OCRWM	SCIENTIFIC ANALYSIS COVER SHEET	1. QA: QA Page 1 of 552

2. Scientific Analyses Title *In Situ* Field Testing of Processes			
3. DI (Including Revision Number) ANL-NBS-HS-000005 REV02			
4. Total Attachments 9		5. Attachment Numbers - Number of pages in each I-6, II-18, III-16, IV-10, V-8, VI-8, VII-4, VIII-22, IX-22	
	Printed Name	Signature	Date
6. Originator	J.S.Y. Wang	Joseph Shyi-Yi Wang	12/5/2003
7. Checker	C. Campbell		12/5/2003
8. QER	S. Harris	Stephen Harris	12/5/03
9. Responsible Manager/Lead	J.S.Y. Wang	Joseph Shyi-Yi Wang	12/5/2003
10. Responsible Manager	P. Dixon		12/5/03

11. Remarks

Block 6. Additional contributors to this report are:

6.1 – P.J. Cook; 6.2 – R.C. Trautz, S. Flexser; 6.3 and 6.4 – Q. Hu; 6.5 – P.J. Cook; 6.6 through 6.9 – R. Salve; 6.10 – R. Salve, D.B. Hudson, P.J. Cook, Q. Hu, M. Conrad; 6.11 – Y. Tsang, P.J. Cook; 6.12 – R. Salve, D.B. Hudson, K. Williams; 6.13 – W. Soll, H.J. Turin, K. Williams, S.S. Levy, T.T. Vandergraaf; 6.14 – Z.E. Peterman, J.B. Paces, G.L. Patterson, J.F. Whelan, L.A. Neymark, B.D. Marshall, R.C. Roback.

Revision History

12. Revision/ICN No.	13. Description of Revision/Change
REV00	Initial Issue
REV01	Complete revision. Numerous changes have been made throughout the document. Table and figure identifiers have been changed throughout. The main revisions are: • Section 4 "Inputs" has been revised to update data inputs and to associate subsections with the various analyses presented in the Section 6 subsections. • Section 5 "Assumptions" has been revised to update assumptions and to associate subsections with the various analyses presented in the Section 6 subsections. • Section 6.1 is revised (1) to include air-permeability data of Niche CD 1620 - Section 6.1.2.2, and (2) to analyze the permeability changes - Section 6.1.2.3. • Section 6.2 is revised (1) to present flow path observations at Niche CD 1620 - Section 6.2.1.2, (2) to present long-term seepage-test data - Section 6.2.1.3, and (3) to compare the seepage threshold data from Niche 4788 with short-term seepage threshold data from Niche 3650 - Section 6.2.2. • Section 6.3 is revised to present additional tracer distribution data on samples collected from the ceiling of Niche 3650 - Section 6.3.1.2. • Section 6.4 is revised to present laser ablation - induced coupled plasma mass spectrometry data for chemical tracer transport and sorption - Section 6.4.3. • Section 6.5 to Section 6.9 are not revised.

2. Scientific Analyses Title
In Situ Field Testing of Processes
3. DI (including Revision Number)
ANL-NBS-HS-000005 REV02

Revision History	
12. Revision/ICN No.	13. Description of Revision/Change
REV01 (continued)	• Section 6.10 is revised (1) to present data of construction water tracer migration below invert Section 6.10.1.3, and (2) to present observations of non-ventilated Cross Drift - Section 6.10.2. • Section 6.11 on systematic hydrologic characterization is a new section. • Section 6.12 on fault test at Alcove 8 and Niche 3107 is a new section. • Section 6.13 on Busted Butte unsaturated zone transport test is a new section.
REV02	Analysis documentation was revised and changes were too extensive to use sidebars per AP-SIII.9Q/Rev. 1/ICN 2, Step 5.6c)1). The following Sections are modified: • Sections 1, 2, 3, 5, 6, 6.1—entire documentation as applicable to AP-SIII-9Q. • Section 4.1 to 4.2 as applicable to AP-SIII.9Q. • Section 6.1 to include air-permeability data for Alcove 8. • Section 6.2.1.3 to include additional seepage test data for Niche CD 1620 (Niche 5). • Section 6.10.1.2.1, 6.10.2, and 6.10.3 to include additional ESF main drift and cross drift observations. • Section 6.11.2.7 through 6.11.2.11, 6.11.3, and 6.11.3.4 to include new tests at boreholes LA#3 and LA#4. • Section 6.12.4 to include new available data from the Alcove 8/Niche 3107 (Niche 3). • Section 6.13 to add neutron probe moisture studies. • Section 6.14 is new from REV01 and includes geochemical and isotopic observations and analysis of the unsaturated zone. • Section 7 is revised to address the new material and modified as applicable to AP-SIII.9Q. • Attachment III to discuss details of seepage tests in Section 6.2. • Attachment VIII to include more information on geology. • Attachment IX to include calculations. All other sections have been modified for editorial purposes, to remove instances of the word "proposed" or "potential" before repository, and to adjust information as applicable to AP-SIII.9Q.

CONTENTS

Page

ACRONYMS AND ABBREVIATIONS xxvii

1. PURPOSE 1-1
   1.1 OBJECTIVES AND PROCESSES ANALYZED BY THE AMBIENT FIELD TESTING ACTIVITIES 1-2
   1.2 LOCATIONS OF TEST SITES 1-2
   1.3 SUPPORT TO FEP ANALYSIS AND TECHNICAL ISSUE RESOLUTION 1-7
   1.4 CONSTRAINTS AND LIMITATIONS 1-8

2. QUALITY ASSURANCE 2-1

3. USE OF SOFTWARE 3-1

4. INPUTS 4-1
   4.1 DIRECT INPUTS 4-1
      4.1.1 Data and Information of Air-Permeability Distributions and Excavation-Induced Enhancements 4-3
         4.1.1.1 Data Used to Illustrate Air-Permeability Distributions and Excavation-Induced Enhancements (Direct Input) 4-3
         4.1.1.2 Information Used to Corroborate Analysis of Air-Permeability Distributions and Excavation-Induced Enhancements (For Reference) 4-4
      4.1.2 Data and Information of Niche Liquid-Release and Seepage-Test Results 4-5
         4.1.2.1 Data Used to Illustrate Niche Liquid-Release and Seepage-Test Results (Direct Input) 4-5
         4.1.2.2 Information Used to Corroborate Analysis and Interpretation of Niche Liquid-Release and Seepage Tests (For Reference) 4-6
      4.1.3 Data Used to Illustrate Tracer-Migration Delineation at Niche 3650 (Niche 5) (Direct Input) 4-6
      4.1.4 Data Used to Illustrate Tracer Penetration and Water Imbibition into Welded Tuff Matrix (Direct Input) 4-7
      4.1.5 Data Used to Illustrate Crosshole Analysis of Air-Injection Tests (Direct Input) 4-7
      4.1.6 Data Used to Illustrate Fracture Flow in Fracture-Matrix Test Bed at Alcove 6 (Direct Input) 4-8
      4.1.7 Data and Information of Flow through the Fault and Matrix in the Test Bed at Alcove 4 4-8
         4.1.7.1 Data Used to Illustrate Flow through the Fault and Matrix in the Test Bed at Alcove 4 (Direct Input) 4-8
         4.1.7.2 Data Used to Corroborate Analysis of Flow through the Fault and Matrix in the Test Bed at Alcove 4 (For Reference) 4-9

CONTENTS (CONTINUED)

Page

4.1.8 Data Used to Compile Water-Potential Measurements in Niches (Direct Input) 4-9
4.1.9 Data Used to Illustrate Observations of Construction-Water Migration (Direct Input) 4-9
4.1.10 Data and Information of Moisture Monitoring and Water Analysis in Underground Drifts 4-10
4.1.10.1 Data Used to Illustrate Moisture Monitoring and Water Analysis in Underground Drifts (Direct Input) 4-10
4.1.10.2 Additional Information on Drift Moisture Monitoring and Water Analysis (For Reference) 4-11
4.1.10.3 Additional Information on Water Potential and Saturation Measurements (For Reference) 4-12
4.1.11 Data and Information of Systematic Hydrological Characterization 4-13
4.1.11.1 Data Used to Illustrate Systematic Hydrological Characterization Results (Direct Input) 4-13
4.1.11.2 Information Used to Corroborate Analyses and Interpretations of Systematic Hydrological Characterization (For Reference) 4-13
4.1.12 Data and Information of Observations from the Test at Alcove 8/Niche 3107 4-14
4.1.12.1 Data Used to Illustrate Observations from the Test at Alcove 8/Niche 3107 (Niche 3) (Direct Input) 4-14
4.1.12.2 Additional Information for Alcove 8/ Niche 3107 (Niche 3) Tests and Summary of the Alcove 1 Tests (For Reference) 4-15
4.1.13 Data and Information of Busted Butte Unsaturated Zone Transport Test 4-16
4.1.13.1 Data Used to Illustrate Busted Butte Unsaturated Zone Transport Test Results (Direct Input) 4-16
4.1.13.2 Information Used to Corroborate Busted Butte Unsaturated Zone Transport Test (For Reference) 4-17
4.1.14 Data and Information of Geochemical Interpretations 4-18
4.1.14.1 Data Used to Support Geochemical Interpretations (Direct Input) 4-18
4.1.14.2 Information Used to Corroborate Geochemical Interpretations (For Reference) 4-21
4.2 CRITERIA 4-23
4.3 CODES AND STANDARDS 4-24

5. ASSUMPTIONS 5-1

6. SCIENTIFIC ANALYSIS DISCUSSION 6.0-1

CONTENTS (CONTINUED)

Page

6.1 AIR-PERMEABILITY DISTRIBUTIONS AND EXCAVATION-INDUCED ENHANCEMENTS 6.1-1
6.1.1 Niche Test Site and Borehole Configuration 6.1-1
6.1.1.1 Site Selection 6.1-1
6.1.1.2 Borehole Configuration 6.1-3
6.1.2 Air-Permeability Testing, Spatial Distribution, and Statistical Analysis ... 6.1-8
6.1.2.1 Data Reduction and Air-Permeability Determination 6.1-9
6.1.2.2 Permeability Profiles 6.1-10
6.1.2.3 Permeability Change as a Function of Initial Permeability 6.1-37
6.1.2.4 Statistical Summary of Air-Permeability Distributions 6.1-40
6.2 ANALYSIS AND INTERPRETATION OF THE NICHE LIQUID-RELEASE AND SEEPAGE-TEST DATA 6.2-1
6.2.1 Review of Data Obtained from Liquid-Release and Seepage Tests Conducted at Niches 6.2-1
6.2.1.1 Pre-Excavation Liquid-Release Test Data 6.2-2
6.2.1.2 Niche Excavation Activities 6.2-3
6.2.1.3 Post-Excavation Seepage Tests 6.2-6
6.2.2 Niche Seepage Threshold and Fracture Characteristic Curves 6.2-34
6.2.2.1 Post-Excavation Liquid-Release and Niche Seepage Threshold 6.2-34
6.2.2.2 Capillary Strength (α^{-1}) of Fractures 6.2-38
6.2.2.3 Estimated Volumetric Water Content (θ) of Fractures 6.2-41
6.2.2.4 Estimated Water Potentials (ψ) of Fractures 6.2-43
6.2.2.5 Fracture-Water Characteristic Curves 6.2-45
6.3 ANALYSES OF TRACER-MIGRATION DELINEATION AT NICHE 3650 (NICHE 2) 6.3-1
6.3.1 Tracer Distribution from the Tracer-Migration Test 6.3-1
6.3.1.1 Field Studies at Niche 3650 (Niche 2) 6.3-1
6.3.1.2 Tracer Migration Test 6.3-1
6.3.2 Delineation of Tracer Distributions from Previous Liquid-Release Tests 6.3-3
6.3.2.1 Detection of Tracers 6.3-4
6.3.2.2 Distribution of Dyes 6.3-7
6.4 ANALYSES OF TRACER PENETRATION AND WATER IMBIBITION INTO WELDED TUFF MATRIX 6.4-1
6.4.1 Penetration of Dyes into Rocks from the Niches 6.4-1
6.4.1.1 Field Observations 6.4-1
6.4.1.2 Dye Penetrations into Rocks 6.4-3
6.4.1.3 Fast Fracture Flow 6.4-4
6.4.1.4 Concentration Profiles of Dye Tracer 6.4-5
6.4.2 Retardation and Tracer Front Movement 6.4-7
6.4.2.1 Dye Retardation Factor Determined by Front Separation 6.4-7

CONTENTS (CONTINUED)

Page
6.4.2.2 Travel-Front Separation 6.4-11
6.4.3 Application of LA-ICP-MS to Investigate Chemical Transport and Sorption 6.4-11
6.5 ANALYSES OF CROSSHOLE AIR-INJECTION TESTS 6.5-1
6.5.1 Crosshole Responses in Welded Tuff 6.5-1
6.5.2 Permeability Distributions and Crosshole Responses in Nonwelded Tuff 6.5-7
6.6 ANALYSES OF FRACTURE FLOW IN FRACTURE-MATRIX TEST BED AT ALCOVE 6 ..... 6.6-1
6.6.1 Liquid-Release Tests in Low- and High-Permeability Zones 6.6-1
6.6.1.1 The Test Bed 6.6-1
6.6.1.2 Instrumentation 6.6-2
6.6.1.3 Liquid-Release Experiments 6.6-2
6.6.2 Observations of Wetting-Front Migration and Fracture Flow 6.6-4
6.6.2.1 Liquid-Release Rates 6.6-4
6.6.2.2 Formation Wetting and Drying 6.6-6
6.6.2.3 Seepage into the Slot 6.6-10
6.6.2.4 Tracer Recovery 6.6-14
6.7 ANALYSES OF FLOW THROUGH THE FAULT AND MATRIX IN THE TEST BED AT ALCOVE 4 ..... 6.7-1
6.7.1 Flow Tests in Paintbrush Tuff Unit Layers and Fault 6.7-1
6.7.1.1 The Test Bed 6.7-1
6.7.1.2 Instrumentation 6.7-4
6.7.1.3 Liquid-Release Experiments 6.7-5
6.7.2 Observations of Fault Flow and Matrix Flow 6.7-6
6.7.2.1 Fault Responses 6.7-6
6.7.2.2 Matrix Responses 6.7-11
6.8 COMPILATION OF WATER-POTENTIAL MEASUREMENTS IN NICHES 6.8-1
6.8.1 Location and Timing of Water-Potential Measurements at Niches 6.8-1
6.8.2 Observations of Dryout in Niche Boreholes 6.8-4
6.8.2.1 Niche 3566 (Niche 1) Pre-Excavation 6.8-6
6.8.2.2 Niche 3566 (Niche 1) Post-Excavation 6.8-7
6.8.2.3 Niche 3650 (Niche 2) Pre-Excavation 6.8-8
6.8.2.4 Niche 3107 (Niche 3) 6.8-8
6.9 OBSERVATIONS OF CONSTRUCTION-WATER MIGRATION 6.9-1
6.9.1 Equipment Setup for Construction-Water Monitoring 6.9-1
6.9.1.1 Starter Tunnel Borehole 6.9-1
6.9.1.2. Electrical Resistivity Probes and Psychrometers 6.9-2
6.9.1.3 Drift Monitoring at the Crossover Point 6.9-3
6.9.2 Wetting-Front Detection and Monitoring Below the ECRB Cross Drift ... 6.9-4
6.9.2.1 Wetting-Front Detection at the Starter Tunnel 6.9-4
6.9.2.2 Wetting-Front Monitoring at the Crossover Point 6.9-13

CONTENTS (CONTINUED)

Page

6.10 MOISTURE MONITORING AND WATER ANALYSIS IN UNDERGROUND DRIFTS 6.10-1
6.10.1 Construction (Drift Excavation) Effects on Moisture Conditions 6.10-1
6.10.1.1 Status of the ESF Moisture Monitoring Study 6.10-1
6.10.1.2 Moisture Conditions and Perturbations Observed in Drifts 6.10-4
6.10.1.3 Construction Water Migration Below Invert from Excavation 6.10-8
6.10.2 Observation along the Nonventilated Sections of the ECRB Cross Drift 6.10-9
6.10.2.1 Water-Potential Measurements and Drift Relative Humidity and Temperature Variations 6.10-12
6.10.2.2 Observations of Wet Zones During Bulkhead Entries 6.10-17
6.10.2.3 Estimates of Mass of Vapor in Nonventilated Sections of the ECRB 6.10-26
6.10.3 Chemical and Isotopic Analysis of Water Samples Collected During Bulkhead Entries 6.10-27
6.10.3.1 Chemical Analysis 6.10-28
6.10.3.2 Isotopic Analysis 6.10-32
6.10.3.3 Summary of ECRB Entries 6.10-33
6.10.4 Ambient Monitoring in Alcove 7 ..... 6.10-33
6.11 ANALYSES AND INTERPRETATIONS OF SYSTEMATIC HYDROLOGICAL CHARACTERIZATION 6.11-1
6.11.1 Systematic Borehole Testing Setup 6.11-1
6.11.1.1 Systematic Borehole Configuration 6.11-1
6.11.1.2 Equipment 6.11-2
6.11.2 Systematic Testing Results and Observations 6.11-7
6.11.2.1 Air-Injection Tests and Liquid-Release Tests in LA2, Initiated on May 11, 2000 ..... 6.11-7
6.11.2.2 Liquid-Release Test in Zone 1, Zone 2, and Zone 3 in LA2, Initiated on May 17, 2000 ..... 6.11-10
6.11.2.3 Liquid-Release Test in Zone 1, Zone 2, and Zone 3 in LA2, Initiated on May 23, 2000 ..... 6.11-11
6.11.2.4 Liquid-Release Test in Zone 2 and Zone 3 in LA2: October 23–December 1, 2000 ..... 6.11-18
6.11.2.5 Liquid-Release Test in Zone 2 of LA1: December 20, 2000 – January 2, 2001 ..... 6.11-20
6.11.2.6 Liquid-Release Test in Zone 2 of LA1: February 28–April 30, 2001 ..... 6.11-23
6.11.2.7 Borehole LA3 and Liquid-Release Test in Zone 1, LA3: May 10 – June 18, 2001 ..... 6.11-25
6.11.2.8 Liquid-Release Test in Zone 2, LA3: May 10–July 23, 2001 ..... 6.11-27

CONTENTS (CONTINUED)

Page

6.11.2.9 Liquid-Release Test in Zone 3, LA3: May 10–July 23, 2001 ..... 6.11-29
6.11.2.10 Borehole LA4 and Liquid-Release Test in Zone 1, LA4: February 5–March 11, 2002 ..... 6.11-30
6.11.2.11 Liquid-Release Test in Zone 2, LA4: October 8 – November 18, 2002 ..... 6.11-32
6.11.2.12 Liquid-Release Test in Zone 3, LA4: February 5– February 28, 2002 ..... 6.11-33
6.11.3 Systematic Testing Discussion and Interpretation 6.11-33
6.11.3.1 Participation of Lithophysal Cavities in Storage and Flow Paths 6.11-34
6.11.3.2 Estimation of the Steady-State Nonintersecting Flow around the Drift 6.11-36
6.11.3.3 Minimum Injection Rate Needed to Induce Seepage 6.11-38
6.11.3.4 Estimation of Evaporation from within the Fracture System 6.11-38
6.11.3.5 Characteristics and Scale of Flow Heterogeneity along the Drift 6.11-39
6.11.3.6 Summary of Systematic Hydrologic Testing 6.11-39
6.12 DRIFT-TO-DRIFT ALCOVE 8/NICHE 3107 (NICHE 3) AND SURFACE-TO-DRIFT ALCOVE 1 TESTS 6.12-1
6.12.1 Drift-to-Drift Alcove 8/Niche 3107 (Niche 3) Tests 6.12-1
6.12.1.1 Test Sequence of Liquid and Tracer Releases 6.12-1
6.12.1.2 The Test Bed 6.12-2
6.12.1.3 Instrumentation 6.12-6
6.12.2 Phase I Observations from the Fault Liquid Test 6.12-7
6.12.2.1 Fault Intake Rates 6.12-8
6.12.2.2 Wetting-Front Migration and Development of the Wetting Plume 6.12-10
6.12.2.3 Seepage in Niche 3107 (Niche 3) 6.12-12
6.12.2.4 Tracer Recovery in Niche 3107 (Niche 3) 6.12-17
6.12.3 Geophysical Imaging of the Drift-to-Drift Test Block 6.12-20
6.12.3.1 Background and Ground-Penetrating-Radar Experimental Approach 6.12-20
6.12.3.2 Results of the Radar Data Acquisition 6.12-21
6.12.4 Large Plot Test 6.12-24
6.12.5 Available Information of Alcove 1 Surface-to-Drift Tests and Implications to Infiltration Process 6.12-29
6.12.5.1 Alcove 1 Test Data 6.12-29
6.12.5.2 Alcove 1 and Pagany Wash Infiltration Comparison 6.12-31
6.13 BUSTED BUTTE UNSATURATED ZONE TRANSPORT TEST 6.13-1
6.13.1 Overview of Unsaturated Zone Transport Test 6.13-1

CONTENTS (CONTINUED)

Page

6.13.1.1 Unsaturated Zone Transport Test Location 6.13-1
6.13.1.2 Unsaturated Zone Transport Test Objectives 6.13-1
6.13.1.3 Unsaturated Zone Transport Test Concept 6.13-2
6.13.1.4 Test Design 6.13-3
6.13.1.5 Site Characterization 6.13-3
6.13.1.6 Borehole Injection and Sampling Systems 6.13-4
6.13.1.7 Electrical-Resistance Moisture Sensors 6.13-5
6.13.1.8 Nonreactive and Reactive Tracers and Microspheres 6.13-6
6.13.1.9 Phase 1 Tracers 6.13-7
6.13.1.10 Phase 2 Tracers 6.13-10
6.13.1.11 Synthetic Pore-Water Recipe 6.13-12
6.13.2 Field-Scale Tracer Transport—Phase 1 ..... 6.13-12
6.13.2.1 Test Phase 1A 6.13-12
6.13.2.2 Test Phase 1B 6.13-17
6.13.3 Field-Scale Tracer Transport – Phase 2 ..... 6.13-22
6.13.3.1 Test Configuration 6.13-22
6.13.3.2 Additional Coring 6.13-24
6.13.3.3 Mineback 6.13-24
6.13.3.4 Pad Analyses 6.13-25
6.13.3.5 Moisture Movement 6.13-26
6.13.3.6 Scaling/Travel Distance 6.13-26
6.13.3.7 Heterogeneity 6.13-26
6.13.3.8 Transverse Dispersion 6.13-30
6.13.3.9 Sorption/Retardation 6.13-32
6.13.4 Tomographic Studies: Geophysical Techniques at the Busted Butte Unsaturated Zone Test Facility 6.13-34
6.13.4.1 Busted Butte Ground Penetrating Radar Tomography 6.13-34
6.13.4.2 Electrical-Resistance Tomography 6.13-45
6.13.5 Neutron Moisture Measurements 6.13-50
6.13.5.1 Neutron Logging Background and Calibration 6.13-50
6.13.5.2 Pre-injection Neutron Logging 6.13-51
6.13.5.3 After Beginning Injection 6.13-53
6.13.6 Summary of Laboratory Radionuclide Migration Experiments 6.13-56
6.14 GEOCHEMICAL AND ISOTOPIC OBSERVATIONS AND ANALYSIS OF THE UNSATURATED ZONE 6.14-1
6.14.1 Pore Water and Rock Geochemistry 6.14-1
6.14.1.1 Analysis and Interpretation of Pore-Water Data 6.14-1
6.14.1.2 Compilation of Rock Chemistry in the Cross Drift 6.14-4
6.14.2 Isoptope Geochemistry Examinations 6.14-9
6.14.2.1 Chlorine-36 Validation Studies 6.14-9
6.14.2.2 Tritium Distribution in the ESF and ECRB 6.14-12

CONTENTS (CONTINUED)

Page

6.14.2.3 Reconstruction of the Paragenetic Sequence and Thermal History of Fracture-Hosted Secondary Mineral Deposits..... 6.14-19
6.14.3 Uranium Isotope Studies..... 6.14-24
6.14.3.1 Mineral-Climate Records of UZ Flow..... 6.14-24
6.14.3.2 U-series Delineation of UZ Flow Zones..... 6.14-33
6.14.4 Fracture Mineral Distribution and Mineralogy..... 6.14-40
6.14.4.1 Results..... 6.14-43

7. CONCLUSIONS..... 7-1
7.1 SUMMARY AND CONCLUSIONS OF AIR-PERMEABILITY DISTRIBUTION AND EXCAVATION-INDUCED ENHANCEMENT IN NICHES..... 7-6
7.2 SUMMARY AND CONCLUSIONS OF LIQUID-RELEASE AND SEEPAGE TESTS IN NICHES..... 7-7
7.2.1 Pre-Excavation Liquid-Release Testing and Niche Excavation Activities..... 7-8
7.2.2 Post-Excavation Seepage Tests at Niche 3650 (Niche 2), Niche 4788 (Niche 4), and Niche CD 1620 (Niche 5)..... 7-8
7.2.3 Constraints and Limitations of the Niche Seepage Test Results..... 7-10
7.3 SUMMARY AND CONCLUSIONS OF TRACER-MIGRATION DELINATION AT NICHE 3650 (NICHE 2)..... 7-11
7.4 SUMMARY AND CONCLUSIONS ON TRACER PENETRATION AND WATER IMBIBITION INTO WELDED TUFF MATRIX..... 7-12
7.5 SUMMARY AND CONCLUSIONS OF SINGLE-HOLE PERMEABILITY DISTRIBUTIONS AND CROSSHOLE CONNECTIVITY ANALYSES..... 7-13
7.6 SUMMARY AND CONCLUSIONS OF FRACTURE FLOW IN THE FRACTURE-MATRIX TEST BED AT ALCOVE 6..... 7-13
7.7 SUMMARY AND CONCLUSIONS OF FLOW THROUGH THE FAULT AND MATRIX IN THE TEST BED AT ALCOVE 4..... 7-15
7.8 SUMMARY AND CONCLUSIONS OF WATER-POTENTIAL MEASUREMENTS CONDUCTED IN THREE NICHES WITHIN THE ESF MAIN DRIFT..... 7-16
7.9 SUMMARY AND CONCLUSIONS OF MONITORING THE CONSTRUCTION-WATER MIGRATION..... 7-16
7.10 SUMMARY AND CONCLUSIONS OF ANALYSES OF CONSTRUCTION EFFECTS..... 7-18
7.11. SUMMARY AND CONCLUSIONS OF SYSTEMATIC HYDROLOGICAL CHARACTERIZATION ALONG THE ECRB CROSS DRIFT..... 7-18
7.12 SUMMARY AND CONCLUSIONS OF DRIFT-TO-DRIFT TESTS BETWEEN ALCOVE 8 AND NICHE 3107 (NICHE 3)..... 7-20
7.13 SUMMARY AND CONCLUSIONS OF BUSTED BUTTE UNSATURATED ZONE TRANSPORT TEST..... 7-21

CONTENTS (CONTINUED)

Page

7.14 SUMMARY AND CONCLUSIONS FOR GEOCHEMICAL AND ISOTOPIC OBSERVATIONS AND ANALYSIS OF THE UNSATURATED ZONE 7-22
7.14.1 Pore Water and Bulk Repository Rock Unit Geochemistry 7-22
7.14.2 Isotope Geochemical Studies 7-22
7.14.2.1 Isotope Geochemical Studies of ^{36}Cl/Cl Signatures 7-22
7.14.2.2 Trituim in Porewater 7-23
7.14.2.3 Thermal Regime 7-23
7.14.3 Uranium Studies 7-24
7.14.3.1 Uranium-Series Dating 7-24
7.14.3.2 U-series Flow Paths in the UZ 7-26
7.14.4 Fracture Mineralogy 7-26

8. INPUTS AND REFERENCES 8-1
8.1 DOCUMENTS CITED 8-1
8.2 CODES, STANDARDS, REGULATIONS, AND PROCEDURES 8-29
8.3 SOURCE DATA, LISTED BY DATA TRACKING NUMBER 8-30
8.4 OUTPUT DATA, LISTED BY DATA TRACKING NUMBER 8-44

ATTACHMENTS
ATTACHMENT I—AUTOMATED AIR-INJECTION SYSTEM I-1
ATTACHMENT II—COMPUTATION TABLES FOR NICHE STUDIES II-1
ATTACHMENT III—SUPPLEMENTAL INFORMATION ON SEEPAGE TESTS AT NICHE CD 1620 ..... III-1
ATTACHMENT IV—SEEPAGE PARAMETER EVALUATION IV-1
ATTACHMENT V—LABORATORY MEASUREMENTS OF RETARDATION AND FRONT SEPARATION V-1
ATTACHMENT VI—FIELD EQUIPMENT FOR CONTROLLED WATER RELEASE, WETTING-FRONT DETECTION, AND SEEPAGE COLLECTION VI-1
ATTACHMENT VII—MEASUREMENT OF WATER POTENTIAL USING PSYCHROMETERS VII-1
ATTACHMENT VIII—GEOLOGY, MINERALOGY, AND HYDROLOGICAL PROPERTIES—BUSTED BUTTE APPLICABILITY VIII-1
ATTACHMENT IX—CALCULATIONS PERFORMED USING EXCEL SPREADSHEETS AND FUNCTIONS IX-1

INTENTIONALLY LEFT BLANK

FIGURES

Page

1.2-1. Schematic Illustration of Alcove and Niche Locations in the Exploratory Studies Facility at Yucca Mountain 1-4
1.2-2. Schematic Illustration of the ESF and ECRB Cross Drift 1-5
1.2-3. Schematic Illustration of Spatial Distribution of Hydrogeologic Units Intersected by the Repository Horizon (Tptpul, Tptpmn, Tptpll, and Tptpln) 1-6
1.2-4. Photo of Yucca Mountain Ridge and Busted Butte, Taken from the Northwest across the Solitario Canyon Fault 1-7
6-1. Schematic Illustration of Flow Tests in the Exploratory Studies Facility at Yucca Mountain 6.0-3
6-2. Schematic Illustration of the Cross-Over Point of ECRB Cross Drift with the Main Drift 6.0-4
6.1.1-1. Schematic Illustration of Location Map for Niche 3107 (Niche 3), Niche 3566 (Niche 1), Niche 3650 (Niche 2), Niche 4788 (Niche 4) and Niche CD 1620 (Niche 5) 6.1-2
6.1.1-2. Schematic Illustration of the End View of Borehole Clusters at Niche Sites 6.1-5
6.1.1-3. Schematic Illustration of the Plan View of Borehole Clusters at Niche Sites 6.1-6
6.1.1-4. Schematic Illustration of the End and Plan Views of Borehole Clusters at Niche CD 1620 (Niche 5) 6.1-7
6.1.1-5. Schematic Illustration of the Plan and End Views of Borehole Clusters at Alcove 8 ..... 6.1-8
6.1.2-1. Pre-Excavation Air-Permeability Profiles along Axial Boreholes at Niche 3566 (Niche 1) 6.1-12
6.1.2-2. Post-Excavation Air-Permeability Profiles along Radial Boreholes at Niche 3566 (Niche 1) 6.1-14
6.1.2-3. Pre- and Post-Excavation Air-Permeability Profiles along Upper Boreholes at Niche 3650 (Niche 2) 6.1-16
6.1.2-4. Pre-Excavation Air-Permeability Profiles along Middle and Bottom Boreholes at Niche 3650 (Niche 2) 6.1-18
6.1.2-5. Pre- and Post-Excavation Air-Permeability Profiles along Upper Boreholes at Niche 3107 (Niche 3) 6.1-21
6.1.2-6. Pre-Excavation Air-Permeability Profiles along Middle and Bottom Boreholes at Niche 3107 (Niche 3) 6.1-23
6.1.2-7. Pre- and Post-Excavation Air-Permeability Profiles along Upper Boreholes at Niche 4788 (Niche 4) 6.1-25
6.1.2-8. Pre-Excavation Air-Permeability Profiles along Middle and Bottom Boreholes at Niche 4788 (Niche 4) 6.1-27
6.1.2-9. Pre- and Post-Excavation Air-Permeability Profiles along Upper Boreholes at Niche CD 1620 (Niche 5) 6.1-30
6.1.2-10. Pre- and Post-Excavation Air-Permeability Profiles along AK Side Boreholes at Niche CD 1620 (Niche 5) 6.1-32
6.1.2-11. Air-Permeability Profiles down Boreholes in Alcove 8 ..... 6.1-34
6.1.2-12. Change Ratio Plot for Niche CD 1620 (Niche 5) Overhead Boreholes 6.1-37
6.1.2-13. Change-Ratio Plots for Niche CD 1620 (Niche 5) AK Boreholes 6.1-38
6.1.2-14. Change-Ratio Plot for Niche 3650 (Niche 2) 6.1-38
6.1.2-15. Change-Ratio Plot for Niche 3107 (Niche 3) 6.1-39

FIGURES (CONTINUED)

Page

6.1.2-16. Change-Ratio Plot for Niche 4788 (Niche 4) 6.1-39
6.2.1-1. Photographic Illustrations of Flow Paths Observed During Niche Excavations: (a) Ambient Flow Path at Niche 3566 (Niche 1), (b) Blue-Dyed Flow Path at Niche 3566 (Niche 1), (c) Pink-Dyed Flow Path at Niche CD 1620 (Niche 5), (d) Pink Stain on the Floor of a Lithophysal Cavity at Niche CD 1620 (Niche 5) 6.2-5
6.2.1-2. Mass of Water Released Versus Aspect Ratio 6.2-6
6.2.1-3. Schematic Illustration of Seepage Capture System and Test Intervals at Niche 3650 (Niche 2) 6.2-8
6.2.1-4. Relative Humidity and Temperature Inside Niche 3107 (Niche 3) 6.2-10
6.2.1-5. Relative Humidity and Temperature Inside Niche 4788 (Niche 4) 6.2-11
6.2.1-6. Stabilized Flow Rates Observed during Test #1 1-5-00 Conducted on Test Interval UR at Niche 4788 (Niche 4) 6.2-12
6.2.1-7. Wetting-Front Sequences Overlying Fracture Map of Niche 4788 (Niche 4) Crown from Seepage Test Begun June 26, 2000 ..... 6.2-14
6.2.1-8. Wetting-Front Area (m^2) versus Time (s) for the Seepage Test Shown in Figure 6.2.1 7 ..... 6.2-15
6.2.1-9. Square Root of Area (m) Plotted versus Perimeter (m) for Each of the Wetting Fronts in the Niche 4788 (Niche 4) Seepage Test 6.2-15
6.2.1-10. Side View Schematic Illustration of the Boreholes at Niche CD 1620 (Niche 5) 6.2-18
6.2.1-11. Plan View Schematic Illustration of the Boreholes at Niche CD 1620 (Niche 5) 6.2-18
6.2.1-12. Schematic Illustration of Front View of Niche CD 1620 (Niche 5) Facing South, Showing Location of Boreholes (#1–7) 6.2-19
6.2.1-13. Schematic Illustration of Front View of Niche CD 1620 (Niche 5) Facing South Showing Profile #1–7–Slot C 6.2-20
6.2.1-14. Photograph of Left (East) Rib of Niche CD 1620 (Niche 5) Facing the Opening of a 3.3-m Long Slot and Showing Ground Support 6.2-21
6.2.1-15. Photograph of Left (East) Rib of Niche CD 1620 (Niche 5) Showing Ceiling of Slot and Ground Support 6.2-22
6.2.1-16. General process diagram for seepage testing at Niche CD 1620 (Niche 5) 6.2-24
6.2.1-17. Capture System Installation Showing Plastic Capture Trays and Tarp in Slot 6.2-26
6.2.1-18. Capture System Showing Tarp Installed Adjacent to Slot 6.2-27
6.2.1-19. Evaporation Rate Inside and Outside Niche CD 1620 (Niche 5) during Test #2 9-17-02 ..... 6.2-30
6.2.1-20. Relative Humidity and Temperature of Air Inside and Outside Niche CD 1620 (Niche 5) during Test#2 9-17-02 ..... 6.2-31
6.2.1-21. Liquid-Release Rate into Borehole #5 and Seepage of Water into the Capture System of Niche CD 1620 (Niche 5) during Test #2 9-17-02 ..... 6.2-32
6.2.1-22. Total Seepage and Seepage into the Tarp Area at the Entrance to the Slot 6.2-33
6.2.1-23. Wetted Area Spreading Down the Sidewall in Niche CD 1620 (Niche 5) 6.2-34
6.2.2-1. Liquid-Release Flux versus Seepage Percentage 6.2-35
6.2.2-2. Niche Seepage Threshold 6.2-37
6.2.2-3. Water Retention Curves for Fractures 6.2-46
6.2.2-4. Effect of Wetting History on Water Retention Curves for Test Interval N3650 UM 4.27–4.57 m 6.2-47

FIGURES (CONTINUED)

Page

6.3.1-1. Schematic of Sampling Borehole Array: (a) Plan View with Liquid-Release/Dye-Application History, and (b) Three-Dimensional View from inside the Niche 6.3-2
6.3.2-1. Dye Detection along Borehole 7: (a) FD&C Blue No. 1 and (b) Sulpho Rhodamine B 6.3-5
6.3.2-2. Dye Detection of: (a) Pyranine Along Borehole 11 and (b) Acid Yellow 7 along Borehole 2 ..... 6.3-6
6.3.2-3. Three-Dimensional View of FD&C Blue No. 1 Detection Related to the Release Intervals above the Niche 6.3-7
6.3.2-4. Three-Dimensional View of Sulpho Rhodamine B Detection Related to the Release Intervals above the Niche 6.3-8
6.3.2-5. Three-Dimensional View of Pyranine Detection Related to the Release Interval above the Niche 6.3-9
6.3.2-6. Three-Dimensional View of Acid Yellow 7 Detection Related to the Release Interval above the Niche 6.3-10
6.3.2-7. Three-Dimensional View of Amino G Acid Detection Related to the Release Interval above the Niche 6.3-11
6.3.2-8. Three-Dimensional View of FD&C Yellow No. 6 Detection Related to the Release Intervals above the Niche 6.3-12
6.4.1-1. Photograph Showing the Wall Face with Fracture Network and Sampling Location of Rock. Stained by FD&C Blue No. 1 during Niche Excavation at Niche 4788 (Niche 4) 6.4-2
6.4.1-2. Sulpho Rhodamine B Penetration Profiles into Rock Matrix from the Fracture Surface 6.4-3
6.4.1-3. Tracer Penetration Profile into Rock Matrix from the Fracture Surface: (a) FD&C Blue No.1 at Niche 3650 (Niche 2); (b) FD&C Blue No.1 at Niche 4788 (Niche 4) 6.4-6
6.4.2-1. Comparison of Tracer Concentration Profiles in a Low-Initial-Saturation Core: (a) Bromide, (b) FD&C Blue No. 1, (c) Sulpho Rhodamine B. Core D had initial saturation of 12.5% and was in contact with saturated boundary for 19.5 hours. 6.4-8
6.4.2-2. Comparison of Tracer Concentration Profiles in a High-Initial-Saturation Core: (a) Bromide, (b) FD&C Blue No. 1, (c) Sulpho Rhodamine B 6.4-9
6.4.3-1. Spatial Distribution along the Tracer Solution Contact Surface of Applied Tracers and the Distribution of Intrinsic Tuff Elements Profiled Using LA-ICP-MS 6.4-12
6.4.3-2. Spatial Distribution Normal to the Tracer Solution Contact Surface (in the Direction of Liquid Imbibition) of Applied Tracers and Distribution of Intrinsic Tuff Elements Profiled Using LA-ICP-MS 6.4-13
6.5.1-1. CrossHole Responses for the Borehole Cluster in Niche 4788 ..... 6.5-3
6.5.1-2. Air-Permeability Profiles along Boreholes in Alcove 6 ..... 6.5-4
6.5.1-3. Crosshole Responses for the Borehole Cluster in Alcove 6 ..... 6.5-6
6.5.2-1. Perspective Illustration of Alcove 4 Test Bed 6.5-7
6.5.2-2. Air-Permeability Profiles along Boreholes in Alcove 4 ..... 6.5-9

FIGURES (CONTINUED)

Page

6.5.2-3. Crosshole Responses for the Borehole Cluster at Alcove 4 PTn Test Bed with All Response Pressure (Resp.) Ratios below 0.2 Included 6.5-13
6.5.2-4. Crosshole Responses for Borehole Cluster at Alcove 4 PTn Test Bed with Small Response Pressure (Resp.) Ratios Filtered 6.5-14
6.6.1-1. Schematic Illustration of (a) Plan view of Location and (b) Vertical View of Layout of Test Bed at Alcove 6 in the ESF at Yucca Mountain 6.6-2
6.6.2-1. Water Intake Rates Observed in the Low Permeability Zone 6.6-5
6.6.2-2. Water Intake Rates Observed in the High Permeability Zone 6.6-5
6.6.2-3. Changes in Electrical Resistance and Water Potential Detected during Liquid Release into the Low Permeability Zone 6.6-7
6.6.2-4. Changes in Electrical Resistance and Water Potential Detected during Liquid Release into the High Permeability Zone 6.6-9
6.6.2-5. Seepage into Slot: (a) Percentage of Injected Water Recovered and (b) Seepage Rates for Various Release Rates 6.6-11
6.6.2-6. Seepage into Collection Trays in the Slot: (a) Tray Configuration and (b) Percentages of Injected Water Recovered for Different Trays 6.6-13
6.6.2-7. Volume of Water Recovered in the Slot after Liquid Injection at Various Rates into the High Permeability Zone was Stopped 6.6-14
6.6.2-8. Tracer Concentrations in Seepage Water Following Injection into the High Permeability Zone 6.6-15
6.7.1-1. Geological Sketch and Schematic Illustration for the North Face of Alcove 4 in the ESF at Yucca Mountain 6.7-2
6.7.1-2. Perspective Illustration of Three-Dimensional View of the Boreholes, Slot, and Lithological Unit Contacts in the Alcove 4 Test Bed 6.7-4
6.7.2-1. Intake Rates along the 0.3 m Zone Located on the Fault in Borehole 12 ..... 6.7-7
6.7.2-2. Wetting-Front Arrival in Borehole 11 Following Liquid Released into the Fault in Borehole 12 ..... 6.7-8
6.7.2-3. Changes in Electrical Resistance in Borehole 11 in Response to Liquid Released into the Fault in Borehole 12 ..... 6.7-9
6.7.2-4. Changes in Electrical Resistance in Borehole 2 in Response to Liquid Released into the Fault in Borehole 12 ..... 6.7-10
6.7.2-5. Intake Rates along a 0.3 m Zone in the Matrix Located 2.44–2.74 m from the Collar in Borehole 5 ..... 6.7-11
6.7.2-6. Changes in Electrical Resistance in Borehole 6 in Response to Liquid Released in Borehole 5 ..... 6.7-12
6.8.1-1. Schematic Illustration of the Location of Psychrometers in Niche 3566 (Niche 1) (a) in Pre Excavation and (b) in Post-Excavation Conditions 6.8-2
6.8.1-2. Schematic Illustration of Location of Psychrometers in Niche 3650 (Niche 2) 6.8-3
6.8.1-3. Schematic Illustration of Location of Psychrometers in Niche 3107 (Niche 3) (Pre-Excavation) 6.8-4
6.8.2-1. Pre-Excavation Water Potential Measured along Borehole U in Niche 3566 (Niche 1) 6.8-7
6.8.2-2. Water Potential Measured along Borehole UM in Niche 3107 (Niche 3) 6.8-8
6.9.1-1. Schematic Illustration of the Location of Wetting-Monitoring Borehole at the Starter Tunnel of the ECRB Cross Drift 6.9-1

FIGURES (CONTINUED)

Page

6.9.1-2. Schematic Illustration of the Borehole Wetting Front Monitoring System with Psychrometers and Electrical Resistivity Probes 6.9-2
6.9.1-3. Schematic Illustration of Sensor Arrays for Wetting Front Monitoring 6.9-3
6.9.2-1. Changes in Water Potential Observed along the Wetting Front Monitoring Borehole at the Starter Tunnel of ECRB Cross Drift 6.9-9
6.9.2-2. Changes in Electrical Resistance Observed along the Wetting-Front Monitoring Borehole at the Starter Tunnel of the ECRB Cross Drift 6.9-10
6.9.2-3. Comparison of Performance of Electrical Resistivity Probe and Psychrometer 6.9-12
6.9.2-4. Example of Time Domain Reflectometry Probe Data at the Crossover Point in the ESF Main Drift 6.9-14
6.10.1-1. Relative Humidity Temporal Variations in the ECRB Cross Drift 6.10-7
6.10.1-2. Relative Humidity Spatial Variations along the ECRB Cross Drift 6.10-7
6.10.1-3. Construction Water Distribution below Exploratory Studies Facility Drift 6.10-8
6.10.2-1. Schematic Illustration of Bulkhead Locations in the ECRB Cross Drift 6.10-10
6.10.2-2. Schematic Illustration showing Berkeley Lab Monitoring Station in Locations in the ECRB Cross Drift 6.10-10
6.10.2-3 As-Built Cross Section of the Terminal End of the ECRB Cross Drift (23+00 m to 26+81 m) Showing the Bulkhead Locations 6.10-11
6.10.2-4. Water-Potential Measurements along the ECRB Cross Drift: (a) Station 15+00; (b) Station 20+00; (c) Station 25+00 ..... 6.10-13
6.10.2-5. Barometric Pressure Measured along the ECRB Cross Drift 6.10-14
6.10.2-6. Temperature Measured in the Four ECRB Cross Drift Stations 6.10-15
6.10.2-7. Relative Humidity Measured in the ECRB Cross Drift Stations 6.10-17
6.10.2-8. Distribution of Wet Zones During ECRB Bulkhead Entries 6.10-18
6.10.2-9. The Green Paint on the Crown of the ECRB Had Condensate Hanging from It, but Surrounding Rock Surface Did Not at CD 24+70 ..... 6.10-21
6.10.2-10. Stalactites near 1st Bulkhead at CD 17+63 ..... 6.10-21
6.10.2-11. Water Puddle and Condensate on Conveyer at CD 18+25 ..... 6.10-22
6.10.2-12. Water Surrounding Inclusions 6.10-22
6.10.2-13. Condensate on Shotcrete after 2nd Bulkhead 6.10-23
6.10.2-14. Solitario Canyon Fault Left Rib 6.10-23
6.10.2-15. Tarp Discoloration before CD 25+99 Bulkhead 6.10-24
6.10.2-16. Inside Bulkhead at CD 25+99 (with TBM)—Quite Dry 6.10-24
6.10.2-17. Vapor Density at Various Temperatures 6.10-26
6.10.2-18. Mass of Vapor in Sections of ECRB Determined from Temperature and Relative Humidity Measurements at Station CD 21+40 and Station CD 25+52 ..... 6.10-27
6.10.3-1. Chemical Analyses of Liquid Samples Collected during Bulkhead Entries 6.10-28
6.10.3-2. Comparison of Chemical Signatures 6.10-29
6.10.3-3. Plot of the Hydrogen and Oxygen Isotope Compositions of Water Samples Collected from the ECRB Cross Drift 6.10-32
6.11.1-1. Schematic of Borehole Configuration in the ECRB Cross Drift for Systematic Characterization of the Lower Lithophysal Unit 6.11-2
6.11.1-2 A Schematic of the Equipment System: Packer Assembly, Water Supply and Air-Injection Component, Seepage Collection Component, and Data Acquisition and Control 6.11-3
6.11.1-3. Schematic Illustration of Front Panel for Control Interface on Computer 6.11-6

FIGURES (CONTINUED)

Page

6.11.2-1. Pressure Responses (Red, Orange, and Green) to Constant Mass Flow of Air-Injection (Blue) for Estimation of Fracture Permeability in ECRB-SYBT LA#2 .....6.11-8
6.11.2-2 Cumulative Water Supplied to ECRB-SYBT-LA#2 Zone 1 and Cumulative Seeped Water into the ECRB Cross Drift for a Test Performed on May 11–May 12, 2000 .....6.11-9
6.11.2-3. Cumulative Water Supplied to ECRB-SYBT-LA#2 Zone 1, Zone 2, and Zone 3 and Cumulative Seeped Water into the ECRB Cross Drift for Tests Performed on May 17–May 18, 2000 .....6.11-11
6.11.2-4. Cumulative Water Supplied to ECRB-SYBT-LA#2 Zone 1 and Cumulative Seeped Water into the ECRB Cross Drift for Tests Performed on May 23–June 1, 2000 .....6.11-12
6.11.2-5. Cumulative Water Supplied to ECRB-SYBT-LA#2 Zone 2 and Cumulative Seeped Water into ECRB Cross Drift for Tests Performed on May 23-June 8, 2000. (a) May 23-June 1, 2000 (b) June 1–June 8, 2000. .....6.11-14
6.11.2-6. Cumulative Water Supplied to ECRB-SYBT-LA#2 Zone 3 and Cumulative Seeped Water into ECRB Cross Drift for Tests Performed on May 23-June 27, 2000: (a) May 23-June 1; (b) June 1 to June 3; (c) June 14-June 18; and (d) June 18–June 27 .....6.11-16
6.11.2-7. Cumulative Water Supplied to ECRB-SYBT-LA#2 Zone 2 and Zone 3 and Cumulative Seeped Water into ECRB Cross Drift for Test Performed on October 23, 2000 to December 1, 2000.....6.11-19
6.11.2-8. Supply Rate, Seepage Rate and Relative Humidity and Temperature for Liquid-Release Test Performed in ECRB-SYBT-LA#2 Zone 2 on October 23, 2000, to December 1, 2000.....6.11-19
6.11.2-9. Supply Rate, Seepage Rate, and Relative Humidity and Temperature for Liquid-Release Test Performed in ECRB-SYBT-LA#2 Zone 3 on October 23, 2000, to December 1, 2000.....6.11-20
6.11.2-10. (a) Cumulative Water Supplied to ECRB-SYBT-LA#1 Zone 2 for Test Performed on December 20, 2000 to January 2, 2001. Also shown are humidity and (b) temperature, and the water level in the evaporation pan.....6.11-22
6.11.2-11. (a) Cumulative Water Supplied to and Seeped from ECRB-SYBT-LA#1 Zone 2 for Test Performed on February 28 to April 30, 2001; (b) Water Supply Rate and Seeped Rate; (c) Humidity, Temperature, and the Water Level in the Evaporation Pan 6.11-24
6.11.2-12. Cumulative Water Volume and Rate Supplied to and Seeped from ECRB-SYBT-LA#3 Zone 1 and Evaporation with Linear Fit and Slope (mm drop per day) for Test Performed on May 17 to June 19, 2001 .....6.11-26
6.11.2-13. Cumulative Water Volume and Rate Supplied to and Seeped from ECRB-SYBT-LA#3 Zone 2 and Evaporation with Linear Fit and Slope (mm drop per day) for Test Performed on June 20 to July 24, 2001 .....6.11-28
6.11.2-14. Rate Supplied to Returned from and Rate of Net Inflow ECRB-SYBT-LA#3 Zone 3 for Test Performed on May 17 to July 24, 2001 .....6.11-30
6.11.2-15. Volume and Rate Supplied to Returned from and Rate of Net Inflow ECRB-SYBT-LA#4 Zone 1 for Test Performed from February 6 to March 9, 2002 .....6.11-31

FIGURES (CONTINUED)

Page

6.11.2-16. Volume and Rate Supplied to Returned from and Rate of Net Inflow ECRB-SYBT-LA#4 Zone 2 and Evaporation with Linear Fit and Slope (mm drop per day) for Test Performed from November 9 to September 18, 2002 ..... 6.11-32
6.11.2-17. Volume and Rate Supplied to Returned from and Rate of Net Inflow ECRB-SYBT-LA#4 Zone 3 for Test Performed from February 6 to February 28, 2002 ..... 6.11-33
6.11.3-1. Depiction of Fast Paths and Storage Areas for Flowing Seepage (a), Pause in Flow and Subsequent Drainage (b) and Refill of Fast Paths (c) 6.11-38
6.11.3-2. Summary Figure of Injection: Return Flow, Evaporation, and Diversion in all Systematic Hydrological Testing studies 6.11-40
6.12.1-1. Schematic Illustration of Liquid Release and Seepage Collection Test Sequence 6.12-2
6.12.1-2. Schematic Illustration of the Test Bed for the Alcove 8/Niche 3107 (Niche 3) Tests 6.12-4
6.12.1-3. Schematic Illustration of the Infiltration Zones along the Floor of Alcove 8: (a) Fault Test and (b) Large Plot Test 6.12-5
6.12.1-4. Schematic Illustration of the Monitoring Boreholes in Niche 3107 (Niche 3) 6.12-6
6.12.2-1. Alcove 8 Trench Infiltration Daily Rates for Saturated and Unsaturated Conditions in the Fault Experiment 6.12-9
6.12.2-2. Cumulative Trench Application from March 5, 200l to August 20, 2002 ..... 6.12-10
6.12.2-3. Wetting-Front Arrival Detected in Borehole 10 in Niche 3107 (Niche 3) 6.12-11
6.12.2-4. Wetting-Front Velocities as determined from Boreholes 1, 9 and 10 in Niche 3107 (Niche 3) 6.12-12
6.12.2-5. Cumulative Seepage (Blue) from All Collection Trays in Niche 3107 (Niche 3) and the Seepage Rate Observed (Red) along a Section of Fault in Niche 3107 (Niche 3) (as Measured in Tray U3-B4) 6.12-13
6.12.2-6. Seepage Rates Measured From 10 Trays Located Along the Ceiling of Niche 3107 (Niche 3) 6.12-14
6.12.2-7. Concentration of Bromide and Seepage Rates Plotted for a Period of 45 Days After First Observations of Drips in Tray 6 ..... 6.12-18
6.12.2-8. Relative Mass Recovery of Tracers Measured in Seepage in Niche 3107 (Niche 3) 6.12-19
6.12.3-1. Radar Velocity Tomograms between Alcove 8 Well Pairs 6.12-23
6.12.3-2. Radar Velocity Tomograms between Alcove 8 and Niche 3107 (Niche 3) Well Pairs 6.12-24
6.12.4-1 Schematic Illustration of the Infiltration Zones along the Floor of Alcove 8 Large-Plot Test 6.12-25
6.12.4-2. Infiltration rates of individual plots from August 20, 2002 to November 19, 2002 ..... 6.12-26
6.12.4-3. Cumulative Application of all Twelve Plots in Alcove 8 Large Plot Experiment 6.12-26
6.12.4-4. Daily seepage rates measured in Niche 3107 (Niche 3) following release of water in the big infiltration plot in Alcove 8 ..... 6.12-27
6.12.4-5. Seepage rates measured in Niche 3107 (Niche 3) following release of water in the big infiltration plot in Alcove 8 ..... 6.12-28

FIGURES (CONTINUED)

Page

6.12.5-1. Schematic Illustration of Alcove 1 Test Site Inside the ESF North Portal 6.12-30
6.13.1-1. Busted Butte Unsaturated Zone Transport Test 6.13-4
6.13.1-2. Vertical Cross Section of Injection and Collection System Configuration 6.13-5
6.13.1-3. Schematic of Phase-1A Borehole Numbers and Relative Locations 6.13-8
6.13.1-4. Phase-1B and Phase-2 Borehole Numbers and Relative Locations 6.13-8
6.13.2-1. Fluorescein Plume at Each of the Four Phase-1A Mineback Faces 6.13-14
6.13.2-2. Fluorescein Plume at 90 cm Mineback Face at Borehole 3 (10 mL/h) 6.13-15
6.13.2-3. Phase-1B Pad Extraction/Analysis Scheme 6.13-18
6.13.2-4a. Bromide Concentrations in Borehole 6 for Phase 1B 6.13-19
6.13.2-4b. 2,6-DFBA Concentrations in Borehole 6 for Phase 1B 6.13-20
6.13.2-4c. Fluorescein Concentrations in Borehole 6 for Phase 1B 6.13-20
6.13.2-4d. Pyridone Concentrations in Borehole 6 for Phase 1B 6.13-21
6.13.2-4e. Lithium Concentrations in Borehole 6 for Phase 1B 6.13-21
6.13.3-1. Borehole Configuration on the Collection Face 6.13-23
6.13.3-2. Schematic Illustration of Locations of Phase 2 Post-Test Overcores 6.13-25
6.13.3-3. Moisture Front Precedes Tracer Front 6.13-27
6.13.3-4. Influence of Scaling/Travel Distance on Tracer Transport in UZTT Phase 2 ..... 6.13-28
6.13.3-5. Influence of Rock Heterogeneity on Tracer Transport in UZTT Phase 2 ..... 6.13-29
6.13.3-6. Extent of Transverse Dispersion on Tracer Transport Measured in Borehole 16 of the UZTT Phase 2 ..... 6.13-31
6.13.3-7. Effect of Sorption/Retardation on Tracer Transport in UZTT Phase 2 ..... 6.13-33
6.13.4-1. Tomography (GPR-T) Results for Well Pair 46-16 from December 1998; March 1999; and April 1999 ..... 6.13-38
6.13.4-2. Tomography (GPR-T) Results for Well Pair 46-9 from April 1999; February 2000; and July 2000 ..... 6.13-40
6.13.4-3. Tomography (GPR-T) Results for Well Pair 11-47 from September 1999, February 2000, and November 2000 ..... 6.13-42
6.13.4-4. Tomography (GPR-T) Results for Well Pair 13-15 from April 1999, February 2000, and July 2000 ..... 6.13-44
6.13.4-5. ERT Layout 6.13-46
6.13.4-6. ERT Electrode Assignments 6.13-46
6.13.4-7. ERT Images of the Test Block Viewed from Test Alcove: Baseline and August Differences 6.13-48
6.13.4-8. ERT Images of the Test Block Viewed from Test Alcove: September Differences 6.13-49
6.13.5-1. Initial Measurements of Moisture Content at Borehole #16 (before smoothing) 6.13-51
6.13.5-2. Moisture Content at Borehole #16 before Injection Compared with Air Permeability 6.13-52
6.13.5-3. Moisture Content at Borehole #46 before Injection 6.13-53
6.13.5-4. Moisture Increase at Borehole #16 at Various Times 6.13-54
6.13.5-5. Moisture Increase at Borehole #46 at Various Times 6.13-55

FIGURES (CONTINUED)

Page

6.14.2-1. $^{36}Cl/Cl$ Ratio Plotted against Sample Location in the Exploratory Studies Facility (ESF) 6.14-10

6.14.2-2. The Average Homogenization Temperatures (T_h) of Two-Phase Fluid Inclusions with Small and Consistent Vapor: Liquid Ratios in Fluid Inclusion Assemblages in Calcite and Fluorite from Secondary Mineral Coating Samples from the Exploratory Studies Facility (ESF) and Enhanced Characterization of the Repository Block (ECRB) Cross Drift Tunnels 6.14-20

6.14.2-3. The $\delta^{18}O$ Values of Calcite from Secondary Mineral Coating Samples in the Exploratory Studies Facility (ESF) and Enhanced Characterization of the Repository Block (ECRB) Cross Drift Tunnels 6.14-21

6.14.2-4. Latest Calcite $\delta^{18}O$ Values Plotted vs. Depth Below the Surface in the ESF, Reflecting Separate Trends in the TCw (squares) and TSw (circles) Welded Tuffs 6.14-22

6.14.2-5. Graph of Calcite Depositional Temperatures versus $^{235}U/^{207}Pb$ or $^{230}Th/U$ (Paces et al. 2001 [156507]) Depositional Ages of Chalcedony or Opal Associated with the Calcite 6.14-23

6.14.3-1. Cross Sections of Two Opal Hemispheres Analyzed by Ion Microprobe Shown under Transmitted Light (Upper Images) and Reflected Light (Lower Images) 6.14-26

6.14.3-2. U/Th Isotope Evolution Plot for Ion-Microprobe Analyses of Opal Hemispheres (Large, Shaded 2σ Error Ellipses) 6.14-27

6.14.3-3. Depth-Age Relations for Profiles of Opal Hemispheres Analyzed by Ion Microprobe (spot locations Shown in Figure 6.14.3-1) 6.14-28

6.14.3-4. Depth-Age Relations for Sequential Microdigestions of Opal Hemisphere HD2074-g2 ..... 6.14-31

6.14.3-5. A. Generalized Geologic Map of Yucca Mountain Showing Sample Locations; B. Cross Sections along the Exploratory Studies Facility (ESF) North Ramp Tunnel Alignment (upper section) and the Enhanced Characterization of the Repository Block (ECRB) Cross Drift Tunnel Alignment (lower section) Showing Sample Locations 6.14-35

6.14.3-6. Variations of (A) Thorium and Uranium Concentration and (B) $^{234}U/^{238}U$ and $^{230}Th/^{238}U$ Activity Ratios (AR) in Yucca Mountain Whole-Rock Subsamples Plotted against Distance from the Fracture Surface 6.14-36

6.14.3-7. Relations between $^{230}Th/^{238}U$ and $^{234}U/^{238}U$ Activity Ratios (AR) for Three Samples from the Cross Drift 6.14-37

6.14.3-8. Map of the Right Rib of the Exploratory Studies Facility Tunnel Showing U-Series Sample Locations 6.14-38

6.14.3-9. U-series Isotopic Compositions (2σ Error Ellipses) for Samples from the Exploratory Studies Facility near the Bow Ridge Fault Zone 6.14-39

6.14.4-1. Relations between Ca Concentration Determined by X-ray Fluorescence and Calcite Concentration Determined by CO_2 Evolution for Cuttings of Tiva Canyon and Topopah Spring High-Silica Rhyolite from Boreholes USW SD-6 and USW WT-24 ..... 6.14-42

6.14.4-2. Hydrogenic Mineral Abundances for 30-m Surveys in the Exploratory Studies Facility (ESF) Plotted against Distance from the North Portal 6.14-43

6.14.4-3. Shaded Topographic Map of the Area Overlying the Underground Workings at the Repository Site 6.14-44

FIGURES (CONTINUED)

Page

6.14.4-4. Histograms Showing Hydrogenic Mineral Abundances in Welded Tuffs in the Exploratory Studies Facility on (A) Linear and (B) Log Scales 6.14-45
6.14.4-5. Variations with Distance in the Exploratory Studies Facility from the North Portal for (A) Fracture Density; (B) Fault and Shear Density; and (C) Hydrogenic Mineral Abundance 6.14-46
6.14.4-6. Relation between Hydrogenic Mineral Abundance in Welded Units of the Topopah Spring Tuff and the Number of Faults and Shears Measured in the Corresponding Intervals in the Exploratory Studies Facility 6.14-47
6.14.4-7. Summary of Hydrogenic-Mineral Abundances in Welded Tuffs in the Exploratory Studies Facility 6.14-49
6.14.4-8. Profiles of Calcite Abundance Calculated from CO_2 Determinations on Cuttings from Boreholes USW SD-6 and USW WT-24 ..... 6.14-50
6.14.4-9. Box and Whisker Plots for Distributions of Calcite Abundance Measurements in Borehole USW SD-6 and the ECRB Cross Drift (gray boxes) Divided into Three Lithostratigraphic Zones, Each Zone Deeper Than the One Above 6.14-52
6.14.4-10. (A) Box and Whisker Plots for Distributions of Lithophysal Cavity Widths and (B) Coating Thicknesses for Both Cavities and Fractures in the Topopah Spring Tuff Welded Unit (TSw) 6.14-53

TABLES

Page

1-1. Features, Events, and Processes Addressed in this Scientific Analysis Report 1-8
3-1. Software and Routines 3-1
4.1-1a. Data Used to Illustrate Air-Permeability Distributions and Excavation-Induced Enhancements (Direct Input) 4-3
4.1-1b. Information Used to Corroborate Analysis of Air-Permeability Distributions and Excavation-Induced Enhancements (For Reference) 4-4
4.1-2a. Data Used to Illustrate Niche Liquid-Release and Seepage-Test Results (Direct Input) 4-5
4.1-2b. Information Used to Corroborate Analysis and Interpretation of Niche Liquid-Release and Seepage Tests (For Reference) 4-6
4.1-3. Data Used to Illustrate Tracer-Migration Delineation at Niche 3650 (Niche 5) (Direct Input) 4-6
4.1-4. Data Used to Illustrate Tracer Penetration and Water Imbibition into Welded Tuff Matrix (Direct Input) 4-7
4.1-5. Data Used to Illustrate Crosshole Analysis of Air-Injection Tests (Direct Input) 4-7
4.1-6. Data Used to Illustrate Fracture Flow in Fracture-Matrix Test Bed at Alcove 6 (Direct Input) 4-8
4.1-7a. Data Used to Illustrate Flow through the Fault and Matrix in the Test Bed at Alcove 4 (Direct Input) 4-8
4.1-7b. Data Used to Corroborate Analysis of Flow through the Fault and Matrix in the Test Bed at Alcove 4 (For Reference) 4-9
4.1-8. Data Used to Compile Water-Potential Measurements in Niches (Direct Input) 4-9
4.1-9. Data Used to Illustrate Observations of Construction-Water Migration (Direct Input) 4-9
4.1-10a. Data Used to Illustrate Moisture Monitoring and Water Analysis in Underground Drifts (Direct Input) 4-10
4.1-10b. Additional Information on Drift Moisture Monitoring and Water Analysis (For Reference) 4-11
4.1-10c. Additional Information on Water Potential and Saturation Measurements (For Reference) 4-12
4.1-11a. Data Used to Illustrate Systematic Hydrological Characterization Results (Direct Input) 4-13
4.1-11b. Information Used to Corroborate Analyses and Interpretations of Systematic Hydrological Characterization (For Reference) 4-13
4.1-12a. Data Used to Illustrate Flow and Transport Test Results at Alcove 8/Niche 3107 (Niche 3) (Direct Input) 4-14
4.1-12b. Additional Information for Alcove 8/ Niche 3107 (Niche 3) Tests and Summary of the Alcove 1 Tests (For Reference) 4-15

TABLES (CONTINUED)

Page

4.1-13a. Data Used to Illustrate Busted Butte Unsaturated Zone Transport Test Results (Direct Input) 4-16
4.1-13b. Information Used to Corroborate Busted Butte Unsaturated Zone Transport Test (For Reference) 4-17
4.1-14a. Data Used to Support Geochemical Interpretations (Direct Input) 4-18
4.1-14b. Information Used to Corroborate Geochemical Interpretations (For Reference) 4-21
4.2-1. Project Requirements and YMRP Acceptance Criteria Applicable to This Scientific Analysis Report 4-23
6-1. Scientific Notebooks 6.0-5
6.1.2-1. Summary Statistics of Air-Permeability (m^2) along Boreholes above Niches 6.1-41
6.1.2-2. Summary Statistics of Air-Permeability (m^2) along Boreholes above Niche CD 1620 (Niche 5) 6.1-42
6.1.2-3. Summary Statistics of Air-Permeability (m^2) in Boreholes alongside Niche CD 1620 (Niche 5) 6.1-43
6.1.2-4. Summary Statistics of Air-Permeability (m^2) along Boreholes under Alcove 8 ..... 6.1-44
6.1.2-5. Comparison of Geometric Means and Standard Deviations of Niches and Alcoves in the Exploratory Studies Facility at Yucca Mountain 6.1-45
6.2.1-1. Borehole Depth Summary 6.2-23
6.2.2-1. Seepage Threshold Fluxes (K_o^*) 6.2-36
6.2.2-2. Alpha (α) Values Estimated for the Fractures 6.2-39
6.2.2-3. Estimated Changes in Volumetric Water Content ($\Delta\theta$) 6.2-42
6.2.2-4. Estimated Water Potential (ψ) for the Fractures 6.2-44
6.3.2-1. Compilation of Tracer Detection versus Borehole Location 6.3-4
6.4.1-1. Liquid-Release Tests and Experimental Conditions 6.4-4
6.4.1-2. Post-Excavation Tracer-Release Tests at Niche 3650 (Niche 2) 6.4-4
6.4.2-1. Measured Properties for Core Samples 6.4-10
6.6.1-1. Amount of Water and Types of Tracers Released into the Injection Borehole 6.6-4
6.6.2-1. Summary of Liquid-Injection Tests in the High Permeability Zone. 6.6-10
6.7.1-1. Summary of Liquid Releases into the Fault Zone in Borehole 12 ..... 6.7-5
6.8.2-1. Water-Potential Measurements in Niche 3566 (Niche 1) 6.8-5
6.8.2-2. Water-Potential Measurements in Niche 3650 (Niche 2) 6.8-6
6.8.2-3. Water-Potential Measurements in Niche 3107 (Niche 3) 6.8-6
6.9.2-1. Psychrometers Response to Excavation at the Starter Tunnel of the ECRB Cross Drift 6.9-5
6.9.2-2. Electrical Resistivity Probe Responses to Excavation at the Starter Tunnel of the ECRB Cross Drift 6.9-6

TABLES (CONTINUED)

Page

6.10.1-1. Moisture-Monitoring Stations in the Exploratory Studies Facility 6.10-2
6.10.1-2. Water-Potential Measurements in the Exploratory Studies Facility 6.10-3
6.10.1-3. Saturation Measurements in the Exploratory Studies Facility 6.10-4
6.10.2-1 Rock Unit Contacts Intersected by the Bulkhead Sections (All within the Topopah Spring Tuff) 6.10-11
6.10.3-1. Chemical and Isotopic Data for Liquid Samples Collected in the ECRB Cross Drift 6.10-30
6.11.2-1. Air-Permeability Estimates for the Three Zones in Borehole LA2 ..... 6.11-8
6.12.5-1. Alcove 1 Infiltration Test Data 6.12-31
6.13.1-1. Tracer C0 Values for Phase 1B Injection 6.13-9
6.13.1-2. Summary of Concentrations Used for Phase 1 Injections 6.13-9
6.13.1-3. Summary of Concentrations Used for Phase 2A Injections 6.13-10
6.13.1-4. Summary of Concentrations Used for Phase 2B Injections 6.13-11
6.13.1-5. Summary of Concentrations Used for Phase 2C Injections 6.13-12
6.13.2-1. Phase 1A Samples Taken from the 90-cm Mineback Face at Borehole 3 ..... 6.13-16
6.14.1-1. Summary of the Most Recent Analyses of Pore Water from Topopah Spring Tuff (TSw), Means and Statistical Parameters 6.14-2
6.14.1-2. Mean Composition of the Phenocryst-Poor member of the Topopah Spring Tuff in the Cross Drift 6.14-6
6.14.1-3. Mean Trace Element Concentrations of the Phenocryst-Poor Member of the Topopah Spring Tuff in the Cross Drift 6.14-7
6.14.1-4. Mean Normative Mineral Contents of the Phenocryst-Poor Rhyolite Member of the Topopah Spring Tuff in the Cross Drift 6.14-8
6.14.2-1. Comparison of Chlorine-36 (^{36}Cl) Validation Study Results with Other ^{36}Cl Results 6.14-11
6.14.2-2. Tritium Activities Found in Samples from Locations in the ESF and ECRB 6.14-16
6.14.3-1. Microstratigraphic Depth, Date and Initial ^{234}U/^{238}U Activity Ratios for HD2074 Opal Determined by Ion Probe. 6.14-25
6.14.3-2. U and Th Isotopic Results from HD2074 Opal Hemispheres 6.14-29
6.14.3-3. Uranium and Thorium Concentrations and ^{234}U-^{230}Th-^{238}U-^{232}Th Isotopic Compositions for Whole Rock-Samples from the ECRB Cross Drift and ESF tunnels, Yucca Mountain, Nevada 6.14-34

INTENTIONALLY LEFT BLANK

ACRONYMS AND ABBREVIATIONS

1-D	one-dimensional
2-D	two-dimensional
3-D	three-dimensional
ACC	Accession Number
AMR	Analysis/Model Report
AMS	Accelerator Mass Spectrometry
AP	Administrative Procedure (DOE)
AR	Activity Ratio
ATDT	Automated Technical Data Tracking
B	Bottom borehole
BBTF	Busted Butte Test Facility
BST	Borehole Sensor Tray
CAMS	Center for Accelerator Mass Spectrometry
CD	ECRB Cross Drift
CDCS	Cross Drift Construction Station
CHn	Calico Hills Non-welded Hydrogeologic Unit
CRWMS	Civilian Radioactive Waste Management System
CS	Construction Station (ESF main loop)
CWAT	Construction Water
DOE	U.S. Department of Energy
DTN	Data Tracking Number
ECM	Effective Continuum Method
ECRB	Enhanced Characterization of Repository Block
ERP	Electrical Resistivity Probe
ERT	Electrical Resistance Tomography
ESF	Exploratory Studies Facility
FBA	Flourobenzoic Acid
FD&C	Food, Drug and Cosmetics
FEP	Features Events and Processes
FI	Fluid Inclusion
FIAs	Fluid Inclusion Assemblages
FY	Fiscal Year
GPR	Ground Penetrating Radar
GPR-T	Ground Penetrating Radar Tomography
HPZ	High Permeability Zone

ACRONYMS AND ABBREVIATIONS (CONTINUED)

ICPAES	Inductively Couples Plasma Atomic Emission Spectrometry
IMP	Ion Microprobe
LA	License Application
LA-ICP-MS	Laser Ablation analyzed by Inductively Coupled Plasma-Mass Spectrometry
LANL	Los Alamos National Laboratory
LBNL	Lawrence Berkeley National Laboratory
LPZ	Low Permeability Zone
M	Middle borehole
MC	Moisture Content
M&O	Management and Operating Contractor
M&TE	Measuring and Test Equipment
ML	Middle Left borehole
MFC	Mass Flow Controller
MR	Middle Right borehole
NRC	Nuclear Regulatory Commission
NTS	Nevada Test Site
OCRWM	Office of Civilian Radioactive Waste Management
PA	Performance Assessment
PMR	Process Model Report
PTn	Paintbrush Non-welded Hydrogeologic Unit
PVC	Polyvinyl Chloride
Q	Qualified
QA	Quality Assurance
QAP	Administrative Procedure (M&O)
QARD	Quality Assurance Requirements and Description
QIP	Quality Implementing Procedure
RH	Relative Humidity
RIS	Records Information System
SDOM	Standard Deviation of the Mean
SMOW	Standard Mean Ocean Water
SR	Site Recommendation
SLPM	Standard Liter Per Minute

ACRONYMS AND ABBREVIATIONS (CONTINUED)

TBM	Tunnel Boring Machine
TBV	To Be Verified
TCO	Test Coordination Office
TCw	Tiva Canyon Welded Hydrogeologic Unit
TDMS	Technical Data Management System
TDR	Time Domain Reflectometry
T_h	Homogenization Temperature
TIMS	Thermal-Ionization Mass Spectrometry
TSPA	Total System Performance Assessment
TU	Tritium Units
TWP	Technical Work Plan
U	Upper borehole
UL	Upper Left borehole
UM	Upper Middle borehole
UR	Upper Right borehole
USGS	United States Geological Survey
UV	Ultraviolet
UV/Vis	Ultraviolet and Visible
UZ	Unsaturated Zone
UZTT	Unsaturated Zone Transport Test
VS	Validation Study
WP	Work Packages
YAP	Administrative Procedure (YMP)
YMP	Yucca Mountain Site Characterization Project
YMRP	Yucca Mountain Review Plan

INTENTIONALLY LEFT BLANK

1. PURPOSE

The purpose of this scientific analysis report is to update and document the data and subsequent analyses from ambient field-testing activities performed in underground drifts through unsaturated zone (UZ) tuff rock units. This scientific analysis report supports Total System Performance Assessment (TSPA) of Yucca Mountain for Licensing Application (LA).

This report is the second revision (REV 02), with the initial issue (REV 00) prepared in March 2000 and the first revision (REV 01) in December 2001. This revision was developed in accordance with the *Technical Work Plan (TWP) for: Performance Assessment Unsaturated Zone* (BSC 2002 [160819], Section 1.10.6, under Work Package (WP) AUZM06) to document available data collected in tests described in the same UZ TWP:

- Moisture studies (in TWP Section 1.1 under WP AUZG01)
- Isotope hydrology (in TWP Section 1.2 under WP AUZG02)
- ESF/ECRB UZ testing (in TWP Section 1.23 under WP AUZT08)
- UZ Seepage Laboratory Testing (in TWP Section 1.24 under WP AUZT09)
- Radionuclide transport laboratory testing (in TWP Section 1.25 under WP AUZT10)
- UZ Busted Butte Transport Test (in TWP Section 1.26 under WP AUZT11).

ESF and ECRB are abbreviations for two existing drifts at Yucca Mountain where testing activities are performed: the Exploratory Studies Facility and the Cross Drift for Enhanced Characterization of Repository Block.

Documentation in this report includes descriptions of how and under what conditions the tests are conducted. The descriptions and analyses provide information useful for refining and confirming the understanding of flow, drift seepage, and transport processes in the UZ. The analyses include the impact of excavation (including use of construction water and effect of ventilation) on the UZ processes. This report is intended to support preparations and revisions of model reports in the UZ TWP (BSC 2002 [160819]) associated with:

- Climate, infiltration, and flow (in TWP Section 1.10 under WP AUZM06)
- Radionuclide mountain scale transport (in TWP Section 1.11 under WP AUZM07)
- Ambient drift seepage (in TWP Section 1.13 under WP AUZM09)
- Drift-scale radionuclide transport (in TWP Section 1.15 under WP AUZM11).

In general, the results discussed in this report are from studies conducted using a combination or a subset of the following three testing approaches: (1) air-injection tests, (2) liquid-release tests, and (3) moisture monitoring. The air-injection tests quantify spatial variability (heterogeneity) of permeability. The liquid-release tests provide an evaluation of *in situ* fracture flow and the

competing processes of matrix imbibition. In addition to active testing, sensors in boreholes and along drifts are used to monitor the *in situ* and perturbed conditions, evaluating the impact of excavation, ventilation, and construction-water usage on the surrounding rocks. The field studies are supplemented by laboratory testing, with addition (in this revision) of hydrochemical data from samples collected in underground drifts. Variabilities and uncertainties in both field and laboratory data are presented for cases with sufficient data to be amenable for statistical analyses.

1.1 OBJECTIVES AND PROCESSES ANALYZED BY THE AMBIENT FIELD TESTING ACTIVITIES

The field-test findings and their implications for drift seepage, fracture flow, matrix imbibition, moisture evolution, and radionuclide transport can be used to address Performance Assessment (PA) uncertainties and repository design issues. The UZ Flow and Transport Model (UZ Model) and the drift-scale models require field data for partitioning UZ flux into a fast fracture-flow component and a slow matrix-flow component (CRWMS M&O 2000 [151940]). This partitioning is controlled by fracture-matrix interaction. The damping of infiltration pulses and diversion by the Paintbrush nonwelded tuff unit (PTn) above the Topopah Spring welded tuff unit (TSw) are potential mechanisms for infiltration and percolation flux redistribution. In the vicinity of the repository, perturbations by drift excavation, air ventilation, and water usage can change the hydrological regime in the UZ. Retardation by rock mass and dispersion through fractures are processes affecting the migration of tracers and the dilution of radionuclides below the drifts to the water table. Some of these processes and related uncertainties, issues, and concerns are addressed by the ambient testing program at underground test sites at Yucca Mountain, further documented in Section 6. The data uncertainties are integral parts of overall model uncertainties in the understanding of processes and in constraining model assessments.

1.2 LOCATIONS OF TEST SITES

The ESF provides underground access to tuff units at and above the repository level. *In situ* testing and monitoring studies are being conducted to directly assess and evaluate the waste emplacement environment and the UZ natural barriers to radionuclide transport at Yucca Mountain. This scientific analysis report summarizes the progress and status of ambient studies of UZ flow conducted at various test sites along the ESF, as illustrated in Figure 1.2-1. The ECRB Cross Drift over the repository block provides access to different subunits of the TSw for ECRB, as illustrated in Figure 1.2-2 and Figure 1.2-3.

Figure 1.2-1 illustrates the locations of four alcoves (Alcoves 1, 2, 3, and 4) along the North Ramp, and three alcoves (Alcoves 5, 6, and 7) and four niches (Niches 3107, 3566, 3650, and 4788) along the Main Drift of the ESF. The numerical identification for each niche denotes the distance in meters from the North Portal. These niches are also referred to as Niches 1, 2, 3, and 4, in accordance to the time sequence of excavation (so that Niche 1 = Niche 3566, Niche 2 = Niche 3650, Niche 3 = Niche 3107, and Niche 4 = Niche 4788, along the ESF Main Drift). The ECRB Cross Drift branches out from the ESF North Ramp, crosses over the Main Drift near Niche 3107 (Niche 3), and reaches the western boundary of the repository block, as illustrated in Figure 1.2-2. Figure 1.2-3 illustrates how the ECRB accesses four hydrogeologic units encountered by the repository: through the entrance in the Topopah Spring upper lithophysal (Tptpul), followed by the middle nonlithophysal (Tptpmn), the lower lithophysal (Tptpll), and

the lower nonlithophysal (Tptpln) units (stratigraphic nomenclature of Buesch et al. 1996 [100106], Table 2, pp. 5–8). In comparison, the ESF Main Drift penetrates predominately the Tptpmn unit.

Many emplacement drifts will be in the lower tuff units. The lower units Tptpll and Tptpln have hydrological characteristics different from Tptpmn, with spatially variable lithophysae and fracture densities affecting the amount of seepage and fracture-matrix flow partition. A systematic study with transient air injection and pulse liquid release along four boreholes drilled into the crown of the ECRB Cross Drift has been conducted to evaluate spatial heterogeneity effects. One alcove (Alcove 8) in Tptpul and one niche (Niche CD 1620 or Niche 5, with CD denoting ECRB Cross Drift) in Tptpll have been excavated in the ECRB Cross Drift. Note that Alcove 8 in the ECRB Cross Drift (illustrated in Figure 1.2-3) is located directly (~ 20 m) above Niche 3107 (Niche 3) in the ESF Main Drift (illustrated in Figure 1.2-1).

The ECRB Cross Drift penetrates the Yucca Mountain block to reach the Solitario Canyon fault. The ECRB Cross Drift has four bulkheads, as illustrated in Figure 1.2-3, to hydrologically isolate particular sections of the Cross Drift, such as the portion which contains the fault. Figure 1.2-4 provides a panoramic view of the Yucca Mountain ridge, with Solitario Canyon in the foreground and Busted Butte in the background to the southeast of the repository block. The Calico Hills tuff unit, not accessible by either the ESF Main Drift or the ECRB Cross Drift, is exposed at Busted Butte, 8 km southeast of the repository area. This Busted Butte outcrop is the site of the Unsaturated Zone Tracer Test (UZTT), which is described in Section 6.13 of this report. The geochemical information collected underground from various experiments and test locations is summarized in Section 6.14 to support hydrological understanding of the *in situ* conditions at the Yucca Mountain site.

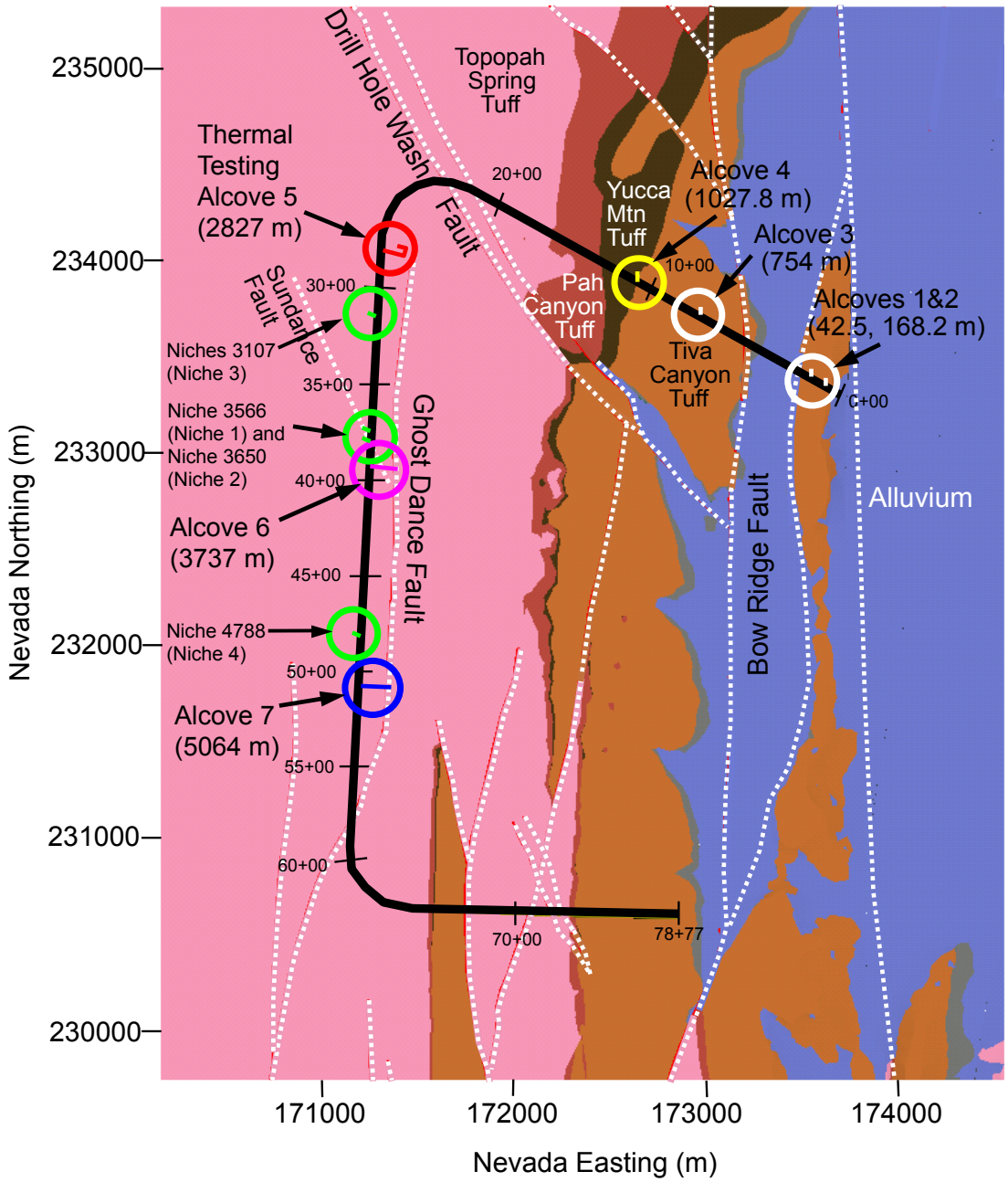

Figure 1.2-1. Schematic Illustration of Alcove and Niche Locations in the Exploratory Studies Facility at Yucca Mountain

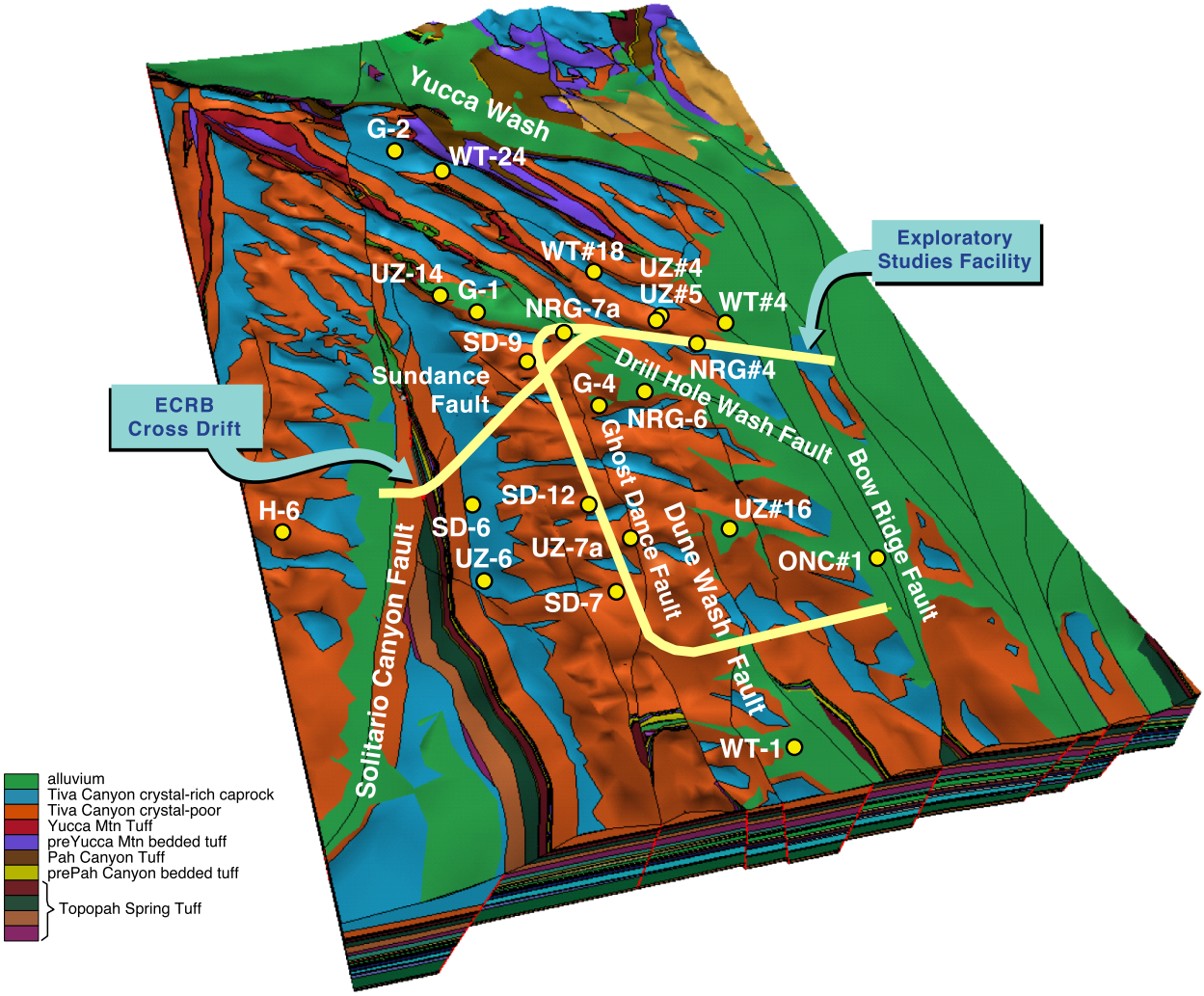

NOTE: The ECRB Cross Drift branches out from the North Ramp of the Exploratory Studies Facility, crosses over the Main Drift, and accesses the western fault boundary of the repository block at Yucca Mountain. Alcoves and niches are illustrated in Figure 1.2-1 for the ESF and in Figure 1.2-3 for the ECRB Cross Drift.

Figure 1.2-2. Schematic Illustration of the ESF and ECRB Cross Drift

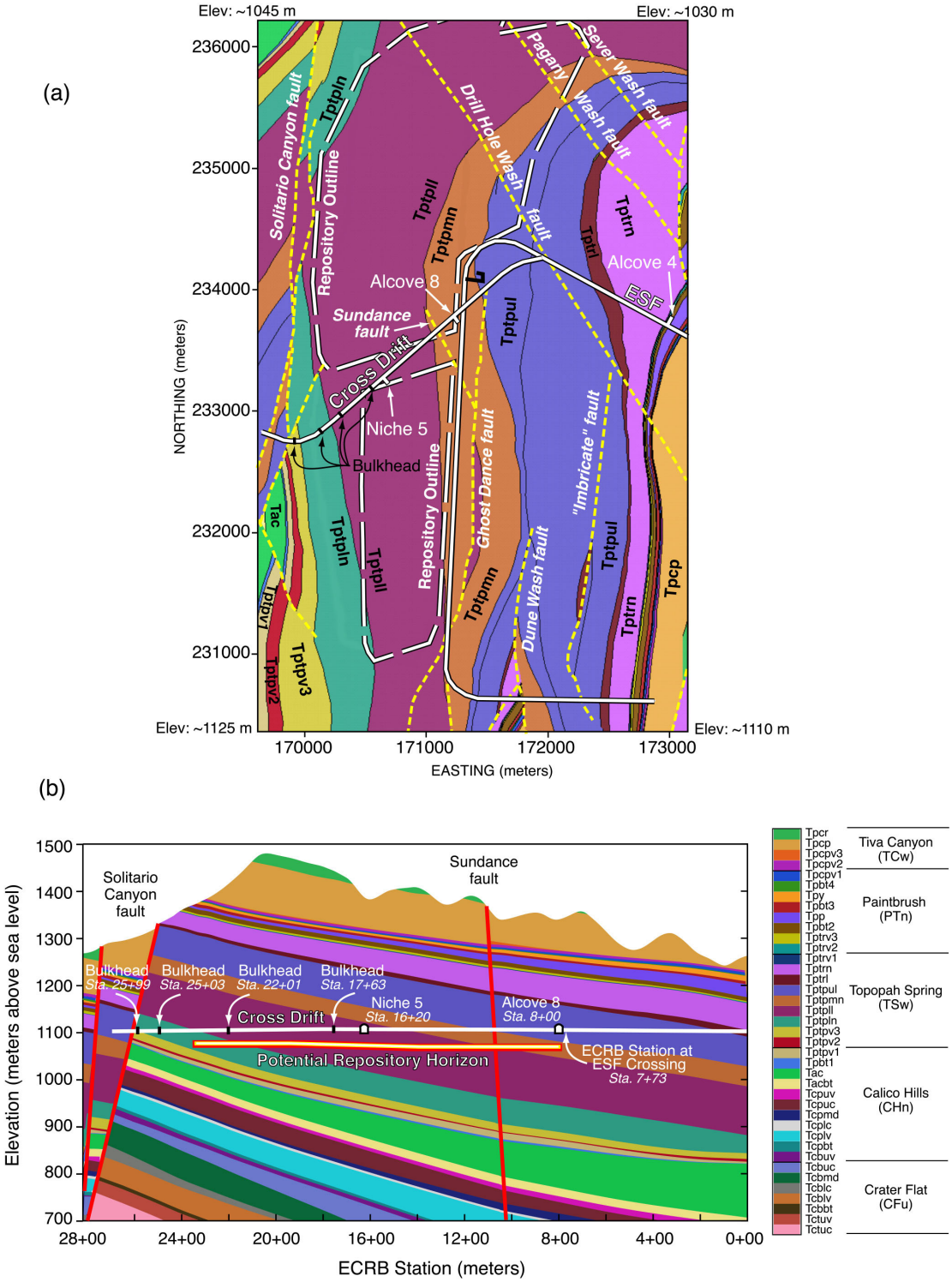

Note: The vertical cross-section in Figure 1.2-3(b) is along the ECRB Cross Drift in nominally the northeast to southwest direction.

Figure 1.2-3. Schematic Illustration of Spatial Distribution of Hydrogeologic Units Intersected by the Repository Horizon (Tptpul, Tptpmn, Tptpll, and Tptpln)

Figure 1.2-4. Photo of Yucca Mountain Ridge and Busted Butte, Taken from the Northwest across the Solitario Canyon Fault

1.3 SUPPORT TO FEP ANALYSIS AND TECHNICAL ISSUE RESOLUTION

This scientific analysis report provides summaries of information which could be used in modeling and abstraction reports (listed in Section 7) and to support the Features, Events, and Processes (FEP) analysis. The following table of FEPs was taken from the LA FEP List (DTN: MO0307SEPFEPS4.000 [164527]). The LA FEP List is a revision to the previous project FEP list (Freeze et al. 2001 [154365]). The selected FEPs are those taken from the LA FEP List associated with the subject matter of this report, regardless of the anticipated status for exclusion or inclusion in TSPA-LA as represented in BSC (2002 [160819]). The results of this analysis are part of the basis for the treatment of FEPs as discussed in the report *Features, Events, and Processes in UZ Flow and Transport* (BSC 2003 [164873]). The UZ FEP report, together with other UZ model reports listed in Section 7, are downstream reports of this scientific analysis report. These reports, rather than this report, provide direct inputs to address issues discussed in *Total System Performance Assessment–License Application Methods and Approach* (BSC 2002 [160146], Section 3.2.2). The cross-reference for each FEP to the relevant sections of this report is also given in Table 1-1 below.

Table 1-1. Features, Events, and Processes Addressed in this Scientific Analysis Report

LA FEP Number	FEP Name	Description Section
1.2.02.01.0A	Fractures	Section 6.1, Section 6.2, Section 6.6, and Section 6.9
1.2.02.02.0A	Faults	Section 6.7 and Section 6.12
2.2.01.01.0A	Mechanical effects of excavation/construction in the near field	Section 6.1
2.2.07.08.0A	Fracture flow in the UZ	Section 6.2, Section 6.6, and Section 6.9
2.2.07.09.0A	Matrix imbibition in the UZ	Section 6.4, Section 6.7
2.2.07.15.0B	Advection and dispersion in the UZ	Section 6.4 and Section 6.12
2.2.07.18.0A	Film flow into the repository	Section 6.2
2.2.07.20.0A	Flow diversion around repository drifts	Section 6.2 and Section 6.11
2.2.08.01.0B	Chemical characteristics of groundwater in the UZ	Section 6.14
2.2.08.03.0B	Geochemical interactions and evolution in the UZ	Section 6.14
2.2.08.08.0B	Matrix diffusion in the UZ	Section 6.3, Section 6.4, Section 6.6, Section 6.7, and Section 6.12
2.2.08.09.0B	Sorption in the UZ	Section 6.3, Section 6.4, Section 6.7, Section 6.12, and Section 6.13
2.2.08.10.0B	Colloidal transport in the UZ	Section 6.13
2.2.09.01.0B	Microbial activity in the UZ	Section 6.10
2.2.11.03.0A	Gas transport in geosphere	Section 6.1 and Section 6.5
2.3.11.03.0A	Infiltration and recharge	Section 6.12

This scientific analysis report also supports the resolutions of technical issues, including: ECRB moisture monitoring, in Section 6.10; Alcove 8/Niche 3107 (Niche 3) testing, in Section 6.11; flow through the Calico Hills nonwelded vitric, in Section 6.13; and analog radionuclide data from test blocks at Busted Butte, in Section 6.13.

1.4 CONSTRAINTS AND LIMITATIONS

The field-testing activities and the associated analyses are subject to the constraints and limitations of spatial locations and temporal durations for tests conducted in the underground drifts. One niche, Niche CD 1620 (Niche 5), has been excavated in the Tptpll unit. Most of the other existing testing alcoves and niches in the ESF (shown in Figure 1.2-3) are located at and

above the horizon of the Tptpmn unit. Test results and analyses from these sites provide information for the upper and middle tuff units. Some of the active flow tests were conducted within a few hours to a few days of each other because of limited accessibility to the test beds in the evenings and on weekends. Depending on system characteristics, the establishment of steady-state conditions requires longer tests. Some tests used automatic data acquisition systems for long-term monitoring and liquid releases, subject to power interruptions and equipment malfunctions. These constraints and limitations are addressed in the analyses of Section 6, if applicable.

The technical scope, content, and management of this scientific analysis report are controlled by the TWP (BSC 2002 [160819]). The update of the LA FEP list from the UZ TWP list is documented in Section 1.3. One deviation from the TWP on YMRP acceptance criteria is documented in Section 4.2. The deviation from the TWP on the status of the ^{36}Cl validation study is documented in Section 6.14.2.

INTENTIONALLY LEFT BLANK

2. QUALITY ASSURANCE

Development of this scientific analysis report and the supporting testing activities have been determined to be subject to the Yucca Mountain Project's quality assurance (QA) program as indicated in *Technical Work Plan for: Performance Assessment Unsaturated Zone,* TWP-NBS-HS-000003 REV 02 (BSC 2002 [160819], Section 8.2, Work Packages (WPs) AUZM06, AUZG01, AUZG02, AUZT08, AUZT09, AUZT10, AUZT11). Approved QA procedures identified in the TWP (BSC 2002 [160819], Section 4) have been used to conduct and document the activities described in this scientific analysis report. The testing and documentation activities follow the TWP for the methods used to control the electronic management of data (BSC 2002 [160819], Section 8.4, WPs AUZM06, AUZG01, AUZG02, AUZT08, AUZT09, AUZT10, AUZT11). There were no variances from the planned methods.

This scientific analysis report provides data for flow, seepage, and transport in natural barriers are classified in the Q-list (BSC 2003 [165179]) as Safety Category because they are important to waste isolation, as defined in AP.2.22Q, *Classification Analyses and Maintenance of the Q-List*. The report contributes to the analyses and modeling data used to support performance assessment (PA). The conclusions of this scientific analysis report do not affect the repository design or permanent items as discussed in AP-2.22Q, *Classification Criteria and Maintenance of the Monitored Geologic Repository Q-List*.

INTENTIONALLY LEFT BLANK

3. USE OF SOFTWARE

The software used in this study are listed in Table 3-1. All qualified software were obtained from Software Configuration Management (SCM), is appropriate for its intended use, and is used only within the range of validation in accordance with AP-SI.1Q, *Software Management.*

For data collection, only acquired software embedded as an integral part of the Measuring and Test Equipment (M&TE) were utilized. The M&TE software were controlled by AP-12.1Q, *Control of Measuring and Test Equipment and Calibration Standards*. Embedded software are exempted from AP-SI.1Q requirements. Software developed or modified for data collection are discussed in the data document associated with each DTN and associated software management reports.

Table 3-1. Software and Routines

Software Name and Version	Software Tracking Number (STN)	DIRS Reference Number	Platform and Operating System
EARTHVISION V4.0	30035-2-V4.0	152835	SGI, IRIX 6.4
ECRB-XYZ V.03	30093-V.03	147402	PC, Windows 98

No models were used for the analyses performed in this scientific analysis report.

Microsoft Excel 97, Microsoft Excel Version 7, Microsoft Excel 2002, CorelDRAW v11.633, Adobe Illustrator 10.0.3, Igor Pro 4.08, Photoshop 7.0.1, MacGPS Pro 4.0.3, DataDesk 6.2, and NOeSYS 2.0 were used for visual display or graphic representation of data; with simple calculations such as mean and standard deviations documented in Attachment IX of this scientific analysis report. These programs are exempted from the requirements of AP-SI.1Q. No developed or modified software is associated with the preparation of this scientific analysis report.

INTENTIONALLY LEFT BLANK

4. INPUTS

Field data collected from underground drifts that characterize ambient and *in situ* field testing conditions include the following:

- Pneumatic pressure and air-permeability data (pre- and post-excavation) for ESF niches
- Pneumatic pressure and air-permeability data from Alcove 4, Alcove 6, and Alcove 8
- Seepage and liquid-release data
- Laboratory dye measurements and sorptivity data
- Water-potential data and electrical resistivity probe data from drift walls and boreholes
- In-drift relative humidity and temperature data (under ventilated and nonventilated conditions)
- Chemical analysis data
- Geologic mapping data
- Unsaturated Zone (UZ) transport testing data from Busted Butte
- Geochemical data and isotope data from underground drifts and boreholes.

The properties resulting from the analyses of the above field data include air-permeability distribution, fracture network connectivity, fracture flow-path distribution, seepage percentage, seepage threshold, fracture characteristic curve, formation intake rate, wetting-front travel time, fracture porosity, fracture volume, fracture flow fraction, tracer distribution, matrix imbibition, retardation factor, fault and matrix flow, water-potential distribution, construction-water migration, relative humidity, moisture conditions, and hydrochemical distributions.

4.1 DIRECT INPUTS

The Q-status of all inputs and a description of the data are shown in the Technical Data Management System (TDMS). The direct inputs to the scientific analysis report were obtained from the TDMS. This scientific analysis report was revised to document recent available *in situ* field-testing data. Results from early revisions with no updates are retained. The input data used in this scientific analysis report are summarized in the tables, which are organized to correspond to equivalent subsections in Section 6.

Since one of the main objectives of this scientific analysis report is to document the data, both direct inputs and collaborating information are summarized together in this section, using separate tables to clearly distinguish different categories. Direct inputs are key data collected, interpreted, illustrated, or tabulated in this scientific analysis report. All other Data Tracking Numbers (DTNs) identified for collaborative information are tabulated in tables without the "direct input" designation.

With the focus of this scientific analysis on the ambient field-testing activities performed in underground drifts through unsaturated zone (UZ) tuff rock units (Section 1), some data collected from monitoring activities, data from surface-based field activities, and data from laboratory testing activities are not included in the "direct input" tables. These data may be important for downstream users for different modeling purposes. The downstream users can make different category selections based on different criteria. If collaborative data are not presented immediately following the direct input data, they are less informative than presentation of the inputs in separated sections.

The direct inputs are presented in the following sections and tables:

- Section 4.1.1.1, Table 4.1-1a on Data and Information Used to Illustrate Air-Permeability Distributions and Excavation-Induced Enhancements
- Section 4.1.2.1, Table 4.1-2a on Data Used to Illustrate Niche Liquid-Release and Seepage-Test Results
- Section 4.1.3, Table 4.1-3 on Data Used to Illustrate Tracer-Migration Delineation at Niche 3650 (Niche 5)
- Section 4.1.4, Table 4.1-4 on Data Used to Illustrate Tracer Penetration and Water Imbibition into Welded Tuff Matrix
- Section 4.1.5, Table 4.1-5 on Data Used to Illustrate Crosshole Analysis of Air-Injection Tests
- Section 4.1.6, Table 4.1-6 on Data Used to Illustrate Fracture Flow in Fracture-Matrix Test Bed at Alcove 6
- Section 4.1.7.1, Table 4.1-7a on Data Used to Illustrate Flow through the Fault and Matrix in the Test Bed at Alcove 4
- Section 4.1.8, Table 4.1-8 on Data Used to Compile Water-Potential Measurements in Niches
- Section 4.1.9, Table 4.1-9 on Data Used to Illustrate Observations of Construction-Water Migration
- Section 4.1.10.1, Table 4.1-10a on Data Used to Illustrate Moisture Monitoring and Water Analysis in Underground Drifts
- Section 4.1.11.1, Table 4.1-11a on Data Used to Illustrate Systematic Hydrological Characterization Results
- Section 4.1.12.1, Table 4.1-12a on Data Used to Illustrate Flow and Transport Test Results at Alcove 8/Niche 3107 (Niche 3)
- Section 4.1.13.1, Table 4.1-13a on Data Used to Illustrate Busted Butte Unsaturated Zone Transport Test Results
- Section 4.1.14.1, Table 4.1-14a on Data Used to Support Geochemical Interpretations

Other associated information are also summarized in different tables.

The uncertainties related to input data and parameters are presented in Section 6 of this scientific analysis report.

4.1.1 Data and Information of Air-Permeability Distributions and Excavation-Induced Enhancements

4.1.1.1 Data Used to Illustrate Air-Permeability Distributions and Excavation-Induced Enhancements (Direct Input)

Table 4.1-1a. Data Used to Illustrate Air-Permeability Distributions and Excavation-Induced Enhancements (Direct Input)

Inputs	Used in			Description
	Section	Figure	Table	
*LB0011AIRKTEST.001 [153155]	Attach. IX.3	6.1.2-1 6.1.2-2 6.1.2-3 6.1.2-4	6.1.2-1 6.1.2-5 IX.3-1	Air-permeability measurements in Niche 3566 (Niche 1) and Niche 3650 (Niche 2) of the ESF
LB980901233124.101 [136593]		6.1.2-5 6.1.2-6 6.1.2-7 6.1.2-8	6.1.2-1 6.1.2-5	Pneumatic-pressure and air-permeability data from Niche 3107 (Niche 3) and Niche 4788 (Niche 4) in the ESF (pre-excavation)
*LB990601233124.001 [105888]		6.1.2-5 6.1.2-7	6.1.2-1 6.1.2-5	Pneumatic-pressure and air-permeability data from Niche 3107 (Niche 3) and Niche 4788 (Niche 4) in the ESF (post-excavation)
LB980912332245.001 [110828]			6.1.2-5	Air-injection data from Niche 3107 (Niche 3) of the ESF (radial boreholes)
*LB0012AIRKTEST.001 [154586]		6.1.2-9	6.1.2-2 6.1.2-5	Air-permeability testing in Niche CD 1620 (Niche 5 upper boreholes, pre-excavation)
*LB0110AKN5POST.001 [156904]		6.1.2-9	6.1.2-2 6.1.2-5	Air-permeability measurement in Niche CD 1620 (Niche 5 upper boreholes, post-excavation)
*LB002181233124.001 [146878]		6.1.2-10	6.1.2-3 6.1.2-5	Air-permeability and pneumatic-pressure data collected from Niche CD 1620 (Niche 5 side boreholes, pre-excavation)
*LB0110AK23POST.001 [156905]		6.1.2-10	6.1.2-3 6.1.2-5	Air-permeability measurement in Niche CD 1620 (Niche 5 side boreholes, post-excavation)
LB980901233124.009 [105856]			6.1.2-5	Pneumatic-pressure and air-permeability data from Alcove 4 in the ESF
LB980901233124.004 [105855]			6.1.2-5	Pneumatic pressure and air-permeability data from Alcove 6 in the ESF
LB0302ALC8AIRK.001 [164748]		6.1.2-11	6.1.2-4 6.1.2-5	Air-permeability data from Alcove 8

NOTE: * Input DTNs for DTN: LB0310AIRK0015.001 [Output].

4.1.1.2 Information Used to Corroborate Analysis of Air-Permeability Distributions and Excavation-Induced Enhancements (For Reference)

Table 4.1-1b. Information Used to Corroborate Analysis of Air-Permeability Distributions and Excavation-Induced Enhancements (For Reference)

Inputs	Used in			Description
	Section	Figure	Table	
MO0008GSC00269.000 [166198]	6.1.1.2		6.1.1-5	As-built ECRB Alcove 8, construction observation alcove boreholes (#1 through 7)
*LB990901233124.004 [123273], Data Table S00017_002			6.1.2-5	Statistical analyses of air-permeability data from Niche 3650 (Niche 2), Niche 3107 (Niche 3), and Niche 4788 (Niche 4), as well as Alcove 4 and Alcove 6.

NOTE: * Other data tables also used as input in Section 6.5 on crosshole connectivity as shown in Table 4.1-5.

4.1.2 Data and Information of Niche Liquid-Release and Seepage-Test Results

4.1.2.1 Data Used to Illustrate Niche Liquid-Release and Seepage-Test Results (Direct Input)

Table 4.1-2a. Data Used to Illustrate Niche Liquid-Release and Seepage-Test Results (Direct Input)

Inputs	Used in			Description
	Section	Figure	Table	
*LB980001233124.004 [136583]	6.2.1.1 6.2.1.2, 6.2.1.3.1 6.2.2.1 6.2.2.3 6.2.2.4 Attach. IV.2 Attach. IV.3.2	6.2.1-2 6.2.2-2	6.2.2-4 II-1 II-4 IV.3-1	Liquid-release test data from Niche 3566 (Niche 1) and Niche 3650 (Niche 2) of the ESF
*LB980901233124.003 [105592]	6.2.1.1 6.2.1.2 Attach. IV.2 Attach. IV.3.2	6.2.1-2 6.2.2-1 6.2.2-2 6.2.2-3 6.2.2-4 IV.2-1	6.2.2-1 6.2.2-2 6.2.2-3 6.2.2-4 II-1 II-4 II-5 II-7 II-8 IV.3-1	Liquid-release and tracer tests in Niche 3566 (Niche 1), Niche 3650 (Niche 2), Niche 3107 (Niche 3), and Niche 4788 (Niche 4) in the ESF, as well as fracture flow and seepage testing in the ESF
*LB0010NICH3LIQ.001 [153144]	6.2.1.3.2	6.2.1-4	II-3a	Niche 3107 (Niche 3) seepage test
*#LB0010NICH4LIQ.001 [153145]	6.2.1.3.3	6.2.1-5 6.2.1-6 6.2.2-2	II-2 II-3b II-8	Niche 4788 (Niche 4) seepage tests measuring injected and captured water masses over time. Time spans include considerations for pumping time, wetting-front arrival time, and dripping duration.
*LB0102NICH5LIQ.001 [155681]	6.2.1.1 6.2.1.2	6.2.1-2	II-1	Niche CD 1620 (Niche 5) seepage tests–pre-excavation
*LB990601233124.001 [105888]			6.2.2-2 II-4	Seepage data feed to UZ drift-scale flow model for TSPA-SR
LB0211NICH5LIQ.001 [160792]	Attach. III.4 Attach. VI Attach. IX.6.1	6.2.1-14 6.2.1-15 6.2.1-17 6.2.1-18 6.2.1-19 6.2.1-20 6.2.1-21 6.2.1-22 6.2.1-23	IV.4-1 IX.6-1	Liquid-release and tracer tests in Niche CD 1620 (Niche 5) in the ECRB

NOTE: * Input DTN for DTN: LB0110LIQR0015.001 [Output].
Input DTN for DTN: LB0110NICH4LIQ.001 [Output].

4.1.2.2 Information Used to Corroborate Analysis and Interpretation of Niche Liquid-Release and Seepage Tests (For Reference)

Table 4.1-2b. Information Used to Corroborate Analysis and Interpretation of Niche Liquid-Release and Seepage Tests (For Reference)

Inputs	Used in			Description
	Section	Figure	Table	
MO0107GSC01069.000 [156941]			II-2	ESF Niche 4788 (Niche 4) borehole as-built information
MO0107GSC01061.000 [155369]	6.2.1.3.5.2 Attach. III.1		6.2.1-13	As-built profile Niche CD 1620 (Niche 5) bat-wing excavation
MO0209GSC02116.000 [160407],	6.2.1.3.5.2			ECRB Niche CD 1620 (Niche 5) borehole as-built information

4.1.3 Data Used to Illustrate Tracer-Migration Delineation at Niche 3650 (Niche 5) (Direct Input)

Table 4.1-3. Data Used to Illustrate Tracer-Migration Delineation at Niche 3650 (Niche 5) (Direct Input)

Inputs	Used in			Description
	Section	Figure	Table	
LB990601233124.003 [106051]		6.3.2-1 6.3.2-2 6.3.2-3 6.3.2-4 6.3.2-5 6.3.2-6 6.3.2-7 6.3.2-8	6.3.2-1	Tracer detection data from core samples for tracers injected in Niche 3650 (Niche 2) in the ESF

4.1.4 Data Used to Illustrate Tracer Penetration and Water Imbibition into Welded Tuff Matrix (Direct Input)

Table 4.1-4. Data Used to Illustrate Tracer Penetration and Water Imbibition into Welded Tuff Matrix (Direct Input)

Inputs	Used in			Description
	Section	Figure	Table	
LB980001233124.004 [136583]			6.4.1-1 6.4.1-2	Liquid-release tests in Niche 3566 (Niche 1) and Niche 3650 (Niche 2)
LB980901233124.003 [105592]			6.4.1-1	Liquid-release and tracer tests in Niche 3566 (Niche 1), Niche 3650 (Niche 2), Niche 3107 (Niche 3), and Niche 4788 (Niche 4) in the ESF.
LB990901233124.003 [155690]	6.4.1.4	6.4.1-2 6.4.1-3 6.4.2-1 6.4.2-2 V-1 V-2	6.4.1-2 6.4.2-1	Tracer lab analyses of dye penetration in Niche 3650 (Niche 2) and Niche 4788 (Niche 4) of the ESF
LB0110TUFTRACR.001 [156979]		6.4.3-1 6.4.3-2		Spatial distribution of applied tracers and the distribution of intrinsic tuff elements profiled using LA-ICP-MS

4.1.5 Data Used to Illustrate Crosshole Analysis of Air-Injection Tests (Direct Input)

Table 4.1-5. Data Used to Illustrate Crosshole Analysis of Air-Injection Tests (Direct Input)

Inputs	Used in			Description
	Section	Figure	Table	
LB980901233124.004 [105855]		6.5.1-2		Pneumatic-pressure and air-permeability data from Alcove 6 in the ESF
LB980901233124.009 [105856]		6.5.2-2		Pneumatic-pressure and air-permeability data from Alcove 4 in the ESF
LB990901233124.004 [123273]		6.5.1-1 6.5.1-3 6.5.2-3 6.5.2-4		Air-permeability crosshole connectivity in Alcove 6, Alcove 4, and Niche 4788 (Niche 4) of the ESF

4.1.6 Data Used to Illustrate Fracture Flow in Fracture-Matrix Test Bed at Alcove 6 (Direct Input)

Table 4.1-6. Data Used to Illustrate Fracture Flow in Fracture-Matrix Test Bed at Alcove 6 (Direct Input)

Inputs	Used in			Description
	Section	Figure	Table	
LB990901233124.002 [146883]		6.6.2-1 6.6.2-2 6.6.2-3 6.6.2-4 6.6.2-5 6.6.2-6 6.6.2-7 6.6.2-8	6.6.1-1 6.6.2-1	Alcove 6 flow data, including electrical resistance, water injection, intake rate, and water-potential measurements
LB990901233124.001 [155694]		6.6.2-8		Alcove 6 tracer tests: the breakthrough of tracers, relating to the volume and the measured tracer concentration of the collected liquid at four collection trays in Alcove 6 experiments

4.1.7 Data and Information of Flow through the Fault and Matrix in the Test Bed at Alcove 4

4.1.7.1 Data Used to Illustrate Flow through the Fault and Matrix in the Test Bed at Alcove 4 (Direct Input)

Table 4.1-7a. Data Used to Illustrate Flow through the Fault and Matrix in the Test Bed at Alcove 4 (Direct Input)

Inputs	Used in			Description
	Section	Figure	Table	
LB990901233124.005 [146884]		6.7.2-1 6.7.2-2 6.7.2-3 6.7.2-4 6.7.2-5 6.7.2-6	6.7.1-1	Alcove 4 flow data, including electrical resistance, water injection, intake rate measurements

4.1.7.2 Data Used to Corroborate Analysis of Flow through the Fault and Matrix in the Test Bed at Alcove 4 (For Reference)

Table 4.1-7b. Data Used to Corroborate Analysis of Flow through the Fault and Matrix in the Test Bed at Alcove 4 (For Reference)

Inputs	Used in			Description
	Section	Figure	Table	
GS960908314224.020 [106059]	6.7.1.1			Analysis report: geology of the north ramp–stations 4+00 to 28+00 data: detailed line survey and full-periphery geotechnical map–Alcoves 3 (UPCA) and 4 (LPCA), and comparative geological cross section–Stations 0+60 to 28+00

4.1.8 Data Used to Compile Water-Potential Measurements in Niches (Direct Input)

Table 4.1-8. Data Used to Compile Water-Potential Measurements in Niches (Direct Input)

Inputs	Used in			Description
	Section	Figure	Table	
LB980001233124.001 [105800]		6.8.2-1 6.8.2-2 VII-1 VII-2	6.8.2-1 6.8.2-2 6.8.2-3	Water-potential measurements in Niche 3566 (Niche 1), Niche 3650 (Niche 2), and Niche 3107 (Niche 3) of the ESF

4.1.9 Data Used to Illustrate Observations of Construction-Water Migration (Direct Input)

Table 4.1-9. Data Used to Illustrate Observations of Construction-Water Migration (Direct Input)

Inputs	Used in			Description
	Section	Figure	Table	
LB980901233124.014 [105858]		6.9.2-1 6.9.2-2 6.9.5-3 6.9.5-4	6.9.2-1 6.9.2-2	Borehole monitoring at the single borehole in the ECRB and ECRB crossover point in the ESF

4.1.10 Data and Information of Moisture Monitoring and Water Analysis in Underground Drifts

4.1.10.1 Data Used to Illustrate Moisture Monitoring and Water Analysis in Underground Drifts (Direct Input)

Table 4.1-10a. Data Used to Illustrate Moisture Monitoring and Water Analysis in Underground Drifts (Direct Input)

Inputs	Used in			Description
	Section	Figure	Table	
LB990901233124.006 [135137]		6.10.1-1 6.10.1-2	6.10.1-1	Moisture data from the ECRB cross drift; relative humidity data from various cross-drift stations
LAJF831222AQ98.007 [122730]		6.10.1-3		Chloride, bromide, and sulfate analysis of salts leached from ECRB-CWAT#1, #2, and #3 drillcore.
GS990908314224.010 [152631]		6.10.2-3		Comparative cross section along the ECRB Cross Drift
GS990408314224.006 [108409]			6.10.2-1	Full periphery geological maps for Station 20+00 to 26+81, ECRB Cross Drift
LB0110ECRBH2OP.001 [156883]		6.10.2.4		Measurements of water potential at three locations between successive bulkhead doors in the ECRB
LB0307ECRBRHTB.001 [164843]	6.10.2.3	6.10.2-5 6.10.2-6 6.10.2-7 6.10.2-17 6.10.2-18		Measurements of relative humidity, temperature, and barometric pressure at four locations between successive bulkhead doors in the ECRB
LB0301ECRBRHTB.001 [164605]	6.10.2.2 6.10.2.2.2 6.10.2.2.3	6.10.2-9 6.10.2-10 6.10.2-11 6.10.2-12 6.10.2-13 6.10.2-14 6.10.2-15 6.10.2-16		Observations of entries made on June 23, 2001, and October 1–2, 2001
LB0110ECRBH2OA.001 [156886]		6.10.3-1 6.10.3-2	6.10.3-1	Anion-cation measurements for water samples from nonventilated sections of the ECRB
LB0110ECRBH2OI.001 [156887]		6.10.3-3	6.10.3-1	Deuterium and DEL O-18 measurements for water samples from nonventilated sections of the ECRB

4.1.10.2 Additional Information on Drift Moisture Monitoring and Water Analysis (For Reference)

Table 4.1-10b. Additional Information on Drift Moisture Monitoring and Water Analysis (For Reference)

Inputs	Used in			Description
	Section	Figure	Table	
LB960800831224.001 [105793]	6.10.1.2.1		6.10.1-1	Relative humidity, temperature, and pressure in ESF monitoring stations
LB970300831224.001 [105794]			6.10.1-1	Moisture data report from October 1996 to January 1997
LB970801233124.001 [105796]	6.10.1.2.1		6.10.1-1	Moisture monitoring data collected at ESF sensor stations
LB970901233124.002 [105798]			6.10.1-1	Moisture monitoring data collected at stationary moisture stations
GS970208312242.001 [135119]			6.10.1-1	Moisture monitoring in the ESF, Oct. 1, 1996, to Jan. 31, 1997
GS970708312242.002 [135123]			6.10.1-1	Moisture monitoring in the ESF, Feb. 1, 1997, to July 31, 1997
GS980908312242.024 [135132]			6.10.1-1	Moisture monitoring in the ESF, August 1, 1997, to July 31, 1998
GS980908312242.035 [135133]			6.10.1-1	Moisture monitoring in the ECRB
GS021008312242.003 [162178]	6.10.1.2.2			Temperature and water-potential data from Alcove 3 and Alcove 4
GS030608312231.002 [165547]	6.10.2.2			Digital image data from the moisture monitoring tests in the ECRB bulkheaded Cross Drift from January 22, 2001, to February 3, 2003
MO0006J13WTRCM.000 [151029]		6.10.3-2		J-13 well water composition
LB0108CO2DST05.001 [156888]		6.10.3-3		Concentration data for CO_2 from gas samples collected from hydrology holes in drift-scale test
LB0011CO2DST08.001 [153460]		6.10.3-3		Contents of gas samples collected from the following drift-scale test holes: 57, 58, 59, 60, 61, 74, 75, 76, 77, 78, 185; and the following control areas: Heater Drift #2 and AO drift air

4.1.10.3 Additional Information on Water Potential and Saturation Measurements (For Reference)

Table 4.1-10c. Additional Information on Water Potential and Saturation Measurements (For Reference)

Inputs	Used in			Description
	Section	Figure	Table	
*LB980001233124.001 [105800]			6.10.1-2	3 main boreholes, 5 lateral boreholes in Niche 3566 (Niche 1) water potential
GS980908312242.022 [135157]			6.10.1-2	Heat-dissipation-probe drill holes water potential
GS980908312242.033 [107168]			6.10.1-2 6.10.1-3	1 core hole in Alcove 3, 2 core holes in Alcove 4 water potential and saturation
GS980908312242.032 [107177]			6.10.1-2 6.10.1-3	1 core hole in Alcove 3, 2 core holes in Alcove 4 water potential and saturation
GS980308312242.004 [107172]			6.10.1-2	18 North Ramp boreholes, 3 Alcove 4 boreholes, and 46 South Ramp boreholes, HQ, 2 m length water potential
GS980308312242.002 [135163]			6.10.1-2	Heat-dissipation-probe drill holes water potential
**LB980901233124.014 [105858]			6.10.1-2 6.10.1-3	43 psychrometers on ESF drift walls, 1 slant borehole below the invert, 43 TDR probes on ESF drift walls
GS980908312242.036 [119820]			6.10.1-2	6 heat-dissipation-probe drill holes water potential
GS970808312232.005 [105978]			6.10.1-2	USW NRG-7a, UE-25 UZ#4, UE-25 UZ#5, USW UZ-7a and USW SD-12 water potential
GS971108312232.007 [105980]			6.10.1-2	USW NRG-7a, UE-25 UZ#4, UE-25 UZ#5, USW UZ-7a and USW SD-12 water potential
GS980408312232.001 [105982]			6.10.1-2	USW NRG-7a, UE-25 UZ#4, UE-25 UZ#5, USW UZ-7a and USW SD-12 water potential
GS981208312232.002 [156505]			6.10.1-2	USW NRG-7a, UE-25 UZ#4, UE-25 UZ#5, USW UZ-7a and USW SD-12 water potential
GS980908312242.018 [135170]			6.10.1-3	3 main boreholes, 6 lateral boreholes in Niche 3566 (Niche 1) and 7 main boreholes in Niche 3650 (Niche 2)
GS980908312242.020 [135172]			6.10.1-3	3 main boreholes, 6 lateral boreholes in Niche 3566 (Niche 1) and 7 main boreholes in Niche 3650 (Niche 2)
GS980908312242.029 [135175]			6.10.1-3	3 boreholes in Alcove 6, 1 borehole in Alcove 7 saturation
GS980908312242.028 [135176]			6.10.1-3	3 boreholes in Alcove 6, 1 borehole in Alcove 7 saturation
GS980308312242.005 [107165]			6.10.1-3	PTn Borehole core saturation
GS980308312242.003 [135180]			6.10.1-3	South Ramp core saturation
GS980308312242.001 [135181]			6.10.1-3	TDR measurements of saturation
GS980908312242.030 [135224]			6.10.1-3	1 slant borehole core saturation

NOTE: * Also used as input in Section 6.8 on niche water-potential measurement, as shown in Table 4.1-8.
** Also used as input in Section 6.9 on construction-water migration, as shown in Table 4.1-9.

4.1.11 Data and Information of Systematic Hydrological Characterization Results

4.1.11.1 Data Used to Illustrate Systematic Hydrological Characterization Results (Direct Input)

Table 4.1-11a. Data Used to Illustrate Systematic Hydrological Characterization Results (Direct Input)

Inputs	Used in			Description
	Section	Figure	Table	
*LB00090012213U.001 [153141]	6.11.2.1	6.11.2-1 6.11.3-2	6.11.2-1	Two sets of air-k (pneumatic conductivity) tests at 3 intervals in title borehole. Air-k derived from steady-state pressure response.
*LB00090012213U.002 [153154]		6.11.2-2 6.11.2-3 6.11.2-4 6.11.2-5 6.11.2-6 6.11.3-2		Eleven sets of seepage tests. Liquid-release tests from borehole SYBT-ECRB-LA#2 at CS 17+26 in cross drift.
*LB0110ECRBLIQR.003 [156877]		6.11.2-7 6.11.2-8 6.11.2-9 6.11.3-2		Measurements of seepage from injection tests in boreholes located in the drift crown of the ECRB
*LB0110ECRBLIQR.001 [156878]		6.11.2-10 6.11.3-2		Measurements of seepage from injection tests in boreholes located in the drift crown of the ECRB
*LB0110ECRBLIQR.002 [156879]	Attach. IX.6.2	6.11.2-11 6.11.3-2	IX.6-2	Measurements of seepage from injection tests in boreholes located in the drift crown of the ECRB
LB0203ECRBLIQR.001 [158462]	Attach. IX.6.3 Attach. IX.6.4 Attach. IX.6.5	6.11.2-12 6.11.2-13 6.11.2-14 6.11.3-2	IX.6-3 IX.6-4 IX.6-5 IX.6-8	Systematic testing in SYBT-ECRB- LA#3 (May–July 2001)
LB0301SYTSTLA4.001 [165227]	Attach. IX.6.4	6.11.2-15 6.11.2-16 6.11.2-17 6.11.3-2	IX.6-6 IX.6-7	Measurements of seepage from injection tests in boreholes located in the drift crown of the SYBT-ECRB-LA#4

NOTE: * Input DTNs for DTN: LB0110SYST0015.001 [Output].

4.1.11.2 Information Used to Corroborate Analyses and Interpretations of Systematic Hydrological Characterization (For Reference)

Table 4.1-11b. Information Used to Corroborate Analyses and Interpretations of Systematic Hydrological Characterization (For Reference)

Inputs	Used in			Description
	Section	Figure	Table	
LB980912332245.002 [105593]	6.11.3.1			Gas tracer data from Niche 3107 (Niche 3) of the ESF
LB0110COREPROP.001 [157169]	6.11.3.1			Data measured from cores drilled in the ECRB: porosity, saturation, bulk density, gravimetric water content, particle density

4.1.12 Data and Information of Observations from the Test at Alcove 8/Niche 3107

4.1.12.1 Data Used to Illustrate Flow and Transport Test Results at Alcove 8/Niche 3107 (Niche 3) (Direct Input)

Table 4.1-12a. Data Used to Illustrate Flow and Transport Test Results at Alcove 8/Niche 3107 (Niche 3) (Direct Input)

Inputs	Used in			Description
	Section	Figure	Table	
GS020508312242.001 [162129]	6.12.2.1	6.12.2-1 6.12.2-2		Trenched fault infiltration in Alcove 8, 3/5/2001–6/1/2001
GS020908312242.002 [162141]	6.12.2.1	6.12.2-1 6.12.2-2		Trenched fault infiltration in Alcove 8, 6/1/2001–3/26/2002
GS030208312242.003 [165544]	6.12.2.1	6.12.2-1 6.12.2-2		Trenched fault infiltration in Alcove 8, 3/26/2002–8/20/2002
LB0110A8N3LIQR.001 [157001]	Attach. IX.6.5	6.12.2-3 6.12.2-4 6.12.2-5 6.12.2-7 IX.6-1	IX.6-9a IX.6-9b IX.6-10	Preliminary observations from the fault test at Alcove 8/Niche 3107 (Niche 3).
LB0204NICH3TRC.001 [158478]		6.12.2-7 6.12.2-8		Fault infiltration test tracer sampling April 2001–March 2002
LB0209A8N3LIQR.001 [165461]		6.12.2-4 IX.6-1	IX.6-9c IX.6-10	Resistance measurements from borehole 10 in Niche 3107 (Niche 3, 5/23/2001–9/3/2002)
LB0303A8N3LIQR.001 [162570]		6.12.2-4 6.12.2-6 6.12.2-8 IX.6-1		Alcove 8/Niche 3107 (Niche 3) seepage data compilation
LB0110A8N3GPRB.001 [156912]		6.12.3-1 6.12.3-2		Pre-seepage test ground penetrating radar tomography in radial borehole arrays between Alcove 8 (ECRB) and Niche 3107 (Niche 3, ESF)
GS031008312242.007 [166089]	6.12.4	6.12.4-2 6.12.4-3		Large plot infiltration in Alcove 8, 8/20/2002–11/19/2002
GS030608312242.005 [166200]		6.12.4-2		Surface infiltration in a large plot in Alcove 8 using permeameters from 11/19/2002–03/24/2003.
LB0306A8N3LIQR.001 [165405]		6.12.4-4 6.12.4-5		Fault infiltration test from Alcove 8 to Niche 3107 (Niche 3, 9/18/2002–10/16/2002)
LB0308A8N3SEEP.001 [166090]		6.12.4-5		Measurements of seepage at Niche 3107 (Niche 3) from injection tests in an infiltration plot located at Alcove 8 of the ECRB, 10/16/2002–4/2/2003

4.1.12.2 Additional Information for Alcove 8/ Niche 3107 (Niche 3) Tests and Summary of the Alcove 1 Tests (For Reference)

Table 4.1-12b. Additional Information for Alcove 8/ Niche 3107 (Niche 3) Tests and Summary of the Alcove 1 Tests (For Reference)

Inputs	Used in			Description
	Section	Figure	Table	
GS030508312242.004 [165545]	6.12.1.2			Photographs from Niche 3107 (Niche 3) of the Alcove 8/Niche 3107 (Niche 3) seepage experiment during construction showing construction water in Niche 3107 (Niche 3), 3/6/2000
*MO9901MWDGFM31.000 [103769]	6.12.1.2			Geologic Framework Model, Version GFM 3.1
GS010608312242.004 [165542]	6.12.1.3.1			Crossover Alcove/Seepage into Niche 3107 (Niche 3): small plot infiltration using a cylinder permeameter, 8/9/2000–8/21/2000
GS010608312242.002 [165543]	6.12.1.3.1			Crossover Alcove/Seepage into Niche 3107 (Niche 3): small plot infiltration using a box permeameter, 8/28/2000–12/14/2000
GS990108312242.006 [162979]			6.12.5-1	Pulse flow meter data for infiltration on surface, Phase I, May 9, 1998–December 4, 1998
GS000308312242.002 [156911]	6.12.5.1		6.12.5-1	Seepage data for water collected in Alcove 1, Phase I, 5/5/1998–9/27/1998
GS000808312242.006 [162980]			6.12.5-1	Pulse flow meter data for infiltration on surface, Phase II, 2/19/1999–6/20/2000
GS000399991221.003 [147024]			6.12.5-1	Preliminary infiltration, seepage, tracer data, Phase II, 2/19/1999–12/15/1999
GS001108312242.009 [165202]			6.12.5-1	Tracer data for water collected in Alcove 1, Phase II, 5/9/1999–7/5/2000

*Note: The TDMS shows DTN: MO9901MWDGFM31.000 [103769] to be superseded by DTN: MO0012MWDGFM02.002 [153777]; however, the new DTN does not include the data used for development of this analysis. The comment section on the Technical Data Information Form for the more recent DTN also states: “GFM2000 does not invalidate GFM3.1.” This scientific analysis report maintains the use of the original DTN.

4.1.13 Data and Information of Busted Butte Unsaturated Zone Transport Test Results

4.1.13.1 Data Used to Illustrate Busted Butte Unsaturated Zone Transport Test Results (Direct Input)

Table 4.1-13a. Data Used to Illustrate Busted Butte Unsaturated Zone Transport Test Results (Direct Input)

Inputs	Used in			Description
	Section	Figure	Table	
LA0302WS831372.001 [162765]		6.13.2-1 6.13.2-2		Fluorescein plumes observed in Phase 1a mineback
LA9909WS831372.001 [122739]	6.13.2.2	6.13.2-4a 6.13.2-4b 6.13.2-4c 6.13.2-4d 6.13.2-4e		Busted Butte UZ transport test: Phase I collection pad extract concentrations
LA9909WS831372.002 [122741]	6.13.2.2	6.13.2-4a 6.13.2-4b 6.13.2-4c 6.13.2-4d 6.13.2-4e		Busted Butte UZ transport test: Phase I collection pad tracer loading and tracer concentrations
LA0112WS831372.001 [157100]		6.13.3-3 6.13.3-4 6.13.3-5 6.13.3-6 6.13.3-7		Busted Butte UZ transport test: Phase II collection pad tracer loading.
LA0112WS831372.002 [157115]		6.13.3-3 6.13.3-4 6.13.3-5 6.13.3-6 6.13.3-7		Busted Butte UZ transport test: Phase II collection pad tracer concentrations.
LA0112WS831372.003 [157106]		6.13.3-3 6.13.3-4 6.13.3-5 6.13.3-6 6.13.3-7		Busted Butte UZ transport test: Phase II normalized collection pad tracer concentrations.
LB00032412213U.001 [149214]		6.13.4-1 6.13.4-2 6.13.4-3 6.13.4-4		Busted Butte ground-penetrating-radar data collected June 1998 through February 2000 at the unsaturated zone transport test (UZTT): GPR velocity data.
LB0110BSTBTGPR.001 [156913]		6.13.4-3 6.13.4-4		Time sequence ground-penetrating-radar tomography for the Busted Butte tracer imbibition test
LL990612704244.098 [147168]	6.13.4.2.1	6.13.4-7 6.13.4-8		ERT data for Busted Butte, electrical properties of the rock were measured during water infiltration.
LA0201WS831372.004 [165422]		6.13.5-1 6.13.5-2 6.13.5-3		Calculated moisture content for the Busted Butte site Phase II collection boreholes
LA0311SD831372.001 [166197]		6.13.5-2		*In situ* air permeability measurements at Busted Butte
LA0008WS831372.001 [156582]		6.13.5-4 6.13.5-5		Calculated daily injection rates for the Busted Butte unsaturated zone transport tests

4.1.13.2 Information Used to Corroborate Busted Butte Unsaturated Zone Transport Test (For Reference)

Table 4.1-13b. Information Used to Corroborate Busted Butte Unsaturated Zone Transport Test (For Reference)

Inputs	Used in			Description
	Section	Figure	Table	
LA9909WS831372.016 [140093]	6.13.1.11			Ion chromatography pore-water analysis for rock samples from Busted Butte (used in AMR as reference for pore-water composition)
LA9909WS831372.017 [140097]	6.13.1.11			pH pore water in rock samples from Busted Butte (used in AMR as reference for pore-water composition)
LA9909WS831372.018 [140101]	6.13.1.11			Gravimetric moisture content of rock samples from Busted Butte (used in AMR as reference for pore-water composition)
LA9910WS831372.008 [147156]	6.13.2.1		6.13.2-1	Busted Butte UZTT: gravimetric moisture content and bromide concentration in selected Phase 1A rock samples
LA9912WS831372.001 [156586]	6.13.3.9			Sorption of fluorinated benzoic acids and lithium on rock samples form Busted Butte
MO0004GSC00167.000 [150300]		6.13.4-1 6.13.4-2		As-built coordinates of boreholes in the test alcove and running drift, Busted Butte test facility (BBTF)
LA0108TV1221313U.001 [161525]	6.13.6			Static batch sorption coefficients and retardation coefficients
GS990708314224.007 [164604]	Attach. VIII.6			Detailed line survey data for Busted Butte access drift and Busted Butte cross drift
LA0204SL831372.001 [164749]	Attach. VIII.7		VIII-1	Mineralogy of the Busted Butte Phase 2 test block
LA0207SL831372.001 [160824]			VIII-3	Lithostratigraphic classification of hydrological-property core-sampling depths, Busted Butte Phase 2 test block
GS990708312242.008 [109822]			VIII-3 VIII-6	Physical and hydraulic properties of core samples from Busted Butte boreholes
GS960808312231.004 [108985]			VIII-4	Physical properties, water content. and water potential for samples from lower depths in boreholes USW SD-7 and USW SD-12. Submitted: 08/30/96.
GS960808312231.005 [108995]			VIII-5	Saturated hydraulic conductivity of Busted Butte.
GS951108312231.009 [108984]			VIII-5	Physical properties, water content, and water potential for borehole USW SD-7. Submitted: 09/26/95.
GS990308312242.007 [107185]			VIII-6	Laboratory and centrifuge measurements of physical and hydraulic properties of core samples from Busted Butte boreholes

4.1.14 Data and Information of Geochemical Interpretations

4.1.14.1 Data Used to Support Geochemical Interpretations (Direct Input)

Table 4.1-14a. Data Used to Support Geochemical Interpretations (Direct Input)

Inputs	Used in			Description
	Section	Figure	Table	
GS020408312272.003 [160899]			6.14.1-1	Collection and analysis of pore-water samples for the period from April 2001 to February 2002. Water chemistry analyses for physical parameters; common anions and cations from 15 ECRB-SYS-Series boreholes, USW SD-9 and USW NRG-7/7A.
GS030408312272.002 [165226]			6.14.1-1	Analysis of water-quality samples for the period from July 2002 to November 2002. Water chemistry analyses for physical parameters; common anions and cations; and trace metals.
GS000308313211.001 [162015]	6.14.1.2 Attach. IX.5		6.14.1-2 6.14.1-3 6.14.1-4	Geochemistry of repository block—chemical composition of rock from ECRB Cross Drift
LAJF831222AQ98.004 [107364]		6.14.2-1	6.14.2-1	Chloride, bromide, sulfate, and chlorine-36 analyses of salts leached from ESF rock samples.
LAJF831222AQ98.009 [145650]		6.14.2-1		Chlorine-36 analyses of salts leached from ESF Niche 3566 (Niche 1) drillcore.
GS951208312272.002 [151649]			6.14.2-2	Tritium analyses of porewater from USW UZ-14, USW NRG-6, USW NRG-7A and UE-25 UZ#16 and of perched water from USW SD-7, USW SD-9, USW UZ-14 and USW NRG-7A from 12/09/92 to 5/15/95.
GS990183122410.001 [146125]			6.14.2-2	Tritium data from pore water from ESF borehole cores, 1997 analyses by USGS. Tritium abundance data from boreholes ESF-AL#3-RBT#1, ESF-AL#3-RBT#4, ESF-AL#4-RBT#1, ESF-NAD-GTB#1A, ESF-NDR-MF#1, ESF-SAD-GTB#1, ESF-SR-MOISTSTDY#1, ESF-SR-MOISTSTDY#2 and ESF-SR-MOISTSTDY#13, for the period 1/16/97 through 11/6/97.
GS990183122410.004 [146129]			6.14.2-2	Tritium data from pore water from ESF borehole cores, 1998 analyses by University of Miami. Tritium abundance data from boreholes ESF-NAD-GTB#1A, ESF-NDR-MF#1, ESF-SR-MOISTSTDY#1, ESF-SR-MOISTSTDY#2, ESF-SR-MOISTSTDY#4, ESF-SR-MOISTSTDY#5, ESF-SR-MOISTSTDY#6, ESF-SR-MOISTSTDY#7, ESF-SR-MOISTSTDY#13 and ESF-SR-MOISTSTDY#16, for the period 3/31/98 through 8/20/98.
GS020408312272.002 [162342]			6.14.2-2	Tritium abundance data from pore water in core samples from Yucca Mountain ESF boreholes for the period of 4/30/1998–3/21/2001
GS021208312272.005 [162934]			6.14.2-2	Tritium abundance data from pore-water in core samples from Yucca Mountain ESF ECRB. May 20, 2001 to July 23, 2002.

Table 4.1-14a. Data Used to Support Geochemical Interpretations (Direct Input, Continued)

Inputs	Used in			Description
	Section	Figure	Table	
GS030208312272.001 [162935]			6.14.2-2	Gas and water vapor chemistry data in Yucca Mountain ESF ECRB bulkheads
GS010808315215.003 [164844]		6.14.2-2 6.14.2-5		Fluid inclusion homogenization temperatures from the ESF, ECRB, and EWCD, 12/99 to 4/01
GS020908315215.003 [164846]		6.14.2-2 6.14.2-3 6.14.2-4 6.14.2-5		Fluid inclusion homogenization temperatures from ESF and ECRB calcite and fluorite samples, 10/01 to 5/02
GS970208315215.005 [107351]		6.14.2-3 6.14.2-4 6.14.2-5		Carbon and oxygen stable isotope kiel analyses of calcite from the ESF and USW G-1, G-2 AND G-4, UE-25 A#1, USW NRG-6 and NRG-7/7A, and UE-25 UZ#16, April 1996–January 1997
GS970808315215.010 [145920]		6.14.2-3 6.14.2-4 6.14.2-5		Carbon and oxygen stable isotope analyses of calcite from the ESF and USW G-1, G-2, AND G-3/GU-3, from 01/16/97 to 07/18/97
GS980908315213.002 [146088]		6.14.2-3 6.14.2-4 6.14.2-5		Carbon and oxygen stable isotopic compositions of Exploratory Studies Facility secondary calcite occurrences, 10/1/97 to 8/15/98
GS990908315213.001 [153379]		6.14.2-3 6.14.2-4 6.14.2-5		Stable carbon and oxygen isotope macro and micro analysis of calcite from the ESF between 2/96 and 5/99.
GS020908315215.004 [164847]		6.14.2-5		Stable carbon and oxygen isotope analyses of ESF/ECRB calcite and USW SD-6 and USW WT-24 whole rock; 1/1999–6/2002.
GS010808315215.004 [164850]		6.14.2-5		Uranium and lead concentrations, lead isotopic compositions, and U-Pb isotope ages for the ESF secondary minerals determined at the Royal Ontario Museum between April 20, 2000 and April 19, 2001
GS021008315215.005 [164848]		6.14.2-5		Uranium, thorium, and lead concentrations, lead isotopic compositions, U-Pb isotope ages and $^{234}U/^{238}U$ and $^{230}Th/^{238}U$ activity ratios for the ESF and ECRB secondary calcite, opal, chalcedony and fluorite determined at the Royal Ontario Museum between 11/16/01 and 4/7/02.
GS021208315215.008 [164851]		6.14.3-1 6.14.3-2 6.14.3-3	6.14.3-1	^{238}U-^{234}U-^{230}Th-^{232}Th isotope ratios and calculated ages for opal hemispheres from sample hd2074 (spc00506577) at Station 30+51 in the Exploratory Studies Facility determined using ion-probe mass spectrometry.

Table 4.1-14a. Data Used to Support Geochemical Interpretations (Direct Input, Continued)

Inputs	Used in			Description
	Section	Figure	Table	
GS021208315215.009 [164750]	Attach. IX.5	6.14.3-4 IX.5-1	6.14.3-2 IX.5-1	U abundances, ^{238}U-^{234}U-^{230}Th-^{232}Th activity ratios, and calculated $^{230}Th/U$ ages, and initial $^{234}U/^{238}U$ activity ratios determined for sequential *in situ* microdigestions of opal hemispheres from the ESF by thermal ionization mass spectrometry
GS021208312272.008 [164609]	6.14.3.2	6.14.3-5 6.14.3-6 6.14.3-7 6.14.3-8 6.14.3-9	6.14.3-3	Uranium and thorium concentrations and ^{234}U-^{230}Th-^{238}U-^{232}Th isotopic compositions from whole rock samples from the ECRB Cross Drift and ESF collected between December 5–6, 2001 and analyzed between February and June 2002.
GS020608315215.002 [162126]	6.14.1.2	6.14.4-1 6.14.4-8 6.14.4-9		Carbon dioxide abundances, carbon dioxide concentrations, and normative calcite concentrations for cuttings from borehole USW SD-6, USW WT-24, and ECRB Cross Drift boreholes, Area 25, Nevada Test Site, determined by carbon dioxide evolution between May 25, 2000 and September 8, 2000.
GS021008315215.007 [162127]	6.14.1.2	6.14.4-1 6.14.4-8		Carbon dioxide abundance, carbon dioxide concentration and normative calcite concentrations in 333 powdered cuttings samples from borehole USW WT-24 determined by CO_2 evolution between July 1998 and August 1999
GS980308315215.008 [107355]		6.14.4-2 6.14.4-3 6.14.4-4 6.14.4-5 6.14.4-7 6.14.4-10		Line survey information from the Exploratory Studies Facility obtained to estimate secondary mineral abundance.
GS030808315215.001 [165426]		6.14.3-5 6.14.4-3 6.14.4-9 6.14.4-10		Calcite and opal mineralization occurrences in lithophysal cavities, fractures, and breccia zones from the line survey in the east-west Cross Drift
GS030908315215.002 [166097]		6.14.4-1 6.14.4-8 6.14.4-9		XRF fluorescence elemental compositions determined on cuttings from USW SD-6 and USW WT-24

4.1.14.2 Information Used to Corroborate Geochemical Interpretations (For Reference)

Table 4.1-14b. Information Used to Corroborate Geochemical Interpretations (For Reference)

Inputs	Used in			Description
	Section	Figure	Table	
LA0002JF12213U.001 [154760]	6.14.1.1			Chemistry data for pore water extracted from drillcore from surfaced-based boreholes USW NRG-6, USW NRG-7A, USW UZ-7A, USW UZ-14, UE-25 UZ#16, USW UZ-N55, USW SD-6, USW SD-7, USW SD-9, and USW WT-24.
LA0002JF12213U.002 [156281]	6.14.1.1			Chemistry data for pore water extracted from ESF, Cross Drift, and Busted Butte drillcore.
LAJF831222AQ98.011 [145402]	6.14.1.1			Chloride, bromide, sulfate, and chlorine-36 analyses of springs, groundwater, perched water, and surface runoff.
LA9909JF831222.012 [122736]	6.14.1.1			Chloride, bromide, and sulfate analyses of porewater extracted from ESF Niche 3566 (Niche 1) and Niche 3650 (Niche 2) drillcore.
LL030408023121.027 [162949]			6.14.2-1	Cl concentrations and Cl ratios obtained from YM rock samples and analyzed by accelerator mass spectrometry and ion chromatography.
LL030605223121.030 [163827]		6.14.2-1	6.14.2-1	Chlorine concentrations and chlorine ratios obtained from YM rock samples and analyzed by accelerator mass spectrometry.
LA0305RR831222.001 [163422]			6.14.2-1	Chlorine-36 and Cl in salts leached from rock samples for the chloride-36 validation study
LA0307RR831222.001 [164091]			6.14.2-1	Chloride, bromide, sulfate, and chlorine-36 analyses of salts leached from Cross Drift samples in FY99 and FY00
LA0307RR831222.002 [164090]			6.14.2-1	Chloride, bromide, sulfate, and chlorine-36 analyses of salts leached from ESF ^{36}Cl validation drillcore samples in FY99
GS990408314224.001 [108396]		6.14.3-5		ESF, ECRB Cross Drift, detailed line survey data collected from stations 00+00.89 to 14+95.18
GS990408314224.002 [105625]		6.14.3-5		ESF, ECRB Cross Drift, detailed line survey data collected from stations 15+00.85 to 26+63.85
GS971108314224.020 [105561]		6.14.3-5 6.14.4-5 6.14.4-6		Revision 1 of detailed line survey data, Station 0+60 to Station 4+00, North Ramp starter tunnel, Exploratory Studies Facility
GS971108314224.021 [106007]		6.14.3-5 6.14.4-5 6.14.4-6		Revision 1 of detailed line survey data, Station 4+00 to Station 8+00, North Ramp, Exploratory Studies Facility
GS950508314224.003 [107488]		6.14.3-8		Provisional results: geotechnical data - full periphery map data from North Ramp of the Exploratory Studies Facility, Stations 0+60 to 4+00.

Table 4.1-14b. Information Used to Corroborate Geochemical Interpretations (For Reference, Continued)

Inputs	Used in			Description
	Section	Figure	Table	
GS960708314224.008 [105617]		6.14.4-6		Provisional results: geotechnical data for Station 30+00 to Station 35+00, Main Drift of the ESF. Detailed line survey data
GS000608314224.004 [152573]		6.14.4-6		Provisional results: geotechnical data for Station 35+00 to Station 40+00, Main Drift of the ESF.
GS960708314224.010 [106031]		6.14.4-6		Provisional results: geotechnical data for Station 40+00 to Station 45+00, Main Drift of the ESF. Detailed line survey data. VA supporting data.
GS960908314224.014 [106033]		6.14.4-5 6.14.4-6		Provisional results - ESF Main Drift, Station 50+00 to Station 55+00. Detailed line survey data
GS970208314224.003 [106048]		6.14.4-5 6.14.4-6		Geotechnical data for Station 60+00 to Station 65+00, South Ramp of the ESF. Provisional results; detailed line survey data.
GS971108314224.022 [106009]		6.14.4-5 6.14.4-6		Revision 1 of detailed line survey data, Station 8+00 to Station 10+00, North Ramp, Exploratory Studies Facility
GS971108314224.023 [106010]		6.14.4-5 6.14.4-6		Revision 1 of detailed line survey data, Station 10+00 to Station 18+00, North Ramp, Exploratory Studies Facility
GS971108314224.024 [106023]		6.14.4-5 6.14.4-6		Revision 1 of detailed line survey data, Station 18+00 to Station 26+00, North Ramp, Exploratory Studies Facility
GS971108314224.025 [106025]		6.14.4-5 6.14.4-6		Revision 1 of detailed line survey data, Station 26+00 to Station 30+00, North Ramp and Main Drift, Exploratory Studies Facility
GS971108314224.026 [106032]		6.14.4-5 6.14.4-6		Revision 1 of detailed line survey data, Station 45+00 to Station 50+00, Main Drift, Exploratory Studies Facility
GS971108314224.028 [106047]		6.14.4-5 6.14.4-6		Revision 1 of detailed line survey data, Station 55+00 to Station 60+00, Main Drift and South Ramp, Exploratory Studies Facility

4.2 CRITERIA

Technical requirements to be satisfied by performance assessment (PA) are based on 10 CFR 63.114 [156605] (*Requirements for Performance Assessment*) and identified in the Yucca Mountain *Project Requirements Document* (Canori and Leitner 2003 [161770]). The acceptance criteria that will be used by the Nuclear Regulatory Commission (NRC) to determine whether the technical requirements have been met are identified in the *Yucca Mountain Review Plan, Final Report* (YMRP; NRC 2003 [163274]). The pertinent requirements and acceptance criteria for this scientific analysis report are summarized in Table 4.2-1.

The only Acceptance Criteria for this scientific analysis report listed in Table 3-1 of the TWP (BSC 2003 [160819]) was Criterion 2 from Section 4.2.1.3.6.3 (*Flow Paths in the Unsaturated Zone*) of NRC (2003 [162418]). NRC (2003 [162418]) has since been superseded by NRC (2003 [163274], with Criterion 2 from Section 2.2.1.3.6). Additional appropriate criteria for this scientific analysis report are Criterion 3 from Section 2.2.1.3.6, Criteria 2 and 3 from Section 2.2.1.3.3.3 (*Quantity and Chemistry of Water Contacting Engineered Barriers and Waste Forms*), and Criteria 2 and 3 from Section 2.2.1.3.7.3 (*Radionuclide Transport in the UZ*) of NRC (2003 [163274]). These criteria are listed in Table 4.2-1. This change of acceptance criteria is one deviation from the TWP (BSC 2002 [160819]) listed in Section 1.4.

Table 4.2-1. Project Requirements and YMRP Acceptance Criteria Applicable to This Scientific Analysis Report

Requirement Number[a]	Requirement Title[a]	10 CFR 63 Link	YMRP Acceptance Criteria
PRD-002/T-015	Requirements for Performance Assessment	10 CFR 63.114(a-c) [156605]	Criteria 2 and 3 for *Quantity and Chemistry of Water Contacting Engineered Barriers and Waste Forms* [b] Criteria 2 and 3 for *Flow Path in the UZ*[c] *Criteria 2 and 3 for Radionuclide Transport in the UZ*[d]

NOTES: [a] from Canori and Leitner (2003 [161770])
[b] from NRC (2003 [163274], Section 2.2.1.3.3.3)
[c] from NRC (2003 [163274], Section 2.2.1.3.6.3)
[d] from NRC (2003 [163274], Section 2.2.1.3.7.3)

The acceptance criteria identified in Section 2.2.1.3.3.3 of the YMRP (NRC 2003 [163274]) are given below, followed by a short description of their applicability to this scientific analysis report.

- Acceptance Criterion 2, *Data Are Sufficient for Model Justification*:

The data on seepage into drifts are collected, described, interpreted, and synthesized.

- Acceptance Criterion 3, *Data Uncertainty Is Characterized and Propagated through Model Abstraction*:

The parameter values and distributions are developed based on Yucca Mountain data for cases of field measurements and laboratory experiments with sufficient data. The results of this report provide information which could be used by, and uncertainties propagated through, UZ process and abstraction models (for a complete list, see Section 7).

The summaries of measurement results are discussed in Section 6.

The acceptance criteria identified in Section 2.2.1.3.6.3 of the YMRP (NRC 2003 [163274]) are given below, followed by a short description of their applicability to this scientific analysis report.

- Acceptance Criterion 2, *Data Are Sufficient for Model Justification*:

The data on hydrology and geochemistry of the unsaturated zone are collected using acceptable techniques.

- Acceptance Criterion 3, *Data Uncertainty Is Characterized and Propagated through Model Abstraction*:

Uncertainties in the characteristics of the natural system are considered.

The summaries of measurement results are discussed in Section 6.

The acceptance criteria identified in Section 2.2.1.3.7.3 of the YMRP (NRC 2003 [163274]) is given below, followed by a short description of their applicability to this scientific analysis report.

- Acceptance Criterion 2, *Data Are Sufficient for Model Justification*:

Data on the transport in the UZ are collected using appropriate techniques.

- Acceptance Criterion 3, *Data Uncertainty Is Characterized and Propagated through Model Abstraction*:

Uncertainty is adequately represented in process evaluation.

The summaries of measurement results are discussed in Section 6.

YMRP criteria are further discussed in Section 7.

4.3 CODES AND STANDARDS

No specific formally established standards have been identified as applying to this analysis.

5. ASSUMPTIONS

This scientific analysis report on ambient field testing of processes presents data collected in underground drifts at Yucca Mountain and its vicinity. No assumptions of parameters were used to supplement the measured data. Discussions on issues related to analysis approximation are included in Section 6. Other than supportable approximations required to utilize various analytic formulas and established scientific methods, physical assumptions were unnecessary, because no predicted values or simulated information was presented.

INTENTIONALLY LEFT BLANK

6. SCIENTIFIC ANALYSIS DISCUSSION

This section describes the field-testing results pertaining to unsaturated zone (UZ) processes in underground drifts at Yucca Mountain and its vicinity. The field activities range from decimeter-scale drift-seepage tests above niches, to meter-scale, fracture-matrix-interaction tests above slots in alcoves, to decameter-scale flow and transport tests in test blocks or between drifts, and to kilometer-scale moisture-monitoring studies along drifts. Niches are room-size excavations, slots are excavations below test beds in alcove walls, and alcoves are side drifts along the ESF Main Loop and ECRB Cross Drift.

Specifically, this section contains data and analysis related to the following topics.

- Section 6.1 and Section 6.5 present the test-site characteristics of niches and alcoves from pneumatic air-permeability test results (with Section 6.1 on permeability profiles and Section 6.5 on crosshole connections).

- Section 6.2 shows that drift-seepage thresholds exist and that seepage threshold data can be interpreted using the capillary barrier theory. It also presents liquid-flow-path data for niche sites.

- Section 6.3 and Section 6.4 present laboratory-measurement results for tracer migration and matrix imbibition for welded tuff samples from the ESF (with Section 6.3 on tracer distribution in the field and Section 6.4 on tracer and fluid penetration into the rock matrix).

- Section 6.6 presents the results of two series of fracture-matrix interaction tests to quantify the partitioning of flux into fast and slow components.

- Section 6.7 presents the results for flow tests in the Paintbrush nonwelded tuff (PTn) test bed.

- Section 6.8 summarizes data collected on ambient water-potential distribution in niches.

- Section 6.9 summarizes observations on construction-water migration.

- Section 6.10 presents data collected on moisture monitoring and water analyses in open drifts under the influence of ventilation and in closed drifts behind bulkheads, including ECRB Cross Drift and Alcove 7.

- Section 6.11 presents the results from systematic hydrological characterization using slanted boreholes along the ECRB Cross Drift.

- Section 6.12 presents the results of drift-to-drift tests from liquid releases in Alcove 8 and wetting-front and seepage detection at Niche 3107 (Niche 3), and on available information of Alcove 1 infiltration tests.

- Section 6.13 presents the results of different phases of transport tests at Busted Butte.

- Section 6.14 summarizes geochemical and isotope data in pore water, rocks, and fracture in-fill minerals collected from test locations in different tuff units.

The tests performed in niches and alcoves along the ESF are illustrated in Figure 6-1. Seepage into drifts at the repository level is related to water percolating down from the ground surface. Drift seepage tests at niche sites quantify the seepage from liquid pulses released above the niches. Percolation flux has a fast fracture-flow component and a slow matrix-flow component. This partitioning of flow is evaluated at the fracture-matrix test bed in Alcove 6. The heterogeneous hydrogeologic setting (with alternating tuff layers) determines the percolation distribution throughout the UZ, with input from infiltration at the ground surface boundary. The mechanism of redistributing near-surface fracture flow by the porous PTn, especially the flow-damping process by the PTn unit, is studied in a test bed in Alcove 4. The PTn unit examined at Alcove 4 consists of layered, altered, and bedded tuffs transected by a fault. Wetter climate conditions increase the infiltration, as quantified in an artificial infiltration test in Alcove 1 and in moisture monitoring at depth in Alcove 7. The seepage threshold data from niches and from systematic hydrological characterization are inputs to the Model Report *Seepage Calibration Model and Seepage Testing Data (U0080)* (BSC 2003 [162267]).

Figure 6-1 lists major TSPA issues (DOE 1998 [100550]) related to UZ flow processes of seepage, percolation, and infiltration. The tests illustrated in Figure 6-1 focus on different issues to quantify the functional relationships among these processes. Seepage is smaller than the percolation flux because of capillarity-induced drift diversion (BSC 2003 [162267], Section 6), and percolation may be smaller than infiltration because of lateral diversion of percolating water along tuff interfaces to bounding faults (BSC 2001 [156609], Section 6.4.3). All tests use tracers to assist the characterization of plume migration.

Figure 6-2 illustrates the ECRB Cross Drift to ESF Main Drift seepage collection system to study the migration of water and tracer flow from one drift to another. The crossover point is located in the northern part of the ESF, as illustrated in Figure 6-2 and Figure 6.1.1-1. In 1998, the seepage monitoring system was used to monitor the migration of construction water from the ECRB Cross Drift. Niche 3107 (Niche 3), originally excavated and used for the drift seepage study, is currently part of the drift-to-drift study as a seepage collection site. The existing horizontal boreholes at Niche 3107 (Niche 3) are used for wetting-front monitoring for liquid released from Alcove 8, excavated from the ECRB Cross Drift and directly above Niche 3107 (Niche 3).

Since neither the ESF Main drift nor the ECRB Cross Drift reaches the Calico Hills hydrogeologic tuff unit (CHn) below the repository block, a dedicated drift complex was excavated at Busted Butte, 8 km southeast of Yucca Mountain, to evaluate flow and transport processes in vitric CHn. Early results were first reported in the AMR *Unsaturated Zone and Saturated Zone Transport Properties (U0100)* (CRWMS M&O 2001 [154024]). The different field-testing phases and recent updates are presented in Section 6.13.

Geochemical and isotope data have been collected from laboratory analyses of samples from various experiments in different test locations. These data have been used to refine the conceptual understanding of the site and for inputs to process models. Early results were reported in the AMR *Analysis of Geochemical Data for the Unsaturated Zone (U0085)* (BSC

2002 [160247]). The updates of geochemical and isotope data are presented in Section 6.14 on pore water and rock compositions; isotope geochemistry examination on chlorine-36 validation studies, tritium distributions, and fluid inclusions for thermal history; uranium isotope studies for UZ flow record and flow zone delineation; and fracture mineral distribution and mineralogy.

Each testing activity has unique findings to contribute to the assessment of unsaturated flow and transport processes at Yucca Mountain. The progress and analyses of field-test results are presented in the following fourteen subsections for fourteen testing activities. Key (and verifiable) scientific notebooks (with relevant page numbers) used for recording the ESF Field Testing activities and analyses described in this scientific analysis report are listed in Table 6-1.

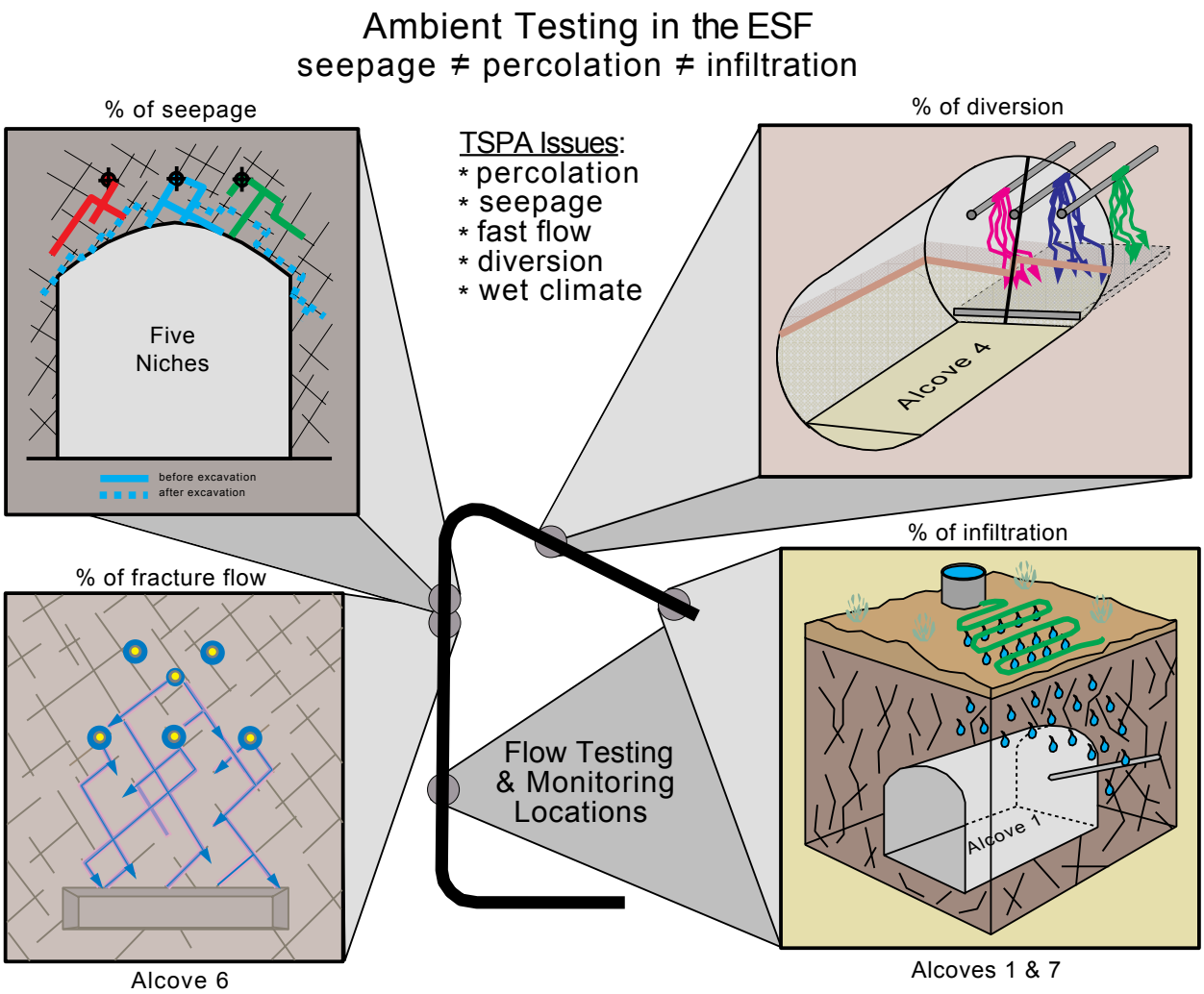

NOTE: The tests evaluate functional relationships between unsaturated zone processes to resolve TSPA issues.

Figure 6-1. Schematic Illustration of Flow Tests in the Exploratory Studies Facility at Yucca Mountain

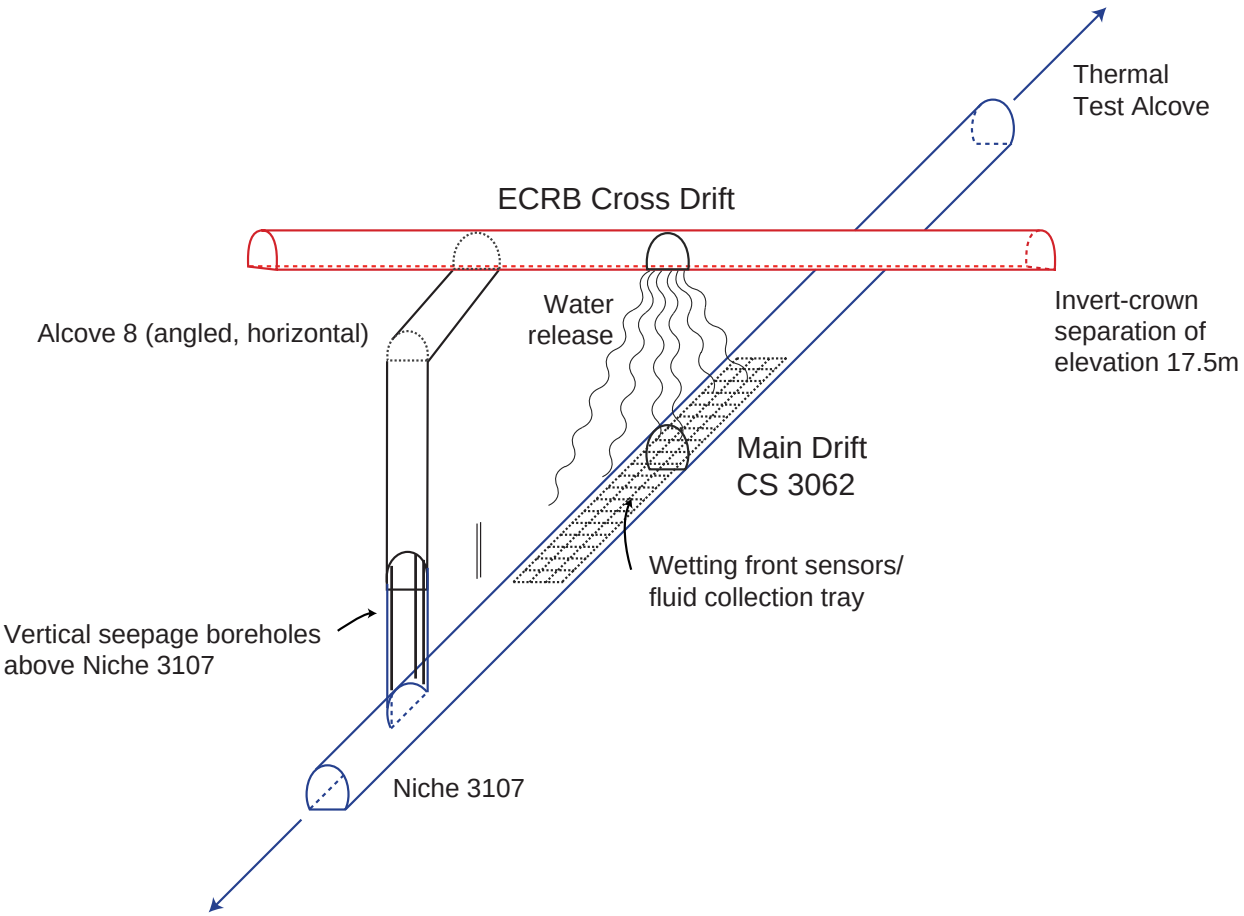

NOTE: Wetting-front sensors and fluid collection trays monitored the construction-water migration. Both the ECRB Cross Drift and the Main Drift, together with Alcove 8 and Niche 3107 and its boreholes, are horizontal in this illustration. Alcove 8 is directly above Niche 3107.

Figure 6-2. Schematic Illustration of the Cross-Over Point of ECRB Cross Drift with the Main Drift

Table 6-1. Scientific Notebooks*

M&O Scientific Notebook ID	Lab Scientific Notebook ID	Cited Pages or Page Range of Scientific Notebook	Relevant AMR Sections	Citation
SN-LBNL-SCI-065-V1	YMP-LBNL-JSW-6	1–158	6.1 (air-K), 6.2 (seepage)	Wang 1997 [156530]
SN-LBNL-SCI-066-V1	YMP-LBNL-JSW-6A	1–159	6.1 (air-K), 6.2 (seepage)	Wang 1997 [156534]
SN-LBNL-SCI-121-V1	YMP-LBNL-JSW-6B	1–159	6.1 (air-K), 6.2 (seepage)	Wang 1999 [156538]
SN-LBNL-SCI-122-V1	YMP-LBNL-JSW-6C	1–159	6.1 (air-K), 6.2 (seepage)	Wang 1999 [153449]
SN-LBNL-SCI-078-V1	YMP-LBNL-JSW-PJC-6.2	1–110, 115–125, 133–135, 144–146, 149–157	6.1 (air-K), 6.5 (cross-hole)	Cook 2001 [156902]
SN-LBNL-SCI-113-V1	YMP-LBNL-RCT-1	62–73, 80–157	6.2 (seepage)	Trautz 1999 [156563]
SN-LBNL-SCI-156-V1	YMP-LBNL-RCT-2	27–160	6.2 (seepage)	Trautz 2001 [156903]
SN-LBNL-SCI-177-V1	YMP-LBNL-RCT-3	4-94	6.2 (seepage)	Trautz 2001 [157022]
SN-LBNL-SCI-177-V2	YMP-LBNL-RCT-4	88–91, 116–117, 120, 130–159, 190–195, 198–221, 298–299	6.2-Attach III.4 (seepage)	Trautz 2001 [161208]
SN-LBNL-SCI- 221-V1	YMP-LBNL-RCT-5	154-160, 162-234, 239-301	6.2-Attach III.4 (seepage)	Trautz 2003 [166248]
SN-LBNL-SCI- 221-V2	YMP-LBNL-RCT-6	14–67	6.2-Attach III.4 (seepage)	Wang 2003 [165376]
SN-LBNL-SCI-089-V1	YMP-LBNL-JSW-QH-1	1–153	6.3 (tracer migration), 6.4 (imbibition)	Hu 1999 [156539]
SN-LBNL-SCI-090-V1	YMP-LBNL-JSW-QH-1A	20–22, 37–48, 54, 68–82, 86–99, 103–126	6.3 (tracer migration), 6.4 (imbibition)	Hu 1999 [156540]
SN-LBNL-SCI-091-V1	YMP-LBNL-JSW-QH-1B	9, 27, 35, 40, 42, 48–73, 77, 81–94, 107–110, 115, 118–119, 123–142, 149, 154–155	6.3 (tracer migration), 6.4 (imbibition)	Hu 1999 [156541]
SN-LBNL-SCI-092-V1	YMP-LBNL-JSW-QH-1C	13, 16–25, 39–41, 51–102, 105–112, 116, 128–133, 139–140, 143–145	6.3 (tracer migration), 6.4 (imbibition)	Hu 1999 [156542]
SN-LBNL-SCI-093-V1	YMP-LBNL-JSW-QH-1D	3–153	6.3 (tracer migration), 6.4 (imbibition)	Hu 1999 [155691]
SN-LBNL-SCI-154-V1	YMP-LBNL-JSW-QH-1E	130-136, 145-146	6.3 (tracer migration), 6.4 (imbibition)	Hu 2000 [156473]

Table 6-1. Scientific Notebooks* (Continued)

M&O Scientific Notebook ID	Lab Scientific Notebook ID	Cited Pages or Page Range of Scientific Notebook	Relevant AMR Sections	Citation
SN-LBNL-SCI-102-V1	YMP-LBNL-JSW-RS-1	1–117	6.6 (fracture-matrix interaction Alcove 6)	Salve 1999 [155692]
SN-LBNL-SCI-104-V1	YMP-LBNL-JSW-RS-1A	1–39	6.6 (fracture-matrix interaction Alcove 6)	Salve 1999 [156547]
SN-LBNL-SCI-105-V1	YMP-LBNL-JSW-RS-2	1–7, 8-127	6.6 (fracture-matrix interaction Alcove 6) 6.7 (PTn Alcove 4)	Salve 2000 [156548]
SN-LBNL-SCI-042-V1	YMP-LBNL-JSW-CMO-1	1–15, 18, 22, 45–-54	6.7 (PTn Alcove 4)	Oldenburg 2000 [156558]
SN-LBNL-SCI-088-V1	YMP-LBNL-JSW-JJH-1	1–71	6.7 (PTn Alcove 4)	Hinds 2000 [156557]
SN-LBNL-SCI-048-VI	YMP-LBNL-JW-1.2	103–152	6.8 (water potential) 6.9 (construction water migration)	Salve 1999 [156552]
SN-LBNL-SCI-133-V1	YMP-LBNL-JW-1.2A	1–43	6.8 (water potential) 6.9 (construction water migration)	Salve 1999 [156555]
SN-LBNL-SCI-116-V1	YMP-LBNL-JSW-4.3	1–24, 61–67, 74–81	6.10 (ESF moisture)	Wang 2000 [156559]
SN-LBNL-SCI-150-V1	YMP-LBNL-JSW-JS-1	18, 148	6.10 (ECRB moisture)	Stepek 2000 [156561]
SN-LBNL-SCI-182-V1	YMP-LBNL-JSW-RS-4	1–147	6.10.1 (ECRB moisture)	Salve 2002 [165378]
SN-LBNL-SCI-182-V2	YMP-LBNL-JSW-RS-6	1–59	6.10.1 (ECRB moisture)	Wang 2003 [165376]
SN-USGS-SCI-110-V1	N/A	1–99	6.10 (Niche Moisture)	Guertal 2000 [165384]
SN-USGS-SCI-128-V1	N/A	1–301	6.10.1 (ECRB moisture)	Hudson 2002 [165391]
SN-USGS-SCI-128-V2	N/A	1–297	6.10.1 (ECRB moisture)	Hudson 2002 [165392]
SN-USGS-SCI-128-V3	N/A	1–141	6.10.4 (Alcove 7)	Hudson 2003 [165273]
SN-USGS-SCI-133-V1	N/A	1–157	6.10.1 (ECRB moisture)	Hudson 2002 [163398]
SN-USGS-SCI-133-V2	N/A	1–147	6.10.1 (ECRB moisture)	Hudson 2003 [165393]
SN-LBNL-SCI-179-V1	YMP-LBNL-JSW-YWT-1	1–44	6.11 (ECRB systematic)	Tsang and Wang 2000 [165375]
SN-LBNL-SCI-179-V2	YMP-LBNL-JSW-YWT-2	8–48, 72–73, 98–99, 114–129	6.11 (ECRB systematic)	Wang 2003 [165376]
SN-LBNL-SCI-216-V1	YMP-LBNL-JSW-PJC-6.3	7–19, 22–27, 46, 58–60, 70–76	6.11 (ECRB systematic)	Wang 2003 [165376]

Table 6-1. Scientific Notebooks* (Continued)

M&O Scientific Notebook ID	Lab Scientific Notebook ID	Cited Pages or Page Range of Scientific Notebook	Relevant AMR Sections	Citation
SN-LBNL-SCI-181-V1	YMP-LBNL-JSW-RS-5	1–156	6.12 (Alcove 8-Niche 3107 [Niche 3])	Salve 2003 [165377]
SN-LBNL-SCI-181-V2	YMP-LBNL-JSW-RS-5.1	1–24	6.12 (Alcove 8-Niche 3107 [Niche 3])	Wang 2003 [165376]
SN-USGS-SCI-120-V1	N/A	1–172	6.12 (Alcove 8-Niche 3107 [Niche 3])	Hudson 2002 [165385]
SN-USGS-SCI-120-V2	N/A	1–182	6.12 (Alcove 8-Niche 3107 [Niche 3])	Hudson 2002 [165386]
SN-USGS-SCI-120-V3	N/A	1–179	6.12 (Alcove 8-Niche 3107 [Niche 3])	Hudson 2002 [165387]
SN-USGS-SCI-120-V4	N/A	1–190	6.12 (Alcove 8-Niche 3107 [Niche 3])	Hudson and Guertal 2002 [165388]
SN-USGS-SCI-120-V5	N/A	1–157	6.12 (Alcove 8-Niche 3107 [Niche 3])	Hudson 2002 [166103]
SN-USGS-SCI-120-V6	N/A	1–147	6.12 (Alcove 8-Niche 3107 [Niche 3])	Hudson 2002 [165389]
SN-USGS-SCI-120-V7	N/A	1–148	6.12 (Alcove 8-Niche 3107 [Niche 3])	Hudson 2003 [165390]
SN-USGS-SCI-108-V1	N/A	1-98	6.12.5 (Alcove 1)	Guertal 2001 [164070]
SN-LANL-SCI-038-V1	LA-EES-1-NBK-99-005	1–161	6.13 (sample analyses)	Bussod 2001 [165281]
SN-LANL-SCI-039-V1	LA-EES-5-NBK-98-020	1–161	6.13 (UZTT)	Bussod 1999 [146978]
SN-LANL-SCI-040-V1	LA-EES-5-NBK-98-010	1–156	6.13 (UZTT)	Bussod 1998 [149129]
SN-LANL-SCI-041-V1	LA-EES-5-NBK-98-011	1– 38	6.13.2 (UZTT injection)	Soll et al. 2001 [165296]
SN-LANL-SCI-042-V1	LA-EES-5-NBK-98-012	1–130	6.13.3 (UZTT injection)	Dunn 2001 [165297]
SN-LANL-SCI-043-V1	LA-EES-5-NBK-98-013	1–26	6.13.5 (UZTT air-K)	Bussod and Stockton 1999 [165324]
SN-LANL-SCI-044-V1	LA-EES-5-NBK-98-014	1–11	6.13.5 (UZTT air-K)	Wyckoff 1999 [165298]
SN-LANL-SCI-046-V1	LA-EES-5-NBK-98-016	1–44	6.13.5 (UZTT air-K)	Lowry 2001 [164632]

Table 6-1. Scientific Notebooks* (Continued)

M&O Scientific Notebook ID	Lab Scientific Notebook ID	Cited Pages or Page Range of Scientific Notebook	Relevant AMR Sections	Citation
SN-LANL-SCI-106-V1	LA-EES-5-NBK-99-003	1–120	6.13 (UZTT)	Soll and Bussod 2001 [165299]
SN-LANL-SCI-127-V1	LA-CST-NBK-99-002	1–7	6.13.1 (tracers)	Bussod and Turin 2000 [165300]
SN-LANL-SCI-133-V1	LA-CST-NBK-98-018	1–7	6.13.3 (tracer analyses)	Bussod and Wolfsberg 2000 [165301]
SN-LANL-SCI-136-V1	LA-CST-NBK-98-017	1–7	6.13.3 (tracer analyses)	Bussod and Wolfsberg 2000 [165303]
SN-LANL-SCI-145-V1	LA-CST-NBK-98-001	1–159	6.13.1 (tracers)	Bussod et al. 2000 [165305]
SN-LANL-SCI-159-V1	LA-CST-NBK-98-002	1–9	6.13.3 (tracer analyses)	Bussod and Wolfsberg 2000 [165306]
SN-LANL-SCI-160-V1	LA-CST-NBK-98-012	1–7	6.13.3 (tracer analyses)	Bussod and Wolfsberg 2000 [165308]
SN-LANL-SCI-161-V1	LA-CST-NBK-98-015	1–7	6.13.2, 6.13.3 (tracer analyses)	Bussod and Wolfsberg 2000 [165310]
SN-LANL-SCI-163-V1	LA-CST-NBK-98-016	1–10	6.13.2, 6.13.3 (tracer analyses)	Bussod and Wolfsberg 2000 [165311]
SN-LANL-SCI-169-V1	LA-CST-NBK-98-009	1–7	6.13.2, 6.13.3 (tracer analyses)	Bussod and Wolfsberg 2000 [165312]
SN-LANL-SCI-184-V1	N/A	1–6	6.13.2, 6.13.3 (tracer analyses)	Soll and Wolfsberg 2000 [165313]
SN-LANL-SCI-188-V1	N/A	1–7	6.13.2, 6.13.3 (tracer analyses)	Soll and Wolfsberg 2000 [165316]
SN-LANL-SCI-191-V1	LA-CST-NBK-99-004	1–10	6.13.2 (sorption)	Bussod et al. 2000 [165317]
SN-LANL-SCI-192-V1	LA-CST-NBK-99-003	1–8	6.13.2, 6.13.3 (tracer analyses)	Bussod and Wolfsberg 2000 [165319]
SN-LANL-SCI-193-V1	N/A	1–8	6.13.3 (tracer analyses)	Soll and Wolfsberg 2000 [165320]
SN-LANL-SCI-199-V1	LA-CST-NBK-98-004	1–810	6.13 (pad collection)	Bussod and Turin 2001 [165321]
SN-LANL-SCI-205-V1	N/A	1–56, photos 1–31	6.13.6 (BBTF block)	Drew 1999 [166105]
SN-LANL-SCI-206-V1	N/A	86326–86406	6.13.6 (BBTF block)	Drew 2001 [165323]
SN-LANL-SCI-206-V2	N/A	99176–99254	6.13.6 (BBTF block)	Drew 2001 [165325]
SN-LANL-SCI-206-V3	N/A	99326–99405	6.13.6 (BBTF block)	Drew 2002 [165326]
SN-LANL-SCI-206-V4	N/A	99551–99630	6.13.6 (BBTF block)	Drew 2002 [165328]
SN-LANL-SCI-206-V5	N/A	99701–99779	6.13.6 (BBTF block)	Drew 2002 [165330]
SN-LANL-SCI-206-V6	N/A	92851–92930	6.13.6 (BBTF block)	Drew 2002 [165333]

Table 6-1. Scientific Notebooks* (Continued)

M&O Scientific Notebook ID	Lab Scientific Notebook ID	Cited Pages or Page Range of Scientific Notebook	Relevant AMR Sections	Citation
SN-LANL-SCI-206-V7	N/A	100226–100303	6.13.6 (BBTF block)	Drew 2003 [165335]
SN-LANL-SCI-207-V1	N/A	83101–83181	6.13.6 (BBTF block)	Drew 2001 [165336]
SN-LANL-SCI-207-V2	N/A	83326–83406	6.13.6 (BBTF block)	Drew 2001 [165348]
SN-LANL-SCI-207-V3	N/A	83476–83556	6.13.6 (BBTF block)	Drew 2001 [165349]
SN-LANL-SCI-207-V4	N/A	97976–98055	6.13.6 (BBTF block)	Drew 2001 [165350]
SN-LANL-SCI-207-V5	N/A	98051–98130	6.13.6 (BBTF block)	Drew 2001 [165351]
SN-LANL-SCI-207-V6	N/A	98126–98205	6.13.6 (BBTF block)	Drew 2001 [165352]
SN-LANL-SCI-207-V7	N/A	99251–99329	6.13.6 (BBTF block)	Drew 2001 [165354]
SN-LANL-SCI-207-V8	N/A	99401–99480	6.13.6 (BBTF block)	Drew 2002 [165356]
SN-LANL-SCI-207-V9	N/A	99626–99705	6.13.6 (BBTF block)	Drew 2002 [165358]
SN-LANL-SCI-207-V10	N/A	99776–99854	6.13.6 (BBTF block)	Drew 2002 [165338]
SN-LANL-SCI-207-V11	N/A	92776–92855 6.13.6	(BBTF block)	Drew 2002 [165340]
SN-LANL-SCI-207-V12	N/A	100151–100229	6.13.6 (BBTF block)	Drew 2002 [165344]
SN-LANL-SCI-207-V13	N/A	100451–100528	6.13.6 (BBTF block)	Drew 2003 [165346]
SN-LANL-SCI-208-V1	N/A	91276–91356	6.13.6 (BBTF block)	Drew 2001 [165360]
SN-LANL-SCI-208-V2	N/A	86701–86780	6.13.6 (BBTF block)	Drew 2001 [165361]
SN-LANL-SCI-208-V3	N/A	99476–99542	6.13.6 (BBTF block)	Drew 2002 [165362]
SN-LANL-SCI-220-V1	LA-EES-1-NBK-94-002	1–101	6.13.1, Attach VIII (CHn mineralogy)	Levy 2001 [165363]
SN-LANL-SCI-228-V1	LA-EES-5-NBK-98-019	1–4	6.13.2 (injection)	Bussod and Wolfsberg 2000 [165364]
SN-LANL-SCI-232-V1	N/A	1–9	6.13.3 (tracer analyses)	Soll and Wolfsberg 2000 [165365]
SN-LANL-SCI-239-V1	N/A	1–103, 290–291	6.13.3 (tracer analyses)	Soll et al. 2002 [165366]
SN-LANL-SCI-241-V1	N/A	1–90	6.13.3 (tracer analyses)	Soll and Wolfsberg 2002 [165367]
SN-LANL-SCI-252-V1	N/A	1–77	6.13.3 (overcore)	Turin 2001 [165368]
SN-LANL-SCI-253-V1	N/A	1–168	6.13.2, 6.13.3 (tracer analyses)	Haga 2001 [165369]
SN-LANL-SCI-256-V1	N/A	1–75	6.13.1, Attach VIII (CHn mineralogy)	Levy 2002 [165370]
SN-LANL-SCI-257-V1	N/A	1	6.13.3	Soll 2001 [165371]

Table 6-1. Scientific Notebooks* (Continued)

M&O Scientific Notebook ID	Lab Scientific Notebook ID	Cited Pages or Page Range of Scientific Notebook	Relevant AMR Sections	Citation
SN-LANL-SCI-261-V1	N/A	1–53	6.13.1, Attach VIII (CHn mineralogy)	Soll and Aldrich 2002 [165372]
SN-LBNL-SCI-119-V1	YMP-LBNL-ELM-KHW-1	1–48	6.13.4 (ground penetrating radar)	Williams 2000 [165373]
SN-LBNL-SCI-119-V2	YMP-LBNL-ELM-KHW-2	1–32	6.13.4 (ground penetrating radar)	Williams 2002 [165374]
SN-LBNL-SCI-193-V1	YMP-LBNL-ELM-JP-1	1–25	6.13.4 (ground penetrating radar)	Peterson 2002 [165379]
SN-LLNL-SCI-421-V1	N/A	1–155	6.13.4 (electrical resistance tomography)	Daily and Buettner 2002 [165380]
SN-USGS-SCI-117-V1	N/A	1–75	6.13.1, Attach VIII (hydrological properties)	Flint 2001 [165381]
SN-USGS-SCI-117-V2	N/A	1–98	6.13.1, Attach VIII (hydrological properties)	Flint 2001 [165382]
SN-USGS-SCI-117-V3	N/A	1–73	6.13.1, Attach VIII (hydrological properties)	Flint et al. 2002 [165383]

* Note: The list of scientific notebooks is sorted first by different tests (represented by the subsection number to the second heading in the fourth column), and then by the scientific notebook IDs (listed in the first column). The listed scientific notebooks contain relevant and corroborating information for testing activities discussed in Section 6. Some scientific notebooks have test pages specified, while others have the whole notebook ranges listed. In addition to data collection, the scientific notebooks in general contain information about test configuration, test design, equipment set-up, sensor calibration, review records, and other test-related information. While data analyses are mostly developed from information in the scientific notebooks, data interpretations are supplemented by open literature surveys and professional exchanges, with the results documented in publications and in the scientific analysis report. Some investigators use technical procedures instead of scientific notebooks in data collections. The technical procedures, together with other information such as test-site configurations and sensor accuracies, are in site-investigation test plans and field work packages governing the testing activities, documented in the UZ TWP (BSC 2002 [160819]).

Alternative scientific approaches and technical methods are evaluated in Section 6. For example, analytic solutions are use to analyze seepage data instead of numerical models, in Section 6.2; psychrometer data are compared with electrical resistivity probe data in Section 6.9; and ion-microprobe results are compared with microdigestion results in Section 6.14. These comparisons are presented for rationales in selection of different methods by the readers of this report. No other identifiable methods are evaluated or used.

Variability and uncertainty are also evaluated in Section 6. The variability and uncertainty, as described in BSC (2002 [158794], Section 4.1), are:

> *Variability*, also referred to as aleatory uncertainty, arises due to natural randomness or heterogeneity. This first type of uncertainty cannot be reduced through further testing and data collection; it can only be better characterized. Thus, this first type of uncertainty is also referred to as irreducible uncertainty. It is typically accounted for using geostatistical approaches, e.g., using appropriate probability distribution functions.
>
> *Uncertainty*, also referred to as epistemic uncertainty, arises from lack of knowledge about a parameter because the data are limited or there are alternative interpretations of the available data. This second type of uncertainty can be reduced because the state of knowledge can be improved by further testing or data collection. As a consequence, this second type of uncertainty is also referred to as reducible uncertainty.

The term *variability* is used for aleatory uncertainty, and the term *uncertainty* is used for *epistemic* uncertainty.

Uncertainty may have different sources depending on how the parameter in question is derived (e.g., whether derived from measurements, analyses, or models), as follows:

> *Measurement uncertainty* refers to the exactness of the actual measurement method and related data processing.
>
> *Spatial variability uncertainty* refers to the uncertainty in parameters describing the spatial variability of data, typically arising from the limited number of samples.
>
> *Conceptual model uncertainty* arises when the most appropriate conceptual model for a system is uncertain.
>
> *Estimation uncertainty* arises if the resulting parameter is estimated from a random process (e.g., from noisy data or from a Monte Carlo analysis), giving a range of possible results.

This scientific analysis report focuses on spatial variability uncertainty of data collected from testing of processes.

The softwares are used for graphic display of data and for simple calculations as documented in Attachment IX. Once the results are acceptable, no other software are needed to be considered.

INTENTIONALLY LEFT BLANK

6.1 AIR-PERMEABILITY DISTRIBUTIONS AND EXCAVATION-INDUCED ENHANCEMENTS

Pneumatic air-permeability tests were undertaken at various locations in the ESF to characterize the potential fluid flow paths in the rock. The repository host rock consists predominantly of unsaturated, fractured welded tuff. Airflow occurs mainly through the fractures. Therefore, air-permeability tests efficiently characterize fractured systems and may be utilized to study fracture heterogeneity. Once the air injections stop, the pressure field returns to ambient conditions within minutes, under most field-test conditions.

To determine fracture location within boreholes at the test sites, packer assemblies were installed along boreholes to isolate intervals in clusters of boreholes drilled into the fractured rock to perform pneumatic testing. In these tests, air is injected into specific intervals at constant mass flux while pressure responses are monitored in other intervals. The specific objectives for pneumatic testing include:

- Profiling the air permeability of boreholes along their length.
- Investigating the effects of nearby excavation on the permeability of a rock mass.
- Enabling a site-to-site comparison of air-permeability statistics and related scale effects.

Two basic types of data are readily available from pneumatic testing and are used to satisfy these testing objectives: (1) single-borehole air-permeability profiles, which are used for borehole-to-borehole and site-to-site comparisons, and (2) crosshole pressure-response data, which enable a determination of connectivity (through fracture networks) between locations at a given site. This section focuses on the permeability profiles for boreholes in niche and alcove sites. Permeability profiles before niche excavation are compared with profiles measured after niche and alcove excavation. In addition, factors such as borehole orientation and host rock type are considered. Section 6.5 focuses on crosshole data analyses.

6.1.1 Niche Test Site and Borehole Configuration

Extensive air-permeability measurements have been made in borehole clusters at five niches and at three alcoves within the ESF tunnel, as part of a program to select locations for liquid-release tests. The air permeability along each borehole in a cluster serves as a guide to the selection of the liquid-release intervals.

6.1.1.1 Site Selection

Various niche and alcove sites were selected for study, based on fracture and hydrological data collected in the ESF, as illustrated in Figure 6.1.1-1. Four niches were excavated along the Main Drift of the ESF and a fifth in the ECRB Cross Drift. The first niche site is located at Construction Station (CS) 35+66 (hereafter referred to as Niche 3566 [Niche 1], located at 3,566 m from the ESF north portal), in a brecciated zone between the Sundance fault and a cooling joint, where a preferential flow path is believed to be present (based on elevated $^{36}Cl/Cl$ ratios described in BSC 2001 [154874], the report on geochemistry data). Niche 3566 (Niche 1) was

sealed with a bulkhead to conduct long-term monitoring of *in situ* conditions. The second niche site is located at CS 36+50 (Niche 3650 [Niche 2]) in a competent rock mass with lower fracture density than Niche 3566 (Niche 1). The third niche is located at CS 31+07 (Niche 3107 [Niche 3]) in close proximity to the crossover point located at CS 30+62. A test alcove (Alcove 8) has been excavated from the ECRB Cross Drift to a position immediately above Niche 3107 (Niche 3), so that a large-scale drift-to-drift test can be conducted at this location. The fourth niche site is located at CS 47+88 (Niche 4788 [Niche 4]) in a 950 m long exposure of the middle nonlithophysal zone, referred to by Buesch and Spengler (1998 [101433], p. 19) as the intensely fractured zone. The fifth niche is located at ECRB Cross Drift CS 16+20 (Niche CD 1620 [Niche 5]) near the center of the repository block. The first four niches described above were excavated on the west side of the ESF Main Drift within the middle nonlithophysal zone (Tptpmn) of the Topopah Spring welded tuff unit (TSw). The fifth niche in the ECRB Cross Drift is excavated in the lower lithophysal zone (Tptpll) of TSw, which is the tuff unit where most of the repository emplacement drifts are planned to be located. Alcove 8 is excavated in the upper lithophysal zone (Tptpul) of the ECRB Cross Drift.

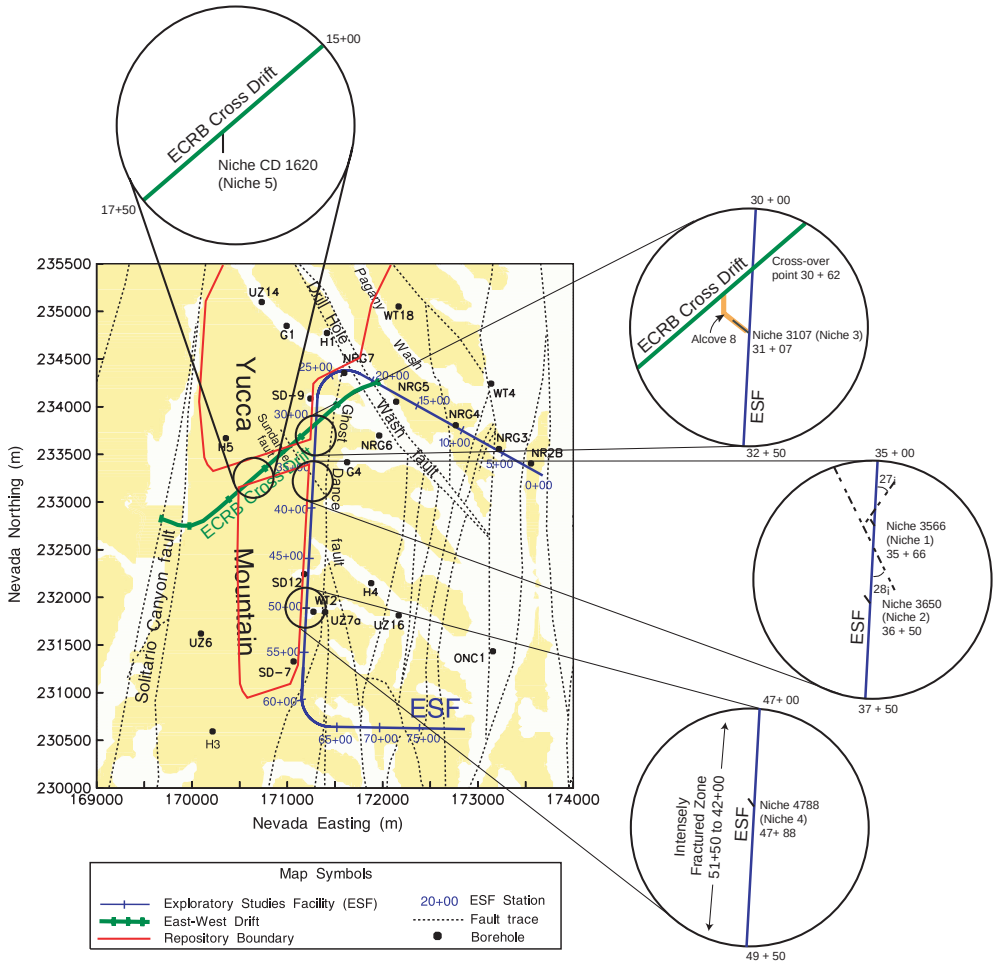

Repository Layout is from BSC (2003 [161726])

Figure 6.1.1-1. Schematic Illustration of Location Map for Niche 3107 (Niche 3), Niche 3566 (Niche 1), Niche 3650 (Niche 2), Niche 4788 (Niche 4) and Niche CD 1620 (Niche 5)

6.1.1.2 Borehole Configuration

Prior to niche excavation, three boreholes were drilled at Niche 3566 (Niche 1), and seven boreholes per niche were drilled at Niche 3650 (Niche 2), Niche 3107 (Niche 3), and Niche 4788 (Niche 4). Boreholes were drilled before excavation into both the rock to be excavated and the surrounding rock to gain access to the testing and monitoring area. Figure 6.1.1-2 shows the schematics of borehole clusters tested at the first four niche sites. Both types of boreholes were tested before niche excavation, and the surrounding boreholes were retested after excavation, allowing a study of excavation effects on the permeability of the surrounding rock. All boreholes shown in Figure 6.1.1-2 are parallel to the niche axis, as illustrated in Figure 6.1.1-3.

Three boreholes were originally drilled at Niche 3566 (Niche 1) along the same vertical plane coincident with the center of the niche (Figure 6.1.1-2a and Figure 6.1.1-3a).[1] The three boreholes were assigned the designation U, M, and B, corresponding to the upper, middle, and bottom borehole, respectively. Borehole M and borehole B were subsequently removed when the rock was mined out to create the niche, and borehole U still remains.

Figure 6.1.1-2b and Figure 6.1.1-3b show the location of the seven boreholes drilled at Niche 3650 (Niche 2). Three of the boreholes, designated UL, UM, and UR (upper left, upper middle, and upper right), were drilled approximately one meter apart and 0.65 m above the crown of the niche in the same horizontal plane. The remaining boreholes (ML, MR, BL, and BR) were drilled within the boundaries of the proposed niche and were subsequently mined out when the niche was excavated as planned.

Figure 6.1.1-2c and Figure 6.1.1-3c contain the final configuration of the seven boreholes drilled at Niche 3107 (Niche 3). The original intent was to drill the middle borehole ML and borehole MR beyond the limits of the proposed excavation to monitor the movement of moisture around the niche during subsequent testing. Unfortunately, the middle boreholes were not drilled at the correct elevation above Niche 3107 (Niche 3) and were partially mined away during excavation.

The final configuration of the seven boreholes drilled at Niche 4788 (Niche 4) is illustrated in Figure 6.1.1-2d and Figure 6.1.1-3d. A misinterpretation of a survey mark, along with bad ground conditions (i.e., falling rock or collapsing ground conditions) at Niche 4788 (Niche 4), also resulted in the partial loss of borehole ML at this site. The original plan was to drill the U and M series boreholes outside the excavation.

After the excavation of Niche 3566 (Niche 1), a special set of horizontal boreholes was drilled from within the niche into the walls and end of the niche in a radial pattern. A similar scheme was used at Niche 3107 (Niche 3) after its excavation. These are not shown on the plan views.

Air-permeability testing has been performed at Niche CD 1620 (Niche 5). Special boreholes to discern the effects of excavation on permeability were drilled alongside the proposed excavation

[1]Figures 6.1.1-2, 6.1.1-3, and 6.1.1-4 were generated using field measurements recorded in Scientific Notebooks (Wang 1997 [156530], Wang 1997 [156534]), Wang 1999 [156538], Wang 1999 [153449], and Trautz 1999 [156563]) and/or using pre-built plans for niche excavation. Therefore, these figures show the idealized shape of the niches and approximate locations of the boreholes. Figure 6.1.1-5 was generated using the as-built information (DTN: MO0008GSC00269.000 [166198]).

site, parallel to the niche wall to-be. These boreholes were designated "AK" because they were intended primarily for air permeability (K) use. Figure 6.1.1-4a and Figure 6.1.1-4c show in plan and elevation view respectively, these three boreholes designated AK1, AK2 and AK3 that were drilled 1 m apart in a horizontal plane, with the first borehole 1 m from the proposed niche wall level with the elevation of the ECRB springline. Before the inner excavation at Niche CD 1620 (Niche 5), seven additional boreholes were drilled as shown in Figure 6.1.1-4b, Figure 6.1.1-4d, and Figure 6.1.1-4e in plan, elevation, and side view respectively, designated B1.75, ML, MM, MR, UL, UM, and UR. All of these boreholes except B1.75 were drilled above the proposed inner-niche location. Subsequent excavation of the inner part of the niche mined out borehole B1.75.

After testing was completed at Niche CD 1620 (Niche 5), air-permeability measurements were performed in the near-vertical boreholes drilled from the invert of Alcove 8 towards Niche 3107 (Niche 3). These boreholes were drilled to surround the area designated for the pond experiment, as described in Section 6.12, to be performed in Alcove 8. These air-permeability tests were made to provide correlation with the ground penetrating radar imaging in the same boreholes, as opposed to providing direct location data for borehole water release experiments (as with the other air-permeability measurements). They were also intended to allow retesting to observe changes in relative permeability caused by possible partial saturation as a result of the pond experiment. The alcove plan and face views are shown with approximate borehole locations, designated as #1 to #6, in Figure 6.1.1-5a and Figure 6.1.1-5b respectively.

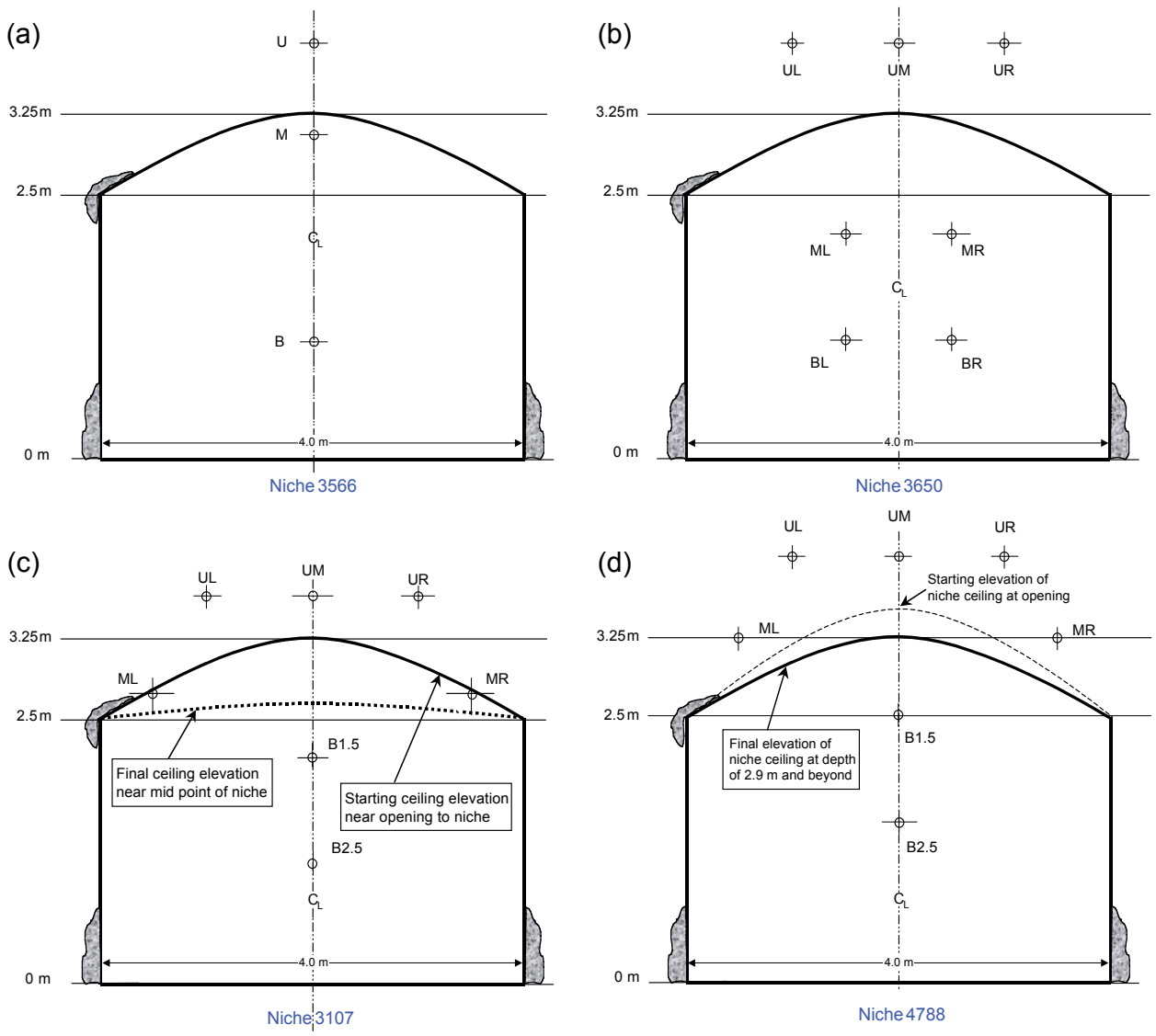

NOTE: All measurements are approximate and do not represent surveyed as-built conditions. The niche faces are on the west wall of the Main Drift of the Exploratory Studies Facility. See Figure 6.1.1-4 for borehole notations. C_L denotes centerline.

Figure 6.1.1-2. Schematic Illustration of the End View of Borehole Clusters at Niche Sites

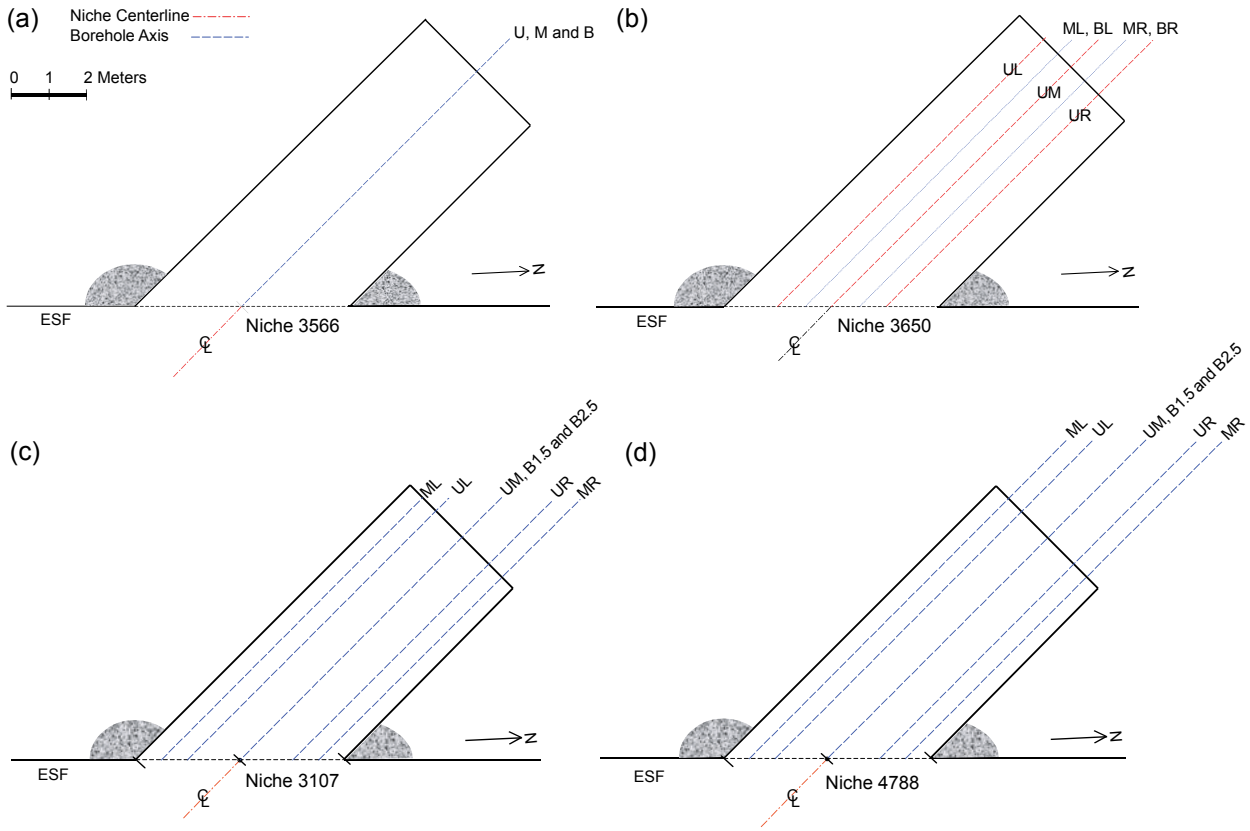

NOTE: All measurements are approximate and do not represent surveyed as-built conditions.
The boreholes shown are oriented horizontally in the northwestern direction parallel to the niche axis.
See Figure 6.1.1-4 for borehole notations. C_L denotes centerline.

Figure 6.1.1-3. Schematic Illustration of the Plan View of Borehole Clusters at Niche Sites

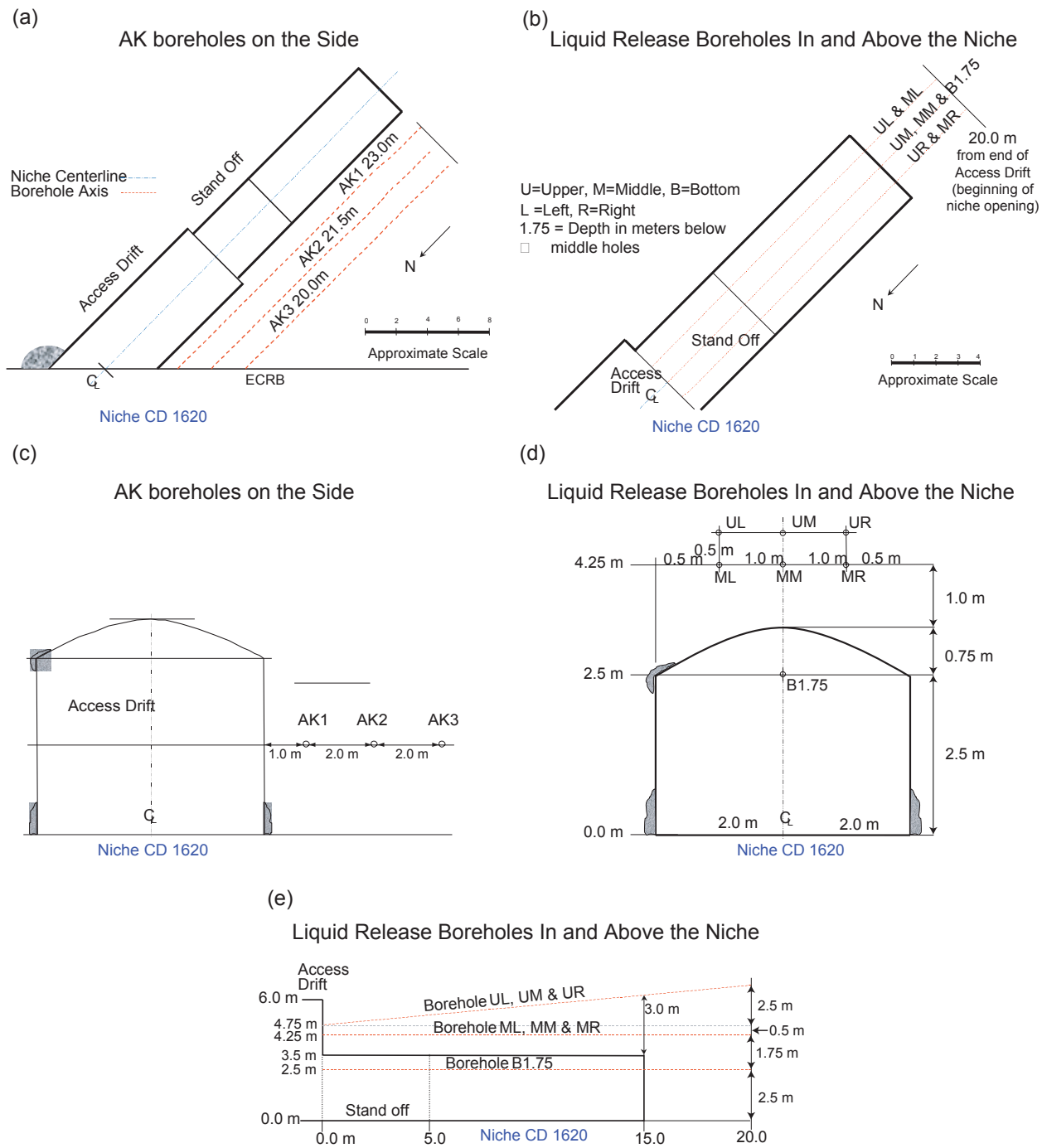

NOTE: All measurements are approximate and do not represent surveyed as-built conditions.
The niche face is on the southeast wall of the ECRB Cross Drift.
C_L denotes centerline.

Figure 6.1.1-4. Schematic Illustration of the End and Plan Views of Borehole Clusters at Niche CD 1620 (Niche 5)

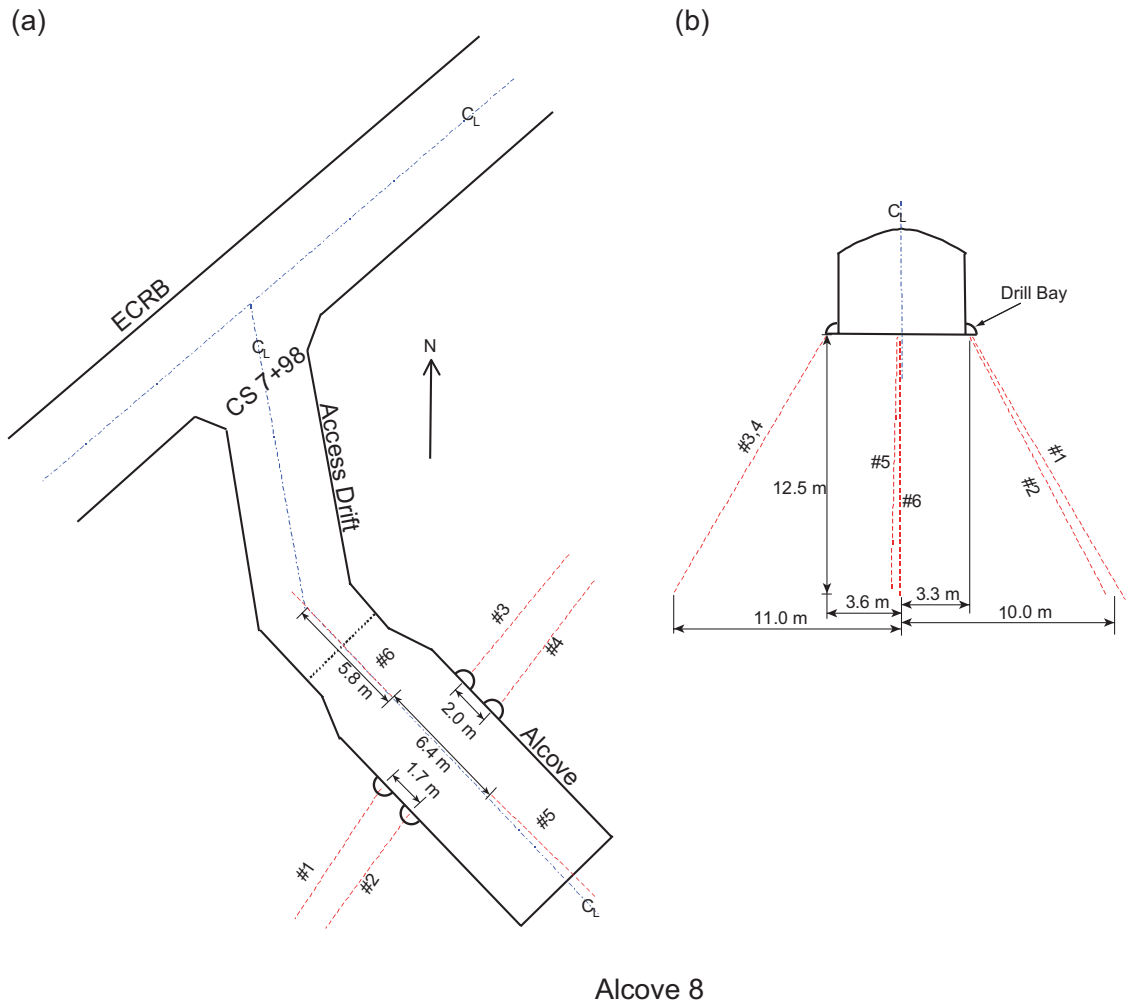

NOTE: All measurements are approximate. Borehole as-built information is in DTN: MO0008GSC00269.000 [166198].
The niche face is on the southeast wall of the ECRB Cross Drift.
C_L denotes centerline.

Figure 6.1.1-5. Schematic Illustration of the Plan and End Views of Borehole Clusters at Alcove 8

6.1.2 Air-Permeability Testing, Spatial Distribution, and Statistical Analysis

To date, an estimated 3,500 separate air injections have been undertaken in the *in situ* studies underground at Yucca Mountain. Nearly a quarter-million pressure-response curves have been logged in the studies. The number of tests lends itself to visualization and statistical comparison of the flow connections and distributions of permeability in the rock mass. The specially designed equipment for pneumatic testing is described in Attachment I. With the equipment, it is feasible to conduct tests for site-to-site and borehole-to-borehole comparisons both before and after nearby excavations.

6.1.2.1 Data Reduction and Air-Permeability Determination

Data in the field were acquired in the form of voltage output from the various instruments and converted in real time or post-test time to physical units, using each instrument's calibration data. At Niche 3107 (Niche 3), Niche 4788 (Niche 4), Niche CD 1620 (Niche 5), and Alcove 8, data acquisition was fully automated, so that log entries for each individual injection test could be done by computer and correlation with the data files linked. Each of these tests was given three minutes to reach steady state. To maximize the signal-to-noise ratio, the maximum flow rate obtainable with the system that did not cause the interval pressure to exceed the packer leak-by pressure was chosen for the purpose of the permeability calculation.

Because each injection test was repeated to accommodate two different observation-packer configurations, there are two tests for each injection location from which to choose flow and pressure data for the single-borehole results. When graphed, the two are usually indistinguishable. Preference is given to the lower of the two if there is a significant difference, because this higher value is likely caused by leaks in the packer sealing.

Reported data consist of the acquisition filename, test location, time, date, channel or interval number, flow rate, ambient pressure, and steady-state injection pressure. The derived steady-state single-borehole permeability can be obtained using the expression described below.

In air-permeability tests to characterize the fracture heterogeneity of the test sites, permeability values are obtained from pressure changes and flow rates using the following modified Hvorslev's formula (LeCain 1995 [101700], Equation 15, p. 10):

$$k = \frac{P_{sc} Q_{sc} \mu \ln\left(\frac{L}{r_w}\right) T_f}{\pi L \left(P_2^2 - P_1^2\right) T_{sc}} \qquad \text{(Eq. 6.1.2-1)}^{a}$$

k	permeability, m^2
P_{sc}	standard pressure, Pa
Q_{sc}	flow-rate at standard conditions, m^3/s
μ	dynamic viscosity of air, Pa-s
L	length of zone, m
r_w	radius of bore, m
T_f	temperature of formation, K
P_2	injection zone pressure at steady-state, Pa

[a] The solution is derived for the steady state ellipsoidal flow field around a finite line source. If the length L in the natural logarithm term in Equation 6.1.2-1 is replaced by an external radius R_e, this formula is identical to the cylindrical flow solution with an ambient constant pressure boundary at the external radius (Muskat 1982 [134132], p. 734). This replacement is used in Section 6.2.2.1 to estimate the saturated hydraulic conductivity for post-excavation liquid flow paths from the borehole interval to the niche ceiling.

P_1 ambient pressure, Pa

T_{sc} standard temperature, K

ln natural log

For the purpose of calculation, standard pressure is 1.013E+05 Pa (one atmosphere). The dynamic viscosity of air used is 1.78E-05 Pa-s. Temperature contributions to Equation 6.1.2-1 are negligible, with $T_f \sim T_{sc}$ for ambient-temperature testing conditions. See Attachment IX.3 for details on how this calculation was performed.

The Hvorslev's equation requires that air behave as an ideal gas. This stipulation is approximately true at the ambient temperatures and pressures used in the air-permeability tests. In addition, a finite line source is used to represent a borehole injection interval. This representation is applied to the borehole injection interval, where all air flow is approximated to be in the radial direction (none in the axial direction). This is justified because in the air-permeability tests, the length of injection zone was 0.3048 m and the radius of the borehole was 0.0381 m. The injection zone is a long, thin cylinder. Flows along axial directions were blocked by packers, and occurrences of packer leaks were monitored by pressures in adjacent borehole intervals, as described in Attachment I.

Although the fractured tuff of the niches is not a homogeneous or infinite medium, the Hvorslev equation provides a consistent method of calculating permeabilities, enabling comparison of the test results for various injection locations. Because the heterogeneity of the surrounding medium is not known *a priori*, the permeabilities calculated by analytic formula are estimates of effective values around the injection borehole intervals. The results of the air-permeability tests are used to characterize the heterogeneity of the medium of niche sites and test beds. Another requirement of this approach is that air flows are mainly through fractures and governed by Darcy's law. Darcy's law is used to relate flux to pressure gradients (Bear 1972 [156269]). The justification for this is that: under the ambient unsaturated conditions in fractured tuff at Yucca Mountain, capillary forces confine the liquid mainly to the matrix. This leaves the fracture network, which is more permeable than the tuff matrix, available for gas flow.

Deviations from Darcy's law may result from either turbulent flow or from the gas slip-flow phenomenon (Klinkenberg 1942 [106105]) but both these effects are considered to be negligible. Slip flow is significant only in pores with dimensions similar to the mean free path of air molecules (Bear 1972 [156269]). Apertures of the fractures in Yucca Mountain are much larger than the molecular mean free path. Pressure drop is proportional to flow rate in laminar flow, which is required for Darcy's law, but not in turbulent flow (Bear 1972 [156269]. These experiments were conducted at multiple flow rates to detect any evidence of deviation from Darcy's law due to turbulence, and none was found. Finally, small effects potentially associated with movement of residual water within the fractures and the multirate approach to check packer leak-by and other nonlinear effects (e.g., turbulence) are discussed in Attachment I.4.

6.1.2.2 Permeability Profiles

All boreholes at niches as illustrated in Figure 6.1.1-2 and Figure 6.1.1-3 are nominally 10 m long and 0.0762 m in diameter. Those in Figure 6.1.1-4 and Figure 6.1.1-5 were nominally 15 m long and 0.0762 m in diameter. The boreholes were drilled dry with compressed air to remove

drill cuttings. Both the packer interval length and the test interval length are 0.3 m in all cases. Further details of equipment configuration and test execution are discussed in Attachment I.

Whereas most of the niches were excavated so as to preserve certain boreholes surrounding them (in order to remeasure the air permeability in these holes after excavation), Alcove 8 was constructed before any drilling near it, so this opportunity did not occur there.

6.1.2.2.1 Pre- and Post-Excavation Permeability Profiles

Permeability profiles along boreholes at the five niches show the permeability value from each test interval, plotted against the location of the middle of the test interval (zone). Figure 6.1.2-1 illustrates three Niche 3566 (Niche 1) permeability profiles along the upper, middle, and bottom boreholes, which are parallel to the niche axis. The air-permeability tests were conducted before niche excavation. Niche 3566 (Niche 1), the first niche excavated in the ESF, is located in the vicinity of the Sundance fault. All three boreholes penetrated brecciated zones in the last one-third of their lengths, with broken rock pieces preventing packer insertion beyond this depth. A wet feature in a brecciated zone was observed at the end of this niche, right after completion of dry excavation (Wang et al. 1999 [106146], Figure (4c), p. 331). The width of the wet feature is comparable to the borehole-interval length of 0.3 m, used in the air-permeability tests (this section) and liquid-release seepage tests (Section 6.2).

After niche excavation, six additional horizontal boreholes were drilled from the inside of the niche, fanning out radially in different directions. Only two radial holes were tested and analyzed in this niche. This niche was sealed for moisture monitoring after testing these two boreholes, and further seepage testing in this niche has been deferred. The permeability profiles for two radial boreholes on the left side of the niche are illustrated in Figure 6.1.2-2. These boreholes also penetrated brecciated zones. The absence of data from the deeper portion of one of the boreholes in Figure 6.1.2-2 is related to the intrinsic difficulties of brecciated zone testing due to poor borehole conditions, which prevent the maintenance of a proper seal (see also Attachment I.4 for discussion about issues of packer leak-by in testing).

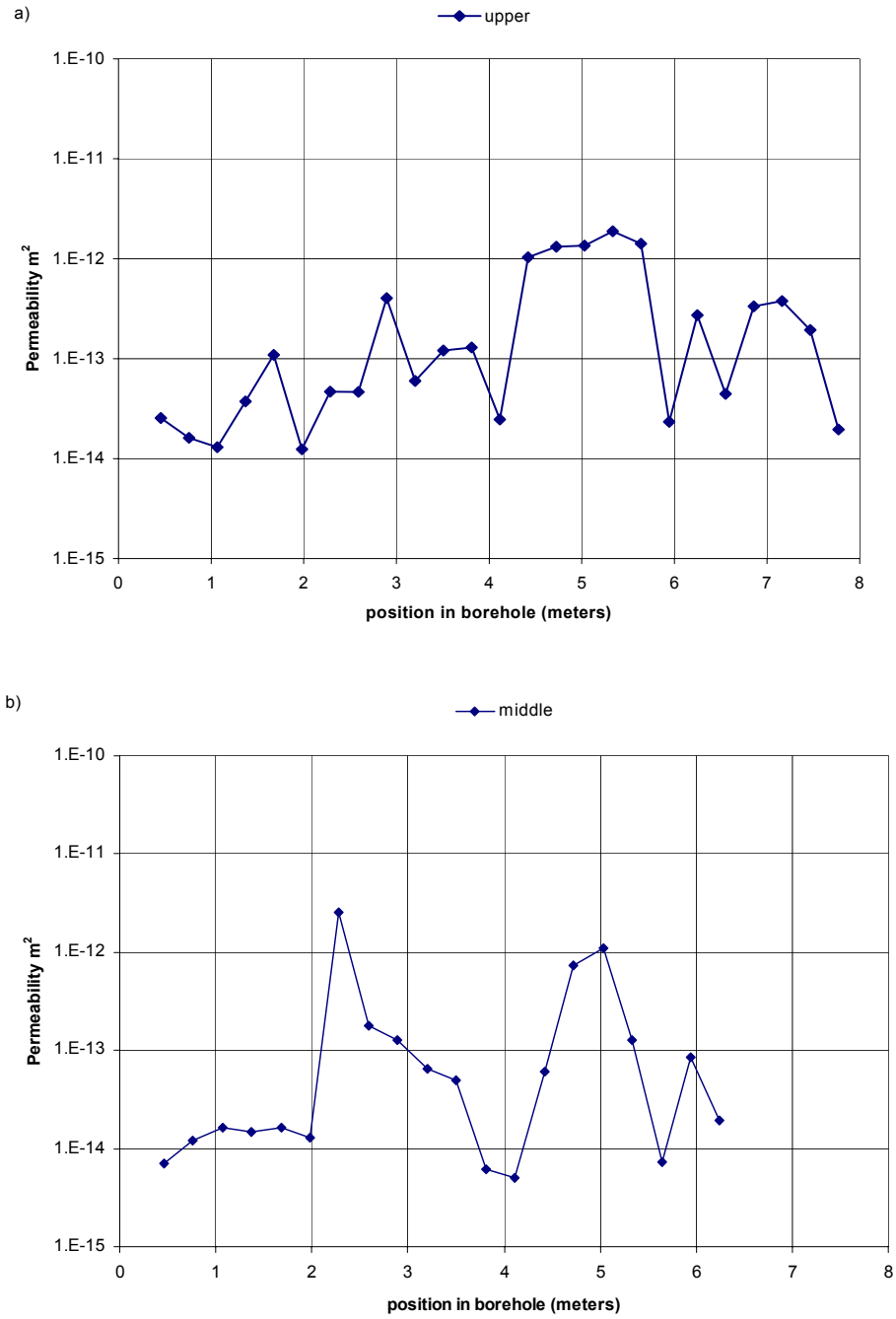

DTN: LB0011AIRKTEST.001 [153155]

NOTE: In DTN: LB0011AIRKTEST.001 [153155], zone numbers are reported, rather than actual position in the borehole. Zone 1 is centered at 0.5 m, and each successive zone is 0.3 m farther into the borehole (e.g., zone 2 is centered at 0.8 m).

Figure 6.1.2-1. Pre-Excavation Air-Permeability Profiles along Axial Boreholes at Niche 3566 (Niche 1)

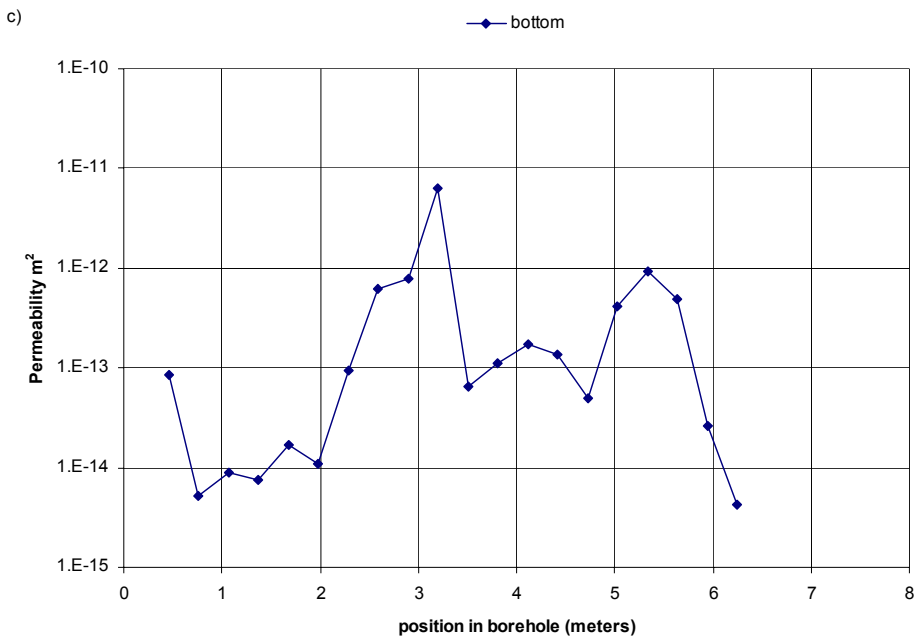

NOTE: In DTN: LB0011AIRKTEST.001 [153155], zone numbers are reported, rather than actual position in the borehole. Zone 1 is centered at 0.5 m, and each successive zone is 0.3 m farther into the borehole (e.g., zone 2 is centered at 0.8 m).

Figure 6.1.2-1. Pre-Excavation Air-Permeability Profiles along Axial Boreholes at Niche 3566 (Niche 1) (continued)

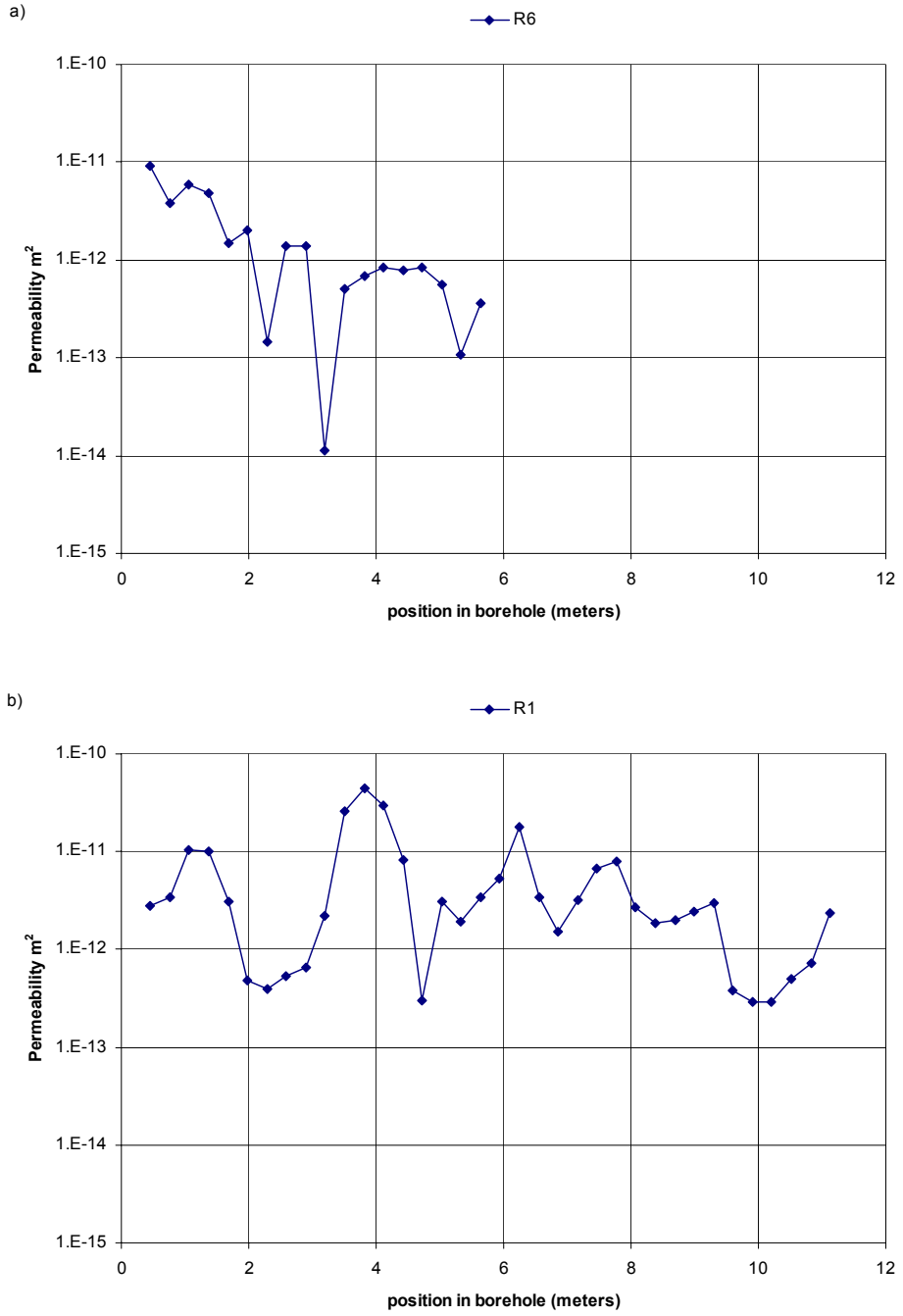

DTN: LB0011AIRKTEST.001 [153155]

NOTE: In DTN: LB0011AIRKTEST.001 [153155], zone numbers are reported, rather than actual position in the borehole. Zone 1 is centered at 0.5 m, and each successive zone is 0.3 m farther into the borehole (e.g., zone 2 is centered at 0.8 m).

Figure 6.1.2-2. Post-Excavation Air-Permeability Profiles along Radial Boreholes at Niche 3566 (Niche 1)

Figure 6.1.2-3 illustrates both the pre- and post-excavation permeability profiles along three upper boreholes at Niche 3650 (Niche 2). On all the plots with both pre- and post-excavation data, a line is drawn through the profiles to indicate the geometric mean of each (see Attachment IX.1 for calculations). This mean includes only intervals that were tested in common both before and after excavation.

The permeability increases could be interpreted as the opening of pre-existing fractures induced by stress releases associated with niche excavation (Wang and Elsworth 1999 [104366], pp. 751–757). The niches were excavated using an Alpine Miner, a mechanical device with a rotary head (as opposed to drill and blast) cutting the rocks below the upper-level boreholes, so that excavation damage itself would not alter permeability.

Intervals with high pre-excavation permeability recorded the smallest post-excavation permeability changes. In additional to mechanical effects, some of the permeability increases can be related to the intersection of previously dead-ended fractures with the excavated free surface. For borehole intervals, beyond the extent of the niche excavation, the permeability values are less altered. Figure 6.1.2-4 illustrates the pre-excavation permeability profiles of the other four boreholes. The middle- and bottom-level boreholes were available for air-injection testing only before niche excavation, since they were subsequently removed by excavation.

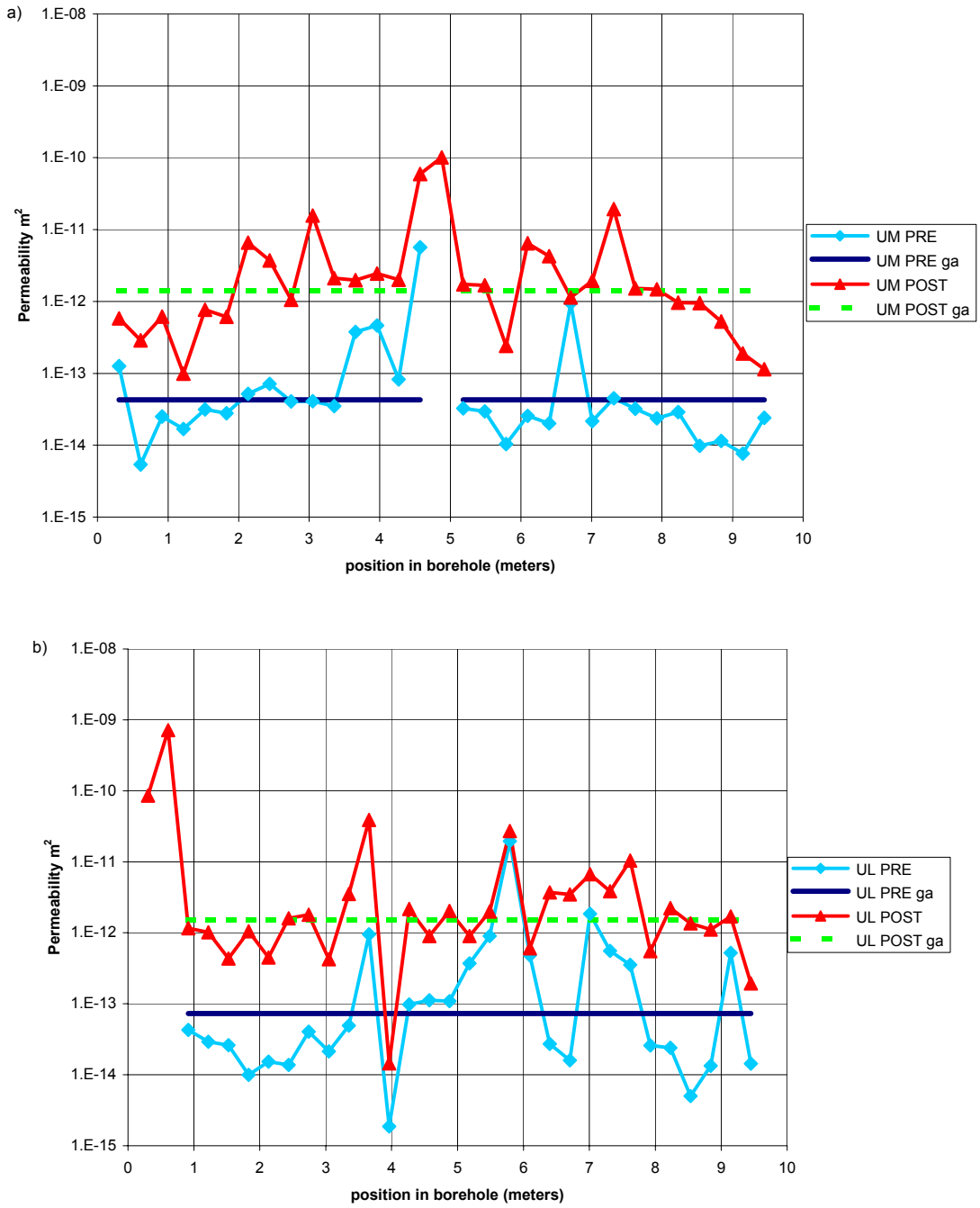

DTN: LB0011AIRKTEST.001 [153155]

NOTE: "ga" is the geometric average.

In DTN: LB0011AIRKTEST.001 [153155], zone numbers are reported, rather than actual position in the borehole. Zone 1 is centered at 0.5 m, and each successive zone is 0.3 m farther into the borehole (e.g., zone 2 is centered at 0.8 m).

Figure 6.1.2-3. Pre- and Post-Excavation Air-Permeability Profiles along Upper Boreholes at Niche 3650 (Niche 2)

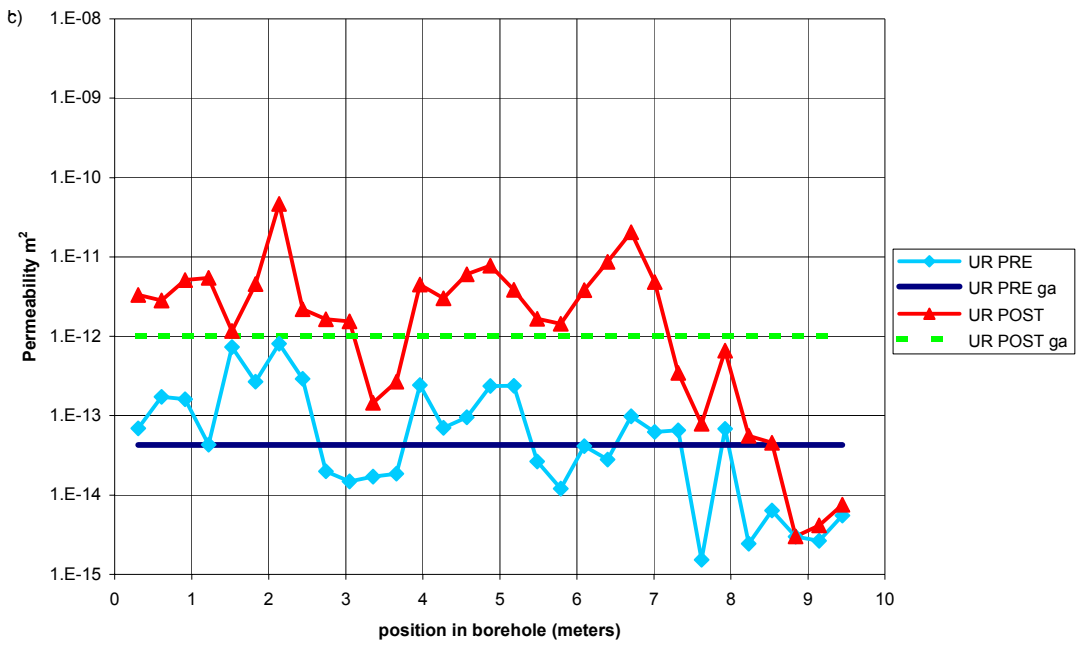

NOTE: "ga" is the geometric average.

In DTN: LB0011AIRKTEST.001 [153155], zone numbers are reported, rather than actual position in the borehole. Zone 1 is centered at 0.5 m, and each successive zone is 0.3 m farther into the borehole (e.g., zone 2 is centered at 0.8 m).

Figure 6.1.2-3. Pre- and Post-Excavation Air-Permeability Profiles along Upper Boreholes at Niche 3650 (Niche 2) (continued)

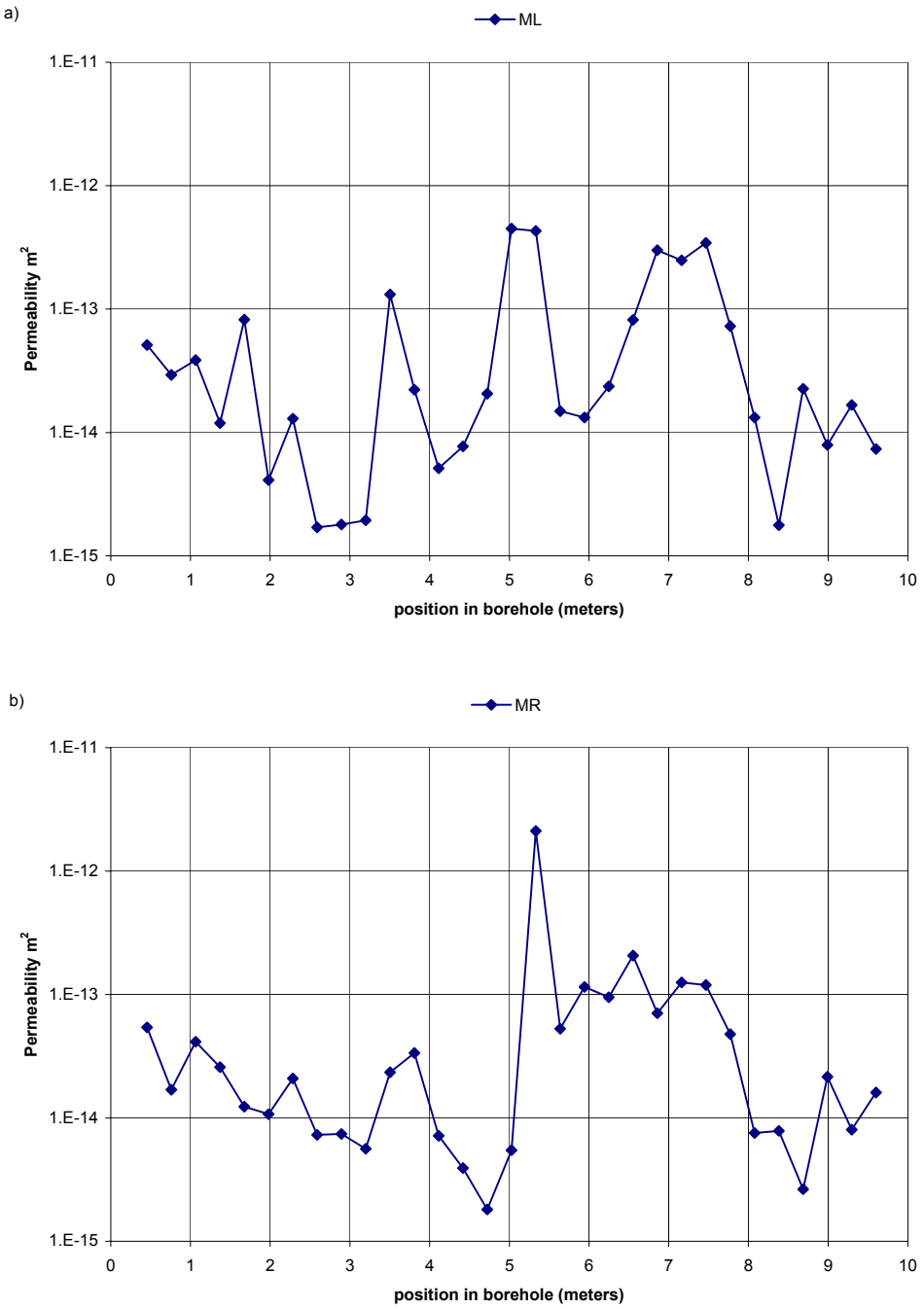

DTN: LB0011AIRKTEST.001 [153155]

NOTE: In DTN: LB0011AIRKTEST.001 [153155], zone numbers are reported, rather than actual position in the borehole. Zone 1 is centered at 0.5 m, and each successive zone is 0.3 m farther into the borehole (e.g., zone 2 is centered at 0.8 m).

Figure 6.1.2-4. Pre-Excavation Air-Permeability Profiles along Middle and Bottom Boreholes at Niche 3650 (Niche 2)

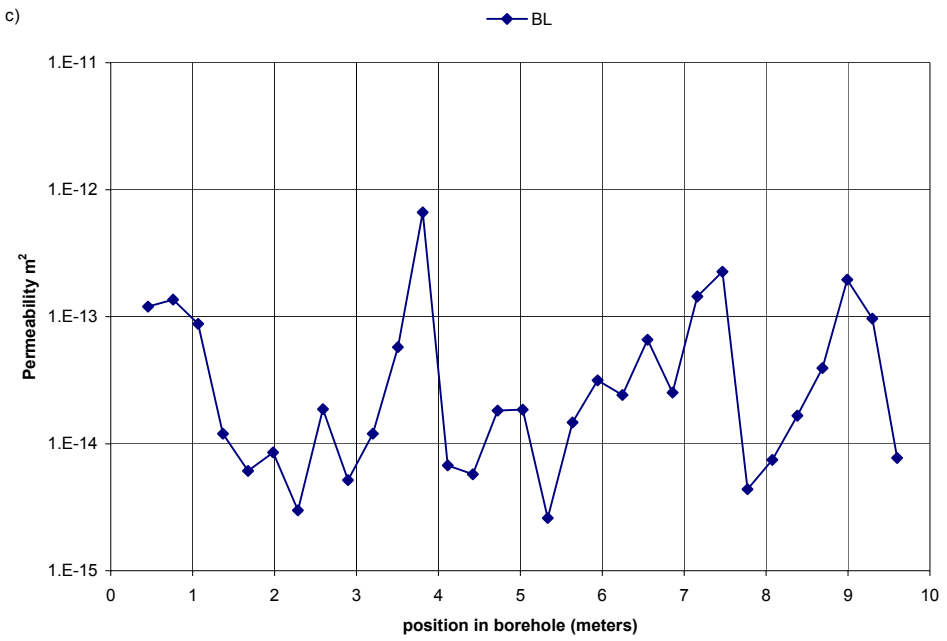

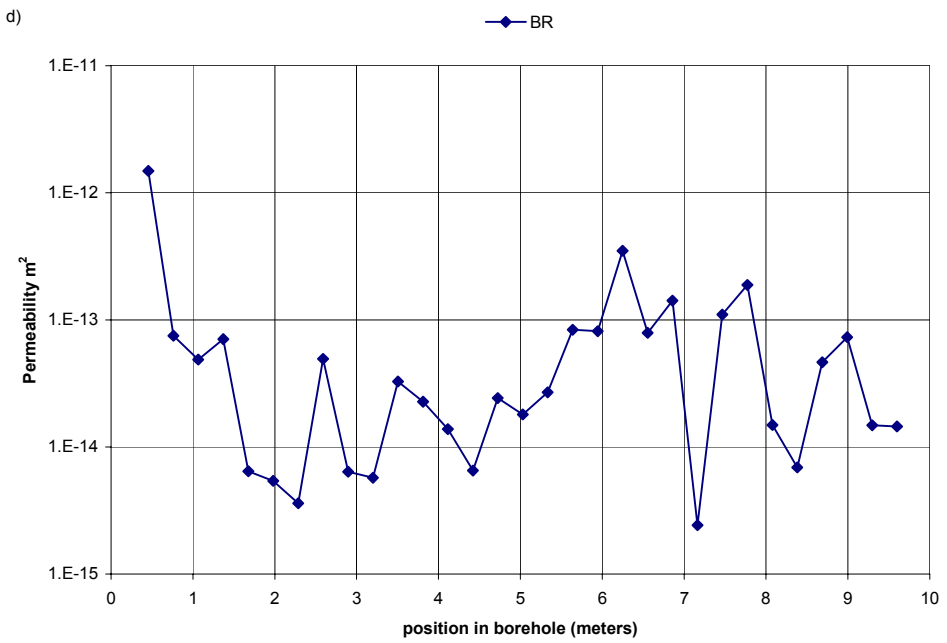

DTN: LB0011AIRKTEST.001 [153155]

NOTE: In DTN: LB0011AIRKTEST.001 [153155], zone numbers are reported, rather than actual position in the borehole. Zone 1 is centered at 0.5 m, and each successive zone is 0.3 m farther into the borehole (e.g., zone 2 is centered at 0.8 m).

Figure 6.1.2-4. Pre-Excavation Air-Permeability Profiles along Middle and Bottom Boreholes at Niche 3650 (Niche 2) (continued)

To compare with Niche 3650 (Niche 2), the corresponding results of the permeability profiles are presented for Niche 3107 (Niche 3) in Figure 6.1.2-5 and Figure 6.1.2-6, and for Niche 4788 (Niche 4) in Figure 6.1.2-7 and Figure 6.1.2-8. Figure 6.1.2-5 and Figure 6.1.2-7, similarly to Figure 6.1.2-3, are for the upper boreholes, with both pre-excavation and post-excavation values presented for the evaluation of excavation-induced enhancements in permeabilities. Figure 6.1.2-6 and Figure 6.1.2-8 are pre-excavation permeability profiles for the middle- and lower-level boreholes that were subsequently mined out from Niche 3107 (Niche 3) and Niche 4788 (Niche 4). The borehole layouts for these two niches are modified from the layout in Niche 3650 (Niche 2), as illustrated in Figure 6.1.1-2.

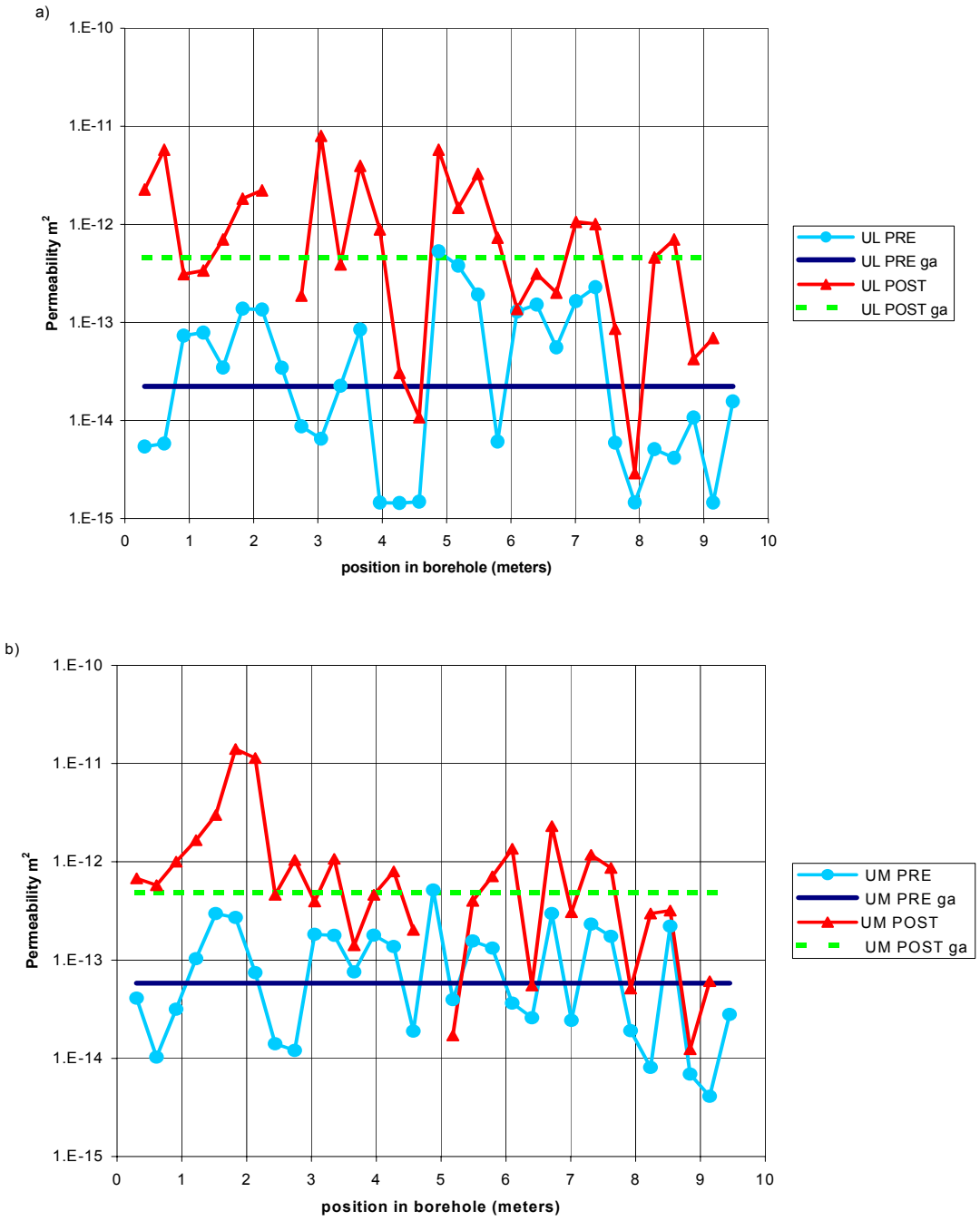

DTNs: LB980901233124.101 [136593] for pre-excavation data,
LB990601233124.001 [105888] for post-excavation data

NOTE: Intervals tested are 0.3 m long; position plotted is at farther end of tested interval.

Figure 6.1.2-5. Pre- and Post-Excavation Air-Permeability Profiles along Upper Boreholes at Niche 3107 (Niche 3)

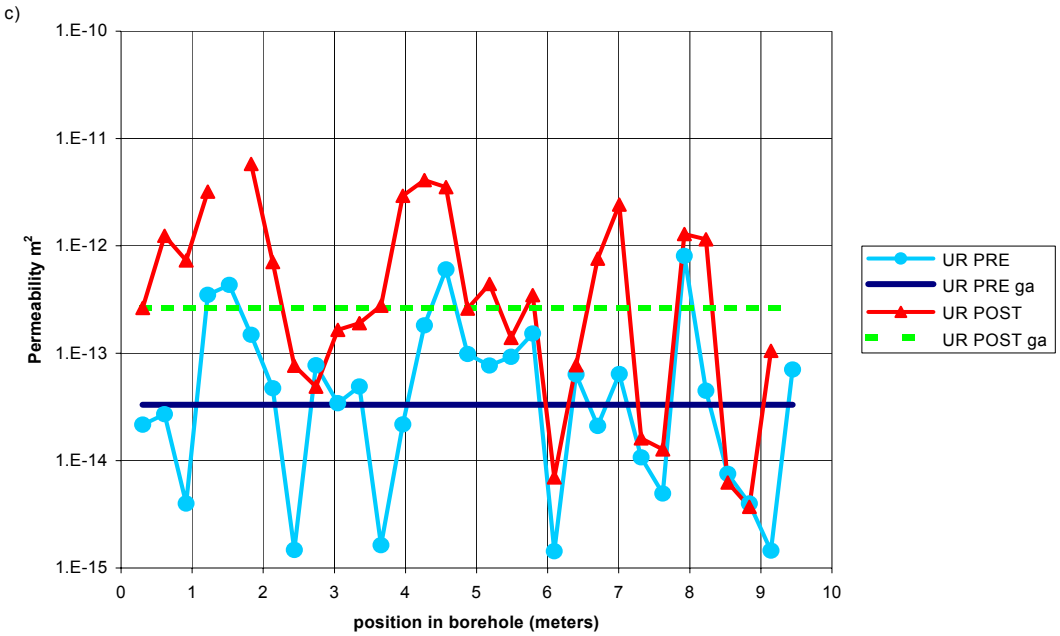

DTNs: LB980901233124.101 [136593] for pre-excavation data,
LB990601233124.001 [105888] for post-excavation data

NOTE: Intervals tested are 0.3 m long; position plotted is at farther end of tested interval.

Figure 6.1.2-5. Pre- and Post-Excavation Air-Permeability Profiles along Upper Boreholes at Niche 3107 (Niche 3) (continued)

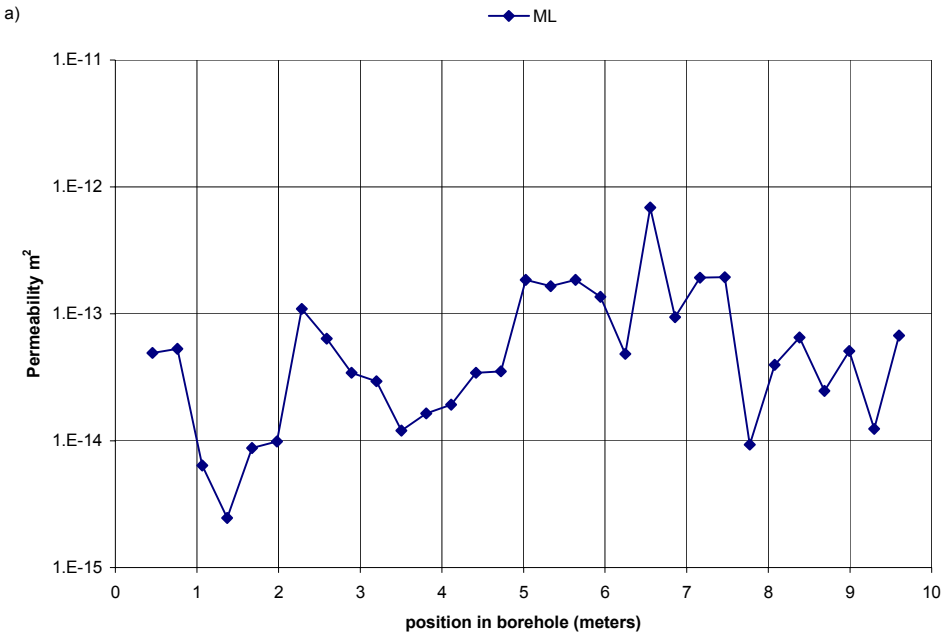

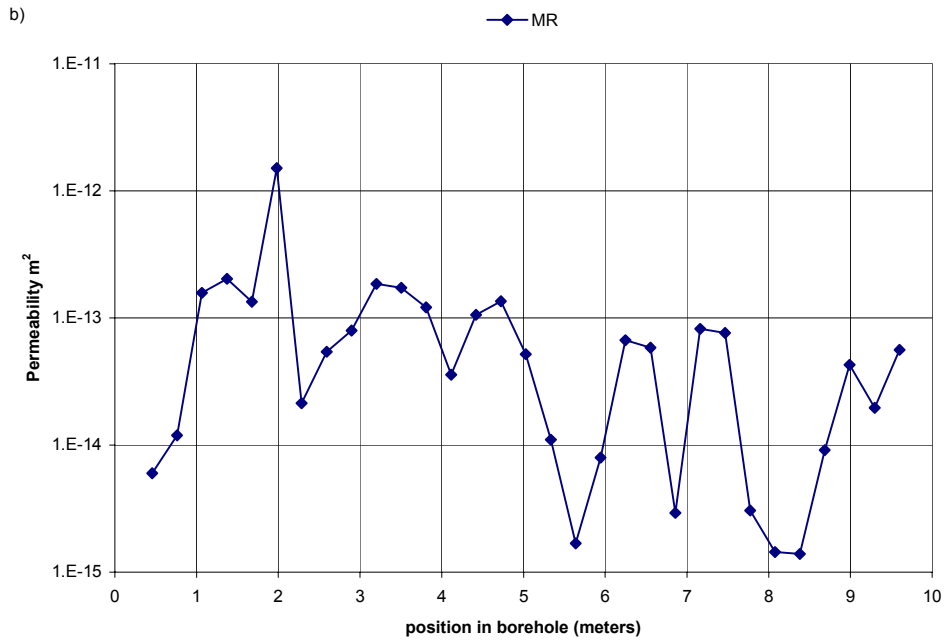

DTN: LB980901233124.101 [136593]

Figure 6.1.2-6. Pre-Excavation Air-Permeability Profiles along Middle and Bottom Boreholes at Niche 3107 (Niche 3)

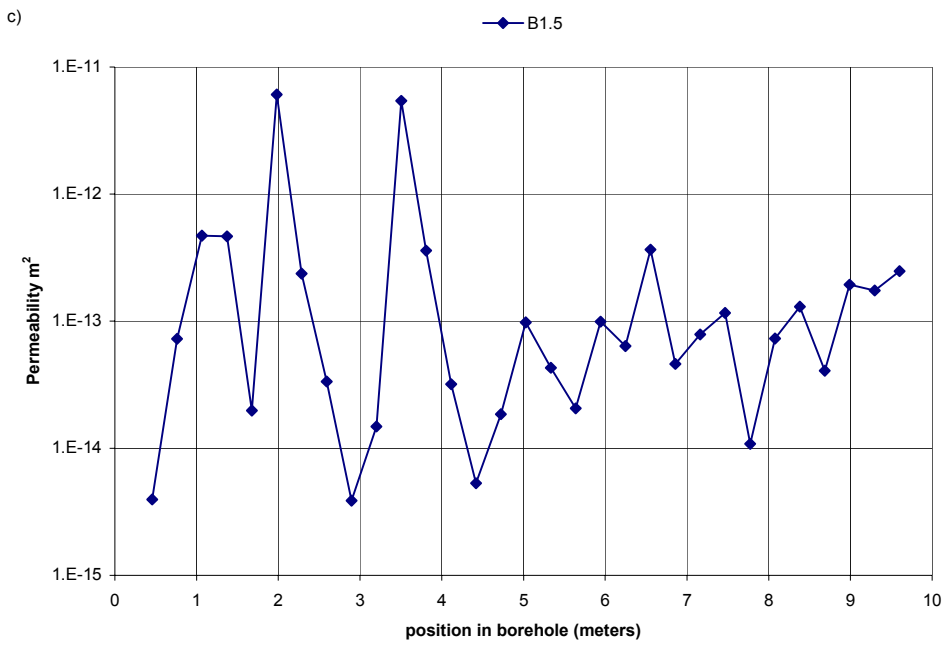

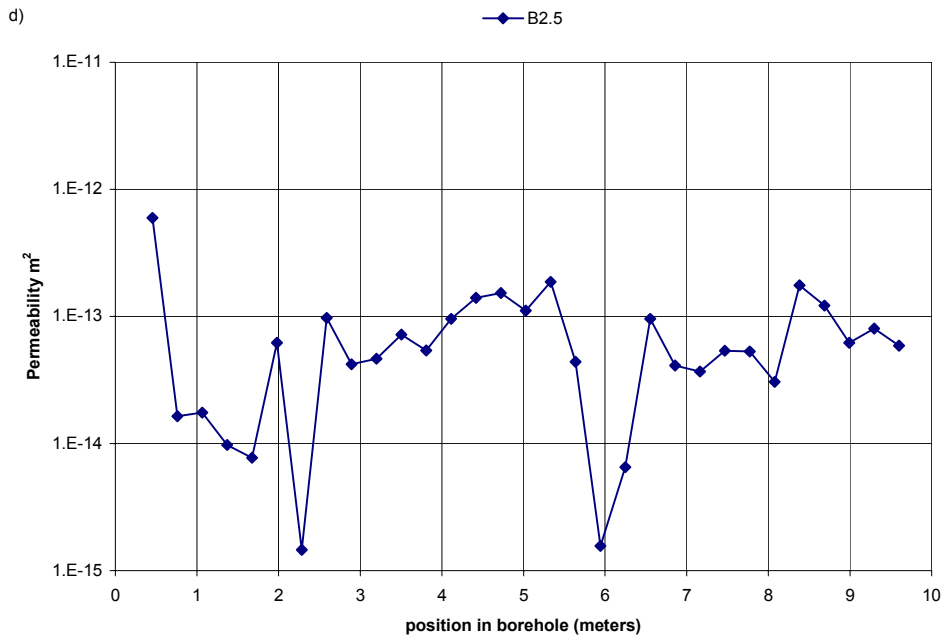

DTN: LB980901233124.101 [136593]

Figure 6.1.2-6. Pre-Excavation Air-Permeability Profiles along Middle and Bottom Boreholes at Niche 3107 (Niche 3) (continued)

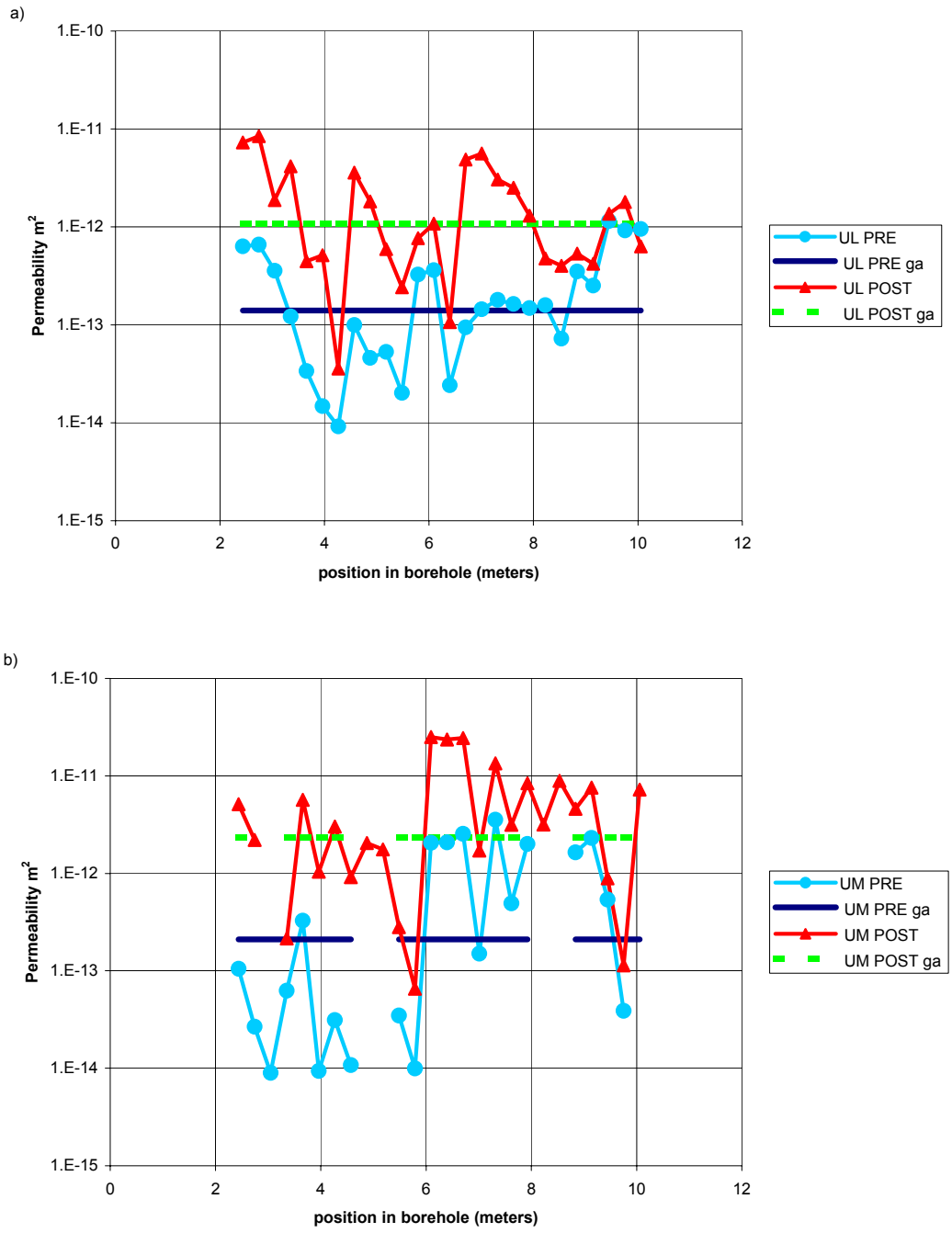

DTNs: LB980901233124.101 [136593] for pre-excavation data,
LB990601233124.001 [105888] for post-excavation data

Figure 6.1.2-7. Pre- and Post-Excavation Air-Permeability Profiles along Upper Boreholes at Niche 4788 (Niche 4)

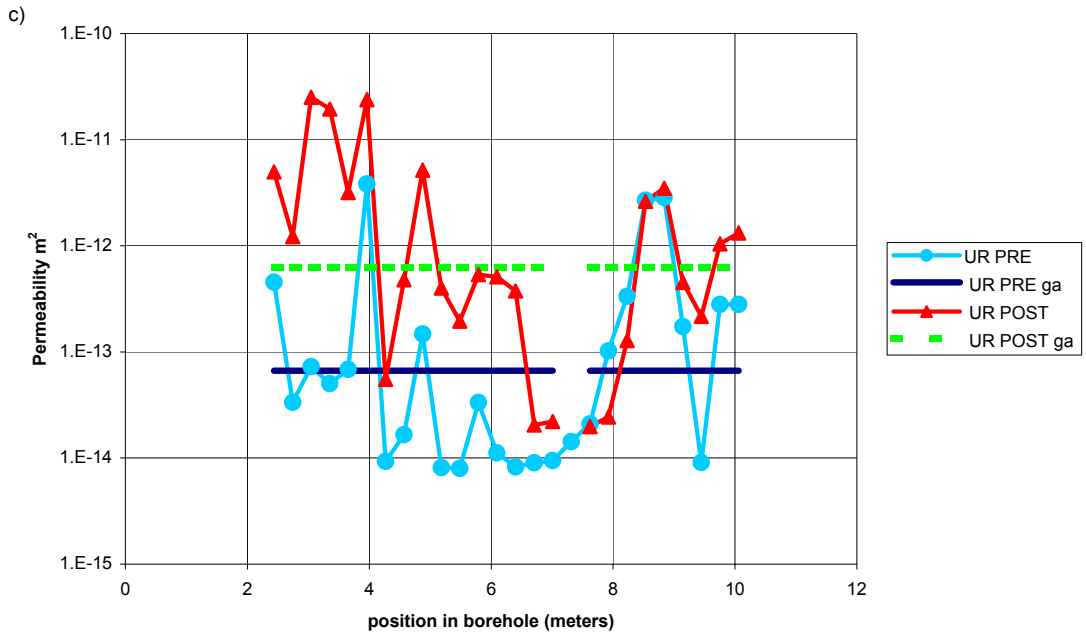

DTNs: LB980901233124.101 [136593] for pre-excavation data,
LB990601233124.001 [105888] for post-excavation data

Figure 6.1.2-7. Pre- and Post-Excavation Air-Permeability Profiles along Upper Boreholes at Niche 4788 (Niche 4) (continued)

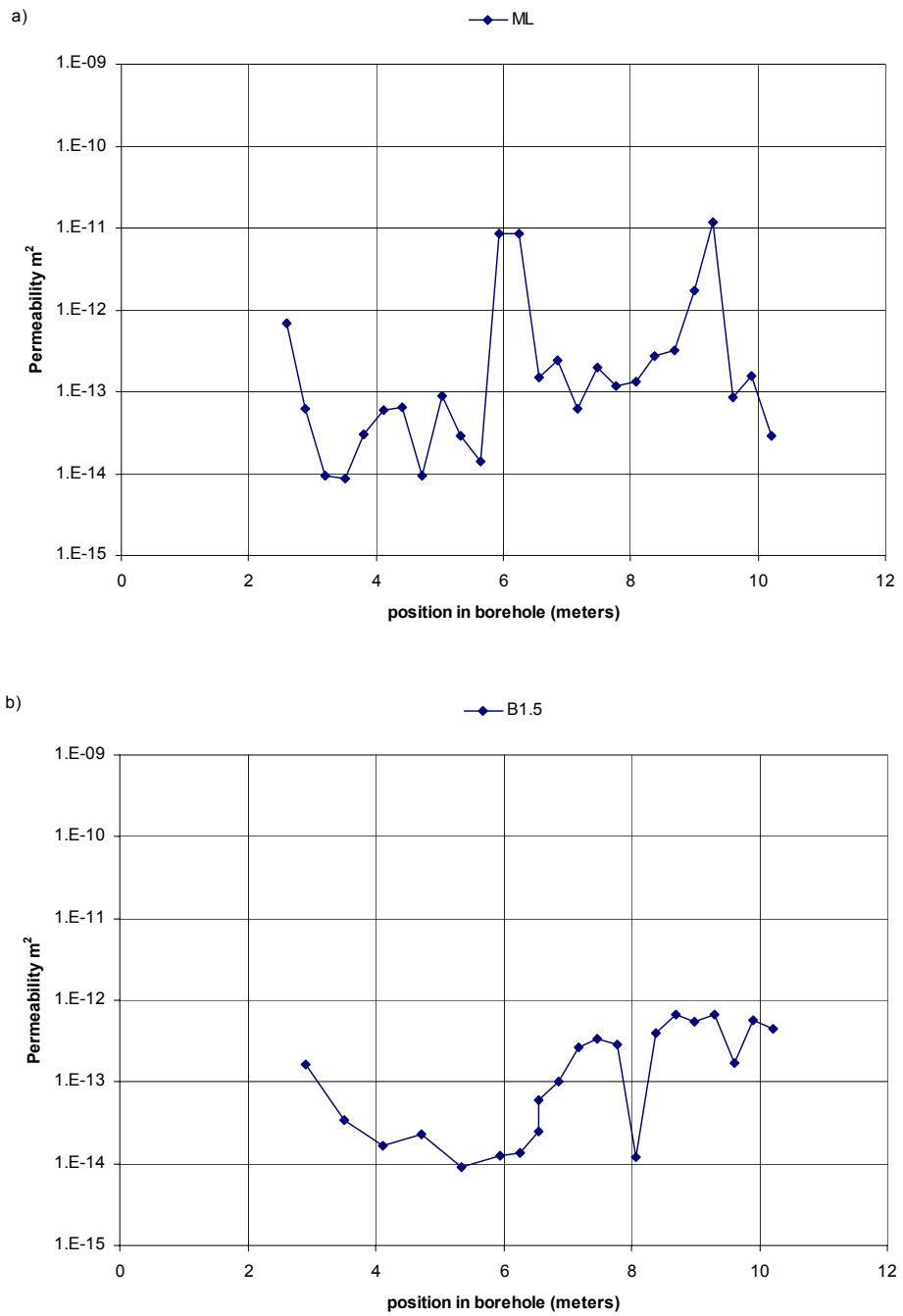

DTN: LB980901233124.101 [136593]

NOTE: Two or more measurements were made at each position. The least value of calculated permeability is reported here as being the most likely to be unaffected by leak-by.

Figure 6.1.2-8. Pre-Excavation Air-Permeability Profiles along Middle and Bottom Boreholes at Niche 4788 (Niche 4)

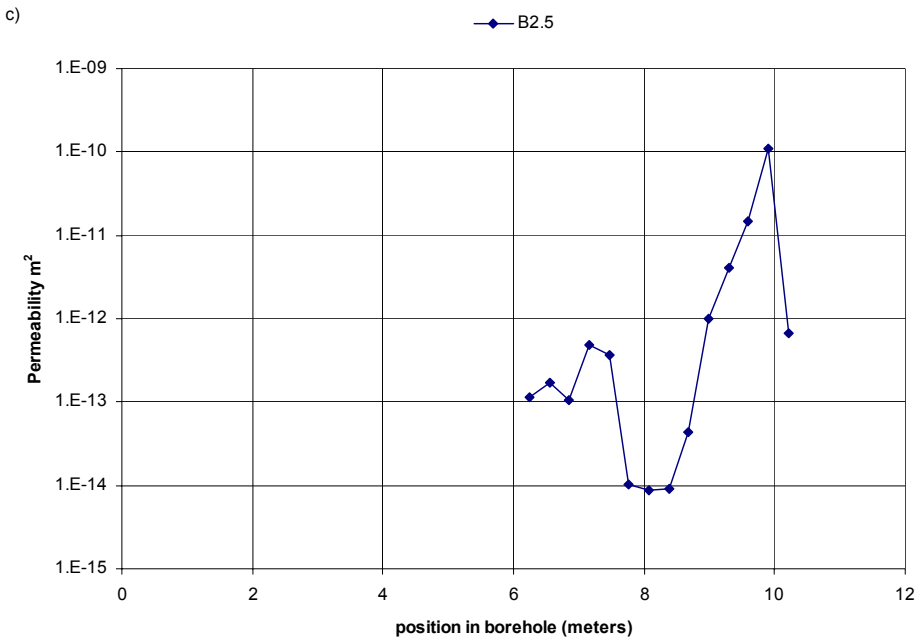

DTN: LB980901233124.101 [136593]

NOTE: Two or more measurements were made at each position. The least value of calculated permeability is reported here as being the most likely to be unaffected by leak-by.

Figure 6.1.2-8. Pre-Excavation Air-Permeability Profiles along Middle and Bottom Boreholes at Niche 4788 (Niche 4) (continued)

At Niche CD 1620 (Niche 5), measurements taken before and after excavation at the inner niche area and alongside the outer niche area allowed comparison of excavation effects on permeability profiles for boreholes situated above excavation versus those situated alongside excavation. Profiles were taken of borehole UL, borehole UM, and borehole ML over the inner niche area both before and after the inner niche excavation, as illustrated in Figure 6.1.2-9. (Only these particular holes out of the overhead holes were testable. The rest were blocked by borehole debris.) Likewise, the AK borehole closest to the proposed niche wall became blocked close to the collar before any measurements could be taken. The other two, AK2 and AK3, were successfully profiled with air-k measurements at 0.3 m intervals. After excavation of the outer niche, the AK boreholes were again profiled. In Figure 6.1.2-10, comparison of the profiles for the two AK boreholes does not show as big a change as the boreholes above the niche in Figure 6.1.2-9. For the overhead boreholes, certain borehole sections change permeability more than others, whereas the change in geometric average (subscript "ga" in figures) for the AK boreholes alongside the excavation is smaller than it is for the overhead boreholes. The UL borehole and the AK2 borehole are roughly the same distance from their respective mined surfaces of the niche, but show a marked difference in change of geometric average of permeability.

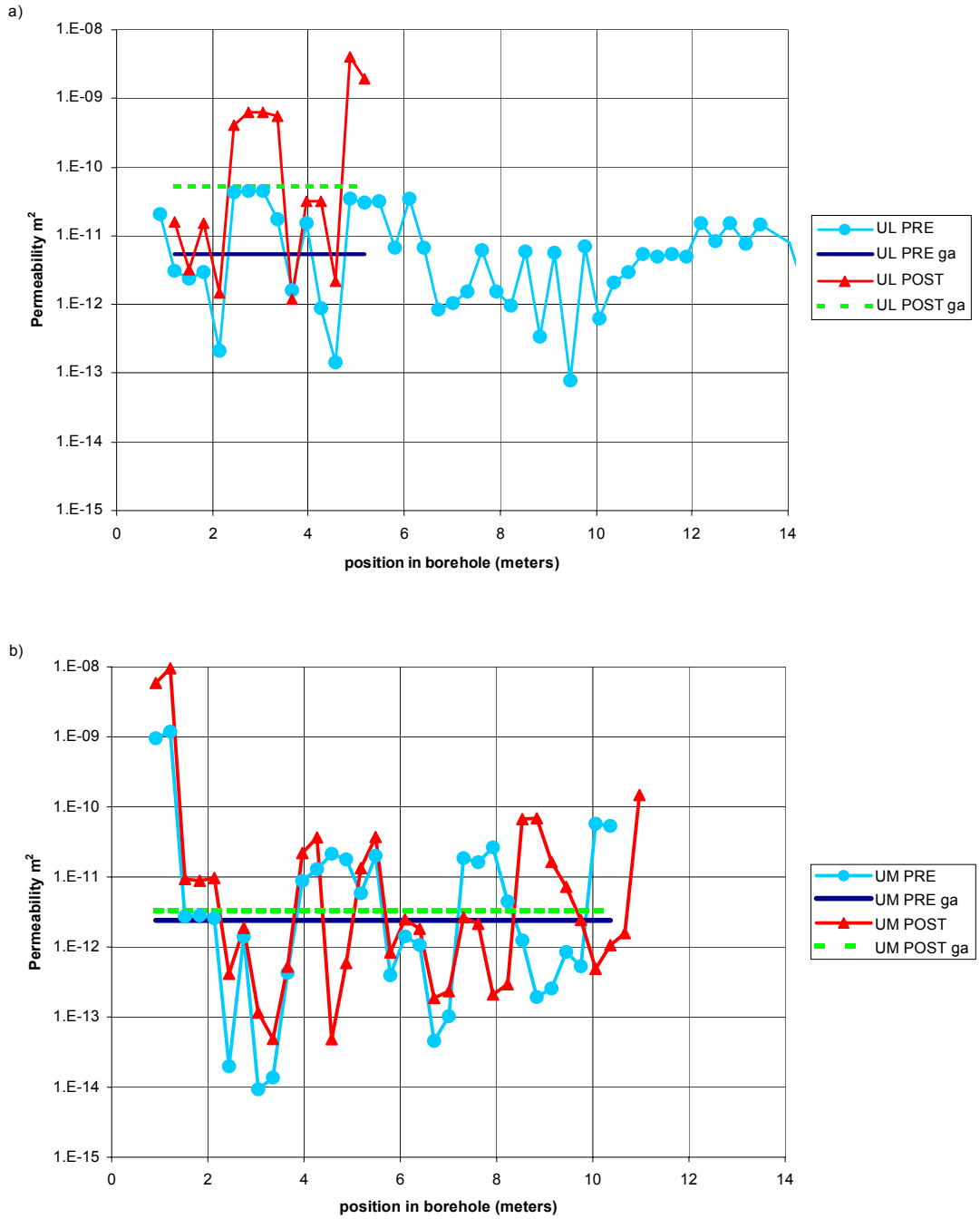

DTN: LB0012AIRKTEST.001 [154586] for pre-excavation data;
LB0110AKN5POST.001 [156904] for post-excavation data

Figure 6.1.2-9. Pre- and Post-Excavation Air-Permeability Profiles along Upper Boreholes at Niche CD 1620 (Niche 5)

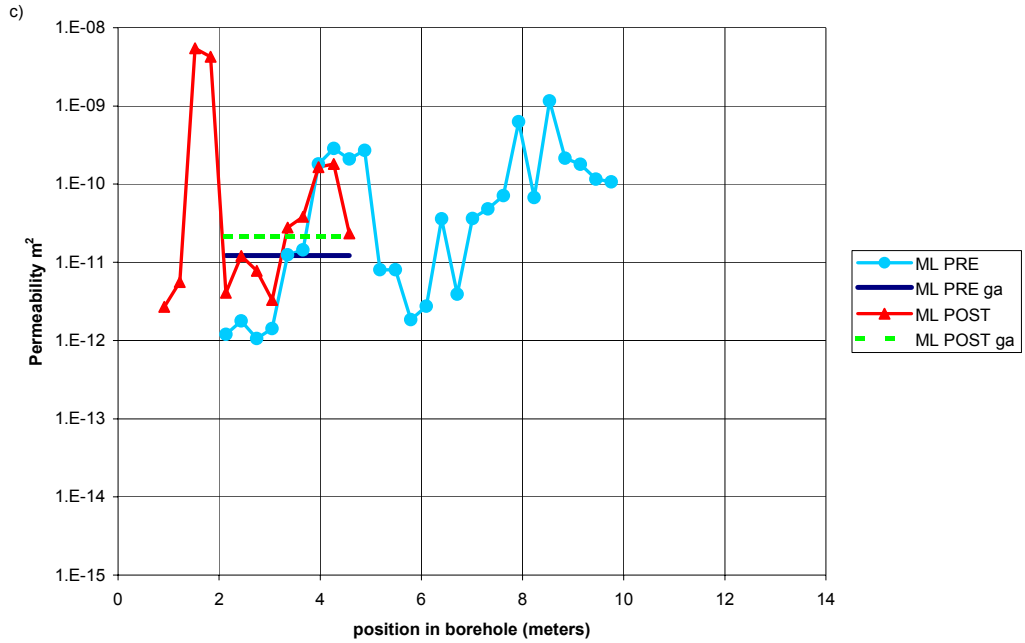

DTN: LB0012AIRKTEST.001 [154586] for pre-excavation data;
LB0110AKN5POST.001 [156904] for post-excavation data

Figure 6.1.2-9. Pre- and Post-Excavation Air-Permeability Profiles along Upper Boreholes at Niche CD 1620 (Niche 5) (continued)

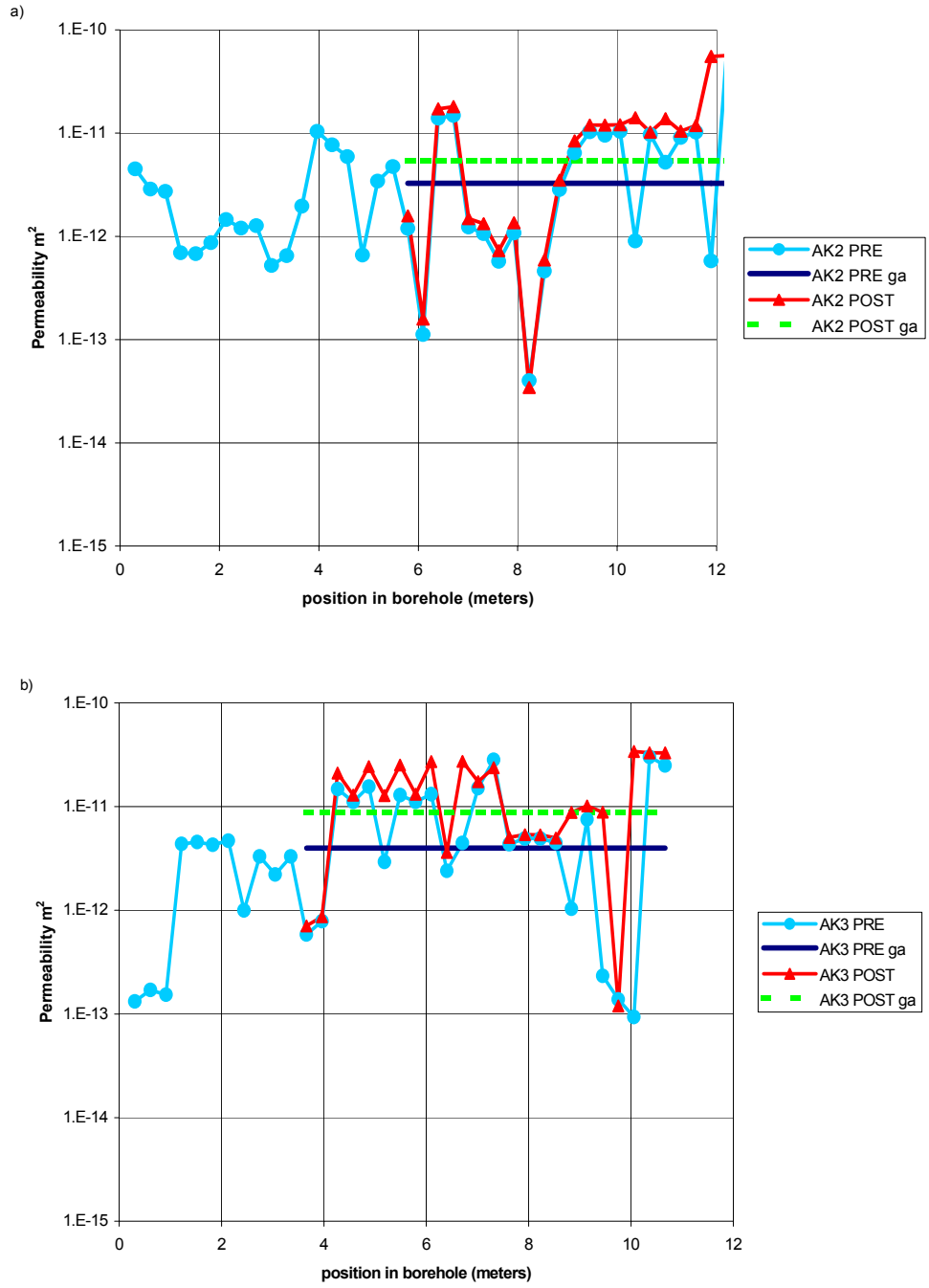

DTNs: LB002181233124.001 [146878]; LB0110AK23POST.001 [156905]

Figure 6.1.2-10. Pre- and Post-Excavation Air-Permeability Profiles along AK Side Boreholes at Niche CD 1620 (Niche 5)

6.1.2.2.2 Vertical Permeability Profiles

Alcove 8 afforded the first opportunity to obtain near-vertical borehole air-permeability profiles in any of the drifts at Yucca Mountain. Figures 6.1.2-11 (a–f) show the permeability as a function of depth for each of the boreholes drilled from the invert of Alcove 8. All boreholes have local peaks and sections of relatively uniform permeabilities along their depths, and high permeabilities towards the bottom. Boreholes 1, 3, and 4 exhibit relatively long sections of low permeability followed by a 3 to 5 order-of-magnitude increase starting at about 6 m for Borehole 1, 10 m for Borehole 3, and 8 m for Borehole 4. These permeability increases could be locally associated with the Tptpul-Tptpmn interface which is approximately midway between Alcove 8 and Niche 3107 (Niche 3), as discussed in Section 6.12.1.2 on the geometry and in Section 6.12.3 on the results of geophysical imaging of the drift-to-drift test bed.

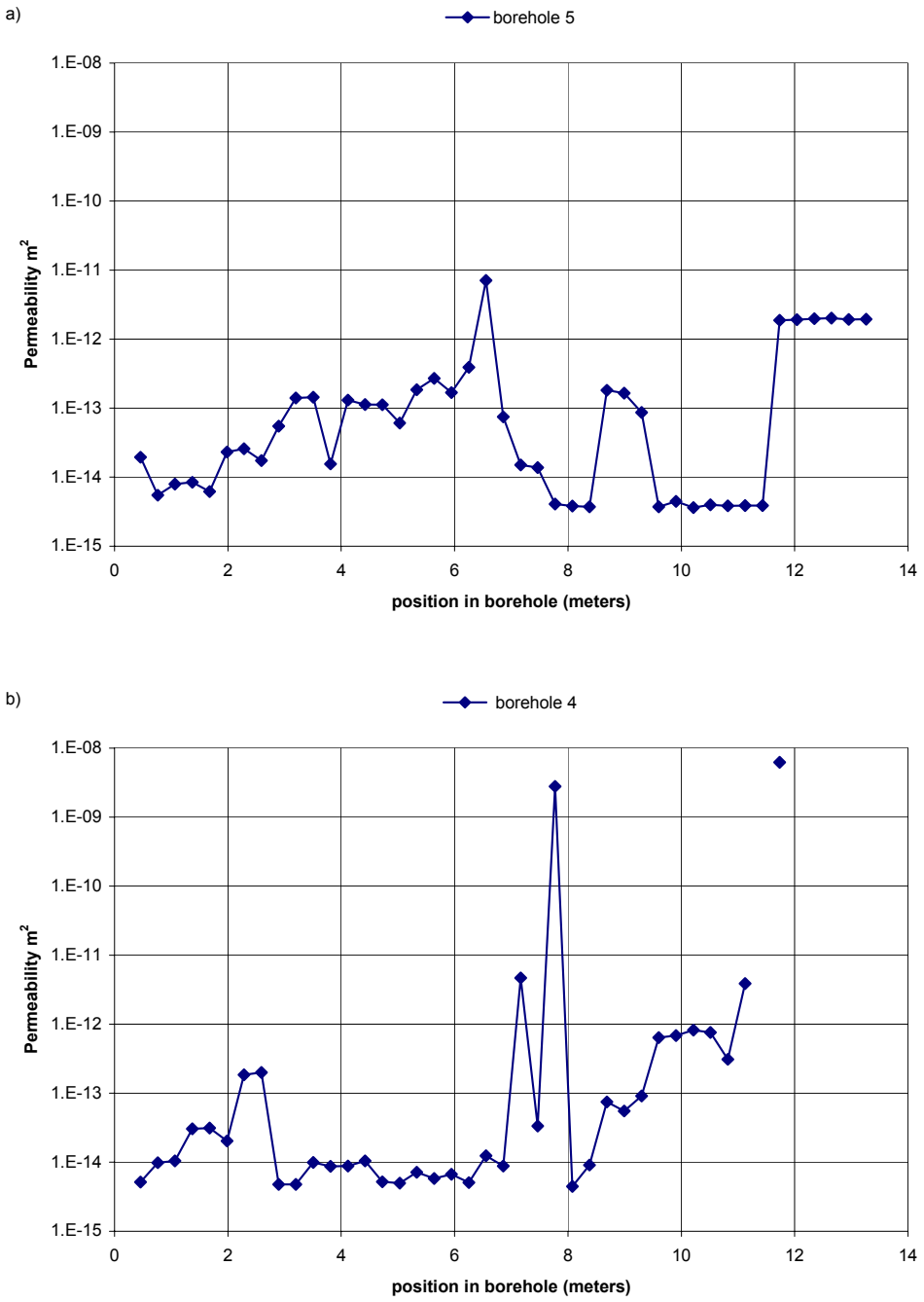

DTN: LB0302ALC8AIRK.001 [164748]

Figure 6.1.2-11. Air-Permeability Profiles down Boreholes in Alcove 8

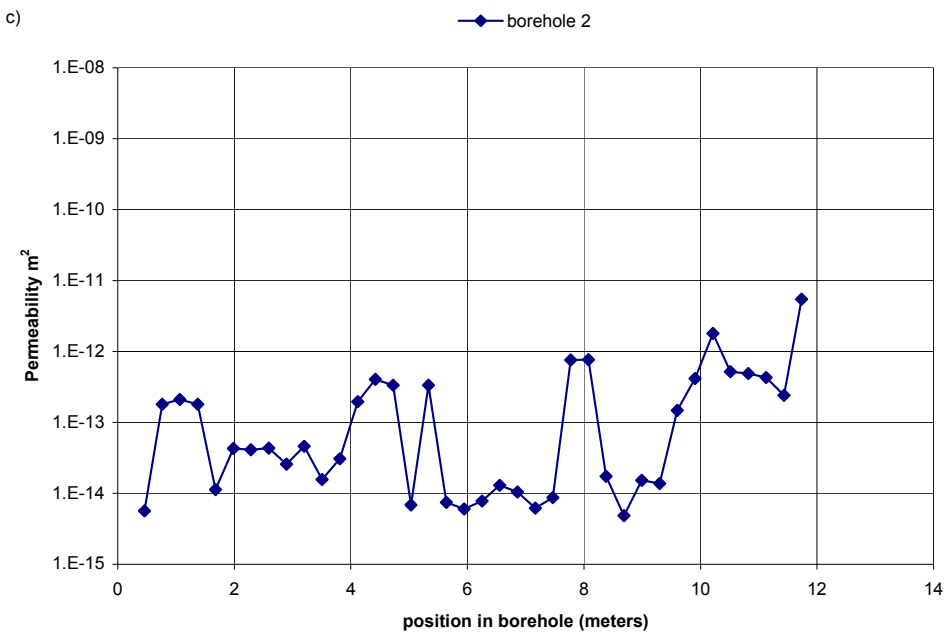

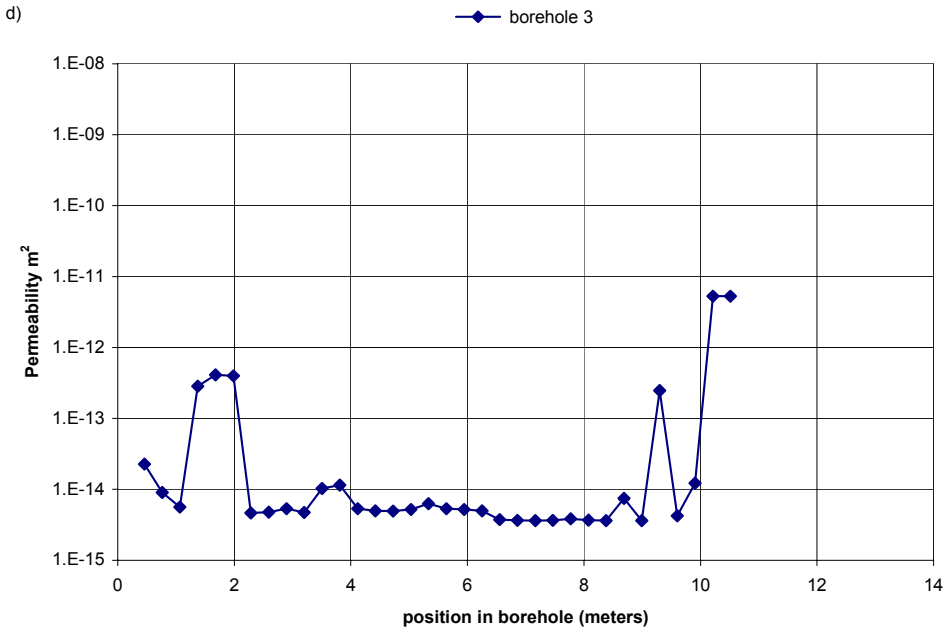

DTN: LB0302ALC8AIRK.001 [164748]

Figure 6.1.2-11. Air-Permeability Profiles down Boreholes in Alcove 8 (continued)

e)

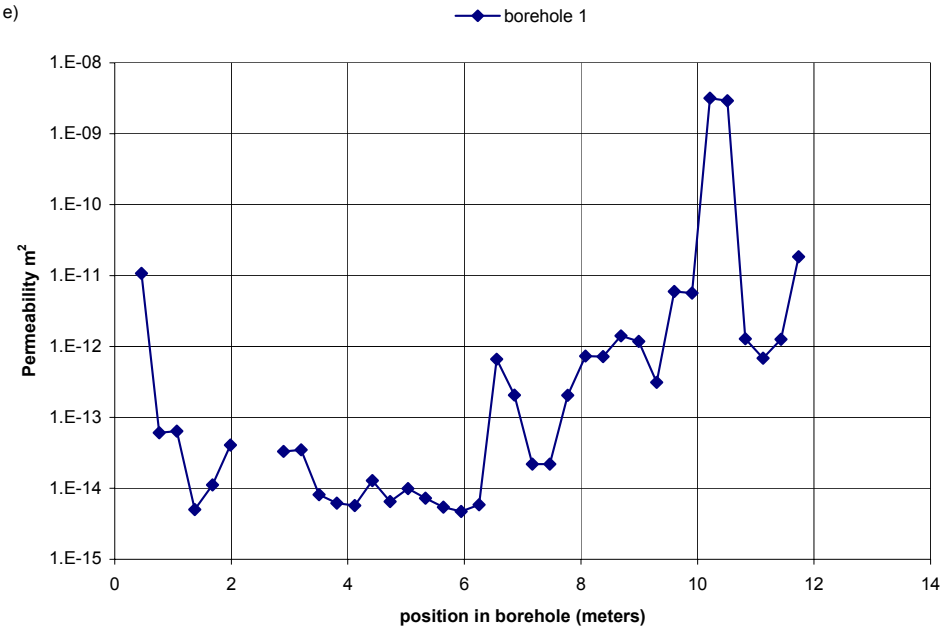

f)

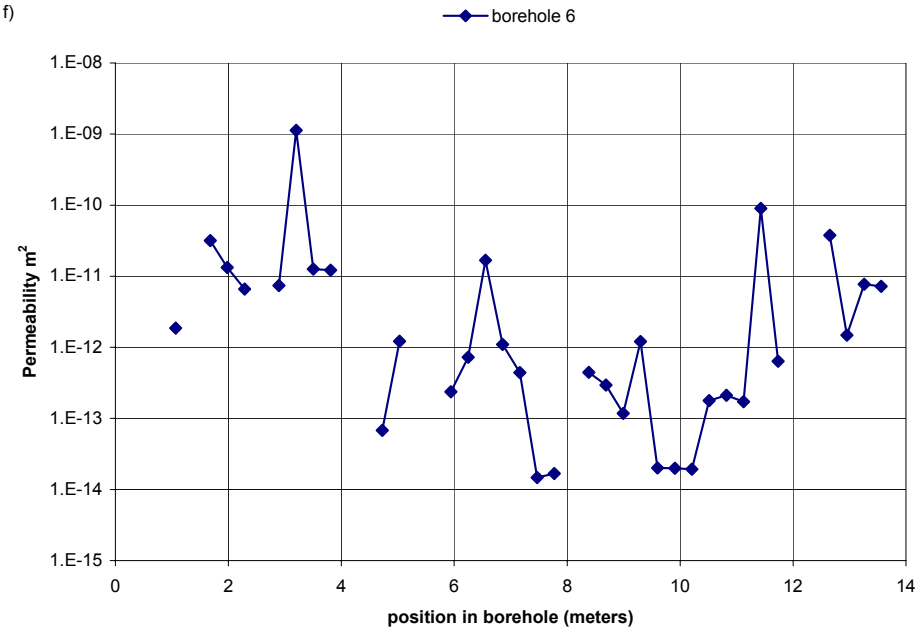

DTN: LB0302ALC8AIRK.001 [164748]

Figure 6.1.2-11. Air-Permeability Profiles down Boreholes in Alcove 8 (continued)

6.1.2.3 Permeability Change as a Function of Initial Permeability

Another type of plot can highlight the difference in the character of borehole permeability changes (caused by nearby excavation). The post-excavation permeability for a particular interval in a borehole, divided by the pre-excavation permeability for the same interval in a borehole, is the interval change ratio caused by excavation. A plot of the log change ratio versus the log pre-excavation permeability value can show a dependence of the change on the initial value. Figure 6.1.2-12 and Figure 6.1.2-13 show the changes for three of the overhead boreholes at Niche CD 1620 (Niche 5) and for two of the side boreholes, respectively. The overhead boreholes show some correlation to the notion that the initially low permeability zones change the most. For the side boreholes, however, there is a much weaker overall trend. See Attachment IX.5 for details on ratio, trend, and slope calculations. The slopes of the trend lines on the change ratio plots indicate some measure of correlation. Two individual slopes can be made out on the plot for the AK holes, one indicating a small population of intervals with strong change dependency, and one indicating a larger population with no dependency. The populations themselves are each evenly distributed over the initial permeabilites.

Change ratios for the pre- and post-excavation testing previously undertaken at Niche 3650 (Niche 2), Niche 3107 (Niche 3), and Niche 4788 (Niche 4) (all in overhead boreholes) are shown in Figure 6.1.2–14, Figure 6.1.2-15, and Figure 6.1.2-16, respectively. The change-ratio plots for these niches in the middle nonlithophysal zone of TSw show stronger correlation between initial permeability and the change ratio. Additionally, from the geometric averages in the profile plots, it can be seen that all these middle nonlithophysal niches show a larger average excavation effect than the boreholes at Niche CD 1620 (Niche 5) in the lower lithophysal zone of the TSw.

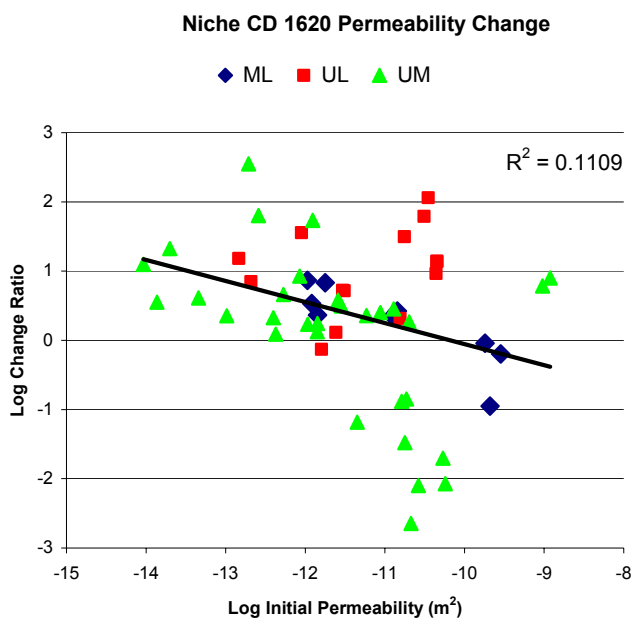

DTN: LB0310AIRK0015.001 [OUTPUT]

Figure 6.1.2-12. Change-Ratio Plot for Niche CD 1620 (Niche 5) Overhead Boreholes

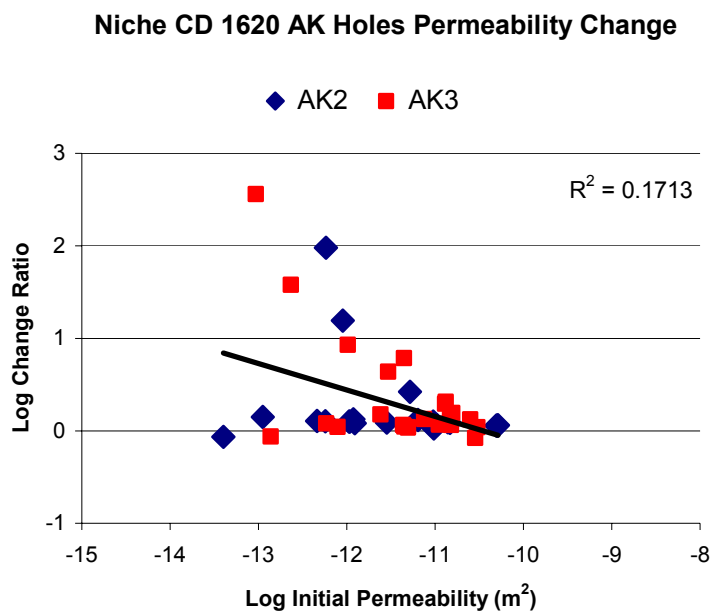

DTN: LB0310AIRK0015.001 [OUTPUT]

Figure 6.1.2-13. Change-Ratio Plots for Niche CD 1620 (Niche 5) AK Boreholes

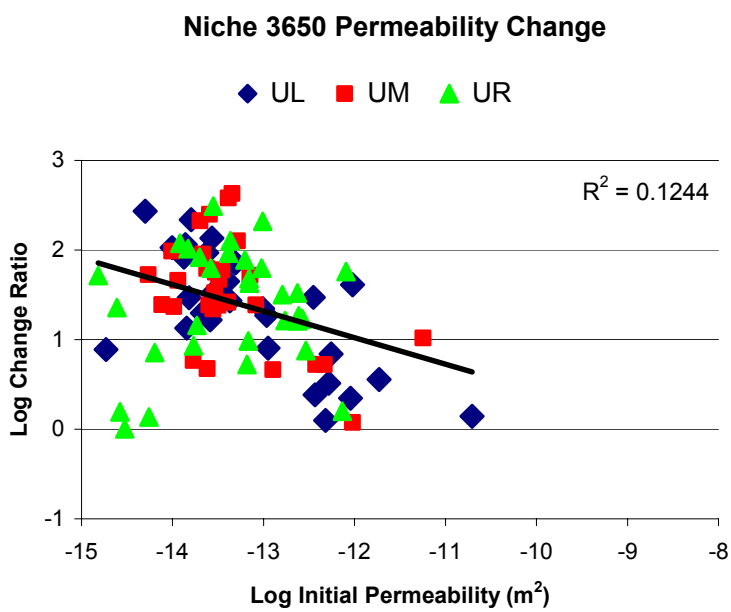

DTN: LB0310AIRK0015.001 [OUTPUT]

Figure 6.1.2-14. Change-Ratio Plot for Niche 3650 (Niche 2)

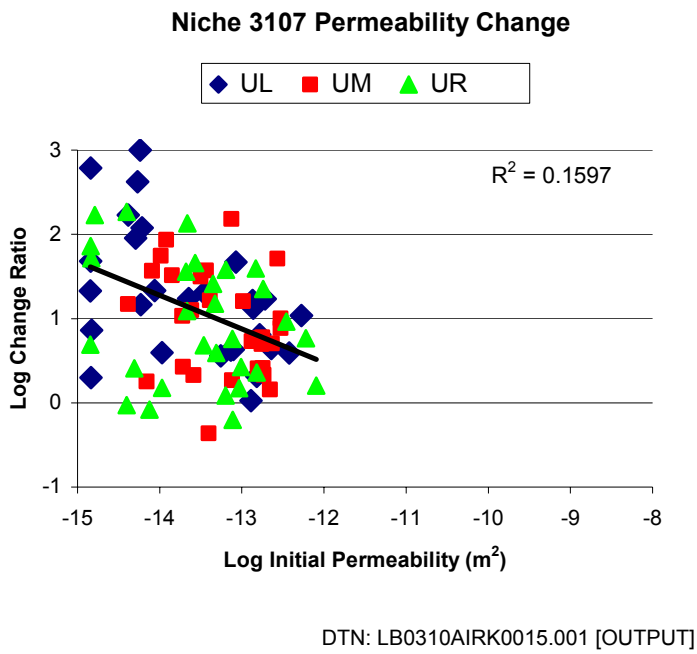

Figure 6.1.2-15. Change-Ratio Plot for Niche 3107 (Niche 3)

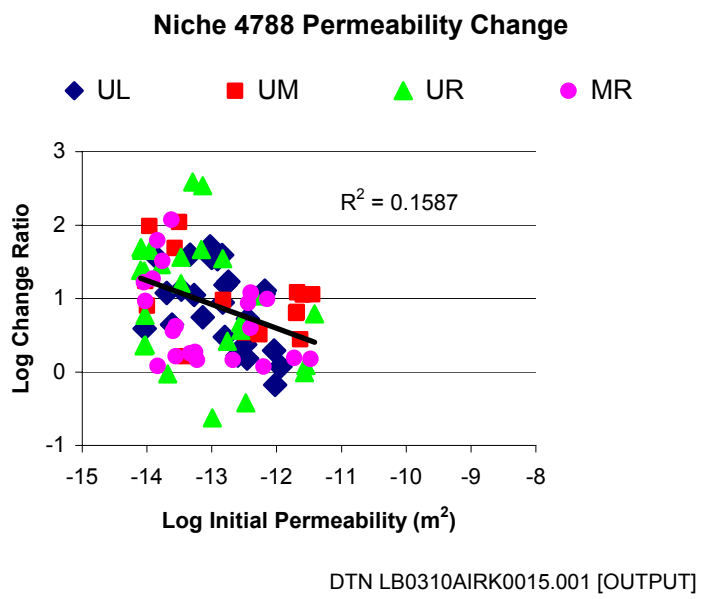

Figure 6.1.2-16. Change-Ratio Plot for Niche 4788 (Niche 4)

6.1.2.4 Statistical Summary of Air-Permeability Distributions

Table 6.1.2-1 summarizes the average (arithmetic and geometric) values, standard deviations, and ranges of variations in pre- and post-excavation permeability of individual boreholes and of whole niche sites (see Attachment IX.1 for calculations). Also included are the averages, deviations, and ranges of interval change ratios for individual boreholes and whole niches. (The ratios are calculated from the pre- and post-excavation permeability values for each interval before the statistical analyses.) Table 6.1.2-2 shows similar information for the overhead boreholes at Niche CD 1620 (Niche 5). Table 6.1.2-3 shows this information for the side holes at Niche CD 1620 (Niche 5). For assessing the excavation-induced impacts, the analyses in Table 6.1.2-1, Table 6.1.2-2, and Table 6.1.2-3 incorporate retested boreholes only. Drift-scale variations along boreholes and among different boreholes within the same niche test site are larger than differences among different sites. Table 6.1.2-4 shows the statistics from the single data set for Alcove 8. Variability among intervals within boreholes in this case straddle that for the whole site. Also, Alcove 8 shows the largest range of values of any site yet tested.

Table 6.1.2-5 summarizes the geometric means and standard deviations of all clusters of boreholes tested in the ESF as a function of site location and rock type. The permeability values from the excavated boreholes are included in these averaging results. Pre-excavation (log geometric) means and standard deviations were derived from averaging over all possible boreholes in each niche or alcove cluster. (The middle- and lower-level boreholes supplement the upper boreholes to characterize the 3-D space in the test beds and locate flow paths under pre-excavation conditions. After excavation with only upper boreholes in a horizontal plane remaining, the air-permeability tests can characterize only the zones above the niche ceilings.) Because the pre-excavation holes at Niche CD 1620 (Niche 5) are the same set as those for post-excavation testing, both types of tests are included for this case.

Each borehole cluster has a distinct air-permeability character. The spatial variability in permeability is considerable at the borehole-interval scale of 0.3 m before averaging over the 10 m scale along the boreholes and the 100 m^3 volume over the borehole clusters (3 to 7 boreholes). Niche 3107 (Niche 3) and Niche 3566 (Niche 1) each have a "radial" entry in the table, which indicates boreholes that are drilled from inside the niches after excavation. Permeability values from these boreholes for Niche 3107 (Niche 3) (profiles not shown) vary little from those of the pre-excavation boreholes, indicative of the uniformity of the formation around Niche 3107 (Niche 3). For Niche 3566 (Niche 1), however, the radial boreholes that were tested ran through the brecciated zone within the niche wall, and thus exhibited higher permeability than that for the pre-excavation boreholes. The results for the borehole cluster at Alcove 8 show highest standard deviation, which may result from the boreholes' traversal of the contact. The entries in Table 6.1.2-5 for Alcove 4 and Alcove 6 are included for completeness and will be discussed in Section 6.5.

Standard deviation from the statistical analysis is a measure of variability, also referred to as aleatory uncertainty, for natural randomness or heterogeneity (as discussed in Section 6 and in BSC 2002 [158794]). The air-permeability measurement is one of the most effective methods to quantify the natural variability of unsaturated fractured rocks (Cook 2000 [165411]).

Table 6.1.2-1. Summary Statistics of Air Permeability (m^2) along Boreholes above Niches

Borehole	Niche 3650 (Niche 2)			Niche 3107 (Niche 3)			Niche 4788 (Niche 4)		
	Pre-Excavation	Post-Excavation	Post/Pre Ratio*	Pre-Excavation	Post-Excavation	Post/Pre Ratio*	Pre-Excavation	Post-Excavation	Post/Pre Ratio*
Geometric Mean									
UL	7.26E-14	2.09E-12	20.75	2.22E-14	4.55E-13	20.51	1.41E-13	1.07E-12	7.62
UM	4.29E-14	1.64E-12	33.29	5.81E-14	4.82E-13	8.72	1.81E-13	2.56E-12	11.09
UR	4.27E-14	1.01E-12	23.56	3.32E-14	2.64E-13	8.94	6.27E-14	6.27E-13	9.42
All 3	5.07E-14	1.51E-12	25.38	3.50E-14	3.87E-13	11.69	1.05E-13	1.20E-12	9.42
Arithmetic Mean									
UL	8.59E-12	2.98E-11	47.06	8.12E-14	1.46E-12	135.48	2.82E-13	2.07E-12	14.28
UM	1.01E-12	7.78E-12	72.98	1.14E-13	1.55E-12	21.36	8.59E-13	6.19E-12	26.43
UR	1.27E-13	4.59E-12	53.62	1.14E-13	1.04E-12	30.95	4.42E-13	3.79E-12	45.09
All 3	3.24E-12	1.40E-11	57.89	1.03E-13	1.35E-12	62.60	5.05E-13	3.99E-12	28.55
Minimum Value									
UL	1.86E-15	1.45E-14	0.67	1.44E-15	2.90E-15	1.06	9.16E-15	3.57E-14	0.67
UM	5.40E-15	9.88E-14	1.19	4.10E-15	1.24E-14	0.43	8.99E-15	6.56E-14	1.64
UR	1.53E-15	3.02E-15	1.01	1.43E-15	3.72E-15	0.63	8.01E-15	1.98E-14	0.24
All 3	1.53E-15	3.02E-15	0.67	1.43E-15	2.90E-15	0.43	8.01E-15	1.98E-14	0.24
Maximum Value									
UL	1.27E-10	7.15E-10	271.15	5.32E-13	7.99E-12	1229.23	1.15E-12	8.44E-12	51.54
UM	2.28E-11	1.01E-10	427.91	5.15E-13	1.40E-11	153.02	3.56E-12	2.50E-11	110.52
UR	8.07E-13	4.66E-11	310.67	8.06E-13	5.80E-12	184.13	3.83E-12	2.51E-11	386.90
All 3	1.27E-10	7.15E-10	427.91	8.06E-13	1.40E-11	1229.23	3.83E-12	2.51E-11	386.90
Range of Log									
UL	4.83	4.69	2.61	2.57	3.44	3.06	2.10	2.37	1.89
UM	3.63	3.01	2.56	2.10	3.05	2.55	2.60	2.58	1.83
UR	2.72	4.19	2.49	2.75	3.19	2.47	2.68	3.10	3.21
All 3	4.92	5.38	2.80	2.75	3.68	3.45	2.68	3.10	3.21
Std. Dev. of Log									
UL	1.18	0.84	0.69	0.81	0.83	0.83	0.58	0.57	0.54
UM	0.80	0.70	0.62	0.57	0.71	0.61	0.95	0.70	0.58
UR	0.73	1.05	0.66	0.79	0.90	0.74	0.85	0.94	0.84
All 3	0.93	0.88	0.66	0.74	0.82	0.75	0.79	0.78	0.67

Input: Niche 3650 (Niche 2) Pre- and Post-Excavation DTN: LB0011AIRKTEST.001 [153155]

Niche 3107 (Niche 3) Pre-Excavation DTN: LB980901233124.101 [136593], Post Excavation DTN: LB990601233124.001 [105888]

Niche 4788 (Niche 4) Pre-Excavation DTN: LB980901233124.101 [136593], Post-Excavation DTN: LB990601233124.001 [105888]

Summary: DTN: LB0310AIRK0015.001 [OUTPUT]

NOTE: *The post/pre ratio is the ratio of post-excavation to pre-excavation permeabilities. This ratio was calculated for each interval in each borehole. Values reported are the statistical measures (maximum, minimum, mean, etc.) of all post/pre ratios calculated for each borehole. For example, mean of (post/pre) ratio is not the same as the ratio of mean(post)/mean(pre).
*Where more than one measurement of permeability was made at a position, the least value is used in averaging.

Table 6.1.2-2. Summary Statistics of Air Permeability (m^2) along Boreholes above Niche CD 1620 (Niche 5)

Niche CD 1620 (Niche 5) Overhead			
Borehole	**Pre-Excavation**	**Post-Excavation**	**Post/Pre Ratio**
Geometric Mean			
ML	1.23E-11	2.14E-11	1.75
UL	5.54E-12	5.48E-11	9.89
UM	2.40E-12	3.32E-12	1.38
All 3	3.88E-12	9.19E-12	2.37
Arithmetic Mean			
ML	7.88E-11	5.15E-11	2.93
UL	1.75E-11	5.90E-10	22.75
UM	7.58E-11	4.90E-10	17.84
All 3	6.14E-11	4.44E-10	16.65
Minimum			
ML	1.06E-12	3.30E-12	0.11
UL	1.46E-13	1.19E-12	0.74
UM	9.28E-15	4.82E-14	0.00
All 3	9.28E-15	4.82E-14	0.00
Maximum			
ML	2.86E-10	1.82E-10	7.33
UL	4.53E-11	4.03E-09	115.10
UM	1.19E-09	9.51E-09	354.12
All 3	1.19E-09	9.51E-09	354.12
Range of Log			
ML	2.43	1.74	1.82
UL	2.49	3.53	2.19
UM	5.11	5.30	5.19
All 3	5.11	5.30	5.19
Std. Dev of Log			
ML	1.03	0.63	0.57
UL	0.87	1.22	0.63
UM	1.25	1.25	1.19
All 3	1.14	1.27	1.04

DTN: LB0012AIRKTEST.001 [154586] for pre-excavation data; LB0110AKN5POST.001 [156904] for post-excavation data

DTN: LB0310AIRK0015.001 [OUTPUT]

Table 6.1.2-3. Summary Statistics of Air Permeability (m^2) in Boreholes alongside Niche CD 1620 (Niche 5)

Niche CD 1620 (Niche 5) Side			
Borehole	**Pre-Excavation**	**Post-Excavation**	**Post/Pre Ratio**
Geometric Mean			
AK2	3.28E-12	5.41E-12	1.65
AK3	3.98E-12	8.81E-12	2.22
Both	3.61E-12	6.90E-12	1.91
Arithmetic Mean			
AK2	1.09E-11	1.58E-11	5.79
AK3	9.00E-12	1.50E-11	18.53
Both	9.93E-12	1.54E-11	12.16
Minimum			
AK2	4.01E-14	3.44E-14	0.86
AK3	1.46E-13	1.19E-12	0.84
Both	4.01E-14	3.44E-14	0.84
Maximum			
AK2	5.14E-11	5.88E-11	95.51
AK3	3.01E-11	3.40E-11	363.64
Both	5.14E-11	5.88E-11	363.64
Range of Log			
AK2	3.11	3.23	2.05
AK3	2.51	2.45	2.64
Both	3.11	3.23	2.64
Std Dev of Log			
AK2	0.82	0.83	0.44
AK3	0.72	0.61	0.61
Both	0.77	0.73	0.53

DTNs: LB002181233124.001 [146878] for pre-excavation data; LB0110AK23POST.001 [156905] for post-excavation data.

Table 6.1.2-4. Summary Statistics of Air Permeability (m^2) along Boreholes under Alcove 8

Alcove 8		
Borehole	**Geometric Mean**	**Arithmetic Mean**
BH1	1.76E-13	1.71E-10
BH2	6.41E-14	3.48E-13
BH3	1.33E-14	3.55E-13
BH4	6.29E-14	2.44E-10
BH5	5.11E-14	4.93E-13
BH6	1.11E-12	4.19E-11
All 6	8.67E-14	7.52E-11
	Minimum	**Maximum**
BH1	4.72E-15	3.17E-09
BH2	4.83E-15	5.46E-12
BH3	3.61E-15	5.28E-12
BH4	4.45E-15	6.25E-09
BH5	3.60E-15	7.06E-12
BH6	1.48E-14	1.13E-09
All 6	3.60E-15	6.25E-09
	Range of log	**Std Dev of log**
BH1	5.83	1.51
BH2	3.05	0.83
BH3	3.17	0.89
BH4	6.15	1.46
BH5	3.29	0.98
BH6	4.88	1.20
All 6	6.24	1.29

DTN: LB0302ALC8AIRK.001 [164748]

Table 6.1.2-5. Comparison of Geometric Means and Standard Deviations of Niches and Alcoves in the Exploratory Studies Facility at Yucca Mountain

Borehole Cluster	**Type of Site**	**log(k) (m^2)**	
		Mean	Standard Deviation
Niche 3566 (Niche 1) Pre-Excavation	Intersects brecciated zone	-13.0	0.92
Niche 3566 (Niche 1) Radial	Predominantly within brecciated zone	-11.8	0.66
Niche 3650 (Niche 2) Pre-Excavation	Moderately fractured welded tuff	-13.4	0.81
Niche 3650 (Niche 2) Post-Excavation	Post-excavation welded tuff	-11.8	0.88
Niche 3107 (Niche 3) Pre-Excavation	Moderately fractured welded tuff	-13.4	0.70
Niche 3107 (Niche 3) Post-Excavation	Post-excavation welded tuff	-12.4	0.82
Niche 3107 (Niche 3) Radial	Moderately fractured welded tuff	-13.8	0.92
Niche 4788 (Niche 4) Pre-Excavation	Highly fractured welded tuff	-13.0	0.85
Niche 4788 (Niche 4) Post-Excavation	Post-excavation welded tuff	-11.9	0.78
Niche CD 1620 (Niche 5) Pre-Excavation side	Highly porous lithophysal cavities; holes on side of excavation	-11.4	0.77
Niche CD 1620 (Niche 5) Post-Excavation side	Highly porous lithophysal cavities; holes on side of excavation	-11.2	0.73
Niche CD 1620 (Niche 5) Pre-Excavation overhead	Highly porous lithophysal cavities; holes above of excavation	-11.4	1.14
Niche CD 1620 (Niche 5) Post-Excavation overhead	Highly porous lithophysal cavities; holes above of excavation	-11.0	1.27
Alcove 4	Discretely faulted and fractured non-welded tuff	-13.0	0.93
Alcove 6	Highly fractured post-excavation welded tuff	-11.9	0.67
Alcove 8	Transition from upper lithophysal to welded fractured nonlithophysal in near-vertical boreholes	-13.1	1.29

DTNs: LB0011AIRKTEST.001 [153155], LB980901233124.101 [136593], LB990601233124.001 [105888], LB980901233124.004 [105855], LB980901233124.009 [105856], LB980912332245.001 [110828]; LB0302ALC8AIRK.001 [164748]; LB0012AIRKTEST.001 [154586]; LB002181233124.001 [146878]; LB0110AK23POST.001 [156905]; LB0110AKN5POST.001 [156904]

Summary: DTN: LB990901233124.004 [123273] (enhanced with Niche CD 1620 [Niche 5] and Alcove 8 results)

INTENTIONALLY LEFT BLANK

6.2 ANALYSIS AND INTERPRETATION OF THE NICHE LIQUID-RELEASE AND SEEPAGE-TEST DATA

The ESF Drift Seepage Test and Niche Moisture Study characterizes the seepage process and furthers our understanding of how moisture could seep into drifts. Specific objectives of the study include:

- Measuring *in situ* hydrological properties of the repository host rock for use in *Seepage Calibration Model and Seepage Testing Data* (BSC 2003 [162267]) and *Seepage Model for PA Including Drift Collapse* (BSC 2003 [163226])
- Providing a database of liquid-release and seepage data that can be used to evaluate seepage and other related UZ processes
- Evaluating drift-scale seepage processes to quantify the extent to which seepage is excluded from entering an underground cavity
- Determining the seepage threshold below which percolating water will not seep into a drift.

The objectives of the study are realized through a combination of field experiments, including air-injection, liquid-release, and seepage tests.

Analytic solutions are used in the data analyses presented in this section to estimate the seepage thresholds, capillary barrier strengths, water-potential values, and characteristic relationships along seepage flow paths. Local homogeneity is the main approximation in the analytic solutions used in estimating the air-permeability values and liquid seepage flow field. Numerical models have been formulated in the Model Report *Seepage Calibration Model and Seepage Testing Data* (BSC 2003 [162267]) to evaluate the effects of spatial heterogeneity on the effective seepage parameters, with the heterogeneity field based on the air-permeability distribution (described in Section 6.1). The seepage calibration model is the basis for other model reports in estimating the seepage fraction and distribution over the potential waste-emplacement drifts. The subsequent model reports include *Seepage Model for PA Including Drift Collapse* (BSC 2003 [163226]) and *Abstraction of Drift Seepage* (BSC 2003 [165564]).

Some of the early results based on short-duration releases of pulses above the first niche tested are enhanced by later tests in other niches with long durations, so that the liquid-release rates and seepage rates can approach steady state. The short-duration tests, originally designed to simulate the arrivals of episodic percolation events through fast flow paths into ventilated drifts, do not provide the data sets needed by the seepage calibration model and other PA models, which emphasize steady-state conditions in sealed drifts under post-emplacement conditions.

6.2.1 Review of Data Obtained from Liquid-Release and Seepage Tests Conducted at Niches

This section provides a general overview of the tests, including field activities performed prior to, during, and after the niches were excavated.

6.2.1.1 Pre-Excavation Liquid-Release Test Data

Before seepage tests in excavated niches, the niche test sites are characterized by air-permeability tests (Section 6.1) and by liquid-release tests. The pre-excavation liquid-release tests introduce a finite amount of dyed water to characterize the flow paths within the niche space. The main objective is to determine the relative strength between the gravity force that moves the liquid downward and the capillary forces that tend to spread the liquid laterally. The characterization of the flow paths is conducted during niche excavation (Section 6.2.1.2).

Hundreds of air-injection tests were conducted in the boreholes at niche sites prior to excavation. The test results were used to determine the distribution of single-borehole air permeabilities within the rock mass (refer to Section 6.1 in this scientific analysis report). These data were then used to select test intervals for subsequent liquid-release tests. The intervals selected for liquid-release testing exhibited a wide range of air permeabilities, including both high and low values.

Liquid-release tests were conducted in the same boreholes as the air-injection tests by pumping water containing colored or fluorescent dyes at a constant rate into various 0.3 m long test intervals. A finite amount of dye-spiked water, typically 1 liter, was introduced into each test interval, slowly to minimize buildup of fluid pressure in the test interval. Various colored and fluorescent tracers were used during the study to document the flow path traveled by the wetting front. Hereafter, the term “water” will be used to describe the test fluid, which may or may not have contained tracer.

Pre-excavation liquid-release tests were performed during early June and early August 1997, in boreholes installed prior to the excavation of Niche 3566 (Niche 1) and Niche 3650 (Niche 2), respectively. Pre-excavation liquid-release tests were performed at Niche 3107 (Niche 3) and Niche 4788 (Niche 4), starting in late April and late June 1998, respectively. Pre-excavation liquid-release tests were also performed at Niche CD 1620 (Niche 5) in the lower lithophysal zone in April 2000. The data from these pre-excavation tests, including the mass of water released, pumping rates and times, and liquid-release rates, were tabulated and entered into the TDMS, and assigned DTN: LB980001233124.004 [136583] for Niche 3566 (Niche 1) and Niche 3650 (Niche 2); DTN: LB980901233124.003 [105592] for Niche 3107 (Niche 3) and Niche 4788 (Niche 4); and DTN: LB0102NICH5LIQ.001 [155681] for Niche CD 1620 (Niche 5). The tables include directly measured mass, pumping rates, return flow rates, and derived quantities of average liquid release rates from the differences of the measured rates.

6.2.1.2 Niche Excavation Activities

The niches were excavated with an Alpine Miner, a mechanical device, using minimal water to observe and photograph the distribution of fractures and dye within the welded tuff. As reported in DTN: LB980001233124.004 [136583], dye was observed along individual fractures as well as along intersecting fractures to depths ranging from 0 to 2.6 m below the liquid-release points at the Niche 3566 (Niche 1) and Niche 3650 (Niche 2) sites. Dye was observed at a maximum depth of about 1.2 m below the release point at Niche 3107 (Niche 3) and about 1.8 m at Niche 4788 (Niche 4), as reported in DTN: LB980901233124.003 [105592]. Dye was observed at a maximum depth of about 1.4 m below the release point at Niche CD 1620 (Niche 5), as reported in DTN: LB0102NICH5LIQ.001 [155681]. (In this scientific analysis report, TDMS DTN and data report table name are both identified if many files are in a given DTN.) Flow of water through a relatively undisturbed fracture-matrix system was documented in this manner.

During the mining operation at Niche 3566 (Niche 1) and Niche 3650 (Niche 2), two types of flow paths were observed in the field, based on the observed pattern of dye: (1) flow through individual or small groups of high-angle fractures; and (2) flow through several interconnected low- and high-angle fractures, creating a fracture network. Dye was observed along individual fractures and fracture networks to a maximum depth of 2.6 m below the release points in the middle nonlithophysal zone (Tptpmn) of TSw. The vertically elongated dye pattern suggests that water is predominantly flowing downwards. In contrast, an approximately spherical dye pattern centered at the release point was observed at Niche CD 1620 (Niche 5), located in the lower lithophysal zone (Tptpll) of TSw. Dye was observed in fractures and lithophysae to a maximum depth of 1.4 m. Here, the dye patterns were more symmetric, with the lateral edges of the wetted area lying about equal distance from the release point.

Figure 6.2.1-1 compares examples of flow paths observed in the Tptpmn at Niche 3566 (Niche 1) with dye patterns observed in the Tptpll at Niche CD 1620 (Niche 5) (See Section 6.1.2.2 for the observation of a damp feature included in the figure). The observed damp feature and the dye patterns suggest that flow through fractures in the Tptpmn is predominately gravity-driven. In contrast, the symmetry of the dye patterns observed in the Tptpll suggests that capillary forces may be more important in this zone.

Dye was observed in numerous lithophysae in the Tptpll. There was no direct field evidence that water accumulated and dripped into the cavities, even though the liquid-release fluxes applied during the test were 1,000 times greater than the natural flux estimated at 10 mm/yr. No dye stains on the ceiling were observed to line up directly above stains on the floor of the cavities. An example of dye observed on the floor of a lithophysal cavity is illustrated in Figure 6.2.1-1d, suggesting capillary-induced upward fluid movement is a likely mechanism to introduce fluid into the cavity.

It is surprising that capillary forces appear to be stronger in the Tptpll, because the average air-permeability of the Tptpll is greater than the Tptpmn. Typically, capillary forces are less important in higher-permeability media than in lower-permeability materials. This may indicate that the air-permeability measurements performed in the Tptpll are influenced by the lithophysal cavities, which may connect relatively large fractures with smaller fractures, effectively contributing to the relatively strong capillarity.

Note that some of the lithophysae had a thick layer of drill cuttings (i.e., dust) coating their surfaces. This layer of dust could influence the flow (dye) patterns and depth of wetting-front migration observed in the Tptpll. This dust was introduced into the cavities intersecting the borings when the boreholes were air cored. The dust could act as a highly transmissive surface zone (compared to the rock matrix) that could enhance the uniform spread of the wetting front. The dust could also impede the movement of water and dye through the fractures by imbibing and retaining the moisture close to the point of release.

In general, the maximum distance that the wetting front traveled through the Tptpmn from the point of injection to the furthest point of observation increased with the mass of water injected. The data did not show that the type of flow (i.e., network or vertical fracture flow) had any significant influence on the maximum travel distance. Figure 6.2.1-2 shows that on average, the wetting front traveled much deeper (i.e., had a larger aspect ratio) for tests conducted in the Tptpmn compared to tests performed in the Tptpll. Computation of the aspect ratio was performed in the Excel spreadsheet documented in Attachment II, Table II-1. The average line for Tptpll in Figure 6.2.1-2 is influenced by a single data point with high aspect ratio (possibly associated with a fracture or fractures connected to the borehole—Trautz 2001 [157022] p. 69). Without this data point, the average is much closer to 1 (i.e., the aspect ratio of a spherical pattern.)

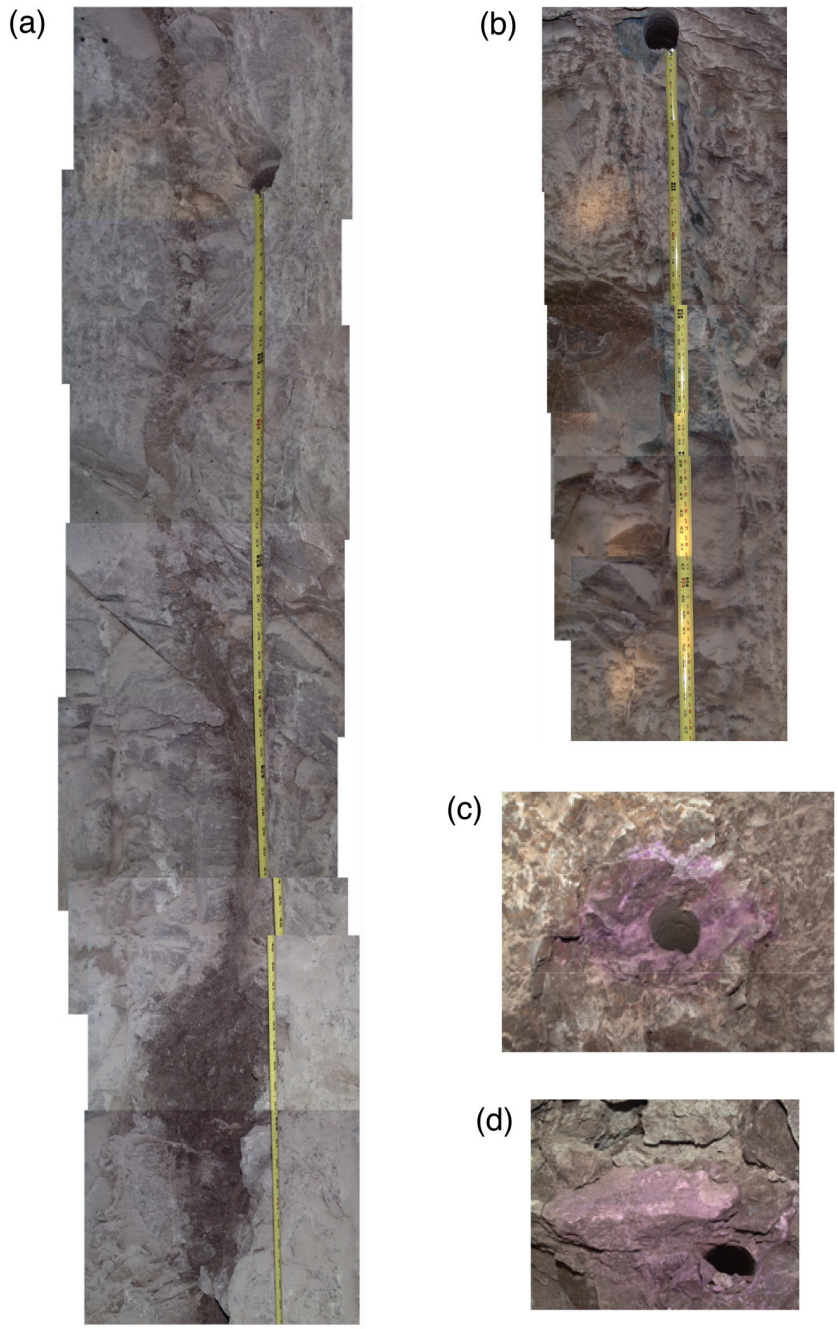

Source: Wang et al. (1999 [106146], Figures 4a, 4c); Trautz (2001 [157022] pp. 79, 84).

Figure 6.2.1-1. Photographic Illustrations of Flow Paths Observed During Niche Excavations: (a) Ambient Flow Path at Niche 3566 (Niche 1), (b) Blue-Dyed Flow Path at Niche 3566 (Niche 1), (c) Pink-Dyed Flow Path at Niche CD 1620 (Niche 5), (d) Pink Stain on the Floor of a Lithophysal Cavity at Niche CD 1620 (Niche 5)

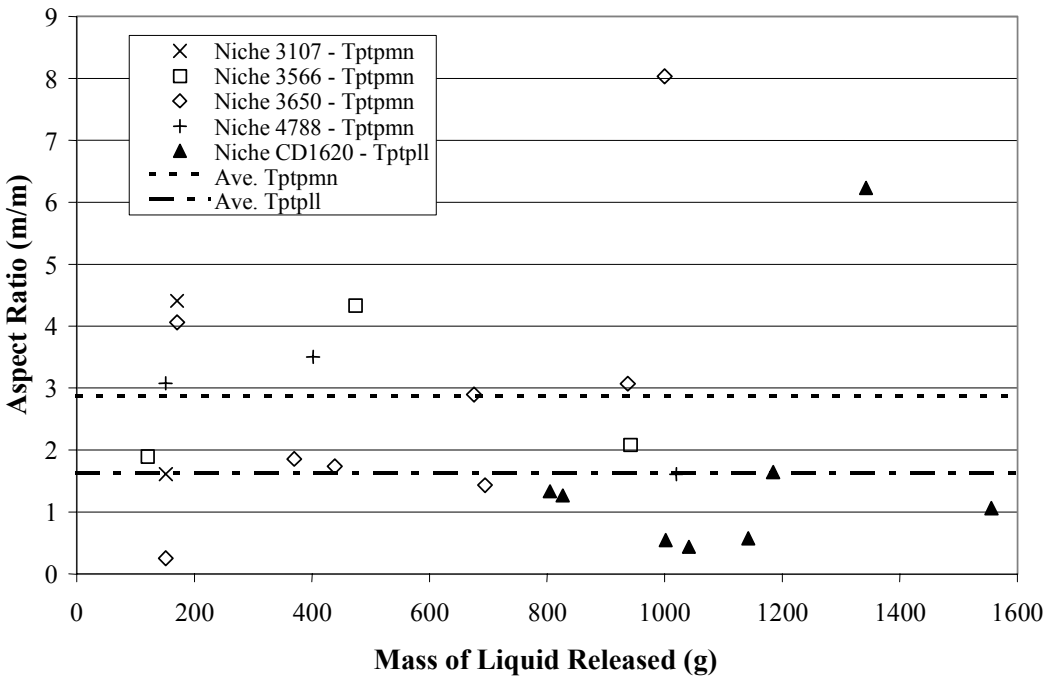

DTN: LB980001233124.004 [136583], DTN: LB980901233124.003 [105592],
DTN: LB0102NICH5LIQ.001 [155681].
DTN: LB0110LIQR0015.001 [OUTPUT]

Figure 6.2.1-2. Mass of Water Released Versus Aspect Ratio

6.2.1.3 Post-Excavation Seepage Tests

A series of seepage tests was performed at Niche 3107 (Niche 3), Niche 3650 (Niche 2), and Niche 4788 (Niche 4). In general, the tests were used to quantify the amount of water seeping into the drift from a localized water source of known duration and intensity. The tests were also used to establish the niche seepage-threshold (K_o^*), defined as the largest flux of water that can be introduced into the test borehole without resulting in seepage into the niche. The borehole flux values were derived from the pumping rate and the wetted area estimated for the borehole interval. This definition of niche seepage threshold is different from the definition used by PA, in which the seepage threshold related to the steady-state background percolation flux averaged over drift scale and site scale areas.

The seepage tests were conducted after the niches were excavated by pumping water into select test intervals in borehole UL, borehole UM, and borehole UR located above each niche. The distance from the test intervals to the niche ceiling ranges from 0.58 to 1.23 m for all the niche sites. (Computation of the distance is inserted in an Excel spreadsheet documented in Attachment II, Table II-2.) The tests were performed by sealing a short interval of borehole using an inflatable packer system, similar to the system used in air-injection tests as described in Attachment I. Any water that migrated from the borehole to the niche ceiling and dripped into the opening was captured and weighed.

For each packer interval, a liquid-return (overflow) line prevented buildup of excess pressure. If the liquid injection rate was high and return flow was observed, the liquid-release rate was

determined by the difference between injection flow rate and return flow rate (if any). The observation of return flows would indicate that the pumping rate exceeded the saturated hydraulic conductivity of the borehole interval. (For tests with small liquid volume in cases with significant storage in the borehole interval, no return flow did not imply that the pumping conditions represented unsaturated conditions.)

6.2.1.3.1 Niche 3650 (Niche 2) Seepage-Test Data

Forty niche seepage tests were performed on 16 test intervals positioned above Niche 3650 (Niche 2) beginning in late 1997 and ending in early 1998. Water migrated through the rock and seeped into the niche in 10 out of the 16 zones tested. The niche seepage threshold was determined for the 10 zones that seeped. Seepage and liquid-release data were tabulated and entered into the TDMS, where it was assigned DTN: LB980001233124.004 [136583].

The mass of water released to the formation was computed by mass balance. In turn, the liquid-release rate (Q_s) for each test was computed by dividing the mass released by the respective duration of each test; thus, these values represent time-averaged rates. The rate at which water was released to the formation ranged from 0.007 to 2.892 g/s, and the total mass released ranged from 274.5 to 5597.5 g per test, as summarized in DTN: LB980001233124.004 [136583].

When water appeared at the niche ceiling during a test and dripped into the opening, it was collected in the capture system and weighed. Figure 6.2.1-3 shows the approximate location of the capture system and test intervals relative to the niche boundaries, and the sequence of dyes and number of tests performed on each test interval. The wetting front typically arrived at the niche ceiling directly below the test zone. Most of the water was typically captured in only one or two 0.3 × 0.3 m cells located directly beneath the test interval.

In the immediate vicinity of locations where the niche ceiling and the conducting fractures intersect, the relative humidity could be high from local evaporation. However, the localized humid conditions were not met everywhere within the niche and/or the ESF Main Drift. Maintenance of high relative humidity conditions was important for long-term seepage tests, since the evaporation effects could have a substantial impact on the analysis of seepage data, with models setting post-emplacement high-humidity conditions in seepage threshold estimation. The potential impact of evaporation effects are discussed in Section 6.7 of the Model Report U0080 *Seepage Calibration Model and Seepage Testing Data* (BSC 2003 [162267]).

The mass of water captured ranged from 0.0 to 568.6 g per test, as reported in DTN: LB980001233124.004 [136583]. The niche seepage percentage is defined as the mass of water that dripped into the capture system, divided by the mass of water released to the rock:

$$\textit{Niche Seepage Percentage} = 100 \times \frac{\text{"}\textit{Mass Captured}\ (g)\text{"}}{\text{"}\textit{Mass Released}\ (g)\text{"}} \qquad \text{(Eq. 6.2.1-1)}$$

The niche seepage percentage ranged from 0% for zones that did not seep, to 56.2% for a predominantly gravity-driven flow through a highly saturated fracture (DTN: LB980001233124.004 [136583]).

The niche seepage tests at Niche 3650 (Niche 2) were conducted with a relatively small amount of liquid over short duration, with multiple tests over multiple borehole intervals. To address the model needs of steady-state data in controlled relative humidity conditions, the later tests in Niche 3107 (Niche 3) and Niche 4788 (Niche 4) were conducted in selected borehole intervals with large amounts of liquid over a long duration, as described in the following two sections.

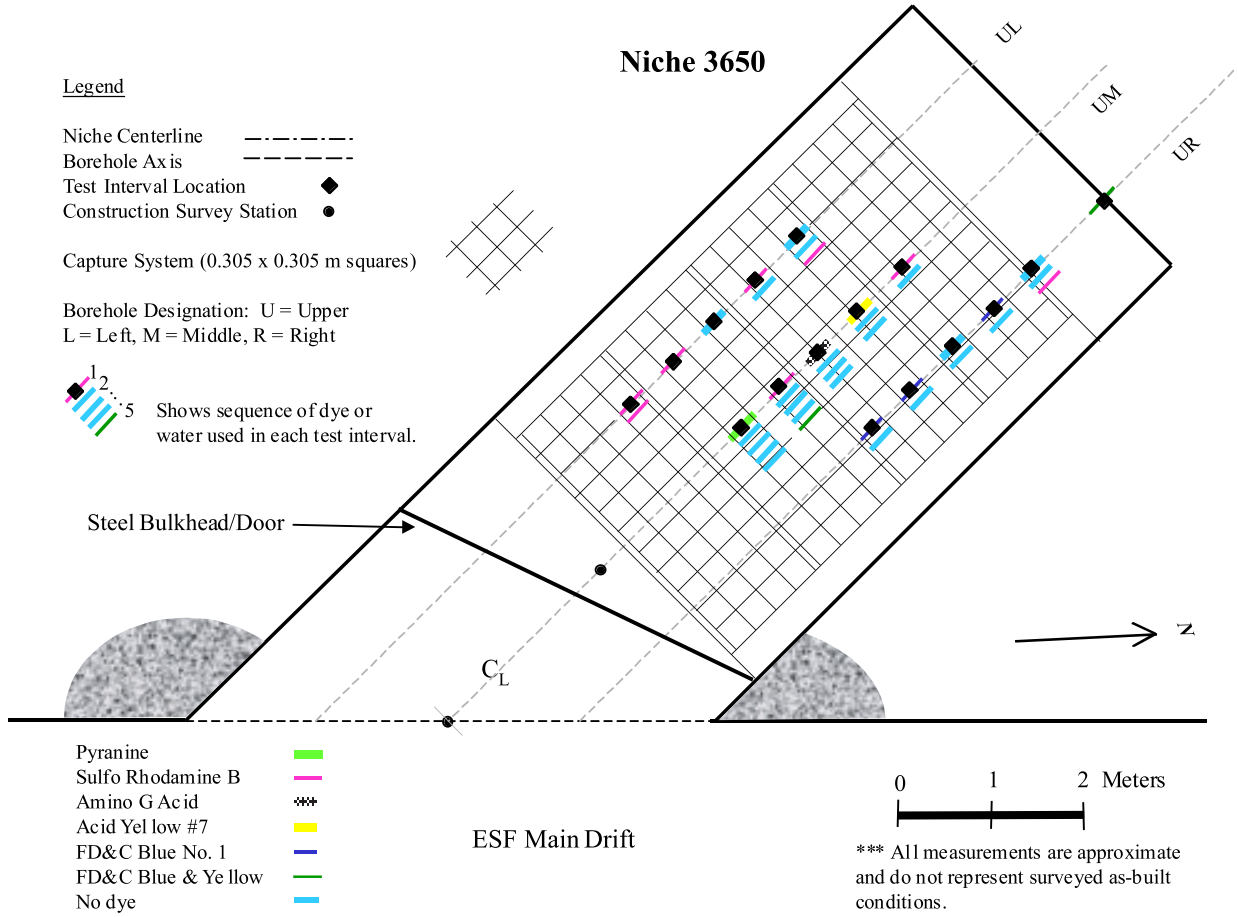

Figure 6.2.1-3. Schematic Illustration of Seepage Capture System and Test Intervals at Niche 3650 (Niche 2)

6.2.1.3.2 Niche 3107 (Niche 3) Seepage-Test Data

Beginning in early 1999 and ending in late 1999, twelve niche seepage tests were performed on two test intervals positioned above Niche 3107 (Niche 3). Water migrated through the rock and seeped into the niche for one out of the two zones tested. Niche seepage threshold was determined for the zone that seeped. The seepage and liquid-release data were tabulated and entered into the TDMS, where it was assigned DTN: LB0010NICH3LIQ.001 [153144]. As noted in Section 6.2.1.3.1, the borehole flux values were derived from the pumping rate and the wetted area estimated for the borehole interval. This definition of niche seepage threshold is different from the definition used by PA, with the seepage threshold related to the steady-state background percolation flux averaged over drift scale and site scale areas.

As with Niche 3650 (Niche 2), the mass of water released to the formation was computed by a mass balance. The liquid release-rate (Q_s) for each test was computed by dividing the mass released by the respective duration of each test; thus, these values represent time-averaged rates. The rate at which water was released to the formation ranged from 0.014 to 0.102 g/s for all of the tests, and the mass released ranged from 4,229.5 to 23,831.4 g per test.

When water appeared at the niche ceiling during a test and dripped into the opening, it was collected in the capture system and weighed. The wetting front typically arrived at the niche ceiling directly below the test zone. Most of the water was typically captured in only one or two 0.3 × 0.3 m cells located directly beneath the test interval. The mass of water captured ranged from 0.0 to 15,715.1 g per test. The seepage percentage defined by Equation 6.2.1-1 ranged from 0% for zones that did not seep to 70.1%.

The niche seepage tests were conducted with the bulkhead doors at the entrance to the niche closed and sealed. Also, the air space within the niche was artificially humidified to increase the relative humidity as high as practical to minimize the effects of evaporation resulting from ESF ventilation. One open-faced water bath was placed inside the niche to freely supply moisture to the niche space. The water loss volume resulting from evaporation was used to estimate the average evaporation rate over the niche space. The test conditions (e.g., high humidity and low evaporation rates) are representative of steady seepage into a drift that could potentially occur after the repository is closed, the heat load and temperature rise from the decaying waste have dissipated, and air in the sealed repository equilibrates with the surrounding rock is at or near 100% relative humidity. The relative humidity and temperature within Niche 3107 (Niche 3) is shown in Figure 6.2.1-4.

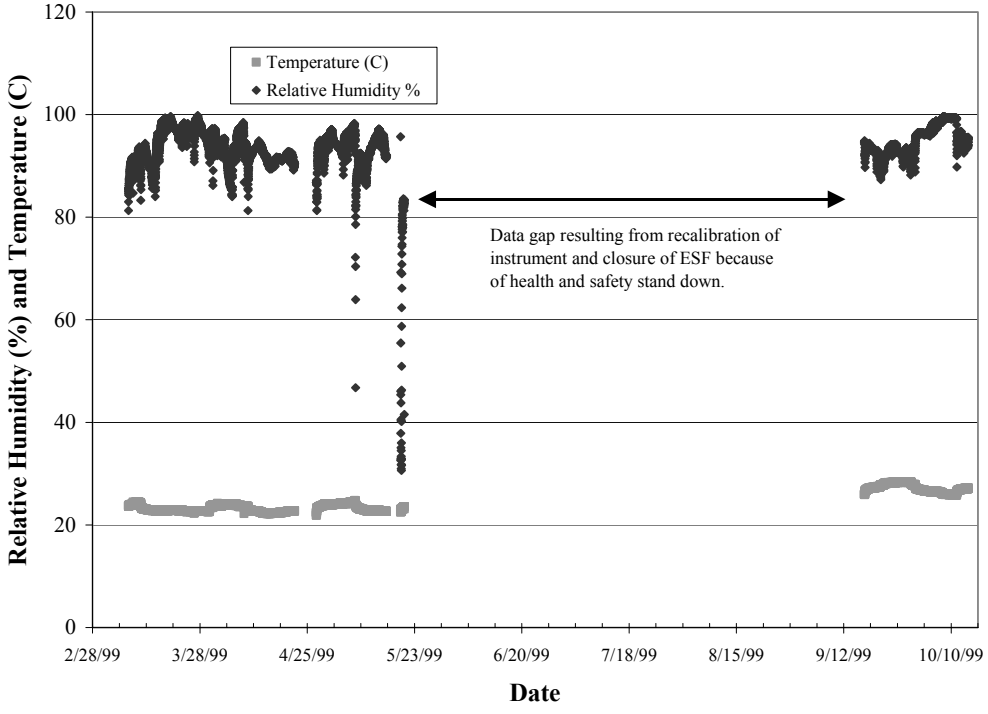

DTN: LB0010NICH3LIQ.001 [153144]

Figure 6.2.1-4. Relative Humidity and Temperature Inside Niche 3107 (Niche 3)

6.2.1.3.3 Niche 4788 (Niche 4) Seepage-Test Data

Beginning in late 1999 and ending in mid-2000, 13 niche seepage tests were performed on three test intervals positioned above Niche 4788 (Niche 4). Water migrated through the rock and seeped into the niche from all zones tested. The niche seepage threshold was determined for two of the three zones that seeped. The seepage and liquid-release data were tabulated and entered into the TDMS, where it was assigned DTN: LB0010NICH4LIQ.001 [153145]. As noted in Section 6.2.1.3.1 for Niche 3650 (Niche 2) and Section 6.2.1.3.2 for Niche 3107 (Niche 3), the borehole flux values for Niche 4788 (Niche 4) were derived from the pumping rate and the wetted area estimated for the borehole interval. This definition of niche seepage threshold is different from the definition used by PA, with the seepage threshold related to the steady-state background percolation flux averaged over drift scale and site scale areas.

The long-duration data from Niche 4788 (Niche 4) were analyzed in Section 6.6 of the Model Report U0080 *Seepage Calibration Model and Seepage Testing Data* (BSC 2003 [162267]). The seepage calibration model analyzed the transient behavior, storage effects, and memory effects between separate tests to determine the effective seepage parameters. The parameters were then used in the Model Report U0075 *Seepage Model for PA Including Drift Collapse* (BSC 2003 [163226]) to determine the seepage threshold flux relative to percolation flux. The final

input to TSPA is evaluated in the Model Report *Abstraction of Drift Seepage* (BSC 2003 [165564]).

As with Niche 3107 (Niche 3) and Niche 3650 (Niche 2), the mass of water released to the formation was computed by a mass balance. The liquid-release rate (Q_s) for each test was computed by dividing the mass released by the respective duration of each test; thus, these values represent time-averaged rates. The rate at which water was released to the formation ranged from 0.008 to 0.092 g/s for all of the tests, and the mass released ranged from 1,474.9 to 39,514.6 g per test.

When water appeared at the niche ceiling during a test and dripped into the opening, it was collected in the capture system and weighed. The wetting front typically arrived at the niche ceiling directly below the test zone. Most of the water was typically captured in only one or two 0.3 × 0.3 m cells located directly beneath the test interval. The mass of water captured ranged from 0.0 to 15,555.1 g per test. The niche seepage percentage defined by Equation 6.2.1-1 ranged from 0% to 68.7%.

Again, the seepage tests were conducted with the bulkhead doors at the entrance to the niche closed and sealed, and the air space within the niche was artificially humidified to minimize evaporation. Figure 6.2.1-5 shows the relative humidity and temperature inside of Niche 4788.

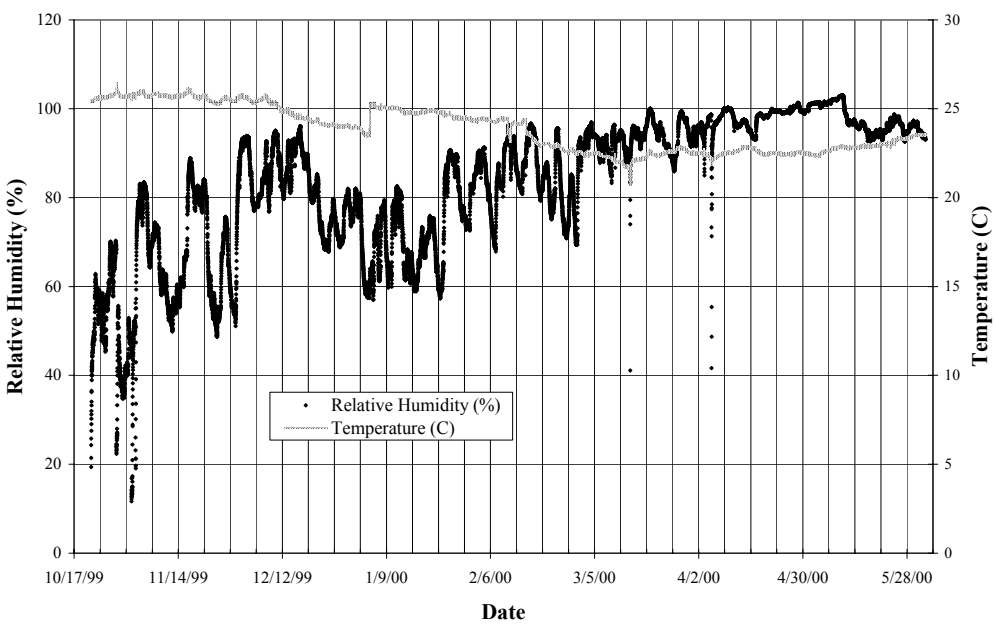

DTN: LB0010NICH4LIQ.001 [153145]:
native data file Niche4 h&T 3-10-00.csv,
Niche4 RH&T 4-1-00.csv, and
Niche4788 R&T 6-8-00.csv;
data report S00429_007.

Figure 6.2.1-5. Relative Humidity and Temperature Inside Niche 4788 (Niche 4)

Figure 6.2.1-6 illustrates the release rate into a borehole interval, the return rate, and the stabilization of niche seepage rate of water collected in the niche trays. If tests were not long enough before niche stabilization, the niche seepage ratio was not well defined. Various operating conditions and niche moisture conditions may contribute to the fluctuations observed in the early time data. The execution of long-duration tests to ensure quasi-steady conditions contributed to the robustness of seepage quantification at selected borehole intervals.

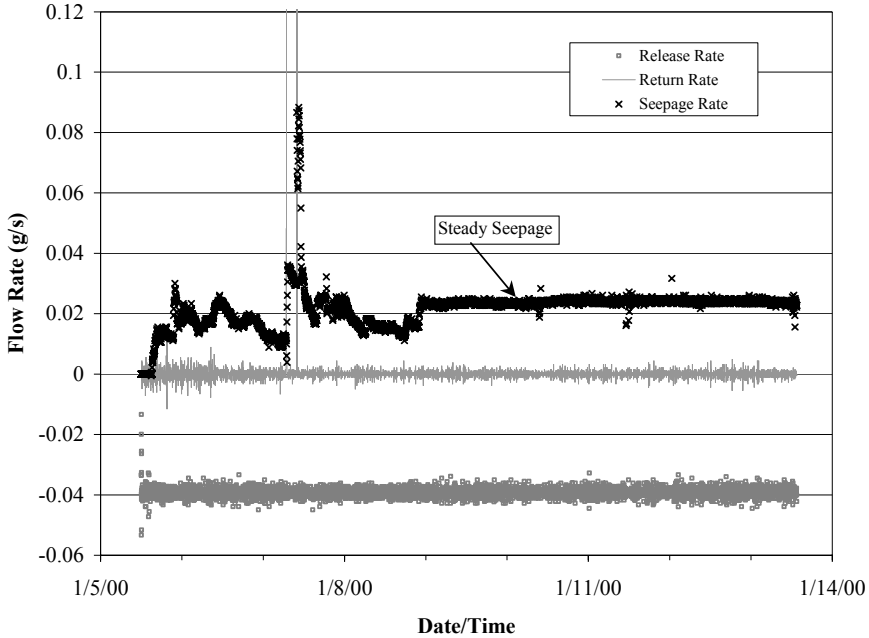

DTN: LB0010NICH4LIQ.001 [153145]:
native data file Niche 4788 UR 5.18-5.48m 1-5-2000.csv,
data report S00429_007.

Figure 6.2.1-6. Stabilized Flow Rates Observed during Test #1 1-5-00 Conducted on Test Interval UR at Niche 4788 (Niche 4)

6.2.1.3.4 Niche 4788 (Niche 4) Wetting-Area Data

In this section, an example of niche wetting-area data from a seepage test run in Niche 4788 (Niche 4) is discussed. The progression of the wetting fronts with time was recorded on videotape, and still images from the videos were captured and digitized. Wetting fronts were traced from these captured still images; they were later adjusted by reference to marked grid points and other features on the niche crown, and to sketches made during the tests, to correct for distortion caused by the camera's oblique angle of view to the niche crown. They were then superimposed over corresponding areas of a fracture map of the niche crown (Trautz 2001 [156903], pp. 57–62).

Figure 6.2.1-7 shows the wetting-front sequence for a seepage test begun June 26, 2000, with water released from the interval 7.62–7.93 m from the collar of the borehole UL. The release rate at the borehole interval was 0.02 g/s, and the seepage into the niche corresponded to 14% of the water released.

Several observations can be made from Figure 6.2.1-7. With regard to fractures, their presence has a variable impact on the progress of the wetting fronts. Influence of fractures appears relatively minor in the June 26, 2000, test (although a general upper-left-to-lower-right elongation of the fronts may reflect preferred fracture orientation). Also, the initial wetting fronts in these tests are displaced laterally from the vertical projections (the shortest paths) of the release intervals onto the crown, and the wetting fronts overall are not symmetrical about those projections, which suggest a role for fractures in directing flow in the niche crown.

Figure 6.2.1-8 shows the wetting-front growth with time for the seepage test. Each data point corresponds to one of the numbered contours in Figure 6.2.1-7. The x-axis refers to time elapsed since the first wet spot appeared on the crown, rather than from the first release of water.

The plot in Figure 6.2.1-9 pertains to the shape progression of the wet spot. If a front's 2-D shape remained constant as it grew, with subsequent fronts expanding uniformly and maintaining shape similarity between them, the slope of its line in Figure 6.2.1-9 would be constant. This is nearly the case through the early part of the test, with somewhat greater irregularity seen after the eight or ninth front (or data point). The average value of the slope for this test is ~0.25, somewhat less than the 0.28 slope, which would apply for a circle; this reflects the slightly elongated wetting fronts observed for this test.

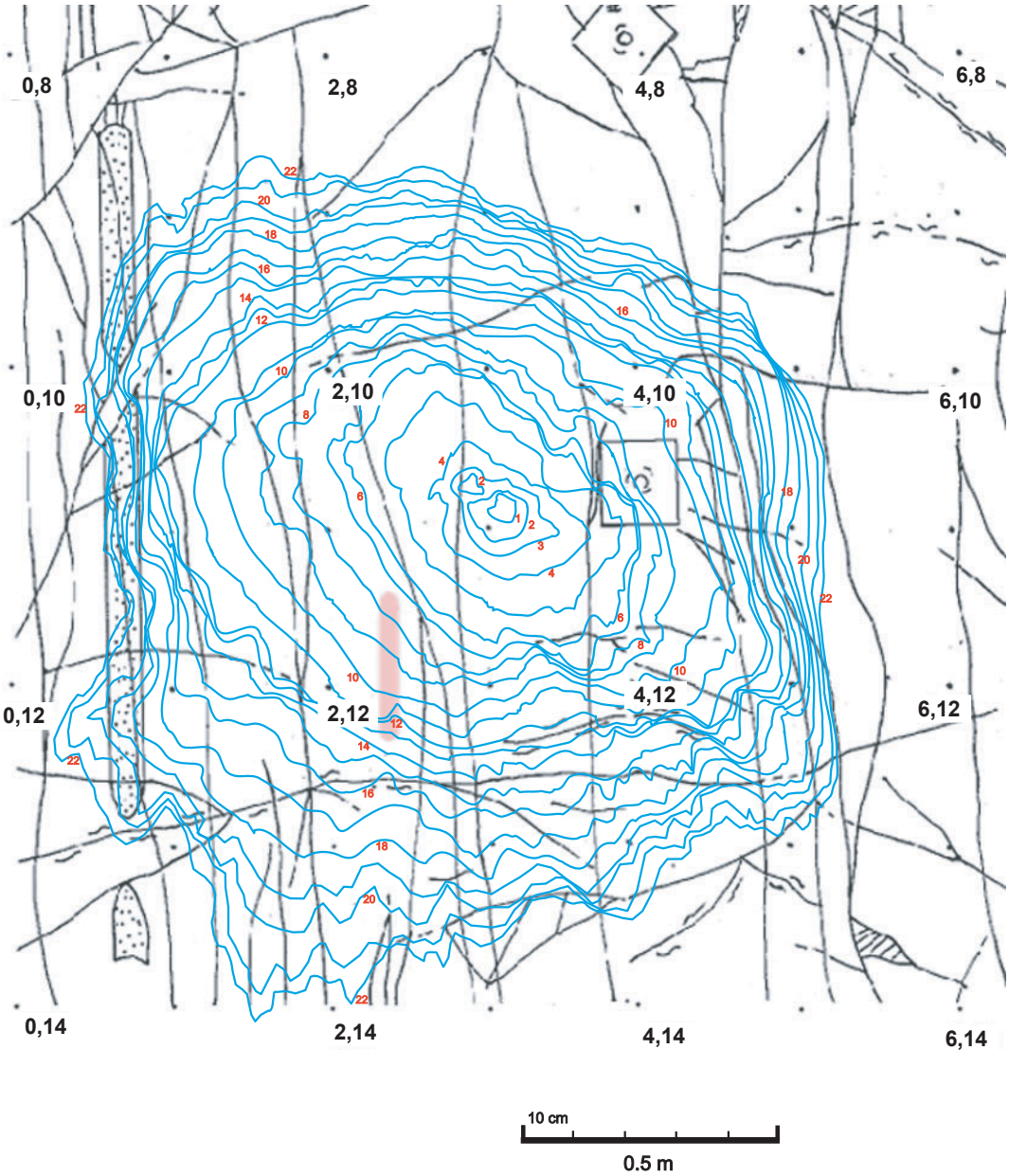

Map symbols:

DTN: LB0110NICH4LIQ.001 [OUTPUT]

NOTE: Blue contours are outlines of wetting fronts. Numbers along wetting fronts correlate with the order of data points in Figure 6.2.1-8, and the time corresponding to each front can be determined from that figure. Pink bars indicate approximate positions of release intervals in boreholes above niche, projected onto crown.

Figure 6.2.1-7. Wetting-Front Sequences Overlying Fracture Map of Niche 4788 (Niche 4) Crown from Seepage Test Begun June 26, 2000

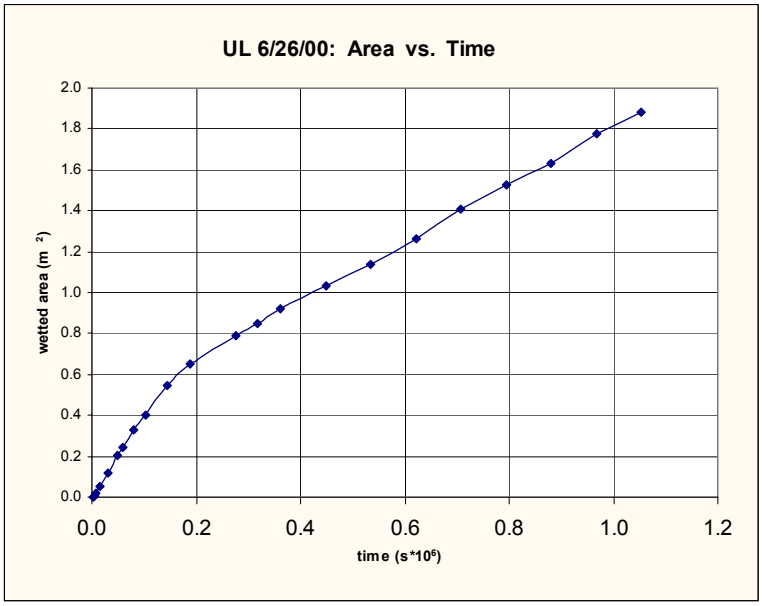

DTN: LB0110NICH4LIQ.001 [OUTPUT]

NOTE: Each plotted point represents data for one of the numbered curves shown in Figure 6.2.1-7.

Figure 6.2.1-8. Wetting-Front Area (m^2) versus Time (s) for the Seepage Test Shown in Figure 6.2.1-7

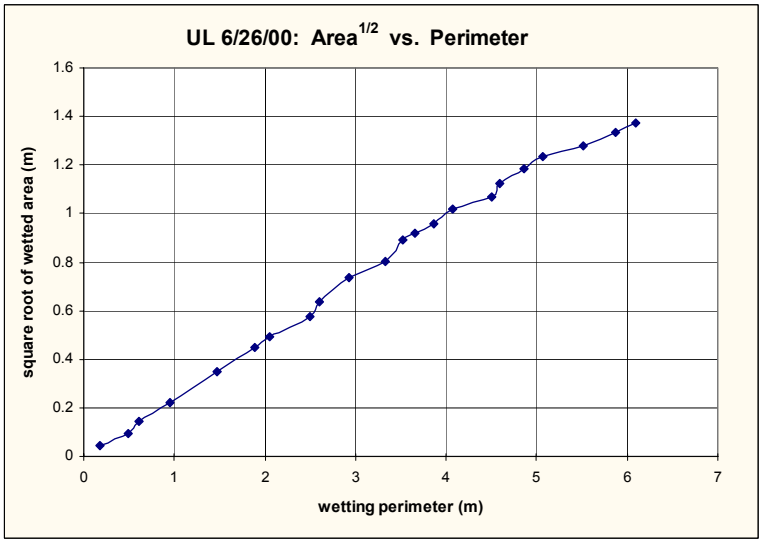

DTN: LB0110NICH4LIQ.001 [OUTPUT]

NOTE: Data points correspond to those in Figure 6.2.1-8.

Figure 6.2.1-9. Square Root of Area (m) Plotted versus Perimeter (m) for Each of the Wetting Fronts in the Niche 4788 (Niche 4) Seepage Test

6.2.1.3.5 Niche CD 1620 (Niche 5) Slot and Seepage-Threshold Tests

6.2.1.3.5.1 Background Information

The study site is located at cross-drift construction station (CD) 16+20 near the center of the ECRB and the repository block shown in Figure 6.1.1-1, and is known as Niche CD 1620 or Niche 5. The site was selected because it is located near the center of the repository block within the lower lithophysal zone (Tptpll) of the Topopah Spring welded tuff (TSw). Approximately 80% of the repository would be constructed within the Tptpll zone, given the current design (BSC 2003 [164491], 800-IED-WIS0-00103-000-00Ab; BSC 2003 [164889] Attachment VIII for area fractions: Tptpul: 4.5%, Tptpmn: 12.4%, Tptpll: 80.5%, Tptpln: 2.6%). Thus, characterization of seepage into waste emplacement drifts constructed in this zone is important to the performance and design of natural and engineered barriers.

The Tptpll contains large naturally occurring cavities called lithophysae that are attributed to gas and vapor-phase constituents entrapped and redistributed during the initial deposition, compaction, and gas migration out of the TSw (Buesch and Spengler 1998 [101433], p. 21). Lithophysae cavities are quite large at the site, with some ranging from 0.5 to 0.75 m in length and 0.2 to 0.3 m in height. Fractures are also present, but the majority of these appear to be cooling features associated with lithophysae cavities. These fractures primarily form halos or rinds around the cavities. Very few through-going fractures of significant length were mapped. However, given the high permeability of the rock observed at Niche CD 1620 (Niche 5) and reported in Section 6.1.2, the fracture rinds and lithophysae cavities do not appear to be dead-end features. Rather, short fractures appear to link the cavities and rinds, giving the entire network a larger overall average permeability than was observed in the densely welded, middle nonlithophysal zone (Tptpmn) of the TSw, where fractures dominate and lithophysae are sparse.

As noted in Section 6.2.1.1, liquid-release tests were performed at Niche CD 1620 (Niche 5) in April 2000 prior to the construction of the access drift and niche in May 2000 described in Section 6.2.1.2. Bulkhead doors were installed across the entrance to the excavation and sealed immediately upon construction to minimize evaporation and drying of the rock surrounding the drift. An initial post-excavation seepage test was performed in late February 2001 and ended approximately 39 days later in April 2001. Water did not seep, nor did the wetting front appear at the niche ceiling during this test after releasing approximately 300 liters of water. (Data are not provided for this test because, with the exception that no seepage was observed after releasing a large volume of water, they are inconsequential.) This test showed that the Tptpll had a high storage capacity (because of the large lithophysae) or was able to divert large quantities of water laterally around the drift through preferential flow paths not connected directly to the opening.

The lack of seepage and the failure of the wetting front to appear at the niche ceiling during the initial test prompted significant changes to the objectives of the seepage-testing program planned for Niche CD 1620 (Niche 5). A slot was constructed in the sidewall of the original niche that could be used to accomplish the following objectives, supplementing those described in Section 6.2:

- Demonstrate that the capillary barrier moves water laterally around the opening to the walls of the niche, where it would collect in the slot.

- Provide a water mass balance. The mass balance was intended to show that the flow field had reached steady state by demonstrating that the amount of water released to the formation was balanced by the amount of water recovered as seepage from the niche ceiling and slot, plus the unrecovered amount of water lost to evaporation as the wetting front spread across the niche ceiling.

The sections that follow describe the test configuration, operation, and equipment used to address these objectives and provide representative test results showing the type of data collected.

6.2.1.3.5.2 Description of Post-Excavation Seepage Tests

Test Configuration

Seven 15 to 17 m long boreholes were drilled in January 2000 at the Niche CD 1620 (Niche 5) site (shown in Figures 6.2.1-10 through 6.2.1-12) prior to niche construction. Each borehole is nominally 0.0762 m (3 inches) in diameter, with the exception of borehole ECRB-Niche1620#7, which was mistakenly drilled to a nominal diameter of 0.1016 m (4 inches) using a larger-diameter core bit. (Boreholes will be referred to hereafter by number only [e.g., #7] and not by their full designation [e.g., ECRB-Niche1620#7].) Post-excavation seepage tests were not performed on borehole #7, because the straddle packer system used to isolate the injection zone was not designed to fit the larger diameter hole.

The first borehole (#1) was installed at the approximate position shown in Figure 6.2.1-10 through Figure 6.2.1-12. Dye-spiked water was released into eight 0.3 m long test intervals within this borehole prior to niche construction, as noted in Section 6.2.1.1. The position of the dye within the rock was then photographed and mapped during niche excavation, and borehole #1 was intentionally removed during the mining process described in Section 6.2.1.2. A set of three boreholes (designated #2, #3, and #4) were drilled parallel to the axis of the niche in the same horizontal plane, located about 1.0 to 1.3 m above the opening of the niche. These boreholes are collectively referred to as the horizontal boreholes. The horizontal boreholes are spaced approximately 1 m apart.

A second set of three boreholes (designated #5, #6, and #7) were drilled parallel to the niche axis, but at a 6 to 8º angle upward (based on as-built information in DTN: MO0209GSC02116.000 [160407], approximately 1º higher than the designed angle in Figure 6.2.1-10). These boreholes are collectively referred to as the inclined boreholes. The collar of the inclined boreholes is located directly above and within 0.4 to 0.5 m of the horizontal boreholes. The upper boreholes are inclined so that the distance between the boreholes and the niche ceiling varies from about 1.4 to 3.0 m. In combination with the horizontal boreholes, the scale of the post-excavation seepage tests can vary from 1.0 to 3.0 m, the latter measurement being slightly larger than the radius of the niche.

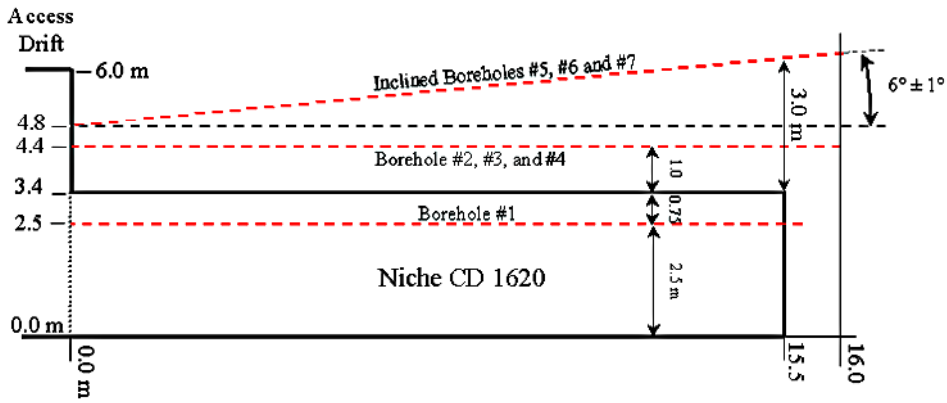

Source: BSC 2001 [158200] Figure 2.

Figure 6.2.1-10. Side View Schematic Illustration of the Boreholes at Niche CD 1620 (Niche 5)

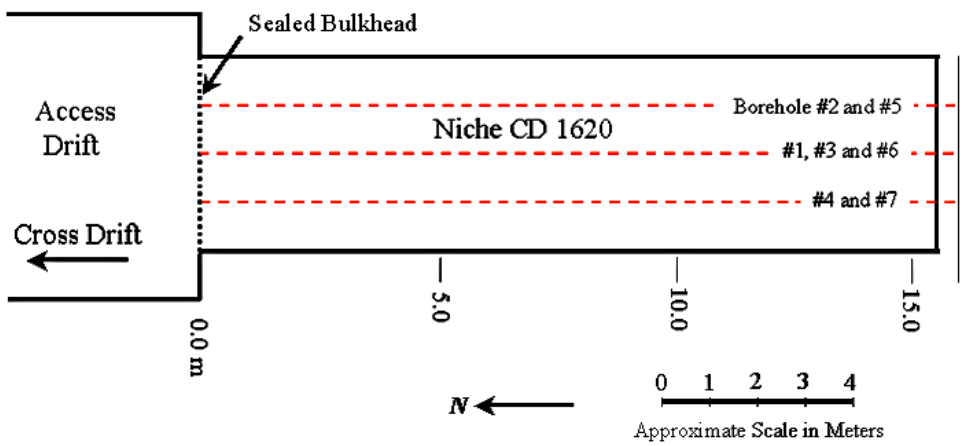

Source: BSC 2001 [158200] Figure 3.

Figure 6.2.1-11. Plan View Schematic Illustration of the Boreholes at Niche CD 1620 (Niche 5)

In May 2000, a mechanical excavator was used to mine out the rock to create Niche CD 1620 (Niche 5). The niche is approximately 15.5 m long by 4 m wide by 3.3 m high (Figure 6.2.1-10 through Figure 6.2.1-12). Niche CD 1620 (Niche 5) was constructed along the south side of the Cross Drift (at the location shown in Figure 6.1.1-1) within the lower lithophysal zone of the Tptpll. Water was used during niche construction to suppress dust generated during mining activities. Split-set rock bolts were installed in the ceiling of the niche immediately following construction to provide ground support for the excavation.

In May 2001, construction began on two slots located in the side walls of the niche called the "bat wing," as shown in Figure 6.2.1-12. The original intent was to construct a 6 m long by 1 m high by 1.5 m deep slot in each wall of the niche to aid in the collection of water. The slot design was based on the premise that, because of the capillary barrier, water would move laterally around the opening, where it would collect at a low spot and drip into the slot (Point A on Figure 6.2.1-12). The initial design was to slope the ceiling of the slot back toward the niche to produce

a low point for water to collect and by creating a capillary barrier, to prevent water from flowing around the backside of the slot.

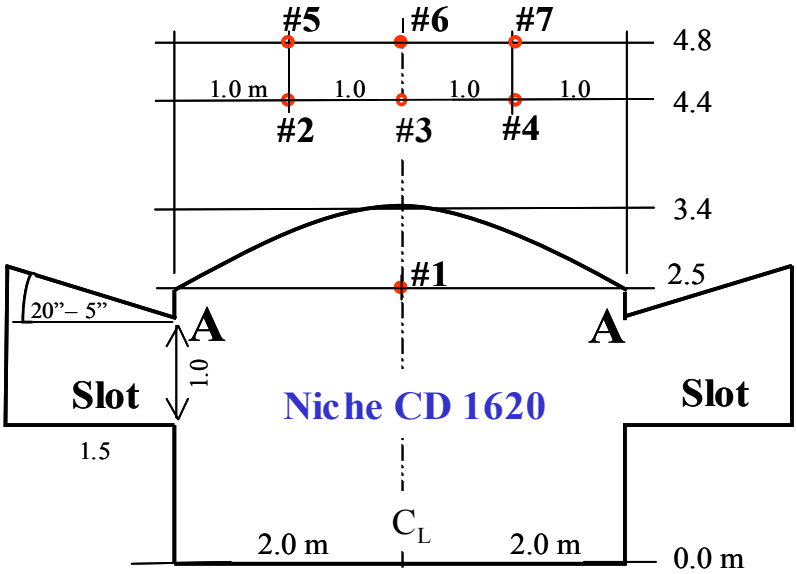

Source: BSC 2001 [158200] Figure 4.

Figure 6.2.1-12. Schematic Illustration of Front View of Niche CD 1620 (Niche 5) Facing South, Showing Location of Boreholes (#1–7)

Additional ground support consisting of Williams' rock bolts was installed in the ceiling of the niche prior to slot construction, to help stabilize the underground opening. These bolts supplemented the split-set rock bolts already in place, effectively doubling the number of bolts and decreasing the rock bolt spacing to about 0.5 m. Even with additional ground support, the unstable rock conditions at Niche CD 1620 (Niche 5) caused sections of the initial slot ceiling (Point A) to collapse during its construction, resulting in an excavation that did not meet the desired construction and testing specifications described above. Slot construction activities were halted after creating a 3.3 m long irregular-shaped excavation in the left rib and a short (< 1m) excavation in the right rib of the niche. Improvements to the 3.3 m long slot were made after construction by installing a wooden header and post system to support the brow of the slot excavation (i.e., Point A) keeping it from collapsing further (Figure 6.2.1-13 through Figure 6.2.1-15). The rock behind the header was then chipped away by hand to create the best sloping ceiling possible, given the circumstances. Additional ground support, consisting of metal house jacks, was installed further back in the slot to provide more stability.

Figure 6.2.1-13 shows the final size and shape of the slots. Note that there are five profiles numbered 2 through 6 in Figure 6.2.1-13, showing the irregular shape of the longest slot. Profile 2 and 6 define the lateral ends of the slot. The remaining profiles (3–5) are spaced sequentially by number between the two lateral ends with a distance of about 0.5 to 1.3 m separating the profiles.

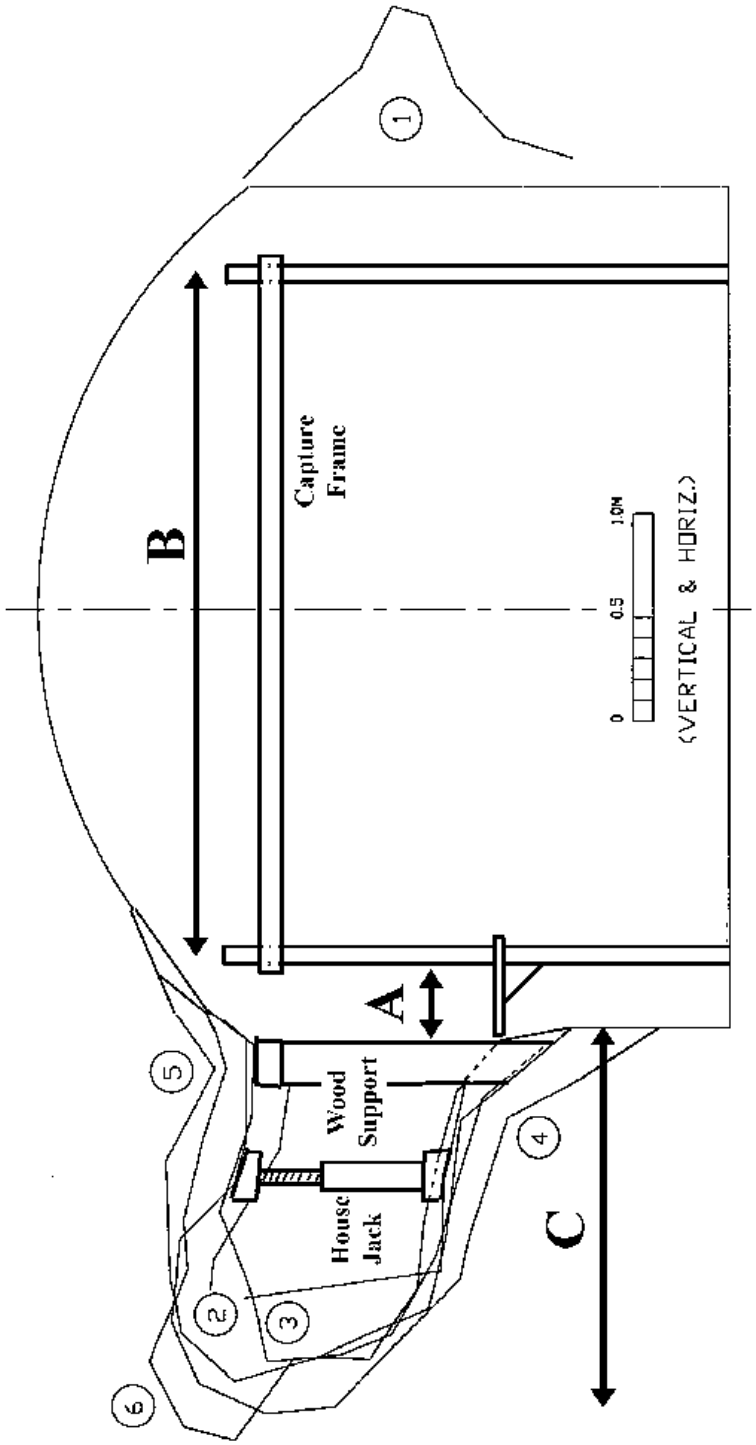

NOTE: Profile #2 is located closest to the niche entrance and # 6 is farthest away, after DTN: MO0107GSC01061.000 [155369].

Figure 6.2.1-13. Schematic Illustration of Front View of Niche CD 1620 (Niche 5) Facing South Showing Profile #1–7–Slot C

DTN: LB0211NICH5LIQ.001[160792]

Figure 6.2.1-14. Photograph of Left (East) Rib of Niche CD 1620 (Niche 5) Facing the Opening of a 3.3-m Long Slot and Showing Ground Support

DTN: LB0211NICH5LIQ.001 [160792]

Figure 6.2.1-15. Photograph of Left (East) Rib of Niche CD 1620 (Niche 5) Showing Ceiling of Slot and Ground Support

‚For additional detail on the slot profiles, refer to the surveyor's drawing (DTN: MO0107GSC01061.000 [155369]) provided in Attachment III.1.

The pilot hole from one of the rock bolts struck test boreholes #2 and #5. A rock bolt was subsequently installed in the pilot hole, blocking both test boreholes at a depth of 5.6 m from their collars, rendering the remaining 10 m of each borehole inaccessible. The rock bolts were subsequently removed by cutting through them laterally from within the test boreholes. This improved the depth available for testing from 5.6 to 7.9 m in borehole #2 and from 5.6 to 10 m in borehole #5. A straddle-packer assembly also got stuck in borehole #4 when air-injection tests were conducted on this hole. Numerous attempts to recover the packer were unsuccessful.

Unstable ground conditions, resulting in loose rock and debris sloughing off the walls of lithophysal cavities intersecting the boreholes, also contributed to several "natural" borehole blockages. The boreholes were vacuumed out to remove as much debris as possible before testing began. Boreholes #3, #4 and #6 were blocked at approximately 12.0, 9.0, and 10.5 m, respectively, by large rocks and debris that could not be extracted during the cleaning process. Table 6.2.1-1 summarizes the total depth and length of boreholes available for testing.

Table 6.2.1-1. Borehole Depth Summary

Borehole Designation	Available for Testing (m)	Total Depth (m)
ECRB-Niche1620#1	--	15.4
ECRB-Niche1620#2	0–7.9	16.0
ECRB-Niche1620#3	0–12.0	15.5
ECRB-Niche1620#4	0–9.0	15.0
ECRB-Niche1620#5	0–10.0	15.9
ECRB-Niche1620#6	0–10.5	16.0
ECRB-Niche1620#7 *	NA	14.8

Source: BSC 2001 [158200] Table 1.

NOTE: -- borehole was intentionally removed during niche construction
NA = not available
* borehole diameter is too large to accommodate test equipment.

Test Operation and Control Equipment

Custom-designed and built test equipment described in this section was used to operate and control the tests. In general, a seepage test is performed by pumping water at a known rate from a release reservoir sitting on an electronic balance through the release line, release manifold, and downhole straddle packer to the release or test interval located in the borehole (Figure 6.2.1-16). The straddle packer consists of a series of rubber glands that the test operator inflates with compressed air (like a balloon) inside the borehole. When inflated with air, the packers create a 0.3 m test interval, isolated from up and downhole sections of the borehole, thus preventing water from migrating throughout the length of the borehole during the experiment.

In the event that the pumping rate exceeds the infiltration capacity of the rock, water may begin to pond in the borehole and pressurize the test interval. An outlet located in the test interval (called the *return port*) prevents this from occurring. Water may rise to the level of the return

port where it will flow by gravity back through the return line, straddle packer, and return manifold, to the return reservoir, where it accumulates and is weighed by the return balance. The overflow line limits the maximum ponding depth of water within the borehole to about 0.05 m, thus preventing overpressurization of the test zone by the pump.

Water that enters the test interval percolates down through the rock, where it may eventually seep into the opening. A capture manifold or seepage collection system is used to capture the water seeping into the drift and to route it to the capture reservoir, where it accumulates and is weighed by the capture balance(s).

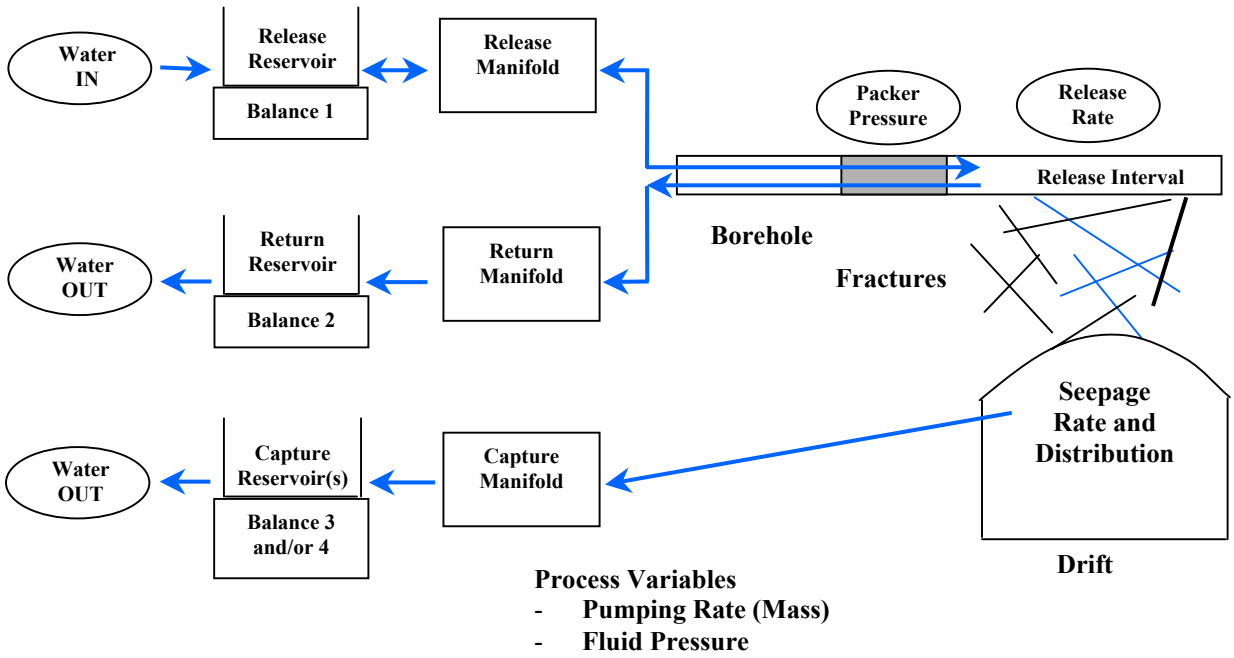

Figure 6.2.1-16. General Process Diagram for Seepage Testing at Niche CD 1620 (Niche 5)

Figure 6.2.1-16 provides a summary of the general processes that the test operator attempts to control during a seepage test, including the release, return, and capture rates. Control variables represent parameters that the operator is attempting to control. These are represented by ovals labeled in Figure 6.2.1-16. Control variables are affected by process variables (e.g., pump speed, valve position) manipulated by the operator. Additional detail on the test operation and control equipment is provided in Attachment III.2.

A plastic tarp was hung from the outside of the aluminum frame (shown in Figures 6.2.1-17 and 6.2.1-18) to the wooden supports at the edge of the slot shown in Figure 6.2.1-13 through Figure 6.2.1-15 to collect water seeping into the slot. The outlet from the slot seepage collection system drained through a pinch valve (that could also be controlled by the operator) to the capture balance.

Field personnel were not allowed to enter the slot, or hang the tarp off of the wooden and steel ground support system inside the slot, because of health and safety issues concerning rock instability. This restriction prevented the entire slot area (corresponding to depth C in Figure 6.2.1-13) from being covered by the slot seepage collection system. Instead, a much smaller area (with corresponding depth A in Figure 6.2.1-13) was covered by the slot seepage collection system. The majority of the slot seepage collection system was not beneath the slot ceiling itself, but rather beneath the sharply curved section of the niche where the niche ceiling meets the wall.

Data Acquisition Equipment

Calibrated instruments and data loggers were used to collect mass (g), mass rate (g/s), temperature (ºC), humidity (%) and pressure (pounds per square inch gauge, psig) data during the tests.

Mettler Toledo model PG, PG-s, and SG series electronic balances were used to measure the mass and rate that water was pumped into the test interval, that flowed back through the return line, and was captured as seepage. Initially, during the early stages of testing (5/3–5/16/02), two Mettler Toledo balances were used to measure the seepage mass and rate into the niche. Starting on 5/16/02, only a single balance was used to measure these same data. Mettler Toledo balances were also set up inside and outside the niche to measure the rate of evaporation from an open pan of water sitting on the balance. The data acquisition software listed in Attachment III.3 were used to query the balance for the mass and to calculate the mass rate on a user-defined time interval.

A calibrated Campbell Scientific, Inc. model CR10x datalogger was used to measure and record the measurements made by 12 calibrated Vaisala model HMP45C temperature and humidity probes located inside and outside the niche. Eleven of the probes were installed at various distances from the bulkhead to measure the air humidity and temperature distribution inside the niche. The twelfth sensor was installed outside the bulkheaded area of the niche to measure the temperature and humidity of the air in the ECRB (Trautz 2003 [166248], p. 162) for a detailed description of the probe locations).

The same calibrated Campbell datalogger was used to measure and record the measurements made by Setra model C204 pressure transducers (0–25 psig). The transducers were used to measure liquid pressures (air or water) inside the release and return lines leading to the test interval during the tests. These data were collected primarily for the purpose of monitoring and controlling the test equipment.7

DTN: LB0211NICH5LIQ.001 [160792]

Figure 6.2.1-17. Capture System Installation Showing Plastic Capture Trays and Tarp in Slot

DTN: LB0211NICH5LIQ.001 [160792]

Figure 6.2.1-18. Capture System Showing Tarp Installed Adjacent to Slot

Time-lapse video recordings of the niche ceiling and bottom of the capture trays were made during the tests to record the spread of the wetting front across the ceiling and dripping into the capture system. Sony model DCR-TRV900 video camcorders (mini-DV format) were utilized for this purpose.

Test Operating Conditions

A seepage test was typically conducted by pumping water at a constant rate through an injection line into a 0.3 m isolated test interval, located in one of the boreholes described in Table 6.2.1-1. Electronic balances were used to monitor the cumulative mass and rate at which water was pumped into the borehole, as well as return flow (if any occurs). Return flow occurs when the pumping rate exceeds the infiltration capacity of the rock.

Water migrating from the release point through the rock to the niche ceiling may drip into the niche, where it is collected in a capture system consisting of plastic trays and a tarp in the slot. Water drains by gravity through a network of tubes into a closed container, resting on an electronic balance. The balance is used to measure the cumulative mass of water that seeps and the seepage rate. One or more containers and balances may be employed for collecting seepage water.

Evaporation of water from the containers, the capture system, and the wetted area of the niche ceiling during seepage tests can influence the outcome of the seepage experiments. The effects of evaporation on the test results were minimized by employing the following techniques:

1. The bulkhead door at the entrance to the niche was closed and sealed during the seepage tests. This helped limit the exchange of dry air in the ECRB (typically <40% relative humidity) with moist air found within the niche (typically >85%).

2. Access to the interior of the niche during testing was limited to authorized field test personnel. Remote monitoring of the niche ceiling, and the capture trays, using digital video and remote monitoring of test equipment, minimized the number of trips inside the niche, thus limiting the exchange of air.

3. Fluid containers and transmission lines are closed systems, minimizing the effect of evaporation.

4. The potential exists for water to evaporate from the niche ceiling and diffuse into the air within the niche. Seepage water may potentially evaporate from the capture trays before the water has time to accumulate and drain into the tubing connecting the trays to the closed container on the seepage balance(s). Therefore, the relative humidity of the air inside the niche was artificially elevated to minimize evaporation, using a centrifugal-type humidifier capable of producing water vapor at a rate of about 1 kg per hour. Humidification occurred 24 hours per day, 7 days a week, under the condition that electrical power was available to operate the humidifier.

5. Electrical lighting within the niche was minimized to limit sources of heat that enhance evaporation. Sufficient lighting was provided, however, for video imaging of the wetted area spreading across the niche ceiling.

6. A small pan, resting on an electronic balance, was set inside the drift to directly measure the mass evaporative flux.

6.2.1.3.5.3 Test Summary

This section provides an overview of the seepage tests performed at Niche CD 1620 (Niche 5) and summarizes the type of data collected by evaluating and interpreting data for Test #2 9-17-02 conducted from 9/17/02 through 10/28/02. The analysis of the Niche CD 1620 (Niche 5) seepage test data for model calibration can be found in the Model Report U0080, *Seepage Calibration Model and Seepage Testing Data* (BSC 2003 [162267]).

Attachment III.4 summarizes general test information, including borehole number, depth of the test interval measured in meters from the datum near the borehole collar, test name, and test start and end dates. Seepage tests were initiated at Niche CD 1620 (Niche 5) in early May 2002 and ran through late May 2002, when the instruments and sensors were removed for routine calibration. Testing resumed in mid-July 2002, upon reinstalling the calibrated instruments, and continued through late October 2002 with seven tests performed over this time period.

Evaporation Pan Data

Evaporation pan data were measured using a single balance loaded with a container filled with water. Figure 6.2.1-19 shows the evaporation flux inside and outside the niche during Test #2 9-17-02. The plot indicates that the average evaporation flux outside of the niche is about a factor of 20 greater than the average evaporation flux inside the niche. (Note that the evaporation data collected during the study and contained in the original data files are the evaporation rates [g/s]. These were converted to evaporation fluxes [g/s-m^2] shown in the Figure 6.2.1-19 by dividing the evaporation rate by the surface area of the evaporation pan [i.e., πr^2, where r is the radius of the pan].) The radius of the evaporation pan inside the niche was 0.075 m (0.15 m diameter reported in Trautz (2003 [166248], p. 187) divided by 2) and outside the niche was 0.244 m (9 5/8 in. diameter reported in Trautz (2003 [166248], p. 187), converted as follows to r in meters (9 5/8 in. * 2.54 cm/in. * 1/100 m/cm)/2). Details of this calculation may be found in Attachment IX.6.1.

The peak evaporation rates associated with the saw-tooth pattern, observed in the evaporation pan data collected outside the niche, correspond to refilling the evaporation container with fresh warm water from the mine's water supply system.

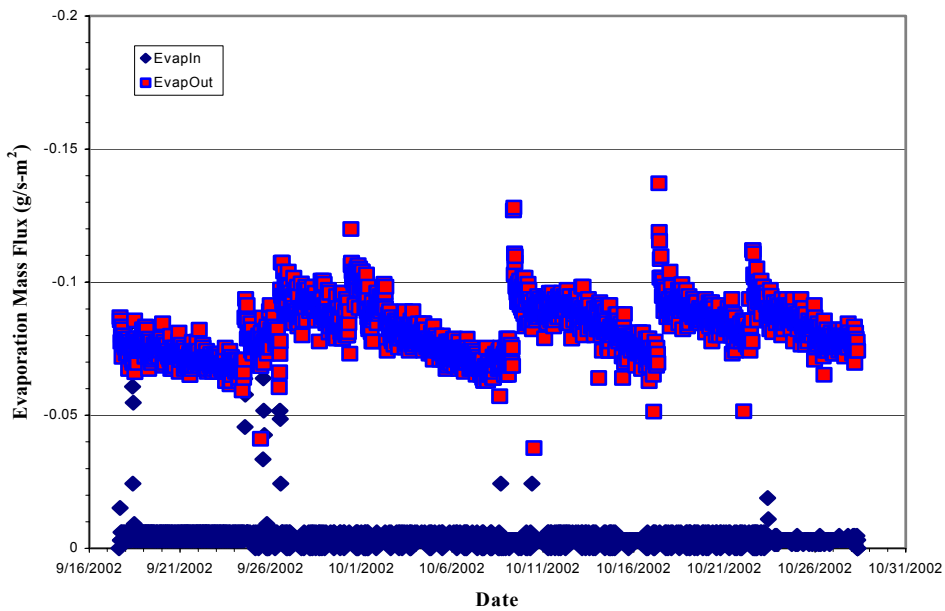

DTN: LB0211NICH5LIQ.001 [160792] Test #2 9-17-02:
native data files Test#1_BH#4_10-11_ft_9-17-02_#1.csv and Test#2_b5_20-21_ft_9-17-02_#1.csv].

Figure 6.2.1-19. Evaporation Rate Inside and Outside Niche CD 1620 (Niche 5) during Test #2 9-17-02

Relative Humidity and Temperature

The data filenames containing the relative humidity and temperature data from inside and outside the niche, and the liquid pressure data measured in the release and return lines during the test, are identified in Attachment III.4. (The pressure in the release and return lines were relatively constant during a given test, so these results will not be discussed further.) These data were collected using the sensors and Campbell Scientific, Inc., dataloggers described in the Data Acquisition Equipment subsection above.

Figure 6.2.1-20 shows the relative humidity and temperature of the air inside and outside the niche during Test#2 9-17-02 (9/17/02–10/28/02). The relative humidity and temperature inside the niche are very stable, ranging from about 90 to 94% and 24 to 25ºC, respectively. The sudden drop in relative humidity observed in mid- and late-September was caused by the exchange of cool moist air inside the drift with dry warm air outside the niche when field personnel opened the bulkhead and entered the niche. A slight rise in inside air temperature is noted over the measurement period. This is probably caused by the cooler inside temperatures slowly equilibrating with the warming temperature outside the niche.

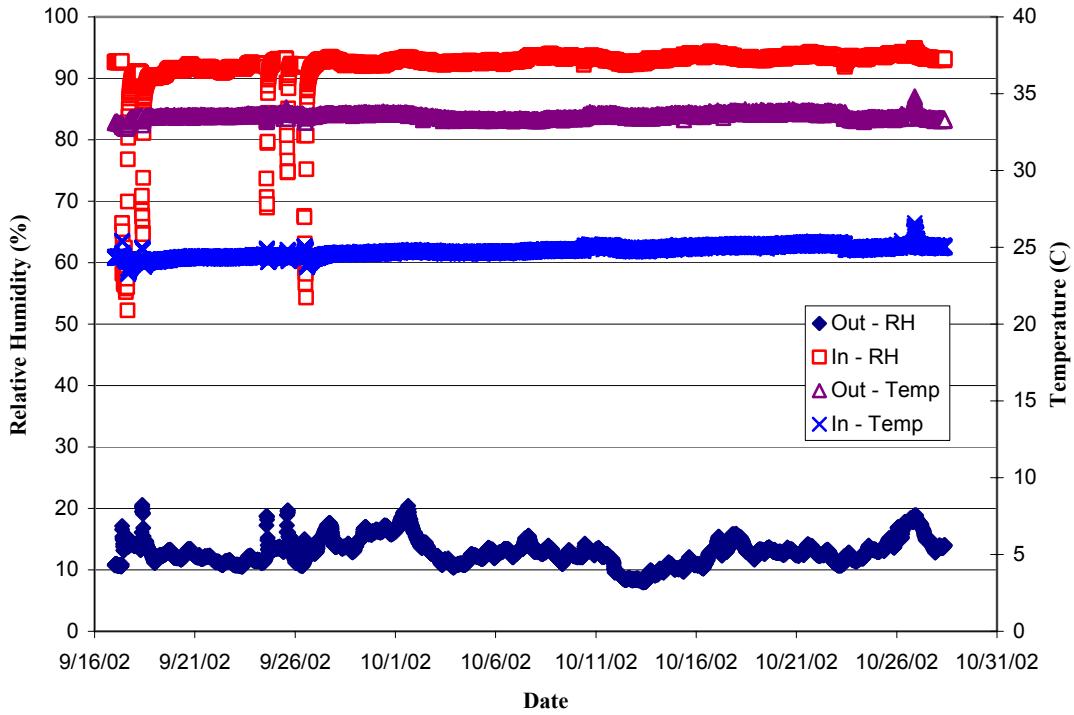

DTN: LB0211NICH5LIQ.001 [160792] Test#2 9-17-02:
native data files N5_RH-T-p_9-18-02.csv, N5_RH-T-p_10-18-02.csv, and N5_RH-T-p_10-29-02.csv.

Figure 6.2.1-20. Relative Humidity and Temperature of Air Inside and Outside Niche CD 1620 (Niche 5) during Test#2 9-17-02

The air temperature outside the niche in the ECRB is also quite stable (33 to 34ºC), but the relative humidity fluctuates from 8 to 21%. The fluctuation in relative humidity can be attributed to the tunnel ventilation system that draws moisture into the ECRB from outside the ESF. Relative humidity conditions in this case are influenced by outside weather conditions.

Test Data–Liquid Release and Seepage Rates

Figure 6.2.1-21 shows a plot of the liquid-release mass flow rate into the formation from the borehole and the total seepage mass flow rate entering the niche during Test #2 9-17-02. A peristaltic pump was used to pump water into the borehole, creating small surges in the rate that give the appearance that the release rate varies with time (i.e., double-line appearance to the release rate in Figure 6.2.1-21). The average release rate (about 0.023 g/s) was quite constant from 9/17 to 10/19/02, and then it steadily declined between 10/20/02 to 10/28/02 to a rate of 0.019 g/s.

Seepage into the niche began on 10/1/02, based on a definitive increase in mass observed on the capture balance. The seepage rate continued to increase through 10/20/02, when it suddenly started to decline and stopped seeping on 10/23/02. This corresponds within a day to the decline in the liquid release rate noted above. The sudden halt in seepage caused by a 10 to 20%

reduction in the release rate suggests that a seepage threshold exists in the Tptpll that is very sensitive to the release mass flow rate.

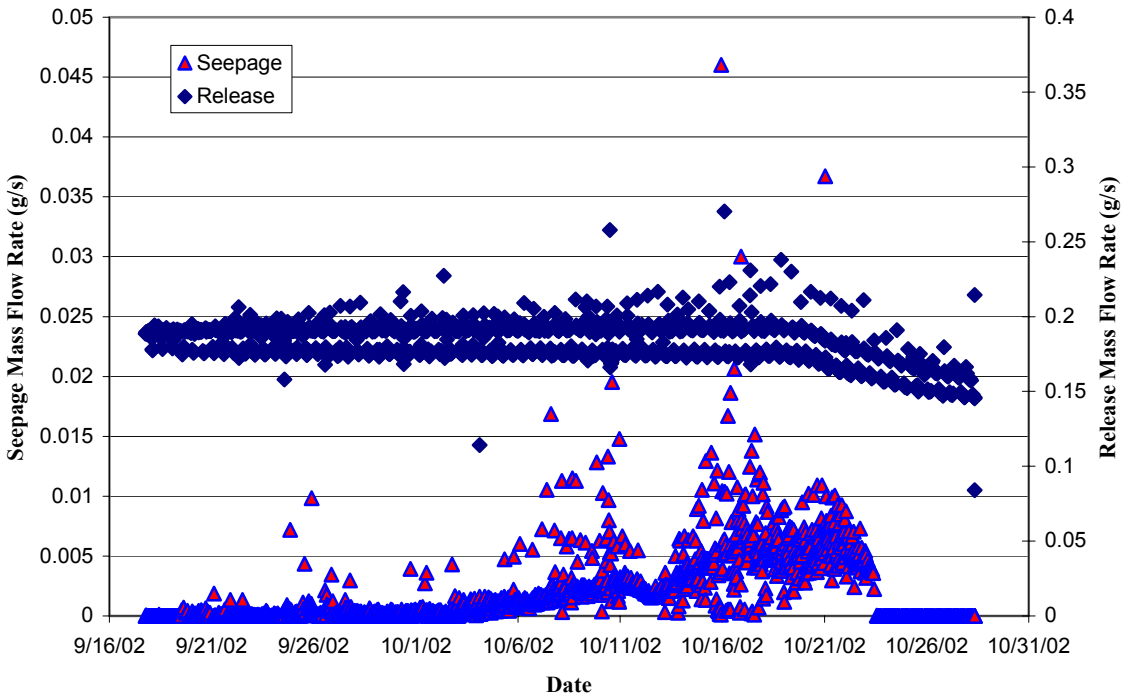

DTN: LB0211NICH5LIQ.001 [160792] Test#2 9-17-02:
native data files Test#2_b5_20-21_ft_9-17-02_#1a (srate).csv and Test#2_b5_20-21_ft_9-17-02_#2 (srate).csv.

Figure 6.2.1-21. Liquid-Release Rate into Borehole #5 and Seepage of Water into the Capture System of Niche CD 1620 (Niche 5) during Test #2 9-17-02

Figure 6.2.1-22 shows a plot of the total seepage rate into the niche (triangles) and the seepage rate captured by the tarp (diamonds) installed at the entrance to the slot (Area A, Figure 6.2.1-13). Seepage captured by the tarp follows the same pattern over time as the total seepage, the latter of which represents water collected from all the capture compartments. Seepage captured by the tarp is a large component of the total seepage into the drift, approaching 80 to 90% of the total during specific periods of time. Both seepage and the seepage captured by the tarp declined and dropped off to zero as the release rate declined after 10/20/02.

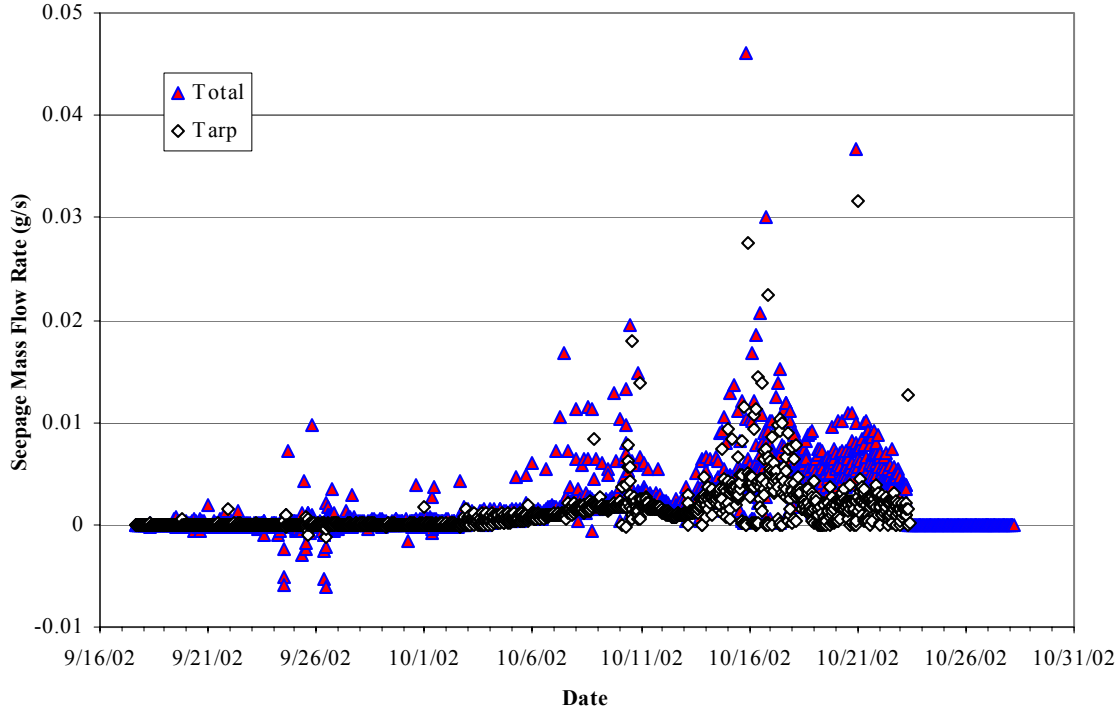

DTN: LB0211NICH5LIQ.001 [160792] Test#2 9-17-02:
native data files Test#2_b5_20-21_ft_9-17-02_#1.csv, Test#2_b5_20-21_ft_9-17-02_#1a (srate).csv, and Test#2_b5_20-21_ft_9-17-02_#2 (srate).csv.

Figure 6.2.1-22. Total Seepage and Seepage into the Tarp Area at the Entrance to the Slot

6.2.1.3.5.4 Summary–Niche CD 1620 (Niche 5)

Tests performed during the study (including the example experiment, Test #2 9/17/02) indicate that a measurable seepage threshold exists for the Tptpll–a stated objective of the niche study. Unfortunately, because of the constraints associated with installation of the slot collection system described in Section 6.2.1.3.5.2.2, investigators were unable to determine whether the water seeping onto the tarp during Test #2 9/17/02 and Test #1 7/15/02 (the only two tests where seepage onto the tarp occurred) originated from the slot or from the niche ceiling adjacent to the slot. Several attempts to observe seepage (i.e., dripping) were made, but the seepage rates were so slow that visual evidence of seepage from the slot was not possible. With the approximation that all of the seepage was derived from the slot, the results of Test #2 9/17/02 demonstrate that the slot did not effectively capture lateral movement of water around the niche, because seepage into the slot ceased when the seepage threshold was reached. The lack of seepage into the slot implies that the revised objectives of the test stated in Section 6.2.1.3.5.1 were not met in this study. Specifically, a mass water balance was not achieved because the lateral movement of seepage water was not collected in the slot. Photographic evidence has been collected in Niche CD 1620 (Niche 5), showing the wetted area spreading down the sidewall during the test (Figure 6.2.1-23), providing qualitative evidence that flow was diverted around the niche. Trautz and Wang (2002 [160335]) showed (using photographic evidence) that the wetted area spreads across the ceiling and down the terminal face and sidewall of Niche 4788 (Niche 4) in Tptpmn.

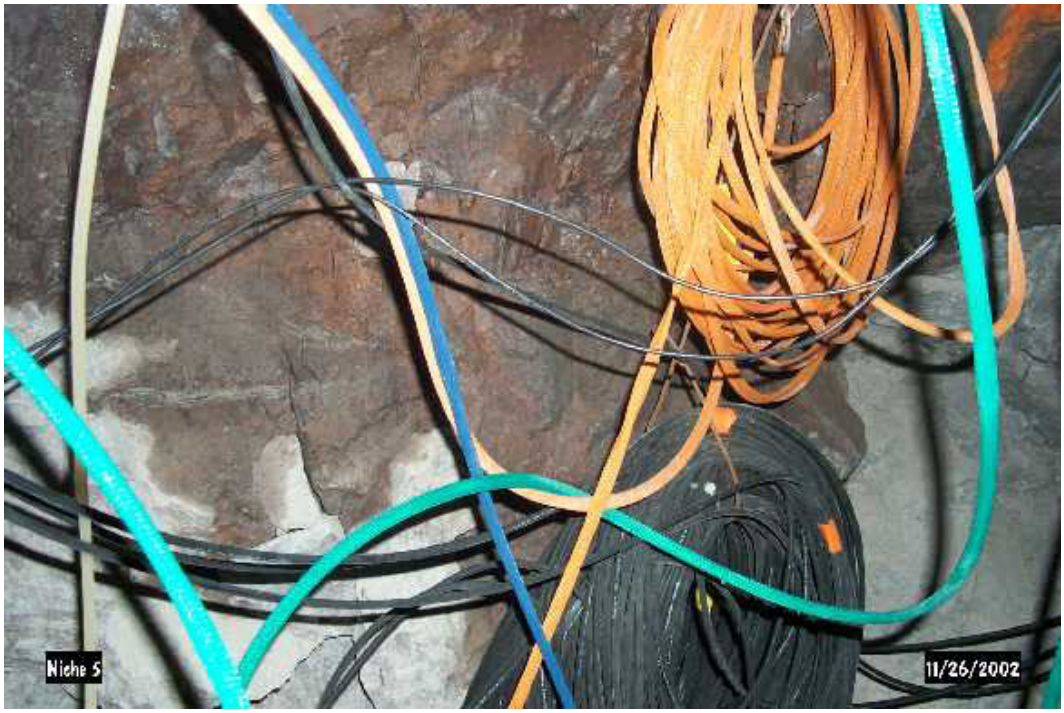

DTN: LB0211NICH5LIQ.001 [160792]

Figure 6.2.1-23. Wetted Area Spreading Down the Sidewall in Niche CD 1620 (Niche 5)

6.2.2 Niche Seepage Threshold and Fracture Characteristic Curves

The niche seepage data collected from short-duration tests in ten intervals at Niche 3650 (Niche 2), long-term tests in one interval at Niche 3107 (Niche 3), and long-term tests in three intervals at Niche 4788 (Niche 4) are analyzed in this section. As stated in Section 6.2.1.3.1, Section 6.2.1.3.2, and Section 6.2.1.3.3, the niche seepage threshold is defined in terms of the pumping rate and the wetted area estimated for the borehole interval. This definition of niche seepage threshold is different from the definition used by PA, which relates the seepage threshold to the steady-state background percolation flux averaged over drift-scale and site-scale areas.

6.2.2.1 Post-Excavation Liquid-Release and Niche Seepage Threshold

For a given test interval, seepage tests were initially conducted at high liquid-release rates (injection rates into borehole interval without excessive pressure buildup). Subsequent tests were performed at lower liquid-release rates to determine whether a threshold could be estimated below which seepage into the cavity would no longer occur.

Figure 6.2.2-1 shows a plot of the seepage percentages observed during four tests conducted at different q_s in borehole UM at the same interval, located 5.49–5.79 m from the borehole collar at Niche 3650 (Niche 2). A linear regression was performed on the four data points to compute the equation for the trendline and the R-squared values (R^2) reported in Figure 6.2.2-1 and tabulated in Table 6.2.2-1. This exercise was repeated for the intervals tested at all the niches to produce the regression data reported in Table 6.2.2-1 for all the zones that seeped. The R-squared values

were computed separately for each interval and are listed for those intervals where three or more data points are available. (The linear regression was performed in an Excel spreadsheet documented in Attachment II, Tables II-3a through -4e.) For the purposes of this analysis, liquid release flux (q_s) is approximately equal to the net downward flux K_o. This approximation is a conservative estimate of K_o (Trautz and Wang 2002 [160335]).

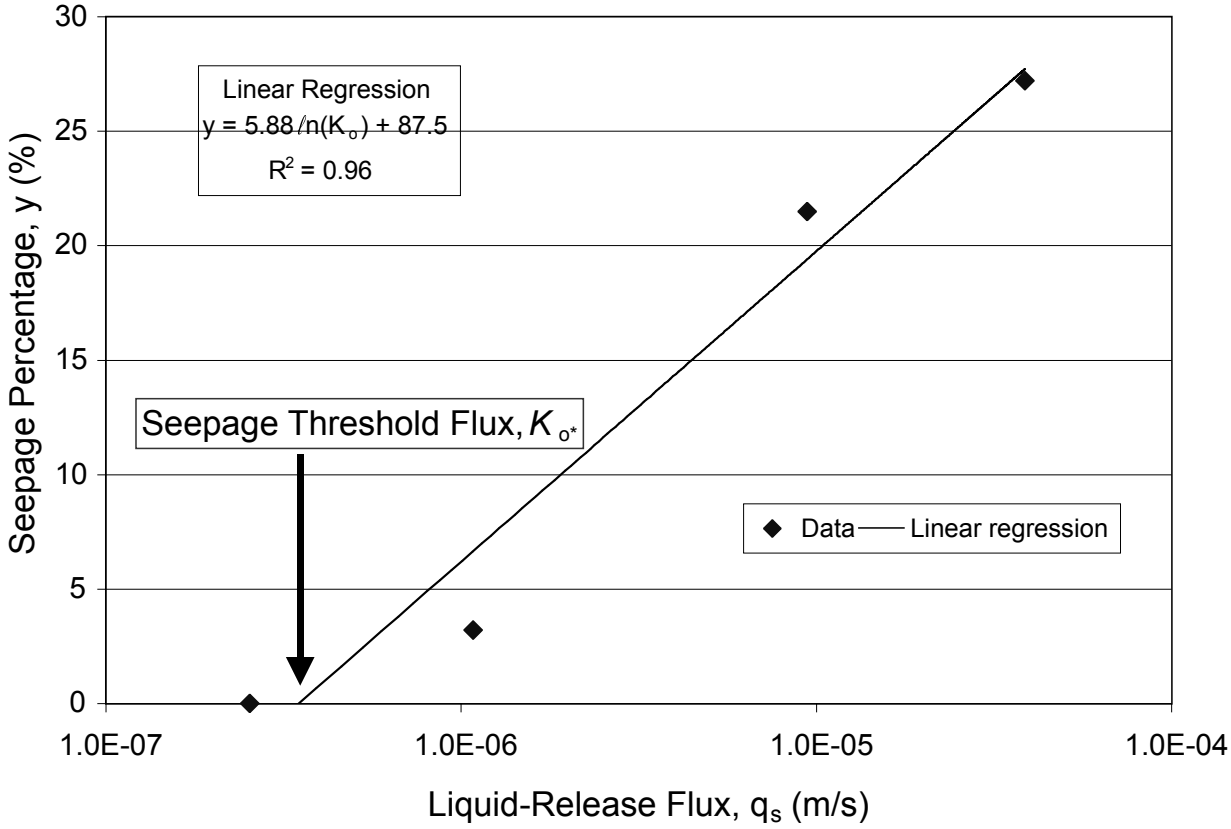

DTN: LB980901233124.003 [105592]

NOTE: Seepage tests were conducted for the interval 5.49–5.79 m from the collar for the upper middle borehole at Niche 3650 (Niche 2).

Figure 6.2.2-1. Liquid-Release Flux versus Seepage Percentage

Table 6.2.2-1. Seepage Threshold Fluxes (K_o^*).

Niche	Borehole and Depth (m)	Linear Regression Equation	Data Points	Correlation Coefficient (R^2)	Niche Seepage Threshold K_o^* (m/s)	Saturated Hydraulic Conductivity K_l (m/s)
3107	UM 4.88-5.18	$y = 30.440\ln(K_o) + 456.085$	8	0.820	3.11E-07	NA
3650	UL 7.01-7.32	$y = 0.6833\ln(K_o) + 8.5742$	2	NR	3.55E-06	8.98E-05
	UL 7.62-7.92	$y = 5.7394\ln(K_o) + 92.627$	3	0.979	9.80E-08	1.51E-04
	UM 4.27-4.57	$y = 5.2757\ln(K_o) + 79.443$	4	0.921	2.89E-07	2.62E-05
	UM 4.88-5.18	$y = 2.304\ln(K_o) + 31.767$	3	0.975	1.03E-06	2.52E-03
	UM 5.49-5.79	$y = 5.8876\ln(K_o) + 87.528$	4	0.963	3.50E-07	2.16E-05
	UR 4.27-4.57	$y = 0.314\ln(K_o) + 4.3283$	2	NR	1.03E-06	4.08E-05
	UR 4.88-5.18	$y = 0.3165\ln(K_o) + 4.3751$	2	NR	9.92E-07	9.87E-05
	UR 5.49-5.79	$y = 28.419\ln(K_o) + 351.09$	2	NR	4.31E-06	1.71E-05
	UR 6.10-6.40	$y = 4.2169\ln(K_o) + 79.596$	2	NR	6.35E-09	3.01E-05
	UR 6.71-7.01	$y = 10.574\ln(K_o) + 165.28$	3	0.974	1.63E-07	2.28E-04
4788	UL 7.62-7.93	$y = 9.273\ln(K_o) + 148.119$	4	0.929	1.16E-07	2.46E-05
	UM 6.10-6.40	$y = 15.697\ln(K_o) + 243.611$	4	0.980	1.82E-07	2.45E-04
	UR 5.18-5.48	$y = 25.415\ln(K_o) + 410.285$	3	0.970	9.75E-08	3.92E-06

DTN: LB980901233124.003 [105592] and LB0110LIQR0015.001 [OUTPUT]

NOTES: Various data sets were used to generate Table 6.2.2-1. Refer to Tables II-3 and II-4 in Attachment II, and Attachment IX.5 for details.
NA = not applicable, the test could not be completed as planned because of rock properties outside the equipment's measurable range.
NR = not reported because two data points result in perfect correlation (R^2 =1.0), therefore, correlation coefficient is meaningless.
y = predicted seepage percentage (%)
K_o = net downward liquid-release flux from regression model (m/s)
ln = natural logarithm

Table 6.2.2-1 also summarizes the niche seepage threshold (K_o^*), defined as the liquid-release flux below which water will not seep into the drift (i.e., see K_o^* defined on Figure 6.2.2-1). The K_o^* values were determined using the regression equations provided in Table 6.2.2-1 by setting the seepage percentage, y, equal to 0, and then solving for $K_o = K_o^*$ [$K_o^* = K_o(y=0)$]. Details on this analysis and calculation procedures may be found in Attachments II and IX. Here, the symbol K_o is used to denote the liquid-release flux used in the regression model to distinguish it from the liquid-release flux computed using the field data (q_s). In terms of K_o and K_o^*, the niche seepage threshold is defined as follows:

- If the liquid-release flux exceeds the seepage threshold flux ($K_o > K_o^*$) for the given interval, then water will seep into the drift.
- If the liquid-release flux is less than the seepage threshold flux ($K_o < K_o^*$), then water will not enter the cavity.

Figure 6.2.2-2 shows a log-log plot of K_o^* versus the saturated hydraulic conductivity (K_l) for 10 test intervals at Niche 3650 (Niche 2) and three test intervals at Niche 4788 (Niche 4) where seepage occurred. For each test interval, multiple tests with different release rates were conducted to estimate the niche seepage threshold. The air permeabilities obtained from the post-excavation gas-injection tests were converted into equivalent saturated hydraulic conductivities (DTN: LB980001233124.004 [136583]) as shown in Wang (1999 [153449], pp. 34–38) for Niche 3650 (Niche 2), to produce the values recorded in Table 6.2.2-1 and plotted in Figure 6.2.2-2. (Computation of K_o^* and K_l was performed in an Excel spreadsheet documented in Attachment II, Table II-4. K_l could not be calculated for Niche 3107 [Niche 3] because the air-permeability test could not be completed as planned: the rock properties were outside the equipment's measurable range.) The straight line in Figure 6.2.2-2 is derived from an analytic solution described in Section 6.2.2.2. The estimation of saturated hydraulic conductivity using air-permeability test data is evaluated in Attachment IV.2.

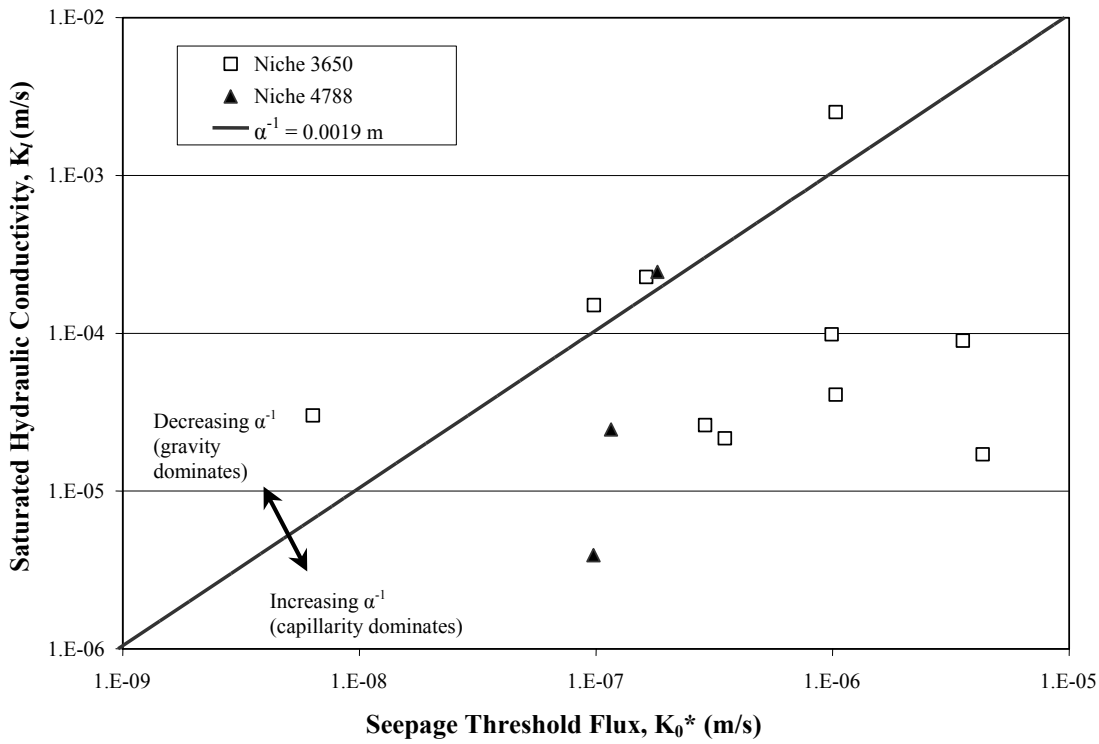

DTN: LB980001233124.004 [136583]; LB0010NICH4LIQ.001 [153145]; LB980901233124.003 [105592]; LB0110LIQR0015.001 [OUTPUT]

NOTE: Various data sets were used to generate this figure. Refer to Table II-4 and Table II-6 in Attachment II for details.

Figure 6.2.2-2. Niche Seepage Threshold

6.2.2.2 Capillary Strength (α^{-1}) of Fractures

Philip et al. (1989 [105743]) recognized that buried cylindrical cavities are obstacles to flow, preventing water from entering the cavity. The following theoretical relation between K_o^* and K_l was provided by Philip et al. (1989 [105743], Section 3.4, p. 19):

$$K_o^* = K_l \left[\vartheta_{\max}(s)\right]^{-1} \qquad \text{(Eq. 6.2.2-1)}$$

where s is the value of the dimensionless cavity length and ϑ_{max} is the maximum value of the dimensionless potential ϑ at the boundary of the cavity. Philip et al. (1989 [105743], Equation 56, p. 20) show that ϑ_{max} occurs at the apex or crown of a cylindrical cavity. The dimensionless cavity length, s, is a measure of the relative importance of gravity and capillarity in determining flow. As $s \rightarrow 0$, capillarity dominates, whereas gravity dominates as $s \rightarrow \infty$.

An exponential functional relation between unsaturated hydraulic conductivity, $K(\psi)$, and water potential, ψ, is used (Philip et.al. 1989 [105743], Equation 12, p. 18):

$$K(\psi) = K_l \, e^{\alpha(\Psi - \Psi_e)} \qquad \text{(Eq. 6.2.2-2)}$$

K_l is the saturated hydraulic conductivity (Pullan 1990 [106141], p. 1221), ψ_e is the air-entry potential, K_l is the conductivity at $\psi = \psi_e$, and α^{-1} is the capillary-strength parameter.

This Gardner exponential functional relation is used by Philip et al. (1989 [105743], Equation 12, p. 18) and by Braester (1973 [106088], Equation 5, p. 688) to transform and linearize the unsaturated governing equations. Equation 6.2.2-2 is also used in Section 6.2.2.4 to estimate water potential.

Another model for unsaturated hydraulic conductivity and water potential is the van Genuchten model with its own capillary-strength parameter and pore-size distribution parameter (BSC 2003 [162267], Section 6.3.2.3). The distinction between model-dependent capillary-strength parameters should be noted in comparing results from the analysis presented in this section and the results from the seepage calibration model and other PA models.

Philip et al. (1989 [105743], Equation 14, p. 18) note that the dimensionless cavity length s in Equation 6.2.2-1 is related to the capillary strength parameter α^{-1} (Equation 6.2.2-2) and a characteristic length of the cavity ℓ by the following expression:

$$s = 0.5\alpha\ell \qquad \text{(Eq. 6.2.2-3)}$$

When s is large, Philip et al. (1989 [105743], Section 6, pp. 23–25) demonstrate that a boundary layer adjoining the ceiling of the cavity surface will develop. This allows the steady flow equation to be replaced by a boundary-layer equation that is readily solved. The asymptotic expansion of ϑ_{max} for large values of s yields (Philip et al. 1989 [105743], Equation 84, p. 23):

$$\vartheta_{\max} = 2s + 2 - \frac{1}{s} + \frac{2}{s^2} - \ldots \qquad \text{(Eq. 6.2.2-4)}$$

Philip et al. (1989 [105743], Table 1, Section 6, p. 25) note that when $s \geq 1$, the first three terms on the right-hand side of Equation 6.2.2-4 produce an adequate estimate that is within 12% or better of the exact value of ϑ_{max}. Therefore, using appropriate values for K_o^*, ℓ, and K_l, we can estimate the capillary strength (α^{-1}) for the porous medium from Equation 6.2.1-1, Equation 6.2.1-3, and the first three terms in Equation 6.2.2-4. This technique was utilized to compute the α^{-1} values reported in Table 6.2.2-2, using the values for K_o^* derived in Section 6.2.2.1. The K_l values were derived from post-excavation air-injection tests summarized in Table 6.2.2-1, and a value of 2 was used for ℓ, which is approximately equal to the radius of the curvature of the niche ceiling. By taking the reciprocal of the α^{-1} reported in Table 6.2.2-2, which in our case also equals s, all the s-values (with the exception of Niche 3107 [Niche 3] UM 4.88–5.18 m) are greater than one, justifying the use of Equation 6.2.2-4. The s-value for Niche 3107 (Niche 3) UM 4.88–5.18 m is slightly less than one (i.e., 0.43), implying that the use of Equation 6.2.2-4 will result in a larger error in α^{-1} for this test.

Table 6.2.2-2. Alpha (α) Values Estimated for the Fractures

Niche	Borehole and Interval (m)	Output Capillary Strength α^{-1} (m)
3650	UL 7.01-7.32	0.0855
	UL 7.62-7.92	0.0013
	UM 4.27-4.57	0.0225
	UM 4.88-5.18	0.0008
	UM 5.49-5.79	0.0334
	UR 4.27-4.57	0.0532
	UR 4.88-5.18	0.0205
	UR 5.49-5.79	0.71
	UR 6.10-6.40	0.0004
	UR 6.71-7.01	0.0014
4788	UL 7.62-7.93	0.0095
	UM 6.10-6.40	0.0015
	UR 5.18-5.48	0.0523
Theoretical limit		0.0019

DTN: LB980901233124.003 [105592]; LB990601233124.001 [105888]

NOTE: Various data sets were used to derive α^{-1}. Refer to Attachment II, Table II-5 for detail.

An early analysis based on visual inspection and straight-line fitting of Niche 3650 (Niche 2) short-duration test data in Figure 6.2.2-2 is documented in Trautz and Wang (2000 [165419]). In

this section of this scientific analysis report, the Niche 3650 (Niche 2) data analyses are compared with the results of long-duration tests at Niche 4788 (Niche 4).

Philip (1989 [156974]) reports that α^{-1} ranges from 0.05 m or less for coarse-grained soils to 5 m or more for fine-textured soils. In comparison, the values reported in Table 6.2.2-2 range from 0.001 to 0.71 m for the fractures tested, with the lower bound below that normally reported in the literature for soils. Philip (1989 [156974]) and White and Sully (1987 [106152], p. 1514) recognized that α^{-1} is a K-weighted mean soil-water potential directly related to the macroscopic capillary length, or pore radius r of the medium, as follows:

$$2\alpha^{-1} = \frac{2\gamma\cos(\theta)}{\rho g r} \qquad \text{(Eq. 6.2.2-5)}$$

where γ, ρ, and θ are the surface tension, density, and contact angle of the fluid, respectively, and g is gravitational acceleration. The right-hand-side of Equation 6.2.2-5 is known as Laplace's capillary formula, which is equal to the height of fluid rise in a small diameter cylindrical tube. Equation 6.2.2-5 can also be used to estimate the height of fluid rise between two smooth parallel plates (analogous to a fracture) by substituting the aperture b, or separation distance between plates for r in Equation 6.2.2-5.

Bouwer (1966 [155682], p. 733) and Raats and Gardner (1971 [155683], p. 922) described the macroscopic capillary length, and hence $2\alpha^{-1}$, as a "mean" height of capillary rise above a water table, or the "mean" air-entry head. In our case, the significance of $2\alpha^{-1}$ is that it represents the mean height that water can be retained in the fractures above the drift (without seeping) because of the capillary barrier.

Figure 6.2.2-2 was generated by plotting the K_o^* values derived in Section 6.2.2.1 along with their corresponding K_l values reported in Table 6.2.2-1. The significance of the line in Figure 6.2.2-2 is that it corresponds to the smallest value of α^{-1} that can be obtained, given the limited range of validity for the capillary mechanism using Laplace's formula. Wang and Narasimhan (1993 [106793], p. 329) show that when the fracture aperture is very large, the radial curvature of the fluid meniscus between two parallel plates will be very large and the capillary effect will be negligible. Using Laplace's formula, they determined for a wetting fluid of contact angle zero (i.e., $\theta = 0$ in Equation 6.2.2-5) that the capillary mechanism is no longer valid when the maximum aperture b_{max} between two smooth-walled parallel plates exceeds

$$b_{max} = \left(\frac{2\gamma}{\rho g}\right)^{1/2} \qquad \text{(Eq. 6.2.2-6)}$$

For $\gamma = 0.072$ kg/s^2, $\rho = 998$ kg/m^3, and $g = 9.8$ m/s^2 the nominal aperture size is 3.84 mm, which, using Equation 6.2.2-5, corresponds to a limiting value for α^{-1} equal to 0.0019 m. The line in Figure 6.2.2-2 represents the practical limit of Equation 6.2.2-1 calculated using the limiting value of α^{-1} derived from Equation 6.2.2-5 and Equation 6.2.2-6. Therefore, values of α^{-1} less than 0.0019 m correspond to nominal apertures that are greater than 3.84 mm, the point at which capillary forces vanish and gravity forces dominate flow. Several data points are

slightly above the line in Figure 6.2.2-2. This implies that gravity forces dominate fluid flow through these features.

6.2.2.3 Estimated Volumetric Water Content (θ) of Fractures

Another useful piece of information that can be derived using the niche seepage data includes estimates of the change in volumetric water content θ, where θ = (volume of water in fractures)/(bulk volume of fractured tuff) of the fractures. Direct measurement of fracture θ in the field is difficult at best using conventional hydrological techniques (e.g., using neutron moisture logs). Therefore, an alternative method of measuring average volumetric water contents indirectly, using wetting-front arrival times observed at the niche ceiling during the seepage tests, is described below.

Based on mass conservation along the vertical flow path, the depth of the wetting front below the water source is:

$$z_p = \frac{q_s t}{(\theta_{ave} - \theta_n)} \qquad \text{(Eq. 6.2.2-7)}$$

where z_p is the depth from the water-supply surface to the leading edge of the wetting front, t is the arrival time of the front at depth z_p, q_s is the constant flux of water supplied at the source, and θ_n is the initial or antecedent (or residual) water content.

Using the arrival time for the wetting front observed at the niche ceiling (DTN: LB980001233124.004 [136583]) and the q_s data (DTN: LB980001233124.004 [136583]), it is possible to estimate the change in volumetric water content change $\Delta\theta = \theta_{ave} - \theta_n$ for each seepage test by applying Equation 6.2.2-7. (Computation of $\Delta\theta$ was performed in an Excel spreadsheet documented in Attachment II, Table II-8 for Niche 4788 [Niche 4]. The $\Delta\theta$ was not computed for Niche 3107 [Niche 3]—refer to Section 6.2.2.4.) Table 6.2.2-3 provides a summary of the estimated $\Delta\theta$ values for zones where three or more seepage tests were conducted. With the approximation that the initial, antecedent, or residual moisture content θ_n is negligible compared to θ_{ave}, then $\Delta\theta$ becomes a measure of the average volumetric water content.

The water-content values shown in Table 6.2.2-3 range from 0.09 to 5.0%. Surprisingly, this indicates that the saturated water contents or porosities of the fractures could be as high as 5.0%, which is greater than expected. In turn, these values could influence travel-time calculations computed for the unsaturated zone, since travel time is proportional to water content. Using larger water content for the fractures would result in longer travel times.

The approach used to estimate water contents for the fractures are evaluated in Attachment IV.1 and Attachment IV.3.

Table 6.2.2-3. Estimated Changes in Volumetric Water Content ($\Delta\theta$)

Niche	Depth (m)	Test Name	Liquid Release Flux q_s, (m/s)	Average Water Content Change $\Delta\theta = \theta_{ave} - \theta_n$ (m^3/m^3)
3650	UL 7.62-7.92	Test #2 1-6-98	9.49E-06	0.0101
	UL 7.62-7.92	Test #1 2-12-98	1.89E-06	0.0017
	UL 7.62-7.92	Test #1 3-4-98	2.33E-07	0.0009
	UM 4.27-4.57	Test 5 Niche 3650 (11-13-97)	3.78E-05	0.0242
	UM 4.27-4.57	Test #1 12-3-97	9.42E-06	0.0146
	UM 4.27-4.57	Test #2 12-3-97	9.47E-06	0.0075
	UM 4.27-4.57	Test #1 1-7-98	8.82E-07	0.0120
	UM 4.27-4.57	Test #2 2-10-98	3.09E-07	0.0063
	UM 4.88-5.18	Test 1 Niche 3650 (11-12-97)	5.41E-05	0.0150
	UM 4.88-5.18	Test #1 12-4-97	9.49E-06	0.0043
	UM 4.88-5.18	Test #2 12-5-97	2.70E-06	0.0040
	UM 4.88-5.18	Test #1 1-8-98	8.75E-07	0.0082
	UM 4.88-5.18	Test #1 3-6-98	2.48E-07	0.0083
	UM 5.49-5.79	Test 4 Niche 3650 (11-13-97)	3.87E-05	0.0124
	UM 5.49-5.79	Test #2 12-4-97	9.43E-06	0.0061
	UM 5.49-5.79	Test #1 1-9-98	1.08E-06	0.0046
	UM 5.49-5.79	Test #1 2-11-98	2.55E-07	0.0040
	UR 6.71-7.01	Test #1 1-13-98	3.68E-06	0.0024
	UR 6.71-7.01	Test #1 2-3-98	1.91E-06	0.0018
	UR 6.71-7.01	Test #1 3-5-98	2.48E-07	0.0017
4788	UL 7.62-7.93	Test #1 11/3/99	1.65E-06	0.0200
	UL 7.62-7.93	Test #1 11-30-99 Niche 4788	9.22E-07	0.0057
	UL 7.62-7.93	Test #1 6-26-2000	3.59E-07	0.0101
	UL 7.62-7.93	Test #1 01-24-00	1.46E-07	0.0115
	UM 6.10-6.40	Test #1 Niche 4788 11/16/99	1.72E-06	0.0489
	UM 6.10-6.40	Test #1 Niche 4788 12-10-99	7.33E-07	0.0503
	UM 6.10-6.40	Test #1 06-08-2000	3.83E-07	0.0331
	UM 6.10-6.40	Test #1 3-14-2000	1.66E-07	0.0355
	UR 5.18-5.48	Test #1 Niche 4788 12/7/99	1.69E-06	0.0092
	UR 5.18-5.48	Test #1 1/5/2000	7.11E-07	0.0055
	UR 5.18-5.48	Test #1 02-14-2000	1.65E-07	0.0055

DTN: LB980901233124.003 [105592] and DTN: LB0110LIQR0015.001 [OUTPUT]

6.2.2.4 Estimated Water Potentials (ψ) of Fractures

The direct measurement of water potentials is difficult to make in unsaturated fractures because hydrological instruments are not readily adaptable to measuring such small features. Therefore, an indirect measure of the water potential (ψ) was formulated using the α-values computed in Section 6.2.2.2, the liquid-release fluxes, air-derived saturated hydraulic conductivities, employing Equation 6.2.2-2 with $q_s = K(\psi)$, and solving for ψ as shown below:

$$\psi = \frac{\ell n\left(q_s / K_l\right)}{\alpha} \qquad \text{(Eq. 6.2.2-8)}$$

Using the values for q_s and K_l reported in DTN: LB980001233124.004 [136583] and the α-values from Table 6.2.2-2, ψ was computed for several Niche 3650 (Niche 2) tests by employing Equation 6.2.2-8. (Computation of ψ was performed in an Excel spreadsheet documented in Attachment II, Table II-7 for Niche 4788 [Niche 4; ψ was not computed for Niche 3107 [Niche 3] because a value for K_l could not be computed: the corresponding air k value was not measurable with the equipment used). A summary of the resulting ψ values is provided in Table 6.2.2-4.

Table 6.2.2-4. Estimated Water Potential (ψ) for the Fractures

Niche	Borehole/Depth (m)	Test Name	Absolute Value of the Water Potential ψ (m)
3650	UL 7.62-7.92	Test #2 1-6-98	3.59E-03
	UL 7.62-7.92	Test #1 2-12-98	5.68E-03
	UL 7.62-7.92	Test #1 3-4-98	8.39E-03
	UM 4.27-4.57	Test 5 Niche 3650 (11-13-97)	8.26E-03
	UM 4.27-4.57	Test #1 12-3-97	2.30E-02
	UM 4.27-4.57	Test #2 12-3-97	2.29E-02
	UM 4.27-4.57	Test #1 1-7-98	7.64E-02
	UM 4.27-4.57	Test #2 2-10-98	1.00E-01
	UM 4.88-5.18	Test 1 Niche 3650 (11-12-97)	3.13E-03
	UM 4.88-5.18	Test #1 12-4-97	4.56E-03
	UM 4.88-5.18	Test #2 12-5-97	5.58E-03
	UM 4.88-5.18	Test #1 1-8-98	6.50E-03
	UM 4.88-5.18	Test #1 3-6-98	7.53E-03
	UM 5.49-5.79	Test 4 Niche 3650 (11-13-97)	1.95E-02
	UM 5.49-5.79	Test #2 12-4-97	2.77E-02
	UM 5.49-5.79	Test #1 1-9-98	1.00E-01
	UM 5.49-5.79	Test #1 2-11-98	1.48E-01
	UR 6.71-7.01	Test #1 1-13-98	5.90E-03
	UR 6.71-7.01	Test #1 2-3-98	6.84E-03
	UR 6.71-7.01	Test #1 3-5-98	9.76E-03
4788	UL 7.62-7.93	Test #1 11/3/99	2.56E-02
	UL 7.62-7.93	Test #1 11-30-99 Niche 4788	3.12E-02
	UL 7.62-7.93	Test #1 6-26-2000	4.01E-02
	UL 7.62-7.93	Test #1 01-24-00	4.86E-02
	UM 6.10-6.40	Test #1 Niche 4788 11/16/99	7.38E-03
	UM 6.10-6.40	Test #1 Niche 4788 12-10-99	8.65E-03
	UM 6.10-6.40	Test #1 06-08-2000	9.61E-03
	UM 6.10-6.40	Test #1 3-14-2000	1.09E-02
	UR 5.18-5.48	Test #1 Niche 4788 12/7/99	4.41E-02
	UR 5.18-5.48	Test #1 1/5/2000	8.93E-02
	UR 5.18-5.48	Test #1 02-14-2000	1.66E-01

DTN: LB980001233124.004 [136583]; DTN: LB980901233124.003 [105592]

NOTE: Various data sets were used to generate this table. Refer to Table II-7 in Attachment II for details.

6.2.2.5 Fracture-Water Characteristic Curves

The volumetric water-content values from Section 6.2.2.3 and the water-potential values derived in Section 6.2.2.4 are plotted on Figure 6.2.2-3 to create a water-characteristic curve for the fractures. Only those test intervals where three or more tests were conducted are included in the figure. (Inclusion of zones having only two data points joined by a straight line contributes little to understanding of the functional relation between θ and ψ.).

Note that the data fall into two groups, exhibiting similar water-retention characteristics. The first group (N3650 UL 7.62-7.92 m, N3650 UR 6.71-7.01 m and N3650 4.88-5.18 m) consists of high-permeability fractures that drain over a narrow range of water potentials and appear to have low residual water contents of about 0.001 to 0.002. The second group (N3650 UM 4.27-4.57 m, N3650 UM 5.49-5.79 m, N4788 UM 6.10-6.40 m, N4788 UL 7.62-7.93 m, and N4788 UR 5.18-5.48 m) consists of lower-permeability fractures that drain over a relatively larger range of water potentials and appear to have a slightly larger residual water content of about 0.005.

Residual water remaining in the fracture after the initial test can cause subsequent test data (collected during a test performed at a similar rate) to shift to the left, parallel to the x-axis, as shown in Figure 6.2.2-4 for zone N3650 UM 4.27-4.57 m. The second and third tests from this interval were conducted at nearly identical fluxes (9.42E-06 versus 9.47E-06 m/s) separated in time by less than 2 hours. The wetting front arrived at the niche ceiling during the second test in about half the time as the first test, resulting in a $\Delta\theta$ value that is half that for the second test compared to the first. The fourth and fifth tests in the sequence were performed approximately one and two months later, respectively. Evidence of the effects of wetting history is not readily apparent for these tests, which were conducted at lower fluxes (corresponding to lower water contents), indicating that the fractures drained or dried out prior to retesting.

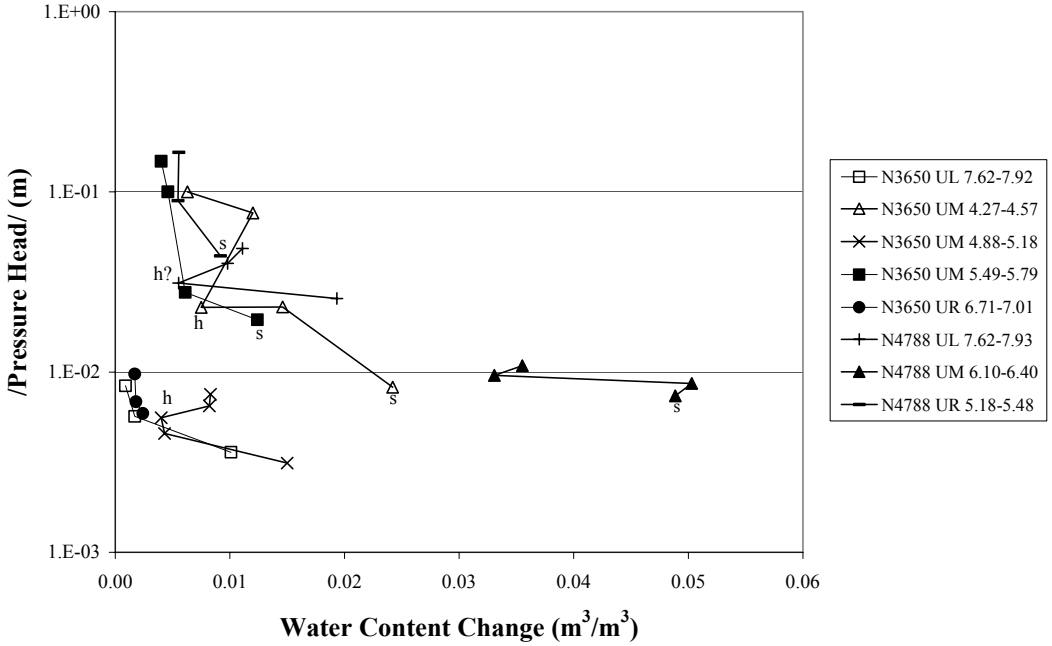

DTN: LB980901233124.003 [105592] and LB0110LIQR0015.001 [OUTPUT]

NOTE: Various data sets were used to generate this Figure. Refer to Table II-7 and Table II-8 in Attachment II for details.

s = saturated conditions
h = data point influenced by wetting history

Figure 6.2.2-3. Water Retention Curves for Fractures

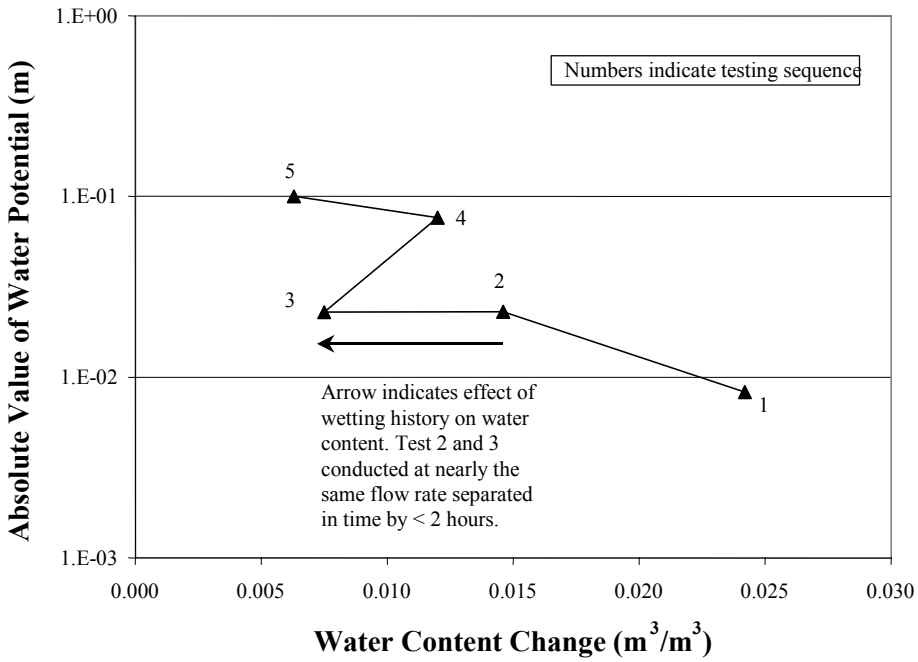

DTN: LB980901233124.003 [105592]

NOTE: Various data sets were used to generate this Figure. Refer to Table II-7 and Table II-8 in Attachment II for details.

Figure 6.2.2-4. Effect of Wetting History on Water Retention Curves for Test Interval N3650 UM 4.27–4.57 m

INTENTIONALLY LEFT BLANK

6.3 ANALYSES OF TRACER-MIGRATION DELINEATION AT NICHE 3650 (NICHE 2)

An additional episodic tracer migration test was conducted at drift-seepage test site Niche 3650 (Niche 2) in the ESF to elucidate the flow paths above the niche ceiling. The distribution of tracers from both the tracer migration test and previous liquid-release and seepage-threshold tests are presented in this section.

6.3.1 Tracer Distribution from the Tracer-Migration Test

6.3.1.1 Field Studies at Niche 3650 (Niche 2)

Seven 0.0762 m diameter boreholes were drilled at Niche 3650 (Niche 2). Three of these boreholes, designated UL, UM, and UR, were drilled approximately one meter apart and 0.65 m above the niche ceiling in the same horizontal plane as shown in Figure 6.1.1-2b. An array of twelve sampling boreholes was drilled to collect core samples for tracer analyses, as shown in Figure 6.3.1-1. The core analyses delineated the extent of tracer migration from an episodic liquid-release event as well as for all tracer and liquid-release tests.

Liquid-release tests were conducted prior to the niche excavation to evaluate how far a finite pulse of liquid would travel through unsaturated fractured rock (Section 6.2.1). Water containing colored dyes was used to mark the wetted area and flow paths resulting from each test. The niche was then excavated dry (using an Alpine Miner) to observe and photograph the distribution of fractures and dye within the welded tuff (Section 6.2.1 and Wang et al. 1999 [106146], pp. 329–332). After niche excavation, a series of short-duration seepage tests were performed to determine the amount of liquid that would seep into the mined opening (Section 6.2.2).

Along the three upper boreholes (UL, UM, UR), two Food, Drug & Cosmetics (FD&C) dyes were released before niche excavation: FD&C Blue No. 1 and FD&C Red No. 40. Blue and red bars in Figure 6.3.1-1a on the upper-left side of test-interval locations represent the pre-excavation liquid-release tests. Post-excavation liquid-injection tests, both with and without tracers, were conducted at various intervals along the boreholes to measure seepage into the niche. Post-excavation tracers included FD&C Blue No. 1, Sulpho Rhodamine B, Pyranine, FD&C Yellow No. 6, Acid Yellow 7, and Amino G Acid. The post-excavation seepage test sequences are summarized schematically on the lower right side of test-interval locations in Figure 6.3.1-1a.

6.3.1.2 Tracer Migration Test

The tracer migration test was conducted at Niche 3650 (Niche 2) six months after the seepage tests. From September 16–18, 1998, water containing six tracers (4.60 g/l NaI, 4.60 g/l CaI_2, 4.60 g/l $CaBr_2$, 1.56 g/l FD&C Blue No.1, 1.76 g/l FD&C Yellow No. 5, 0.019 g/l 2,3-difluorobenzoic acid, and 0.018 g/l pentafluorobenzoic acid) was released into a highly permeable zone located in borehole UM 4.88–5.18 m from the borehole collar. Iodide, bromide, and fluorinated benzoic acids were used as nonreactive tracers, while the others were applied as sorbing tracers. The release rate was 0.013 g/s, with a total released volume of about 1.52 liters.

The wetting front was observed to reach the niche ceiling in a large fracture/breakout, but water did not drip into the niche.

Between September 23 and October 1, 1998, twelve sampling boreholes, nominally 1.5 m long, were drilled into the niche ceiling around and below the liquid-release interval to determine the extent of the tracer migration. Rock-core samples were collected during the drilling process for subsequent laboratory chemical analyses. (Refer to Wang 1999 [153449], p. 99–107, 123, and 124 for detailed description of this tracer migration test.)

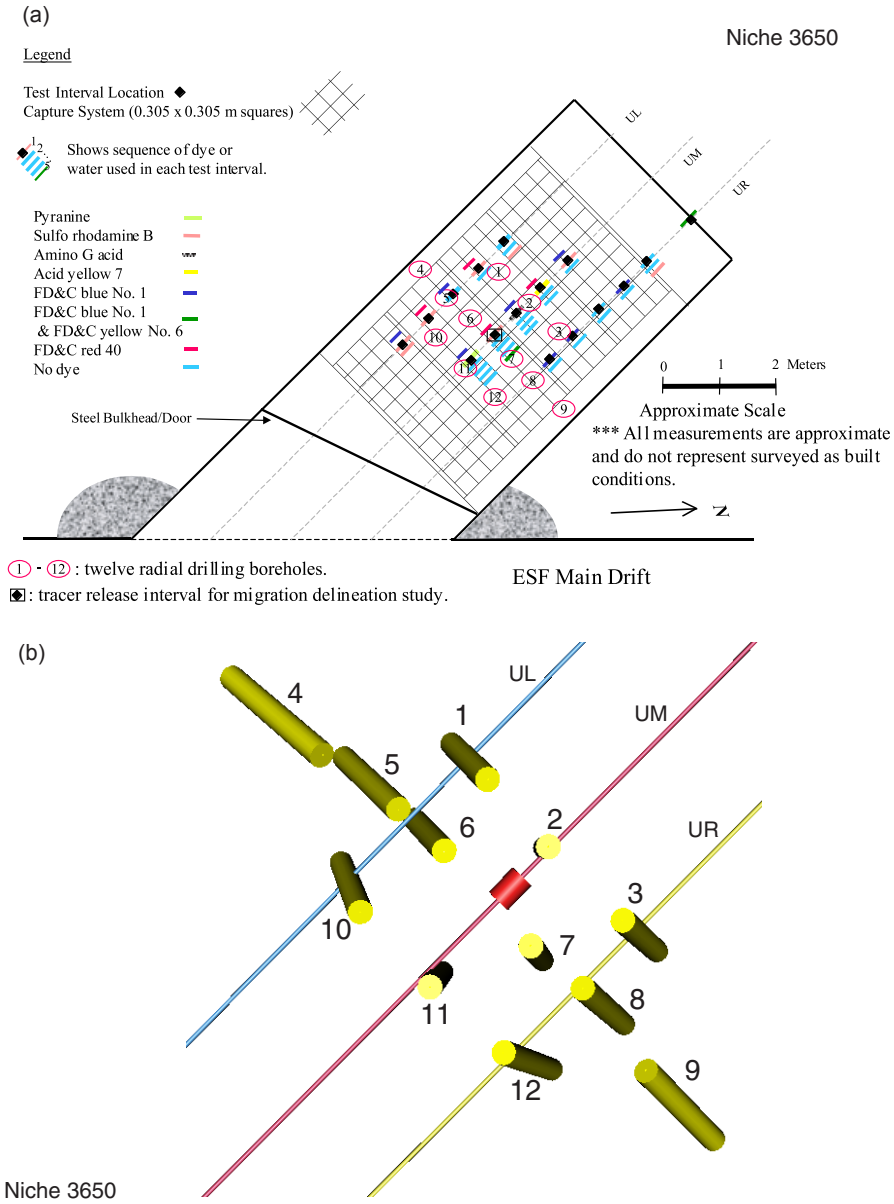

NOTE: The red-colored cylinder denotes the release interval of the tracer migration test.

Figure 6.3.1-1. Schematic of Sampling Borehole Array: (a) Plan View with Liquid-Release/Dye-Application History, and (b) Three-Dimensional View from inside the Niche

Figure 6.3.1-1b shows a 3-D perspective view of the sampling borehole array. The cores from the boreholes were 4.47 cm in diameter and were divided into sections during coring, with each section separately wrapped in Saran wrap. Each wrapped sample was placed inside a Lexan liner (with tape wrapping sealing both ends of the liners) and sealed in a Protecore® packet. The interval for each section was noted on the packet, which was assigned a unique numeric identifier.

The tracer chemical information is shown in Hu 1999 ([156541], pp. 154–155), and Hu 1999 ([155691], p. 151). Tracer analysis results and discussions are presented as concentration ratios (independent of chemical purity). Attachment V describes core sample processing and aqueous tracer measurement for the analyses of tracer distribution.

Iodide and FD&C Yellow No. 5 concentrations were not detected above background levels in the samples collected from the twelve boreholes drilled around the release interval. Iodide and FD&C Yellow No. 5 were applied only during the tracer migration test and were not used in earlier seepage tests at Niche 3650 (Niche 2). These results indicate that the sampling borehole array did not capture the tracer plume of the tracer migration test. Liquid migration was most likely localized and very possibly confined within the 1.0 m × 1.6 m area directly below the liquid-release interval.

Several rock-chip samples were collected from the ceiling of Niche 3650 (Niche 2) in March of 2001. These samples were obtained directly under the release interval of the tracer migration test (within a radius of about 20 cm), and within the twelve sampling boreholes. Six samples have been processed for chemical concentration measurements as documented in Hu 1999 ([155691], pp. 143–144), and Hu 2000 ([156473]). Iodide was detected in all six of the analyzed samples, confirming the arrival of iodide from the wetting front observed at the niche ceiling during the tracer migration test. FD&C Yellow No. 5 was not found among the samples, possibly because of its higher sorption compared to iodide.

6.3.2 Delineation of Tracer Distributions from Previous Liquid-Release Tests

Tests prior to the tracer migration test were conducted at different borehole intervals at various flow rates to determine the seepage thresholds for each interval. A total of 40 liquid-release tests over 16 borehole intervals were conducted at Niche 3650 (Niche 2), using both water with and without dye tracers as shown in Figure 6.3.1-1a. The distributions of these tracers were evaluated through the analyses of cores from the twelve sampling boreholes drilled into the flow domains. Examples of measured dye concentration versus borehole interval are shown in Figure 6.3.2-1 and Figure 6.3.2-2. The distribution of the tracers above the niche is used to assess the extent of tracer spreading and to provide data for the evaluation of seepage processes.

Tracer data are presented as dimensionless ratios of the detected tracer level to the background level. A higher ratio indicates the stronger presence of the tracer in the particular interval of a borehole. These detection ratios provide sufficient information about the spatial distributions of tracers, reconcile the difference in measurement techniques (i.e., ultraviolet/visible and fluorescence spectrophotometers), and eliminate the need to use and verify chemical purity information provided by the manufacturers. In Section 6.3.2.2, the measured dye distributions

are illustrated in three dimensions, based on as-built borehole survey coordinates using EARTHVISION-2 V4.0 software (LBNL 1998 [152835]).

6.3.2.1 Detection of Tracers

Several dyes from previous applications of seepage tests (Section 6.2.1.3.1) were detected within the borehole samples, as summarized in Table 6.3.2-1. FD&C Blue No.1 was present in seven out of 12 boreholes, with some of the boreholes containing relatively high concentrations of the tracer. Sulpho Rhodamine B was detected within four borehole samples. Overall, the dye distribution pattern was relatively spotty, reflecting the complex interplay of preferential flow paths and liquid application history. All of the previous liquid-release and seepage tests were conducted at least six months prior to the tracer migration test (Section 6.3.1).

Table 6.3.2-1. Compilation of Tracer Detection versus Borehole Location

Borehole ID	FD&C Blue No. 1	Sulpho Rhodamine B	FD&C Yellow No. 6	Pyranine	Acid Yellow 7	Amino G Acid
1	-	+++	-	-	-	-
2	+++	-	-	-	+++++	+
3	+++	-	-	-	-	-
4	-	-	-	-	-	-
5	-	-	-	-	-	-
6	-	-	-	-	-	-
7	+++++	+++++	+++	-	-	-
8	+++	-	-	-	-	-
9	+	-	-	-	-	-
10	+++	+++++	-	+	-	-
11	+++++	+	-	+++	-	-
12	-	-	-	-	-	-

DTN: LB990601233124.003 [106051]

NOTES: -: detection ratio < 3 (treated as absent)
+: The highest detection ratio is between 3–100 within this particular borehole.
+++: The highest detection ratio is between 100–1000 within this particular borehole.
+++++: The highest detection ratio is >1,000 within this particular borehole.

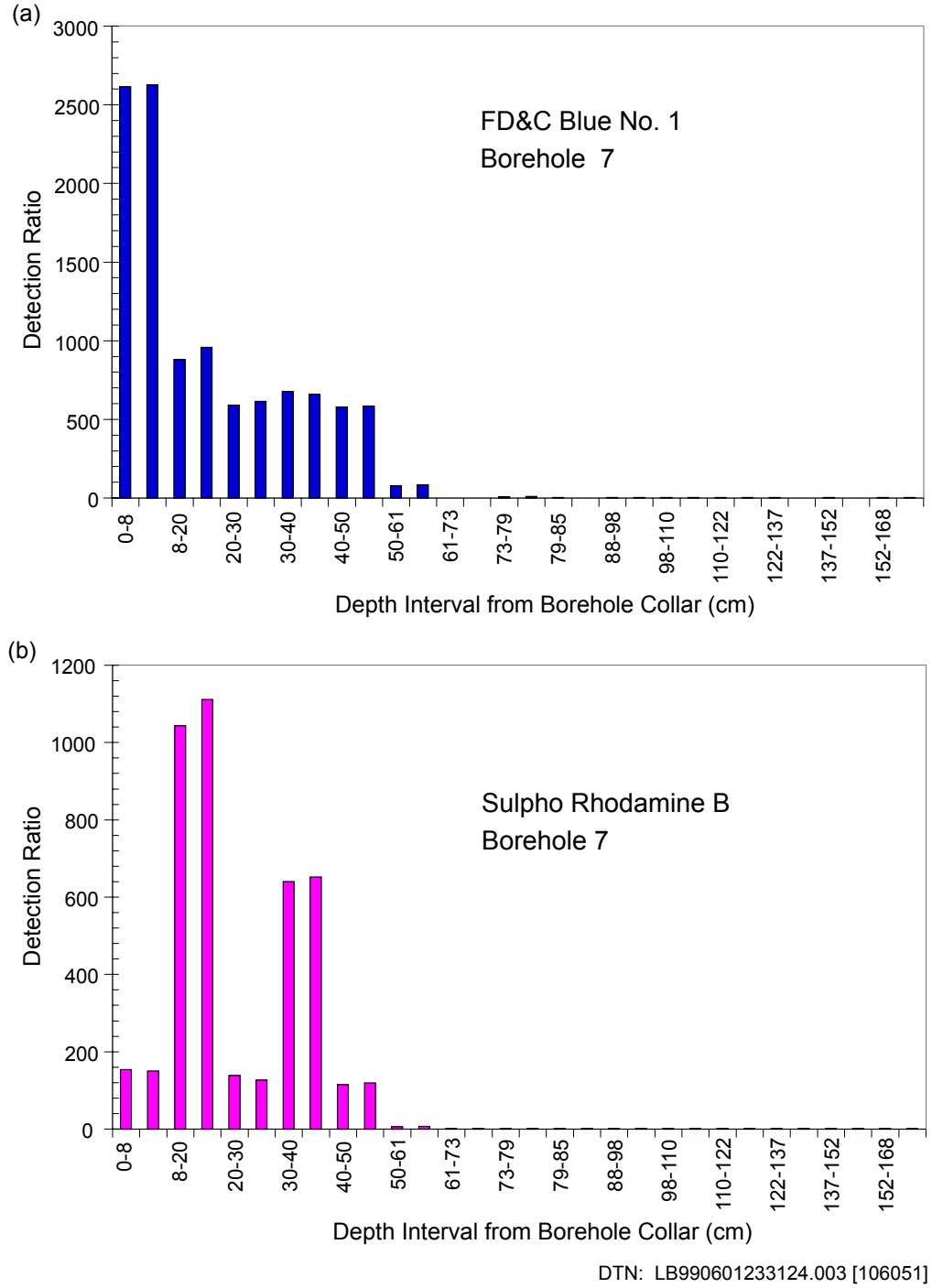

DTN: LB990601233124.003 [106051]

NOTE: Duplicate measurements were conducted in each specific interval.

Figure 6.3.2-1. Dye Detection along Borehole 7: (a) FD&C Blue No. 1 and (b) Sulpho Rhodamine B

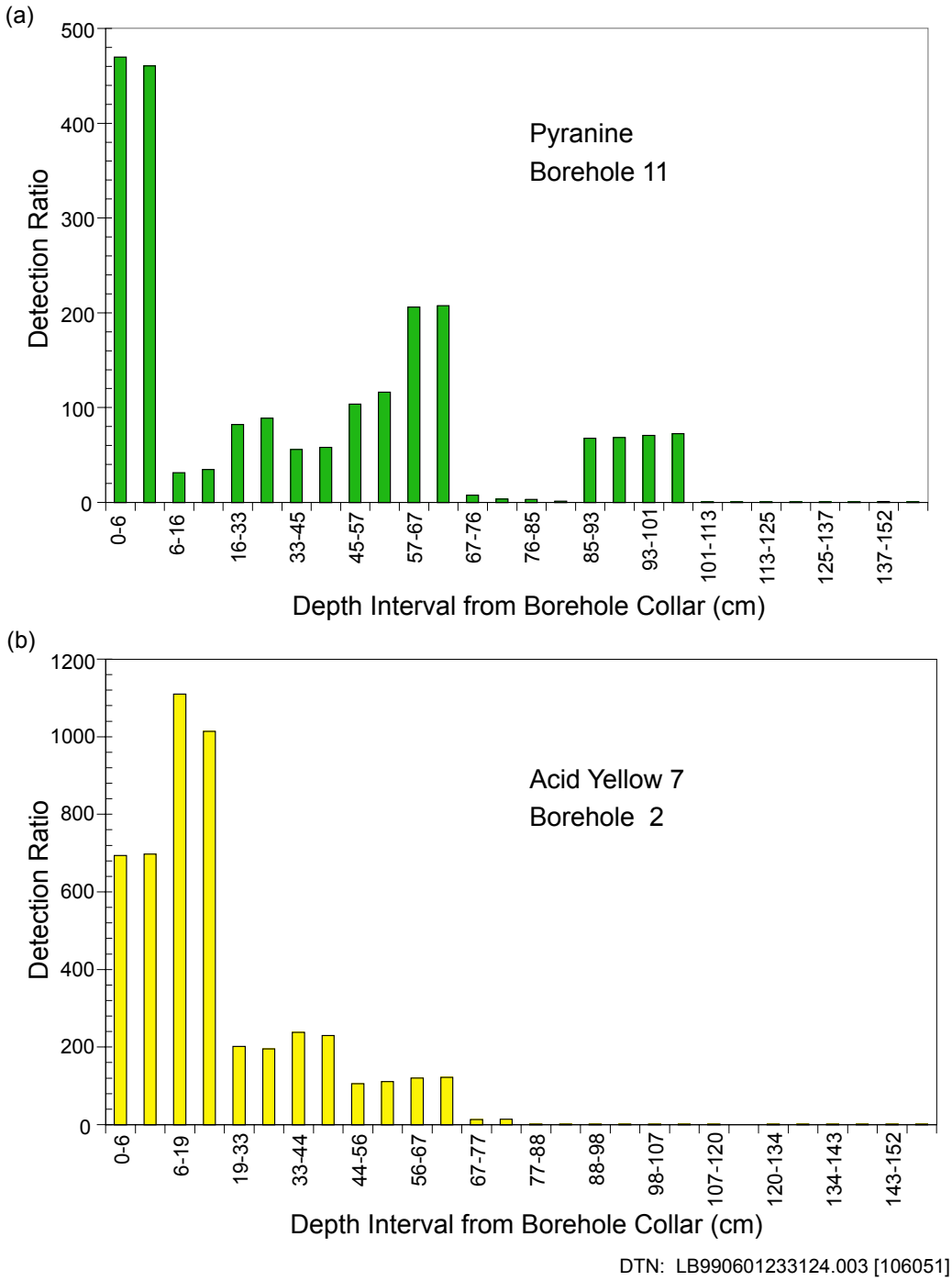

Figure 6.3.2-2. Dye Detection of: (a) Pyranine Along Borehole 11 and (b) Acid Yellow 7 along Borehole 2

6.3.2.2 Distribution of Dyes

FD&C Blue No. 1 was released in six intervals during pre-excavation liquid-release tests and in four intervals during post-excavation seepage tests (including one with a mixture of blue and yellow dyes). The blue dye distributions, together with release-interval locations, are illustrated in Figure 6.3.2-3. Boreholes where the tracer was not detected are represented by narrow lines. The multiple releases and dilutions introduced a complex application history. Overall results suggested that most regions containing blue dye were associated with tracer tests from nearby release intervals.

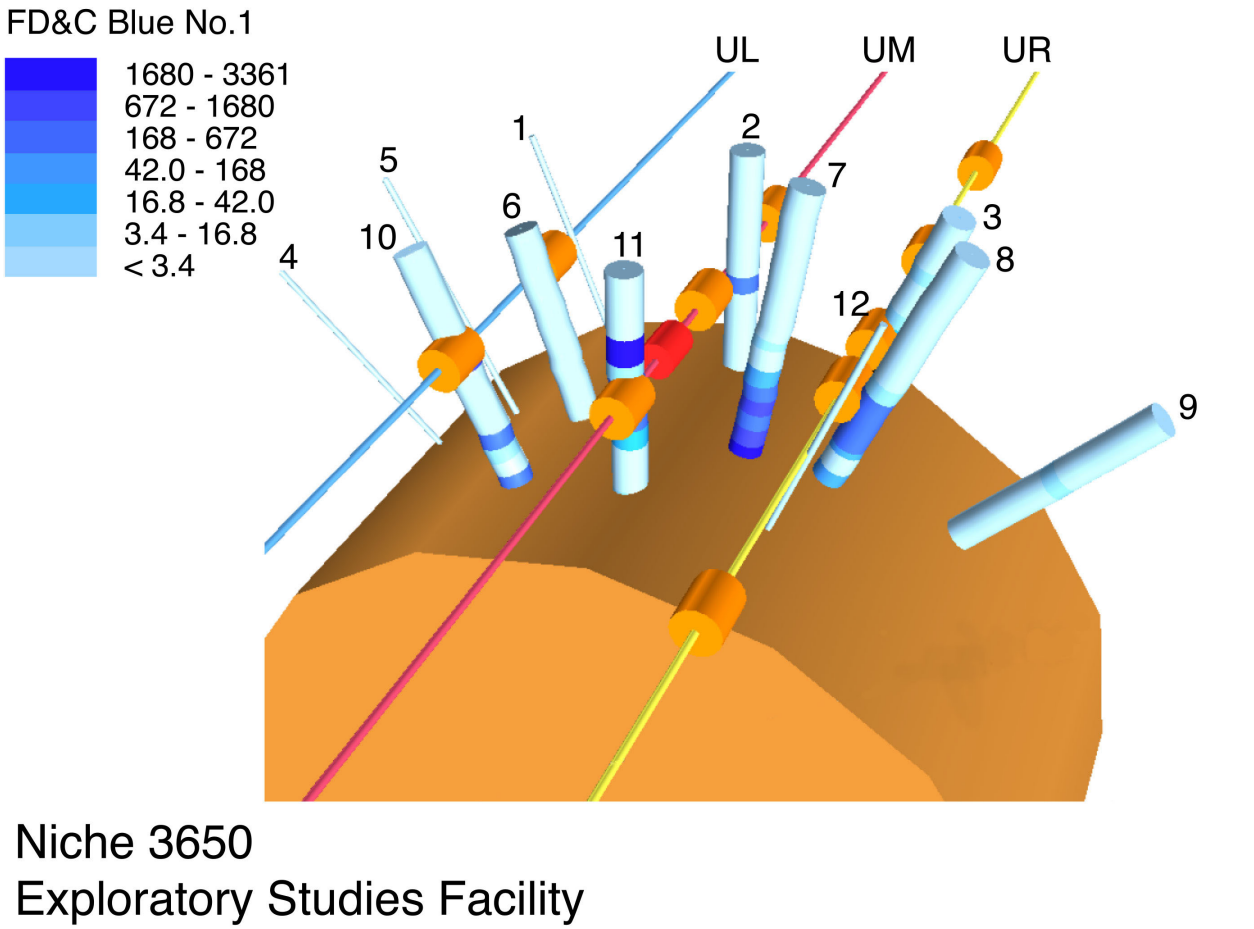

DTN: LB990601233124.003 [106051]

NOTE: The red cylinder denotes the tracer release interval of the tracer migration test and the other orange cylinders for intervals of early-release events. The sampling boreholes are individually identified. Detection ratios (dimensionless) are presented in the legend. Tracer concentrations are presented in dimensionless detection ratios as described in Section 6.3.2.

Figure 6.3.2-3. Three-Dimensional View of FD&C Blue No. 1 Detection Related to the Release Intervals above the Niche

Sulpho Rhodamine B was used in eight seepage tests along seven borehole intervals. Figure 6.3.2-4 illustrates the results for Sulpho Rhodamine B. Near borehole 7, Sulpho Rhodamine B was released once (in the interval UM 4.88–5.18 m), followed by three releases of water without dyes, and once with a mixture of FD&C Blue No. 1 and FD&C Yellow No. 6. The Sulpho Rhodamine B in borehole 7, and near the niche ceiling in borehole 8, most likely originated from this release episode. There was no Sulpho Rhodamine B detected in boreholes 3, 9, and 12. This suggested that the Sulpho Rhodamine B was likely migrating downward, rather than spreading laterally.

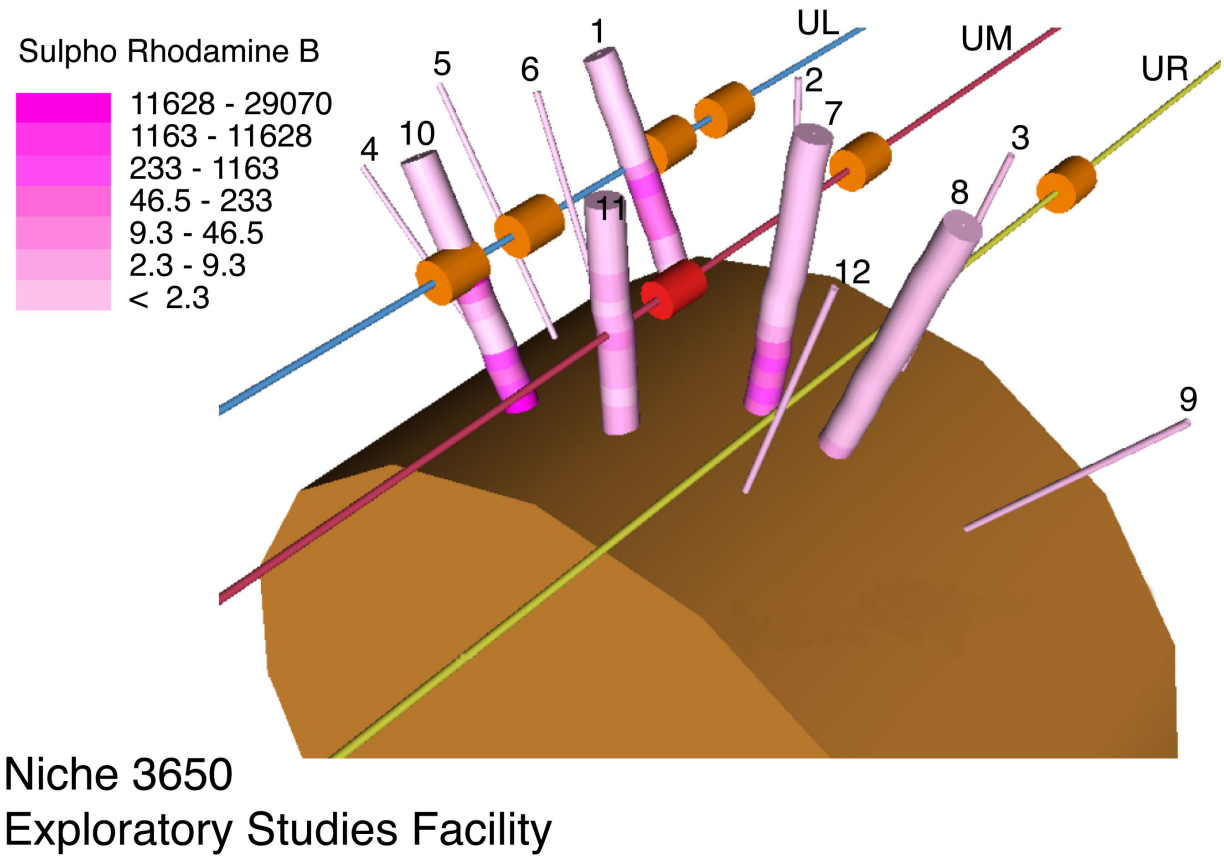

DTN: LB990601233124.003 [106051]

NOTE: The red cylinder denotes the tracer release interval of the tracer migration test and the other orange cylinders for intervals of early-release events. The sampling boreholes are individually identified. Detection ratios (dimensionless) are presented in the legend. Tracer concentrations are presented in dimensionless detection ratios as described in Section 6.3.2.

Figure 6.3.2-4. Three-Dimensional View of Sulpho Rhodamine B Detection Related to the Release Intervals above the Niche

In Niche 3650 (Niche 2), Pyranine, Acid Yellow 7, and Amino G Acid were used only once. Pyranine, Acid Yellow 7, and Amino G Acid are fluorescent dyes, and the low detection limits achievable with the fluorescence spectrophotometer provide confidence for the delineation of dye-stained flow paths within the sampling borehole array. Additionally, FD&C Yellow No. 6 was used once at UM 4.88–5.18 m within the sampling borehole array, and another time at Interval UL 7.62–7.92 m outside the borehole array (Figure 6.3.1-1a). The observations from

these tracer distributions also showed localized distributions of tracers, confirming downward migration (as opposed to the lateral spreading observed in the earlier tests).

Pyranine, for example, was detected at neighboring boreholes 10 and 11, with its presence much lower at borehole 10 than that at borehole 11 (Table 6.3.2-1 and Figure 6.3.2-5). Borehole 11 is located almost exactly below the interval of UM 4.27–4.57 m where Pyranine was released. Four episodes of water-only seepage tests were conducted following this Pyranine application. These liquid releases did not seem to enhance extensive lateral spreading. Overall, the lateral spreading of Pyranine was observed to be about 0.75 m to the left (i.e., borehole 10), resulting from these five release tests. However, its presence at borehole 10 was only slightly above the background level.

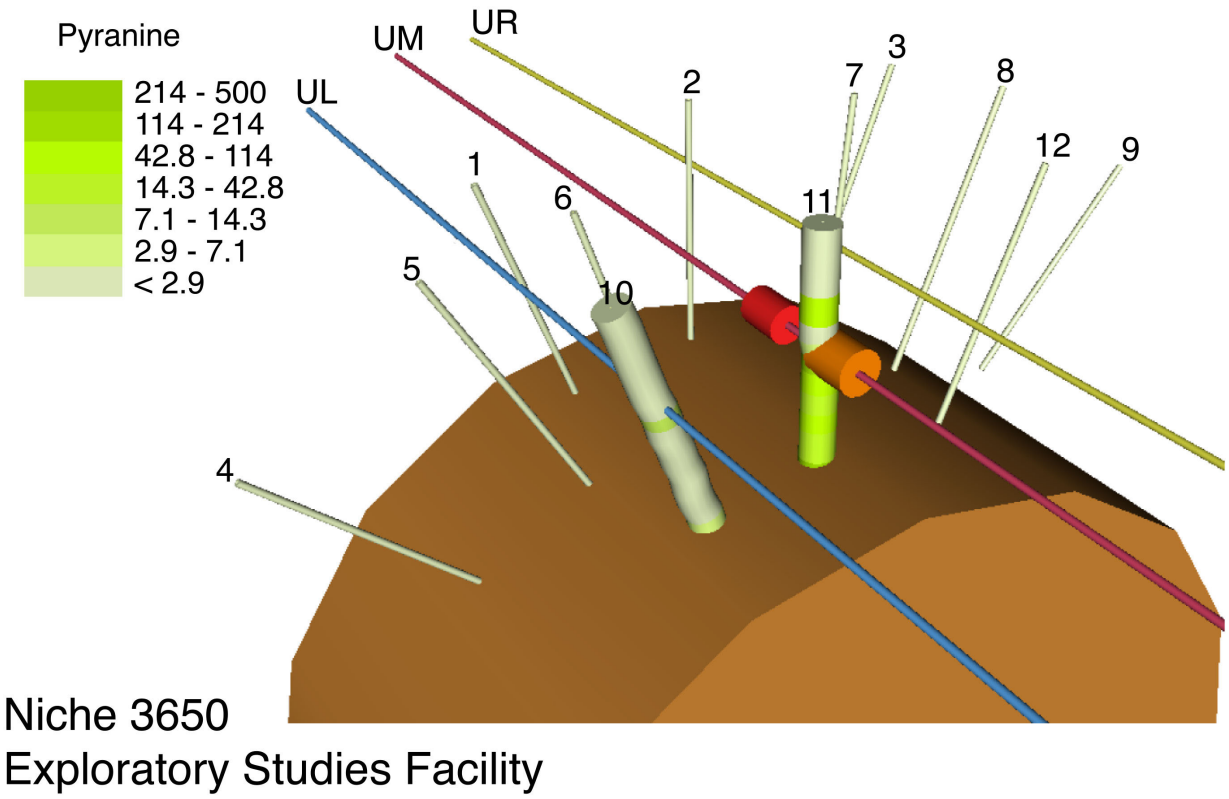

DTN: LB990601233124.003 [106051]

NOTE: The red cylinder denotes the tracer release interval of the tracer migration test and the other orange cylinder for interval of an early-release event. The sampling boreholes are individually identified. Detection ratios (dimensionless) are presented in the legend. Tracer concentrations are presented in dimensionless detection ratios as described in Section 6.3.2.

Figure 6.3.2-5. Three-Dimensional View of Pyranine Detection Related to the Release Interval above the Niche

Acid Yellow 7 was detected only at borehole 2, about 0.3 m from Interval UM 6.10–6.40 m where it was released (Figure 6.3.2-6). Amino G Acid was also detected near the detection limit at borehole 2, about 0.3 m from Interval UM 5.49–5.79 m where it was released (Figure 6.3.2-7). Note that although the Interval UM 5.49–5.79 m was encompassed within the sampling borehole array, Amino G Acid was not detected in any other borehole.

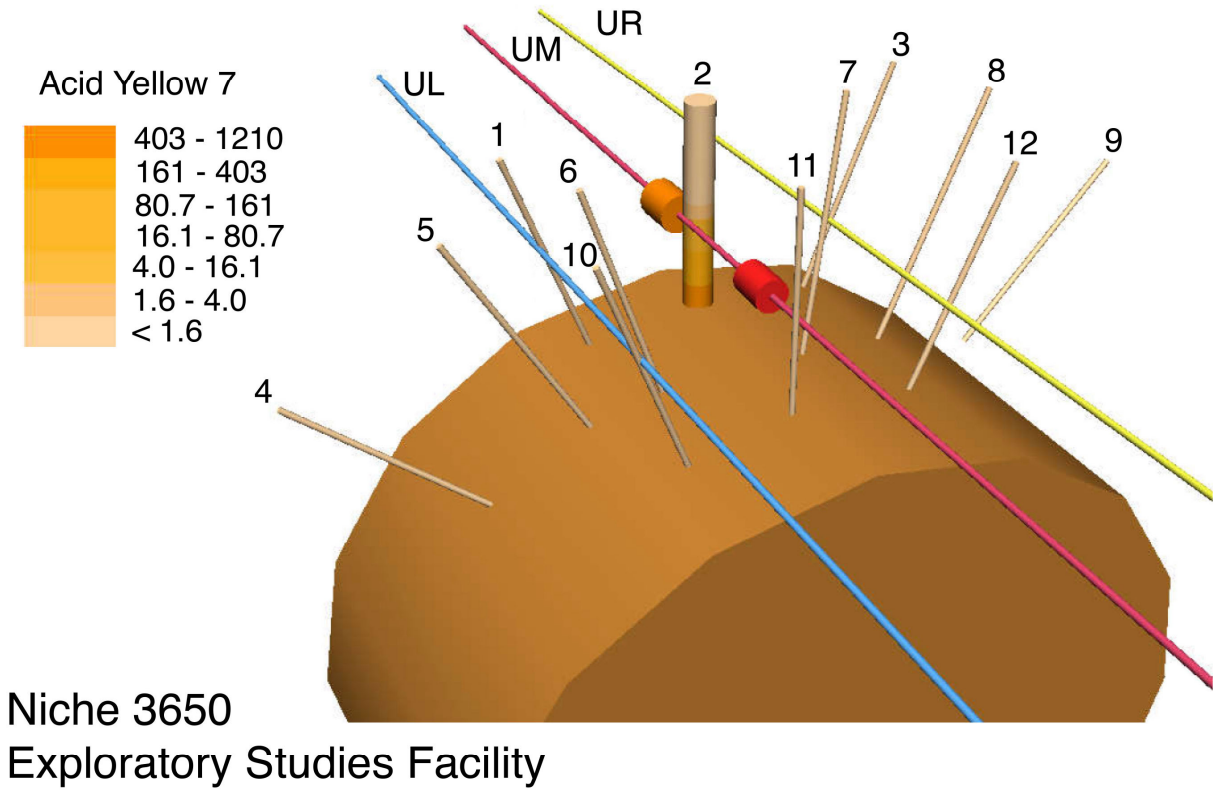

DTN: LB990601233124.003 [106051]

NOTE: The red cylinder denotes the tracer release interval of the tracer migration test and the other orange cylinder for intervals of an early-release event. The sampling boreholes are individually identified. Detection ratios (dimensionless) are presented in the legend. Tracer concentrations are presented in dimensionless detection ratios as described in Section 6.3.2.

Figure 6.3.2-6. Three-Dimensional View of Acid Yellow 7 Detection Related to the Release Interval above the Niche

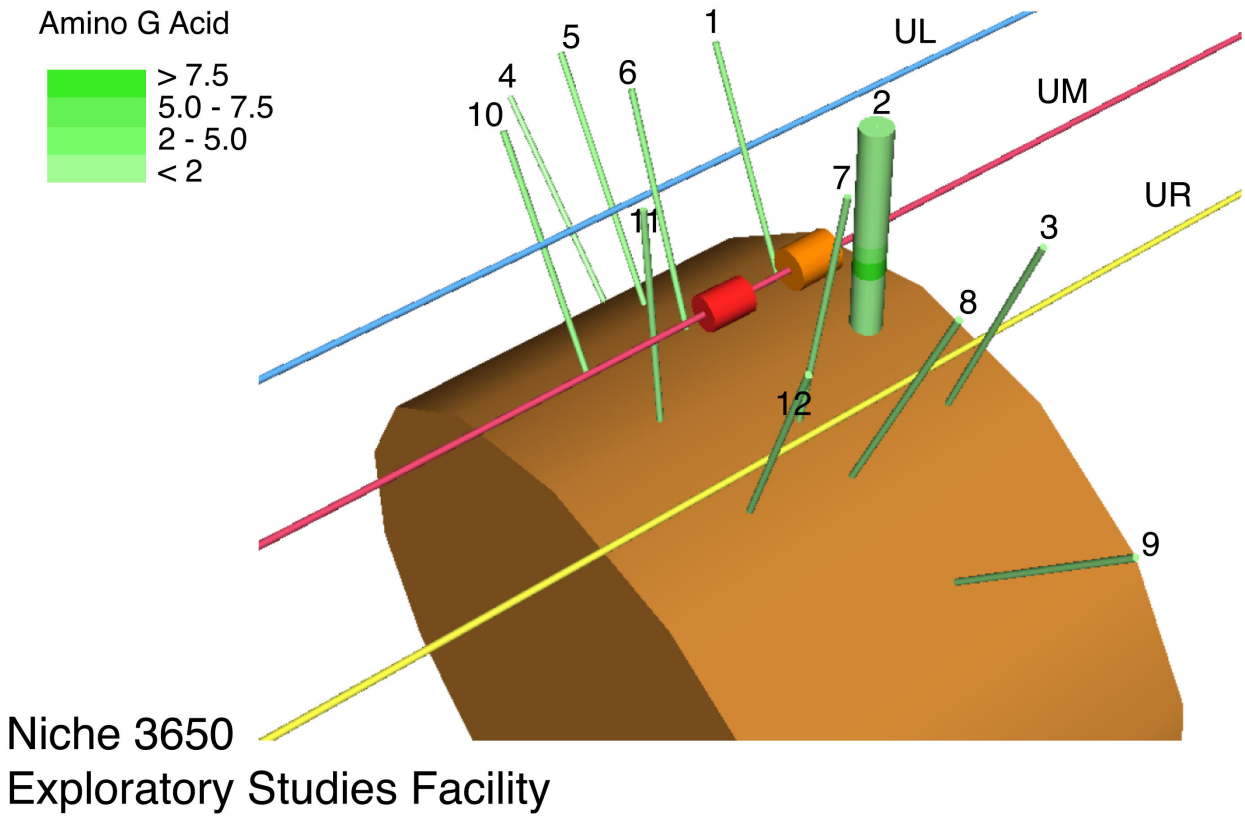

DTN: LB990601233124.003 [106051]

NOTE: The red cylinder denotes the tracer release interval of the tracer migration test and the other orange cylinder for interval of an early-release event. The sampling boreholes are individually identified. Detection ratios (dimensionless) are presented in the legend. Tracer concentrations are presented in dimensionless detection ratios as described in Section 6.3.2.

Figure 6.3.2-7. Three-Dimensional View of Amino G Acid Detection Related to the Release Interval above the Niche

The last dye distribution shown is for FD&C Yellow No. 6 (Figure 6.3.2-8). The dye was present at borehole 7. Borehole 7 was about 0.5 m from Interval UM 4.88–5.18 m where both FD&C Yellow No. 6 and FD&C Blue No. 1 were simultaneously released. This release episode had one of the lowest release rates (0.013 g/s) with one of the largest release volumes (5,597 g) among all the liquid-release tests conducted at Niche 3650 (Niche 2) (see Section 6.2 of this report). Borehole 7 is located in the middle of the sampling borehole array. The observation that FD&C Yellow No. 6 was only present in borehole 7 further demonstrated the localized characteristics of liquid flow with limited lateral spreading, even in this case with comparatively large release volume.

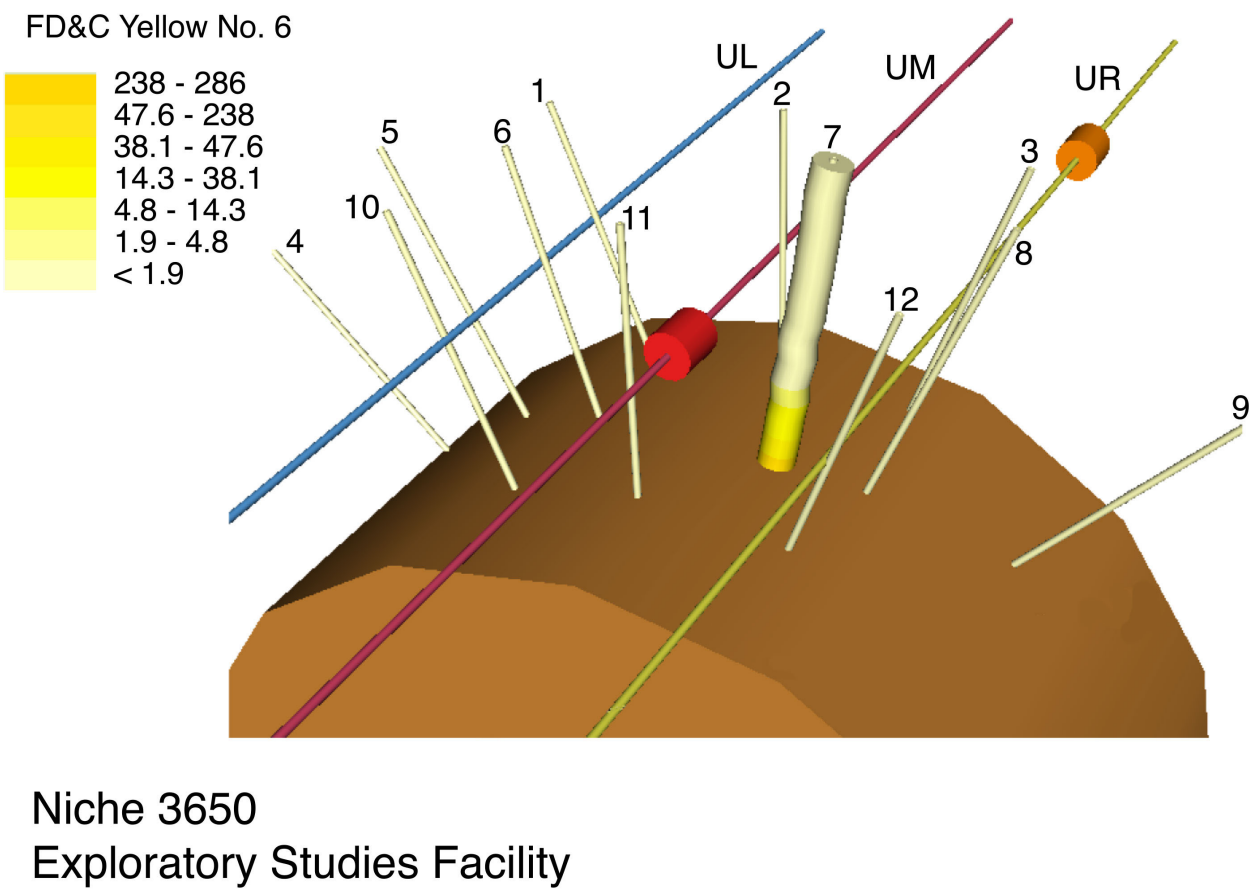

DTN: LB990601233124.003 [106051]

NOTE: The red cylinder denotes the tracer release interval of the tracer migration test and the other orange cylinders for intervals of early release events. (One of the two release intervals is the same as the last release event, represented by the red cylinder.) The sampling boreholes are individually identified. Detection ratios (dimensionless) are presented in the legend. Tracer concentrations are presented in dimensionless detection ratios as described in Section 6.3.2.

Figure 6.3.2-8. Three-Dimensional View of FD&C Yellow No. 6 Detection Related to the Release Intervals above the Niche

The dye distribution plots also indicated that some dyes have migrated above the injection intervals, as illustrated in Figure 6.3.2-3 for FD&C Blue No. 1, in Figure 6.3.2-5 for Pyranine; and to a lesser degree in Figure 6.3.2-4 for Sulpho Rhodamine B, in Figure 6.3.2-6 for Acid Yellow 7, and in Figure 6.3.2-7 for Amino G Acid. This is an interesting observation, indicating that fairly strong capillary forces may induce upward movements against gravity. Similar behavior was also observed in the Busted Butte test, as described in Section 6.13.3.1.1. However, further verification would be needed to determine the exact spatial extents of upward suction and tracer distribution. The locations of subsamples were derived from sample packets, and the spatial resolutions were poor, especially for fragmented core samples. The tracer subsample locations could be further checked against borehole logs (digital version if available) and core logs to improve spatial resolution.

6.4 ANALYSES OF TRACER PENETRATION AND WATER IMBIBITION INTO WELDED TUFF MATRIX

The objectives of this study are to investigate water flow and tracer transport, focusing on the relative extents of fracture flow and fracture-matrix interaction in the unsaturated, fractured tuff through a combination of field and laboratory experiments. Fieldwork was conducted in the ESF niches with liquid containing tracers released at specified borehole intervals. Tracer-stained rock samples were collected during niche excavation for subsequent laboratory analyses. Clean rock samples, collected from the same stratigraphic unit, were machined into cylinders for laboratory studies of tracer penetration into the rock matrix under different initial water-saturation levels. The use of laser-ablation inductively coupled-plasma mass spectrometry (LA-ICP-MS) to investigate chemical transport and sorption in unsaturated tuff is also presented.

6.4.1 Penetration of Dyes into Rocks from the Niches

Samples for laboratory analyses were collected from Niche 3650 (Niche 2) and Niche 4788 (Niche 4). The niche test sites, borehole configurations, liquid-release tests, and tracers used in the field are described in Section 6.2 and Section 6.3. Laboratory tests under controlled conditions were conducted to compare the travel front behavior of moisture, nonreactive bromide, and sorbing dye tracers (FD&C Blue No. 1 and Sulpho Rhodamine B). Sample drilling and tracer profiling techniques were developed. The descriptions and evaluations of laboratory analyses are presented in Attachment V.

6.4.1.1 Field Observations

During the niche excavation, as described in Section 6.2.1.2, dye was observed along individual fractures and intersecting fractures to a maximum depth of 2.6 m below the liquid-release points at Niche 3650 (Niche 2), and to a maximum depth of about 1.8 m at Niche 4788 (Niche 4). In general, the dye remained relatively close to the release interval and did not spread laterally more than 0.5 m. Figure 6.4.1-1 is a photograph taken during the excavation of Niche 4788 (Niche 4), showing the wall face with the fracture network stained by FD&C Blue No. 1. Results of post-excavation liquid-seepage tests at Niche 3650 (Niche 2) also indicated fast fracture flow with limited lateral spreading, since seepage water was captured directly below in trays beneath or immediately adjacent to the test interval.

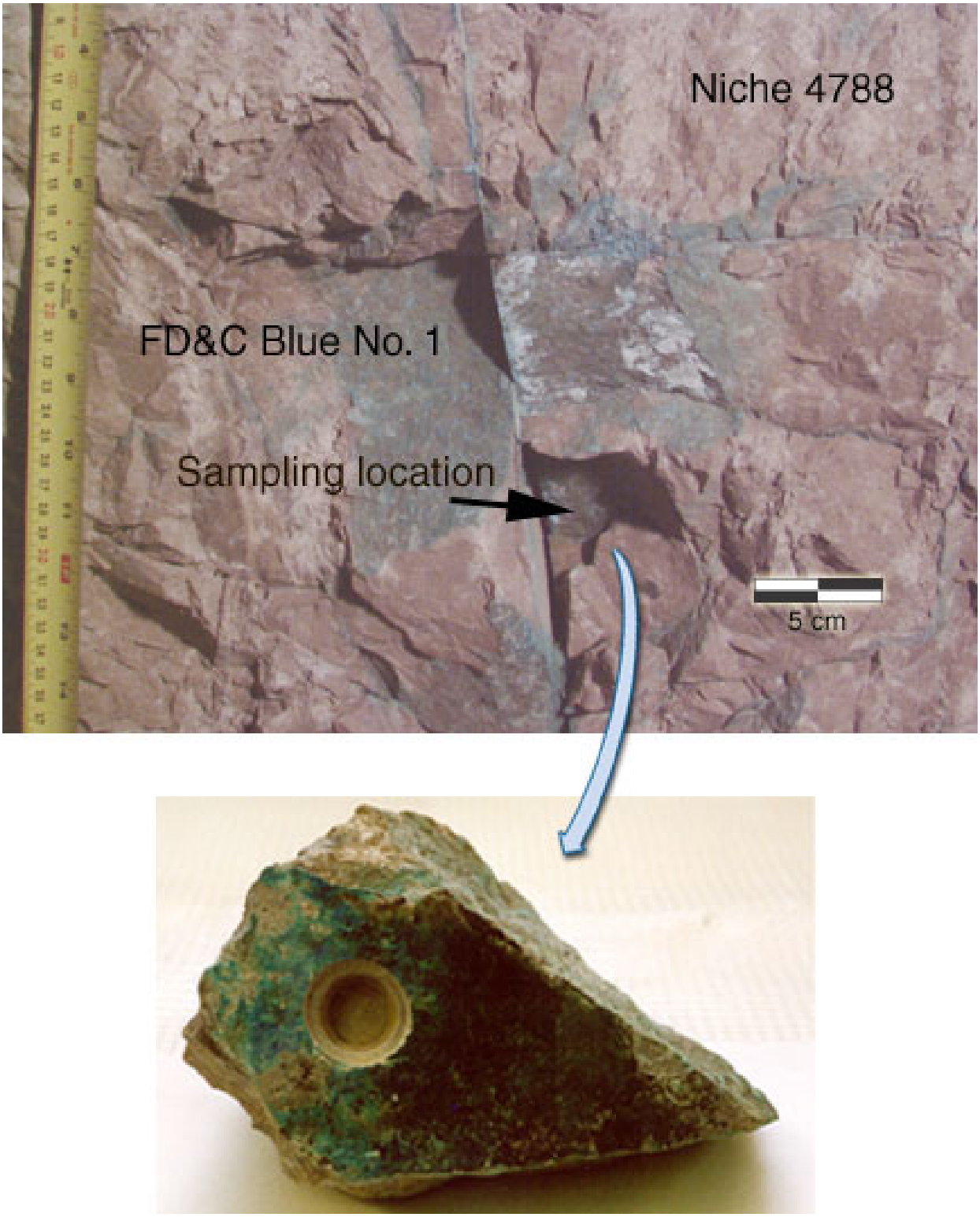

SOURCE: Hu et al. 2002 [165412], Figure 2.

Figure 6.4.1-1. Photograph Showing the Wall Face with Fracture Network and Sampling Location of Rock. Stained by FD&C Blue No. 1 during Niche Excavation at Niche 4788 (Niche 4)

6.4.1.2 Dye Penetrations into Rocks

Visual inspection of dyed rocks collected from the field studies showed that the dye stained the fracture surfaces and the color decreased with the distance and disappeared within a few millimeters from the fracture surfaces (Figure 6.4.1-1). The plot of Sulpho Rhodamine B detection ratio versus depth from the fracture surface is shown in Figure 6.4.1-2. (The dimensionless detection ratio is the measured tracer level divided by the background level.) The depth on the x-axis denotes the mid-point of the drilling interval. For example, the measured tracer concentration from a 1–2 mm drilling interval is shown at the 1.5 mm location from the sample surface. For three rock samples stained with either FD&C Blue No.1 or Sulpho Rhodamine B, each dye concentration decreased from the highest concentration to the background level in less than 6–7 mm. These results quantify the noticeable tracer matrix imbibitions from liquid flowing through the fractures.

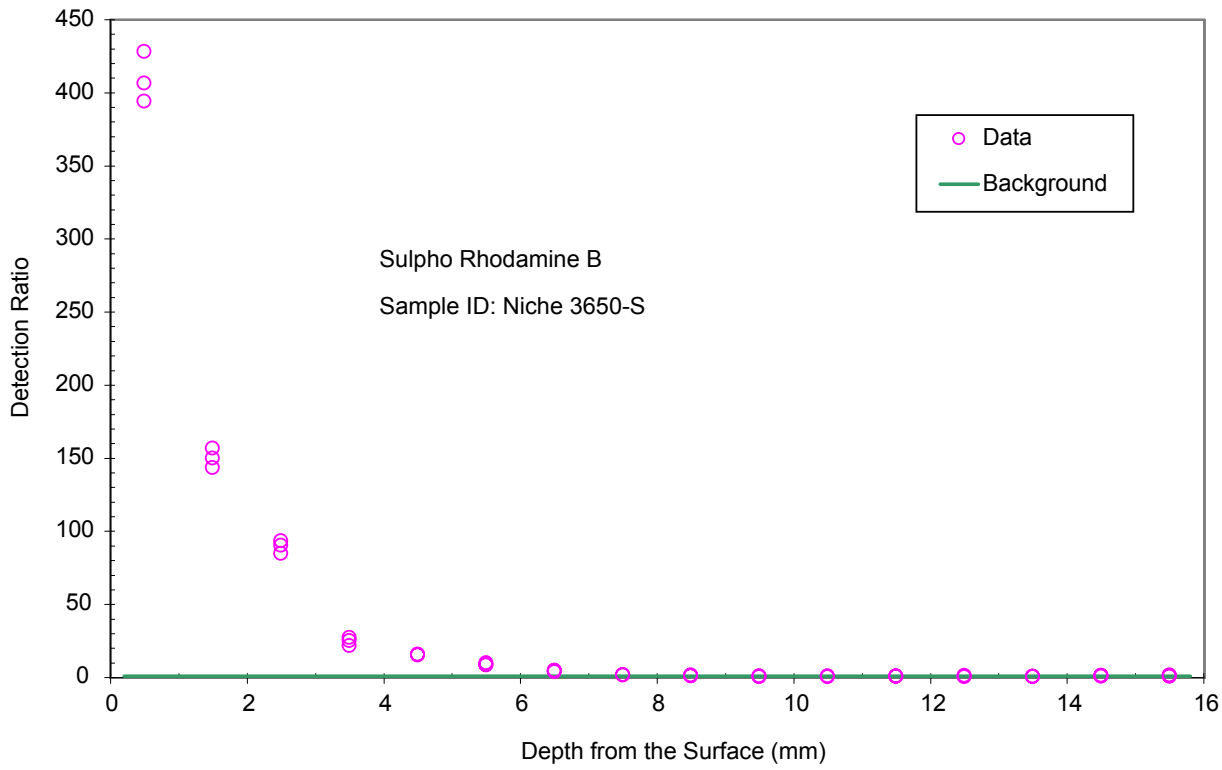

DTN: LB990901233124.003 [155690]

Figure 6.4.1-2. Sulpho Rhodamine B Penetration Profiles into Rock Matrix from the Fracture Surface

Table 6.4.1-1 provides relevant experimental conditions used during the liquid-release tests resulting in the three dyed rock samples collected during excavation. The samples were collected 7–13 days after the dye-spiked water was released into the formation. Water flow in post-excavation seepage tests was found to be very rapid, traversing 0.65 m in 4 minutes under the release rate of about 1.9 g/s (Table 6.4.1-2). It is therefore expected that the fluid-rock contact time is relatively short. Short travel times, together with high ratios of dye concentration in seepage water versus release water (in the far-right column of Table 6.4.1-2), indicated that the

contacts between flowing water in the fractures and the adjacent tuff matrix were highly transient. The exact duration of contacts on the fracture surfaces could not be measured.

Table 6.4.1-1. Liquid-Release Tests and Experimental Conditions

Tracer	Test Date	Test Location [c]	Tracer Conc. (g/l)	Release Rate (g/s)	Release Duration (min)	Mass Released (g)	Sampling Date
Sulpho Rhodamine B [a]	8/8/97	ML 6.71–7.01 m	2.0	2.0	8.22	170.9	8/19/97
FD&C Blue No. 1 [a]	8/6/97	UM 6.71–7.01 m	7.7	1.9	8.20	438.7	8/19/97
FD&C Blue No. 1 [b]	7/2/98	UM 6.40–6.70 m	6.77	0.49	35.0	1019.7	7/9/98

DTN: LB980001233124.004 [136583], LB980901233124.003 [105592]

NOTES: [a]Tests conducted at Niche 3650 (Niche 2) location

[b]Test conducted at Niche 4788 (Niche 4) location

[c]UM: upper middle borehole; ML: middle left borehole. Depth measurement (in meters) is from the collar of the borehole to the test interval.

Table 6.4.1-2. Post-Excavation Tracer-Release Tests at Niche 3650 (Niche 2)

Tracer	Test Location [a]	Release Rate (g/s)	Mass Released (g)	Mass of Seepage Recovered (g)	Wetting Front Arrives at (min:sec) [b]	Ratio of Seepage vs. Release Conc. (%)
Sulpho Rhodamine B	UL 7.01 – 7.32 m	1.949	1005.5	16.0	4:00	95.6
FD&C Blue No. 1	UR 4.27 – 4.57 m	0.198	995.7	4.0	56:08	77.0
FD&C Blue No. 1	UR 4.88 – 5.18 m	0.190	1016.4	4.0	29:50	103.9

DTN: LB980001233124.004 [136583]

NOTES: [a]UL: upper left borehole; UR: upper right borehole. Depth measurement (in meters) is from the collar of the borehole to the test interval.

[b]Time wetting front arrives at niche ceiling following the start of water release to the formation

Summary data are contained in DTN: LB990901233124.003 [155690]

6.4.1.3 Fast Fracture Flow

Fast fracture flow was demonstrated during the post-excavation seepage tests where dye-spiked water was released and collected, if possible, at the collection system below the niche ceiling. The last column of Table 6.4.1-2 shows the ratios of collected to released concentrations for FD&C Blue No. 1 and Sulpho Rhodamine B. Average seepage versus release-concentration ratio is 92.2 ± 13.8% over three tests with dyes. The seepage solution is a composite sample, which could be diluted from the resident water, if any, in the flowing fractures. Also, note that the release concentrations were obtained from the known dye mass dissolved in the known liquid, and no liquid sample was collected for the released solution during these tests. This uncertainty could contribute to the ratio of 103.9% (over the theoretical limit of 100%) for one of the FD&C Blue No. 1 tests. Significant dilutions (about 1,000 times), needed to bring down the sample

concentration within the linear standard curve needed for measurement, could also contribute to the uncertainty. More accurate ratios could be obtained if both the seepage and release solutions were measured simultaneously.

6.4.1.4 Concentration Profiles of Dye Tracer

For the dye-stained samples from the field, tracer concentrations were measured on rock powders collected from drilling intervals of the rock. Two FD&C Blue No. 1 dye profiles are illustrated in Figure 6.4.1-3. The scales of detection ratios described in Section 6.4.1.2 are plotted on the left-hand side. The scales of concentration ratios of measured concentration C divided by the released concentration C_o, C/C_o, are plotted on the right-hand side. The first few millimeters from the fracture surface contain the key portion of the tracer concentration profiles that indicate the extent of fracture-matrix interaction (Hu et al. 2002 [165412], p. 106).

Figure 6.4.1-3a for the sample Niche 3650-F has relative low values of C/C_o (compared with those obtained with Core D and Core H to be discussed in Section 6.4.2) for the first millimeter (i.e., 0–1 mm from the fracture surface). This sample could be associated with fast transient flow. Noticeable water and tracer imbibition into the surrounding matrix was observed, even though fracture flow could be fast.

In contrast, Figure 6.4.1-3b for the sample Niche 4788 has high value of C/C_o in the first millimeter. This sample was collected adjacent to a vertical flowing fracture that apparently dead-ended near the sampling location (Figure 6.4.1-1). For this sample, the fluid-rock contact time could have been longer, contributing to the higher concentration ratio at the first interval. The measured concentration ratio in the second (1–2 mm) interval drops drastically to the level similar to the samples in Figure 6.4.1-3a. With longer contact time, stronger surface sorption of the dye might also have occurred in this rock sample.

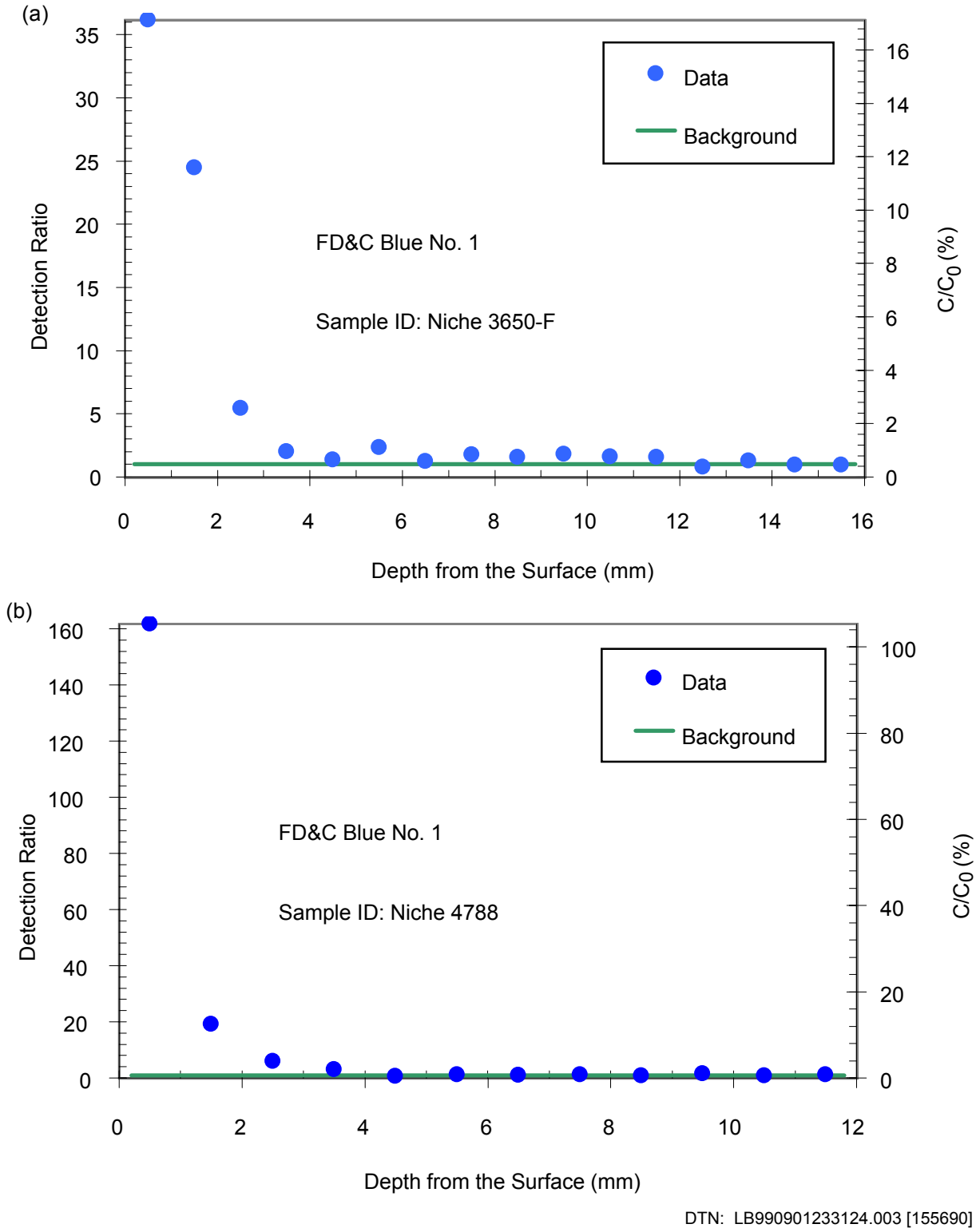

Figure 6.4.1-3. Tracer Penetration Profile into Rock Matrix from the Fracture Surface: (a) FD&C Blue No.1 at Niche 3650 (Niche 2); (b) FD&C Blue No.1 at Niche 4788 (Niche 4)

6.4.2 Retardation and Tracer Front Movement

Laboratory tests were conducted to quantify the imbibition of water and the retardation of tracers into rock cores. In the laboratory, tests can be conducted under controlled conditions, with concentrations in rock samples and in the core reservoir measured simultaneously. The flow paths along cores are well defined compared to the flow paths in the field. The laboratory test results can assist in interpreting data collected on dye-stained samples from the field tests.

There are two approaches presented for measuring the retardation factor: front separation and local 'saturated' measurements at the core-reservoir contact. The consistency between these two approaches lends credence to the quantification of retardation factors on core samples.

6.4.2.1 Dye Retardation Factor Determined by Front Separation

The descriptions and evaluations of laboratory tracer tests on core samples are presented in Attachment V. Figures 6.4.2-1 and 6.4.2-2 compare the concentration profile of nonreactive bromide with the concentration profiles of both FD&C Blue No. 1 and Sulpho Rhodamine B, relative to the moisture fronts obtained from visual inspection. The dyes lag behind the bromide front, indicating dye sorption to the rock. FD&C Blue No. 1 and Sulpho Rhodamine B were the most visible in the tuffs of the tested dyes. Sorption of these dyes on rock is not surprising, considering their complex chemical structure with various functional groups, even though they are negatively charged under normal pH conditions.

From the tracer profiles, the retardation factor R can be derived as the ratio of travel distance of nonreactive tracer divided by the travel distance of sorbing tracer. Bromide is approximately a nonreactive tracer in tuff, as indicated by its nearly coincident front with the wetting front at low initial water saturation. In Figure 6.4.2-1 for Core D at low initial saturation, the bromide front is located at 17–18 mm from the core bottom ($d_{0.5}$ = 17.5 mm, where $d_{0.5}$ is the depth at which the concentration is half of the steady-state concentration in the profile). The first data point at the 0-1 mm interval was excluded for bromide front determination. The 0–1 mm interval measurement was systematically higher than deeper intervals and was consistently observed for bromide in all core measurements. Because the 0–1 m interval at the core-reservoir interface is in direct contact with the tracers, it is not included in the calculation of the travel distance used to determine the retardation factor R. This does not seem to affect the sorbing tracers (FD&C Blue No. 1 and Sulpho Rhodamine B), as evident in the steady-state concentration of the first three intervals in Core D (Figure 6.4.2-1). For the sorbing tracers, $d_{0.5}$ is located at 3.5 mm (Figure 6.4.2-1). The retardation factor for both dyes is estimated to have the value 5 (= 17.5 mm/3.5 mm). Similarly, R is estimated to be 2.33 (= 3.5 mm/1.5 mm) for both dyes in Core H with high initial S_w (Figure 6.4.2-2).

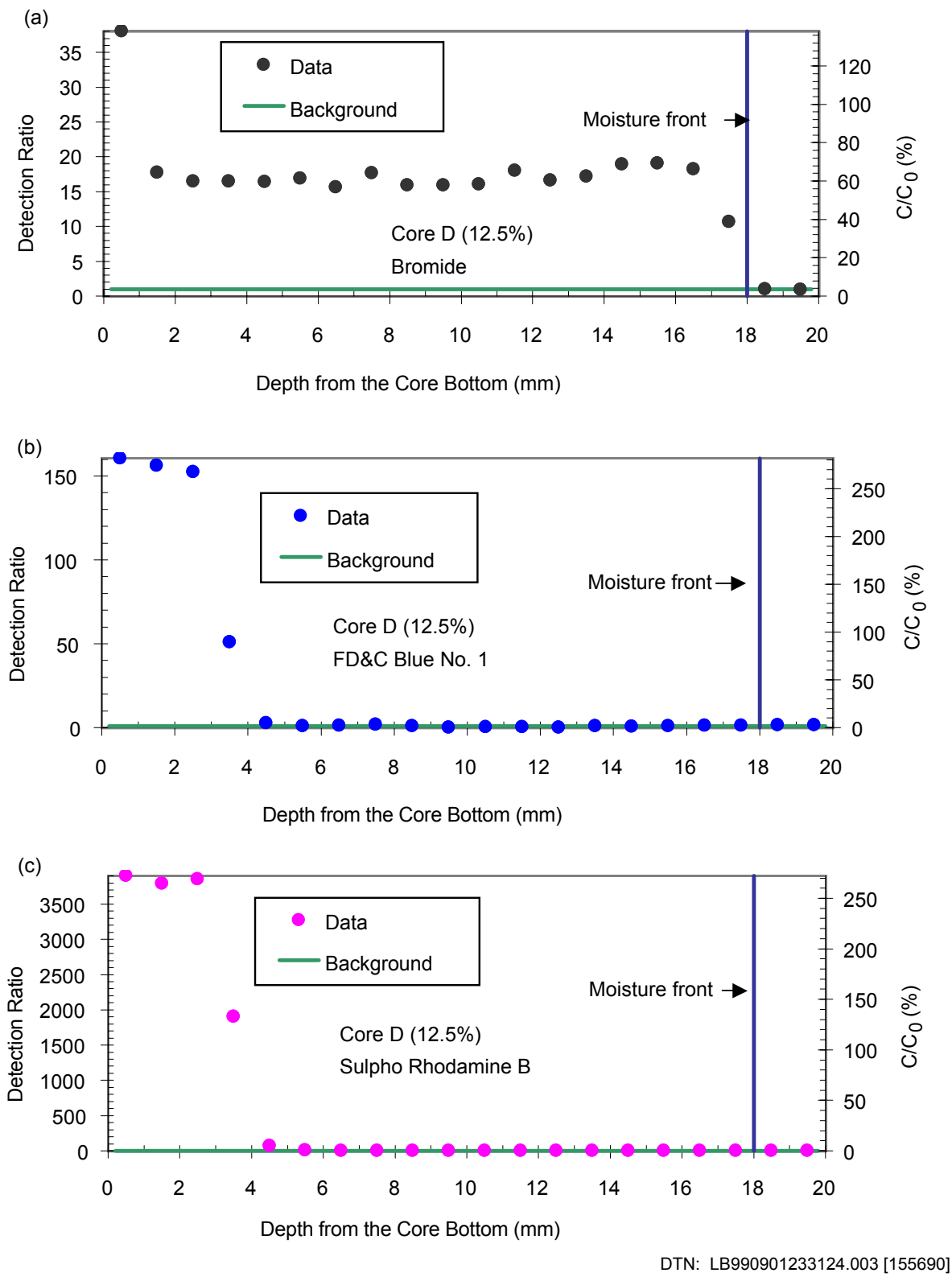

Figure 6.4.2-1. Comparison of Tracer Concentration Profiles in a Low-Initial-Saturation Core: (a) Bromide, (b) FD&C Blue No. 1, (c) Sulpho Rhodamine B. Core D had initial saturation of 12.5% and was in contact with saturated boundary for 19.5 hours.

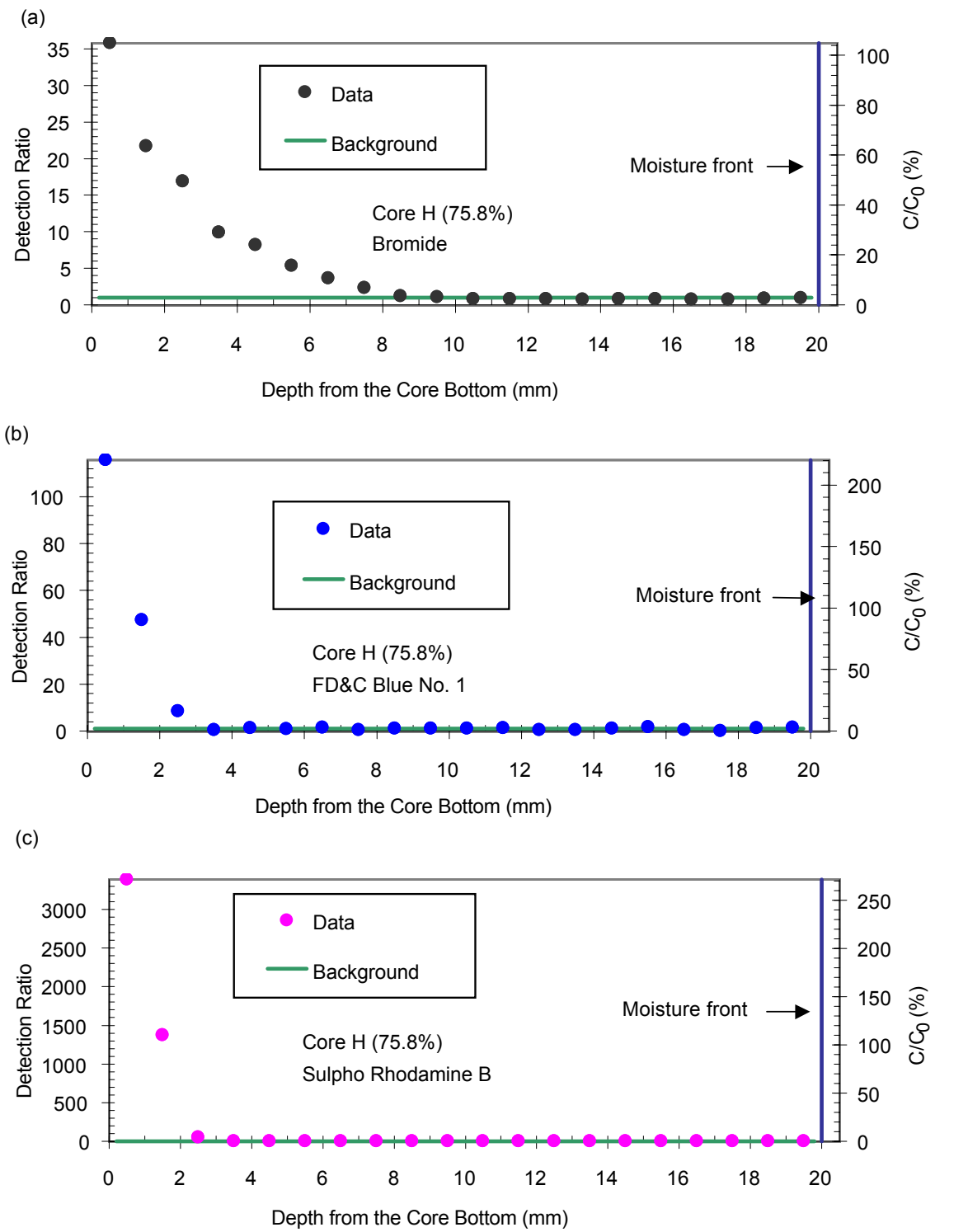

DTN: LB990901233124.003 [155690]

NOTE: Core H had initial saturation of 75.8% and was in contact with saturated boundary for 17.9 hours.

Figure 6.4.2-2. Comparison of Tracer Concentration Profiles in a High-Initial-Saturation Core: (a) Bromide, (b) FD&C Blue No. 1, (c) Sulpho Rhodamine B

The saturation dependence of the retardation factor is derived from the following functional relationship (Porro and Wierenga 1993 [134083], pp. 193–194):

$$R = 1 + \rho_b \times K_d / \theta \qquad \text{(Eq. 6.4.2-1)}$$

where K_d (mL/g) is the sorption distribution factor representing the distribution of solutes between aqueous and solid phase, ρ_b is the bulk density (g/mL), and θ is the water content. This equation explicitly shows that solute retardation is inversely related to water content. If the effective θ value is estimated as the average of the initial water content and the final water content (here set to be the measured porosity), the K_d value can be derived from the R-value. For the two core samples, the K_d value was calculated to be 0.089 mL/g for Core D and 0.047 mL/g for Core H (Attachment IX.3). The bulk density and porosity values for each core were measured independently, with values listed in Table 6.4.2-1. These measured values in Table 6.4.2-1 were used in calculating K_d values from measured R values.

Table 6.4.2-1. Measured Properties for Core Samples

Sample ID	Porosity (cm^3/cm^3)	Bulk Density (g/cm^3)
Core D	0.0888	2.248
Core E	0.0849	2.251
Core F	0.0890	2.239
Core H	0.0896	2.245
Core J	0.0823	2.266

DTN: LB990901233124.003 [155690]

As an additional consistency check, the calculations can be inverted and the R values derived from the K_d values for a fully saturated condition (i.e., 100% saturation). The $R_{100\%}$ is 3.25 for Core D and 2.17 for Core H from the inverse calculations. The average $R_{100\%}$ is 2.71 ± 0.76 for both FD&C Blue No. 1 and Sulpho Rhodamine B. Both K_d value and $R_{100\%}$ are constants independent of saturation. The simple checking verifies the functional relationship of Equation 6.4.2-1. For comparison, Andreini and Steenhuis (1990 [106071], pp. 85, 98) found that the retardation factor for FD&C Blue No. 1 ranged from 1.5 to 7 in a fine, sandy loam soil.

Note that the core measurements presented in this study can generate K_d values for intact rock under *in situ* partially saturated conditions. Most of the K_d values for sorbing solutes have been acquired by batch experiments using crushed rock, with the sizes chosen more or less arbitrarily and mainly for experimental convenience. The batch experiments were performed under saturated conditions with large water/rock ratios. There are concerns regarding the use of crushed-rock samples versus solid-rock samples in batch experiments on tuff rocks. The water/rock ratios used in the sorption experiments with crushed samples were large in comparison with the water/rock ratios likely to exist in the UZ. This unsaturated transport-sorption approach can be used to check the results commonly obtained from batch sorption experiments as well as to provide a more representative sorption under field conditions (Hu et al. 2002 [165412], p. 111).

6.4.2.2 Travel-Front Separation

As a nonreactive tracer, bromide is frequently used for flow tracking. The bromide front is comparable to the moisture front in the rock core at the initial water saturation of 12.5%, as illustrated in Figure 6.4.2-1a. The bromide front lags significantly behind the moisture front at the higher initial water saturation of 75.8%, as shown in Figure 6.4.2-2a. Note that the core top (20 mm) was wet when the experiment was ended, although the moisture front is shown at the 18 mm location in Figure 6.4.2-1b. This observation of nonreactive solute front lagging behind the moisture front agrees with the findings in moist soils (Warrick et al. 1971 [106150], pp. 1216, 1221; Ghuman and Prihar 1980 [106099], pp. 17, 19; Porro and Wierenga 1993 [134083], pp. 193, 196). Warrick et al. (1971 [106150]) first reported that the advance of a solute front was highly dependent on the soil moisture content during infiltration. During infiltration, no solute was found in the advancing wetting front where soil moisture contents were increasing, although the initially infiltrating water contained nonreactive tracer. The importance of this front separation, observed under a transient flow condition, might be more pronounced for low porosity materials under high moisture saturation, such as tuff at Yucca Mountain. Under these circumstances, a relatively small amount of invading solution can push the antecedent water further into the matrix.

For the imbibition experiment in Core D with low initial water saturation, the bromide front is sharp, with the strong capillary force driving the advection-controlled transport. Conversely, for the Core H with high initial water saturation, the bromide front is quite diffuse, since dispersion and dilution become important processes (on account of weaker capillarity) compared to advective flow. Sharp and diffused front separations between the bromide nonreactive tracer front and the moisture front, as well as between sorbing tracer front and bromide front, would provide the data for elucidating flow and transport in unsaturated, fractured tuff.

6.4.3 Application of LA-ICP-MS to Investigate Chemical Transport and Sorption

Laser ablation refers to the process in which an intense burst of energy delivered by a short laser pulse is used to vaporize a minute sample from a specific location. Chemical composition of the vaporized sample is then analyzed with inductively coupled plasma-mass spectrometry (ICP-MS). Laser ablation, coupled with ICP-MS (LA-ICP-MS), has recently evolved as a powerful analytical tool for solid samples (Russo et al. 2000 [155697]). LA-ICP-MS can determine simultaneously a large number of chemical elements, with very low detection limits. The applications of LA-ICP-MS have been recently reported in studies of tree rings, airborne particulates, and geochemistry. However, we are not aware of any studies where transport, sorption, or diffusion of contaminants in rocks are investigated by LA-ICP-MS. The high spatial resolution achieved by a focused laser beam makes LA-ICP-MS a very attractive approach to such environmental pollution studies.

This section describes the investigation of transport and sorption of chemicals that are of interest to the Yucca Mountain Project in unsaturated tuff. Laboratory tracer imbibition tests are similar to those presented in Attachment V, except that an initially dry tuff cube (1.5 cm in each side) was used in this LA-ICP-MS work, compared to core cylinders used in the drilling work as described in Section 6.4.1 and Section 6.4.2. Compared to the drilling technique presented in Attachment V, employment of LA-ICP-MS provides a quick way of profiling tracer chemical

concentration with high spatial resolution. Surrogate compounds are chosen based on their chemical similarity to radionuclides of interest. The tracer solution used in this study contained a mixture of NaBr, $NaReO_4$, CsBr, and RbBr. Both Br^- and perrhenate (ReO_4^-) are used as nonsorbing tracers, with perrhenate serving as an analog to technetium, which exists in a form of pertechnetate ($^{99}TcO_4^-$). Cesium (Cs^+) and rubidium (Rb^+) were used as cationic tracers to examine the sorption effect on delayed transport of radionuclides in unsaturated tuff. Non-radioactive cesium is directly used for radioactive ^{137}Cs. Experimental conditions and analyses are recorded in Hu (2000 [156473] pp. 130–136, 145–146).

Figure 6.4.3-1 shows the spatial-distribution results obtained from LA-ICP-MS profiling for the tuff cube face in contact with the tracer solution. Intensity in the y-axis indicates the signal, measured by ICP-MS, from the laser-abated mass for both the applied tracers and elements (Al, K, Ce, Th) intrinsic to the tuff sample. Peterman and Cloke (2001 [155696]) reported a very uniform distribution of elemental compositions in tuff. Signals shown in Figure 6.4.3-1 are in direct relationship to the reported elemental compositions: percent weight level for Al and K, trace (parts per million) level for Ce and Th. As expected, the spatial distribution of all elements measured is fairly uniform, because this cube face was in contact with the tracer solution throughout the imbibition test duration.

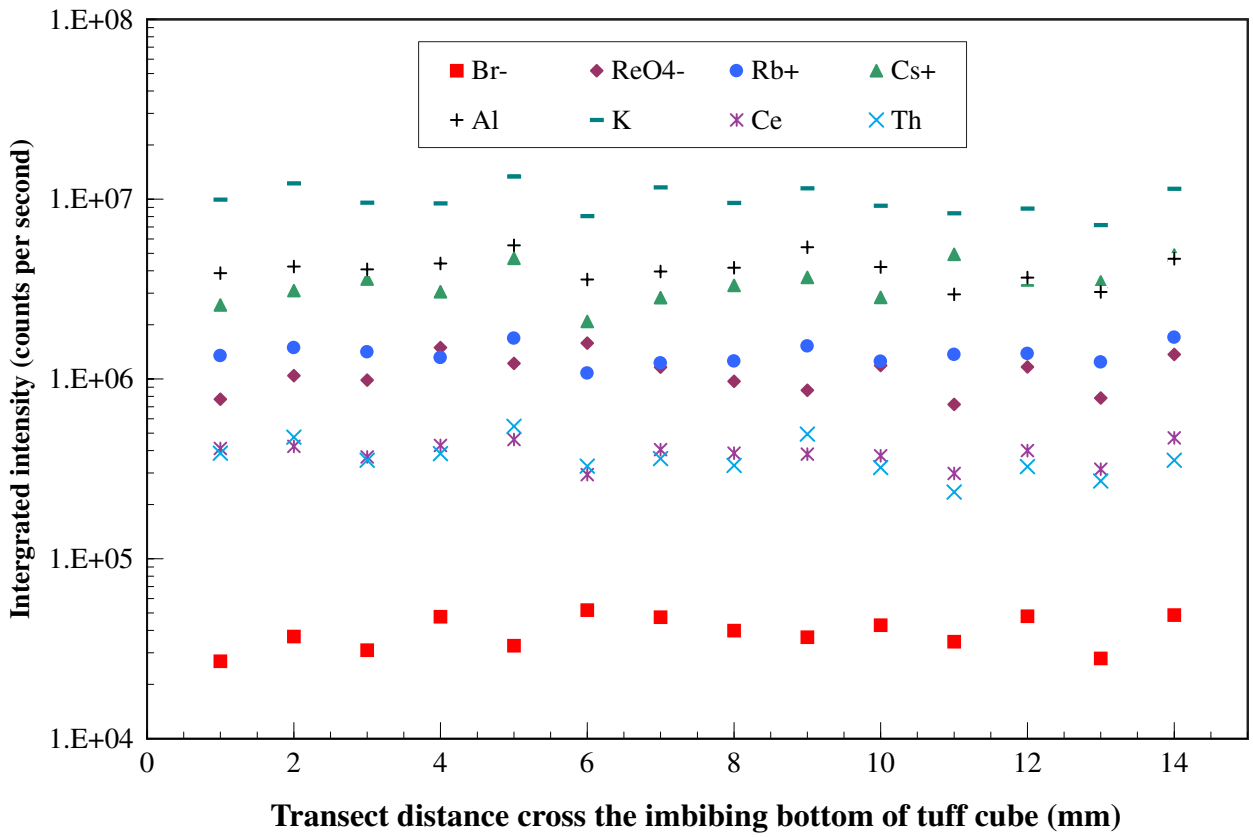

DTN: LB0110TUFTRACR.001 [156979]

Figure 6.4.3-1. Spatial Distribution along the Tracer Solution Contact Surface of Applied Tracers and the Distribution of Intrinsic Tuff Elements Profiled Using LA-ICP-MS

Figure 6.4.3-2, on the other hand, presents the spatial distributions of applied tracers, as well as uniform distribution of element K as it exists inherently in the tuff sample, for a side cube face parallel to the direction of imbibition. Anionic tracers, Br^- and ReO_4^-, travel much further than cationic tracers (Cs^+ and Rb^+) that sorb to the tuff. This is similar to those tracers discussed in Section 6.4.2.1, where sorption of dyes is observed. By the same approach, $d_{0.5}$ is located at about 10.15 mm for both Br^- and ReO_4^-, and $d_{0.5}$ is located at about 2.95 mm and 3.50 mm for Cs^+ and Rb^+, respectively. The retardation factors for Cs^+ and Rb^+ are, therefore, estimated to have the value of 3.44 (= 10.15 mm/2.95 mm) and 2.90 (10.15 mm/3.50 mm), respectively. Similar behavior is observed from the measurements made on another side cube face parallel to the direction of imbibition. Overall, LA-ICP-MS provides a useful way of sampling and understanding tracer, and by extension radionuclide, imbibition and transport in the rock matrix at small spatial scales and reasonable sampling times.

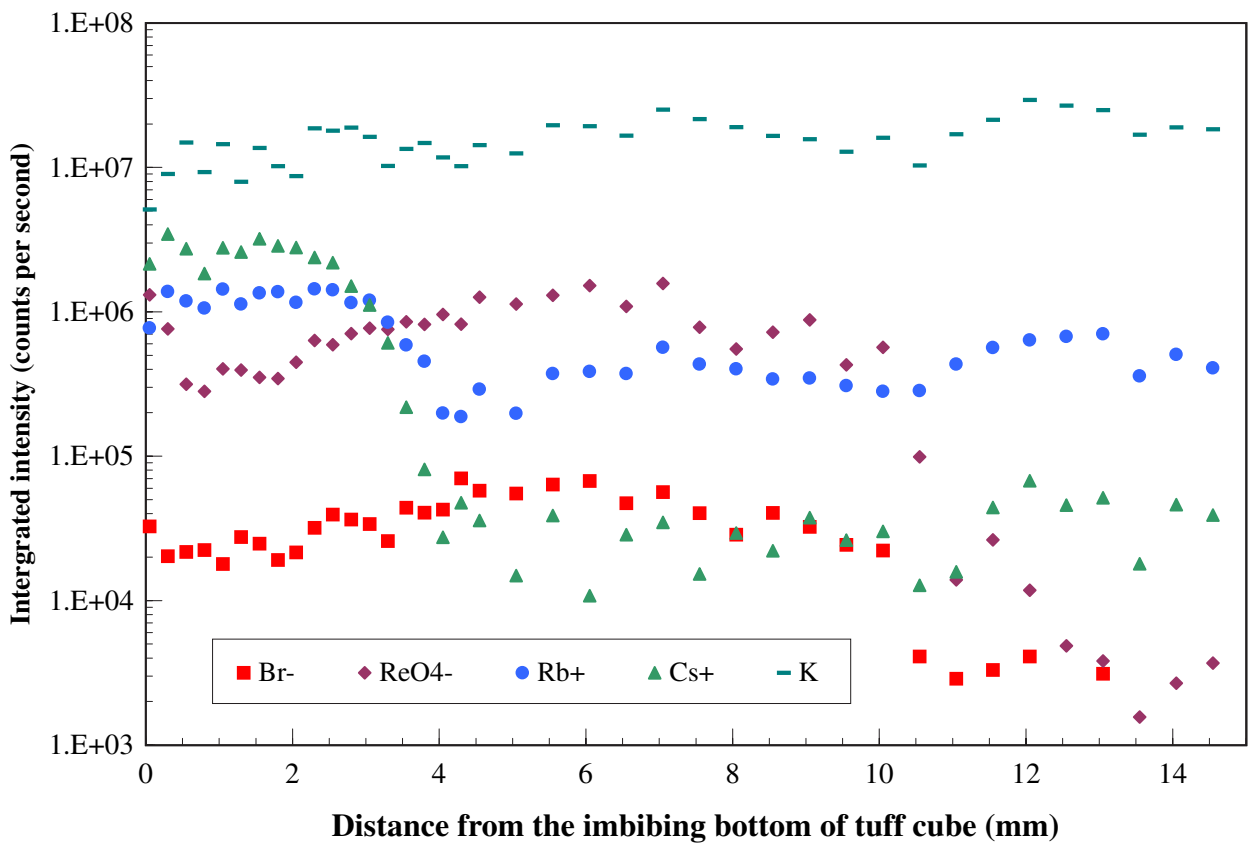

DTN: LB0110TUFTRACR.001 [156979]

Figure 6.4.3-2. Spatial Distribution Normal to the Tracer Solution Contact Surface (in the Direction of Liquid Imbibition) of Applied Tracers and Distribution of Intrinsic Tuff Elements Profiled Using LA-ICP-MS

INTENTIONALLY LEFT BLANK

6.5 ANALYSES OF CROSSHOLE AIR-INJECTION TESTS

This section continues the pneumatic air-permeability test analyses first presented in Section 6.1. Section 6.1 focuses on the air-permeability variations along boreholes in niches. The permeability profiles provide initial inputs to liquid-release-test interval selection, as described in Section 6.2. The permeability profiles were also used in a seepage-calibration study documented in the Model Report, on seepage calibration in defining the heterogeneity of the permeability structure used in modeling.

This section focuses on analyses of crosshole data for fracture-network connectivity. Fracture-network connectivity is one of the most important characteristics in evaluating flow paths from the inlets to the outlets of a given regime. The larger the system, the more elusive it is to determine the dominant flow paths. Air flow paths elucidated in this section are used to characterize test beds for liquid-flow test design and analysis, as described in Section 6.6 and Section 6.7 below for two slotted test beds in the ESF.

Crosshole tests used the same pneumatic testing equipment described in Attachment I. Up to seven identical packer strings were fabricated and installed in the boreholes to test a rock volume in the niches and in the test beds. The packer can isolate 0.3 m intervals along its length. Each interval can become either an observation or response zone, used to monitor pressure, or an injection zone, where air is introduced under pressure during the test. The automation system controls the permutations through pre-assigned sequences of injection tests in all borehole intervals in the borehole cluster.

Crosshole data is acquired at the same time as single-borehole data, by logging the steady-state pressure response in all observation zones while performing an injection. The observation response pressure is divided by the injection pressure to provide a measure of how well a response zone is connected to an injection zone in relation to that response zone's connections to the rest of the site. The normalization with injection pressure enables all the observation responses from all injections at a site to be directly compared. The crosshole connections can all be viewed on a single 3-D diagram instead of individual diagrams for each tested injection zone.

The niches and Alcove 6 are located within the TSw unit in the repository horizon. The Alcove 4 test site is in the PTn unit along the North Ramp of the ESF. Both the fractured TSw and the predominately porous PTn were evaluated by the pneumatic air-permeability tests.

6.5.1 Crosshole Responses in Welded Tuff

In Section 6.1.2, the single-borehole permeability profiles were presented for niches as the bases for selecting liquid-release intervals for drift seepage testing. The first example of crosshole analysis in fractured rock is on Niche 4788, located in an intensely fractured zone. The crosshole analysis for Niche 4788 is illustrated in Figure 6.5.1-1. The single-borehole permeability values (presented in Section 6.1 as profile plots in Figure 6.1.2-7 and Figure 6.1.2-8) are represented by circles in the crosshole plot, with each circle centered along the test interval within each of the boreholes. The size of the circles scales with the single-borehole permeability at each interval. Grayscale pins are shown with their points at the centers of the circles of the injection zones and heads intersecting through the centers of other circles at the observation zones. Direction of flow

is towards the pinhead, and the grayscale indicates the normalized response ratio ("Resp. Ratio" in the figure) from zero to one.

Figure 6.5.1-1 for Niche 4788 is fairly representative of a fractured site, showing discrete connections. It should be noted that very few of the connections have an opposite counterpart; the connections are predominantly one-way. This observation by no means indicates that flow is limited to one direction between points in the rock, but rather that the influence of local connections on the pressure response is strong. The pressure at a response zone discretely connected to the injection zone (and no other zone) will yield a large response. However, if the original injection zone in the reversed injection-observation combination is also well connected to the fracture network or a free surface, then it will not respond strongly to an injection in the original observation zone.

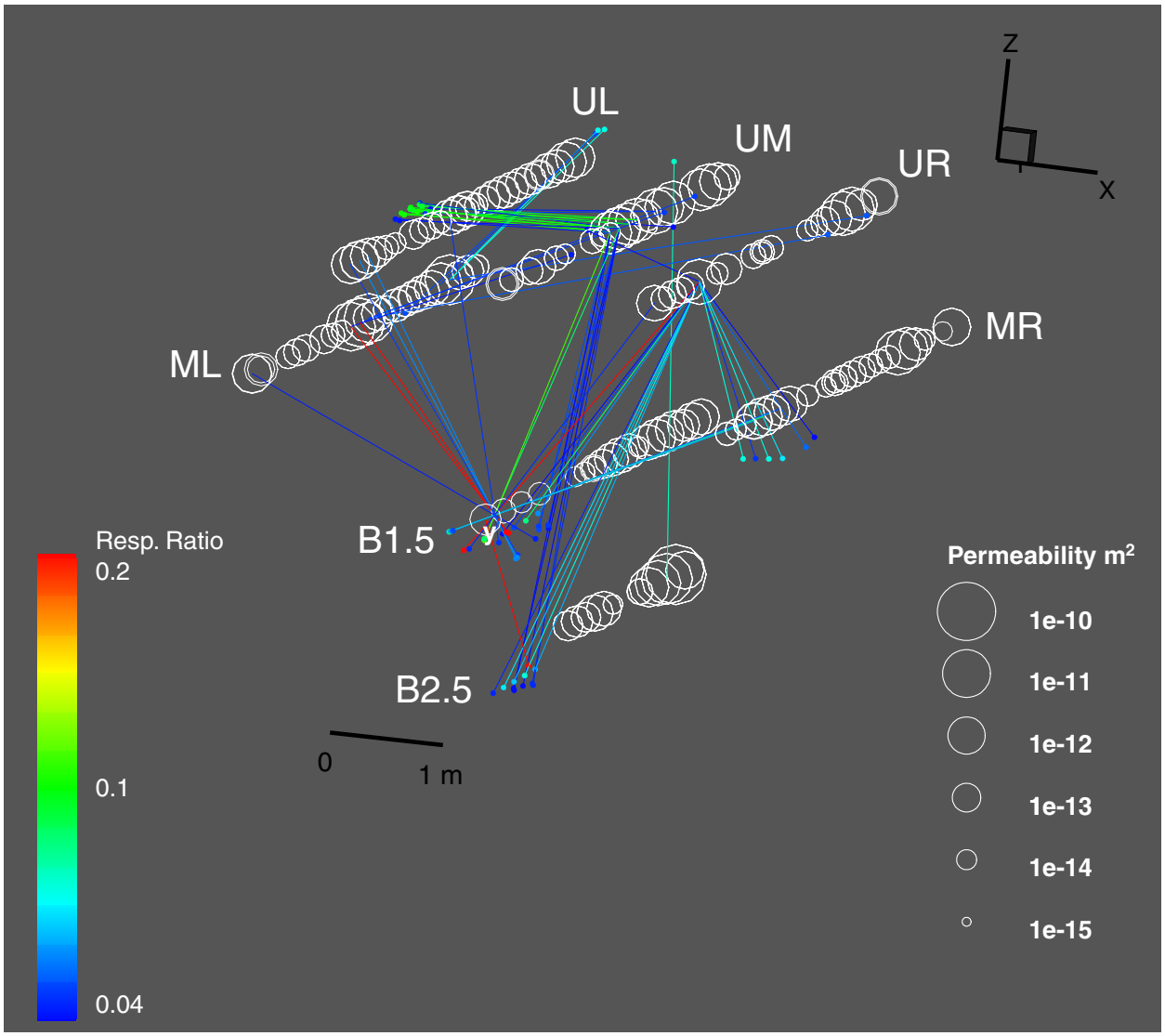

DTN: LB990901233124.004 [123273]

Figure 6.5.1-1. CrossHole Responses for the Borehole Cluster in Niche 4788

The fracture-matrix interaction test site in Alcove 6 of the ESF is in rock that is fractured, with discrete, subvertical fractures and relatively few subhorizontal fractures. The single-borehole permeability profiles for three boreholes tested in Alcove 6 are illustrated in Figure 6.5.1-2. Borehole A was used for a series of liquid-release tests, as described in Section 6.6. Boreholes C and D were used for wetting-front monitoring. Boreholes C and D are located 0.7 m and 0.6 m below Borehole A, respectively, and 0.7 m apart. The crosshole responses for this triangular cluster of boreholes are illustrated in Figure 6.5.1-3. Both Figure 6.5.1-2 and Figure 6.5.1-3 correspond to the first series of tests conducted in the region between 1.3 m and 5.3 m from the borehole collars. Another series of tests was conducted with a straddle packer system (two-packer string to isolate one zone for liquid releases) right before liquid-release tests along the injection borehole.

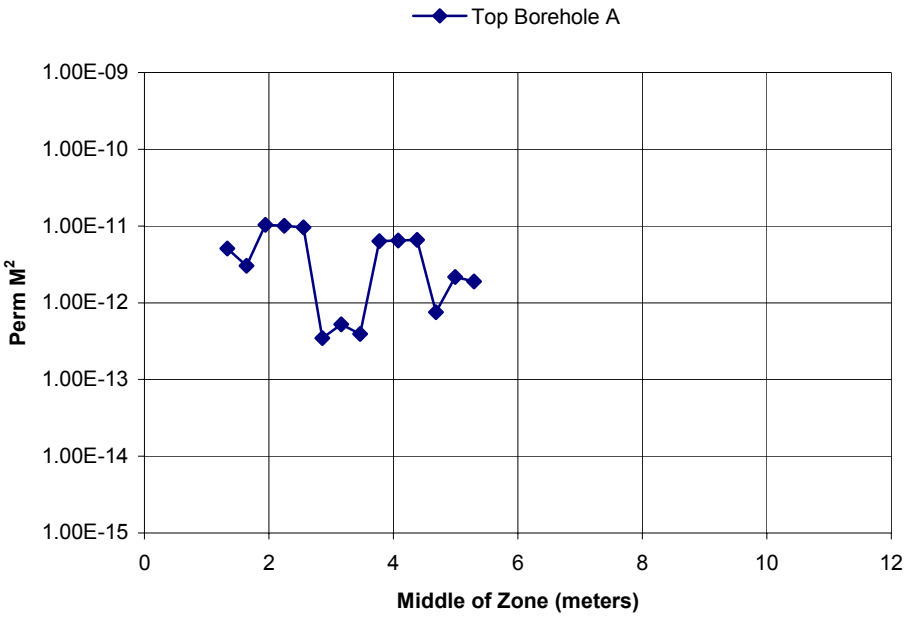

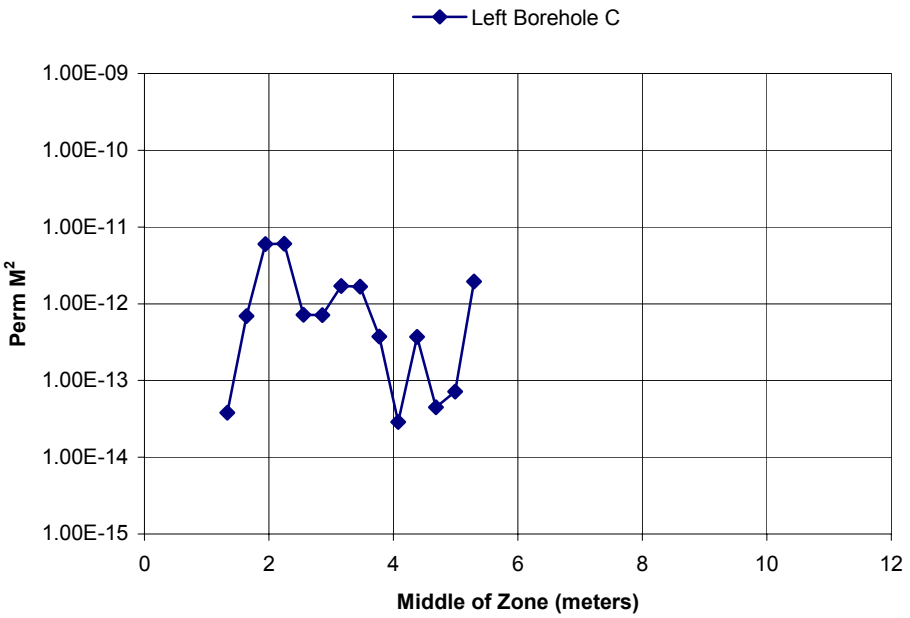

DTN: LB980901233124.004 [105855]

Figure 6.5.1-2. Air-Permeability Profiles along Boreholes in Alcove 6

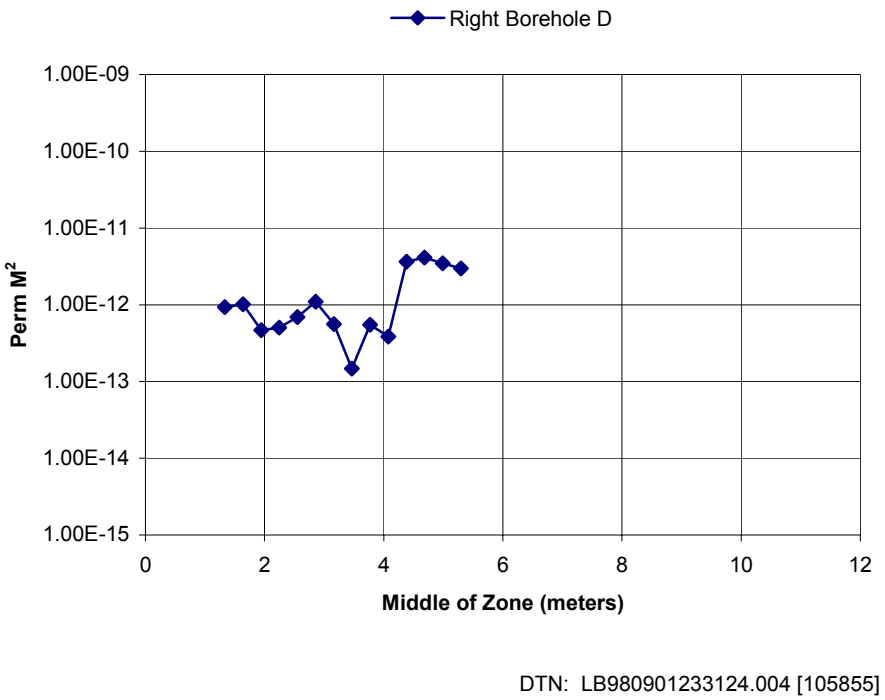

DTN: LB980901233124.004 [105855]

Figure 6.5.1-2. Air-Permeability Profiles along Boreholes in Alcove 6 (continued)

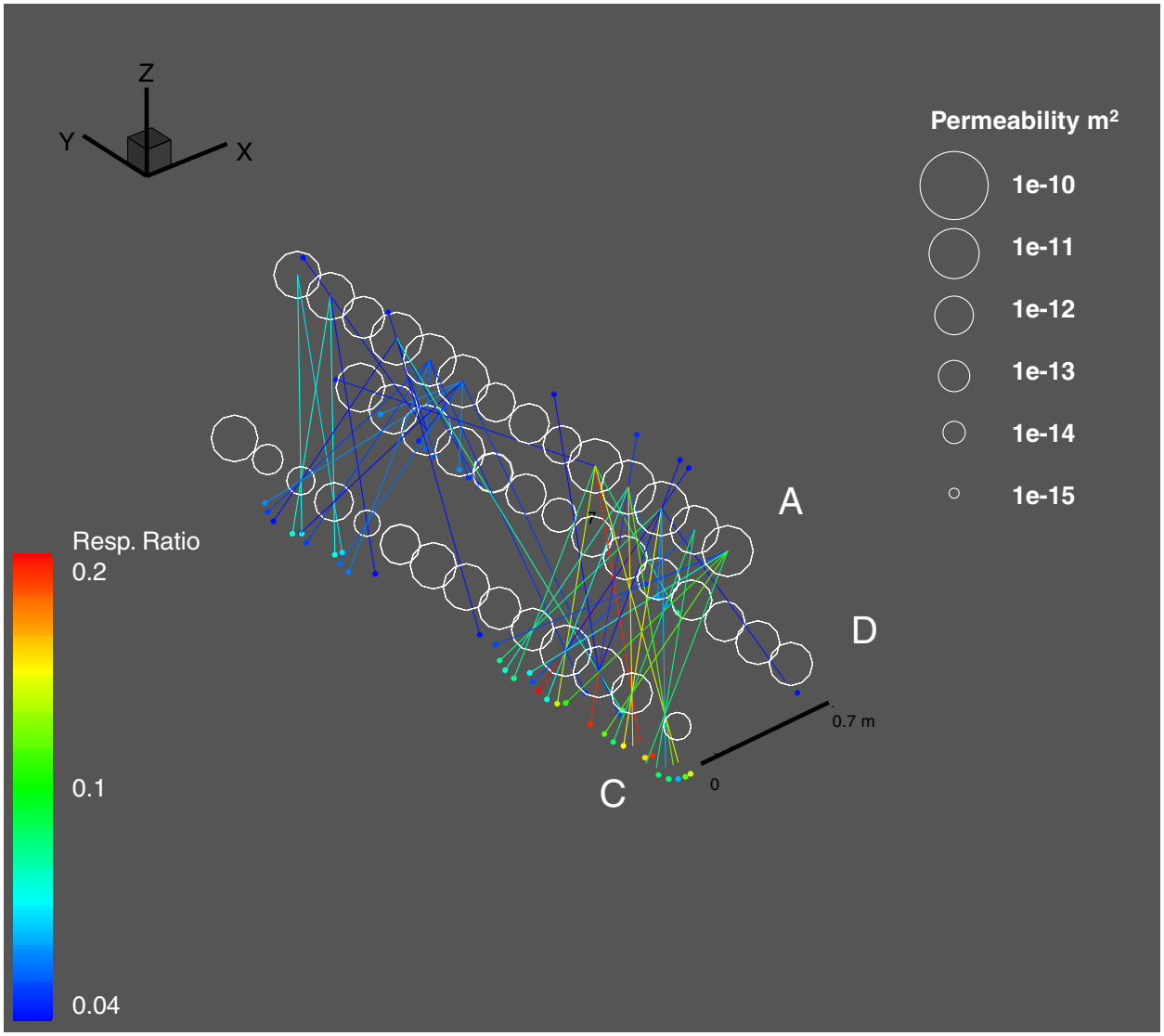

DTN: LB990901233124.004 [123273]

Figure 6.5.1-3. Crosshole Responses for the Borehole Cluster in Alcove 6

Both Figure 6.5.1-1 for Niche 4788 and Figure 6.5.1-3 for Alcove 6 represent crosshole responses in fractured rock. The ratios of pressure response in the observation borehole interval to pressure in the injection borehole interval (Resp. in figure scales) were displayed in the figures for the maximum value of 0.2 (or 20%). Niche 4788, in an intensely fractured zone, has wider range (or larger standard deviation, as shown in Table 6.1.2-3) of distribution in permeability than the variations over a smaller scale at Alcove 6. Both fracture sites contain discrete and well-defined flow paths between boreholes.

During liquid-release tests in the welded tuff (Section 6.2 on niche seepage tests and Section 6.6 on fracture flow tests), it was observed, in some cases, that liquid flux at certain zones was not always commensurate with the air-permeability values at these zones (see Attachment IV.2). Besides the capillary mechanism (that water will prefer smaller aperture fractures), another

possible explanation for this observation is that liquid tries to flow downward following gravity and is thus more sensitive to the directionality of permeability than is air. Directionality of flow is not available from single-borehole data and requires crosshole data analyses.

6.5.2 Permeability Distributions and Crosshole Responses in Nonwelded Tuff

The Alcove 4 test bed is located in the PTn unit. The test bed contains several nonwelded and bedded subunits, including a pinkish-colored argillic layer. The test bed contains a fault plane as illustrated in Figure 6.5.2-1. Section 6.7 below describes in more detail the borehole configuration and specifications. In this section, the focus is on the cluster of seven boreholes. Boreholes 1, 4, 11, and 12 intersected the projected fault plane in the front part of the test block, while boreholes 2, 15, and 16 penetrated other features in the test block, with potential fault zone influences (if any) confined near the ends of the boreholes. If the fault is perfectly planar, the last three holes would not be intercepted by the fault.

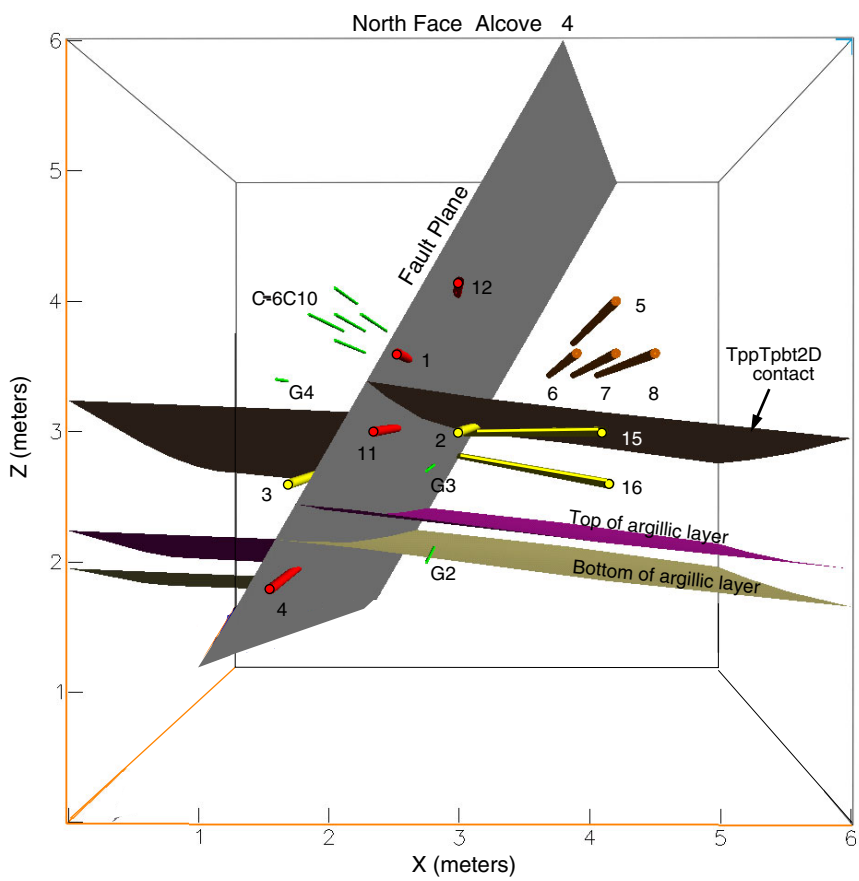

Figure 6.5.2-1. Perspective Illustration of Alcove 4 Test Bed

Figure 6.5.2-2 illustrates the single-borehole air-permeability profiles along the boreholes. Layer variations and the influence of faults could contribute to the widely distributed set of permeabilities over a broad range, both along individual boreholes and among different boreholes. With the exception of borehole 12, the other six boreholes penetrate a high-permeability zone near the end of the boreholes. Among all the borehole clusters tested in the ESF to date, the Alcove 4 PTn cluster shows the largest standard deviation of any of the sites (see Table 6.1.2-3 in Section 6.1.2.3). Even the cluster at the intensely fractured site at Niche 4788 has lower standard deviation of log permeability (0.85) than the value at Alcove 4 (0.93). The mean permeabilities of these two distinctly different sites (in lithological, geological, and fracture characteristics) are incidentally nearly identical. In comparison, the standard deviation for the Alcove 6 cluster was 0.67, and mean was nearly one order of magnitude higher.

Figure 6.5.2-3 shows the connections for Alcove 4 at the same shading scale used in welded tuff plots (Figure 6.5.1-1 and Figure 6.5.1-3). The number of connections is much higher for this nonwelded tuff site. To better display the stronger connections, Figure 6.5.2-4 portrays the data at Alcove 4 on a more appropriate scale legend and trims off the weaker connections. The salient features of the site now become apparent. Strong vertical connections are apparent between the upper and middle boreholes, but very little connectivity exists between the middle borehole and the lower-left borehole, despite similar flow rates and distances. The argillic layer exists between these locations, and the slot provides a nearly impermeable barrier. The single strong connection running from left to right is most likely associated with a high-permeability zone identified by the single-borehole profiles. The high-permeability zone could be associated with the fault intersecting the boreholes near the end. Interceptions were not identified in pre-test design in Figure 6.5.2-2. The connections were identified by crosshole analyses of pneumatic air-permeability test data.

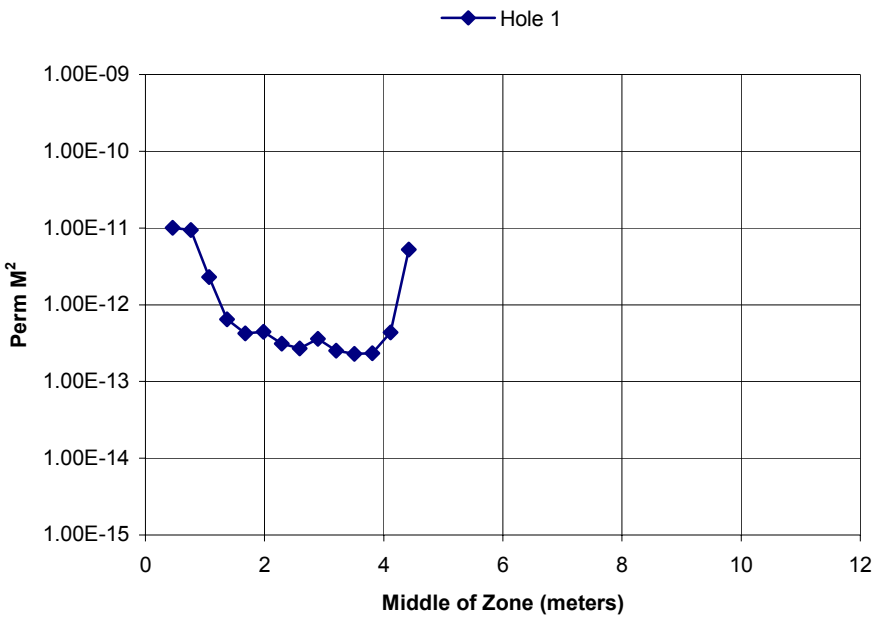

DTN: LB980901233124.009 [105856]

Figure 6.5.2-2. Air-Permeability Profiles along Boreholes in Alcove 4

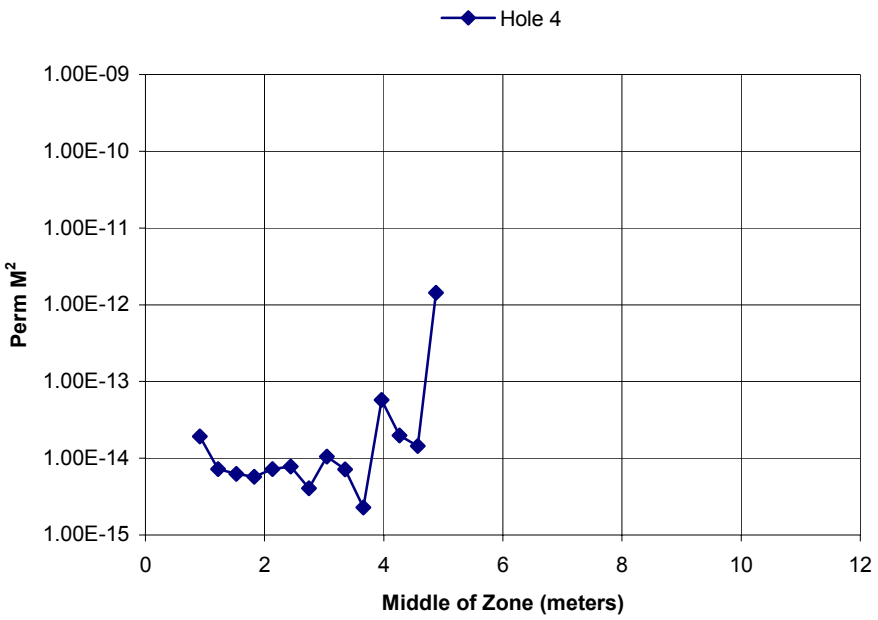

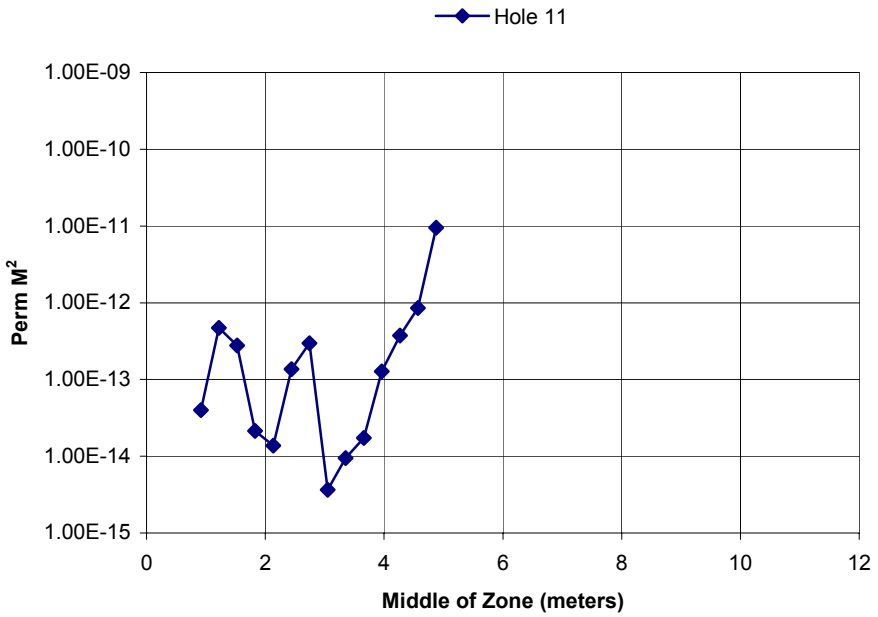

DTN: LB980901233124.009 [105856]

Figure 6.5.2-2. Air-Permeability Profiles along Boreholes in Alcove 4 (continued)

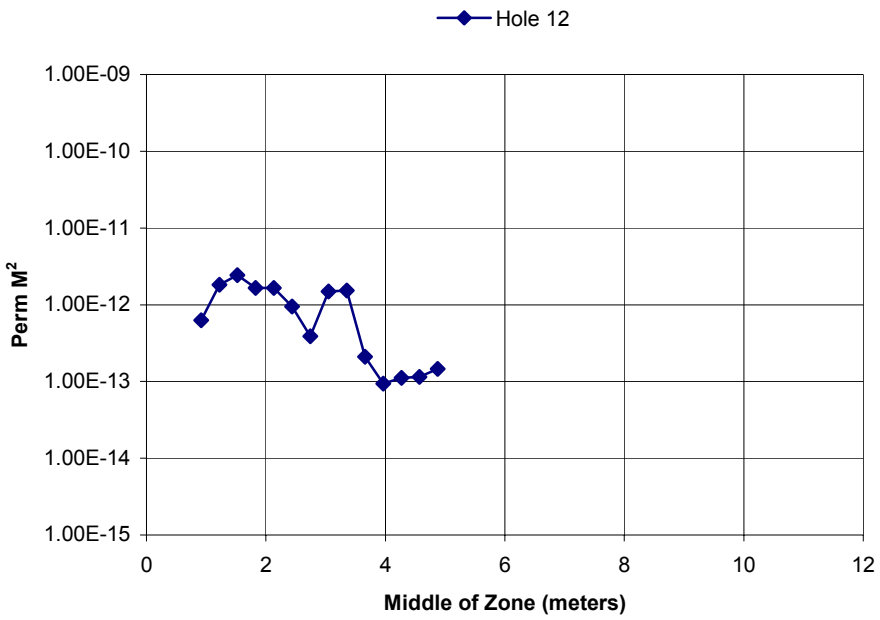

DTN: LB980901233124.009 [105856]

Figure 6.5.2-2. Air-Permeability Profiles along Boreholes in Alcove 4 (continued)

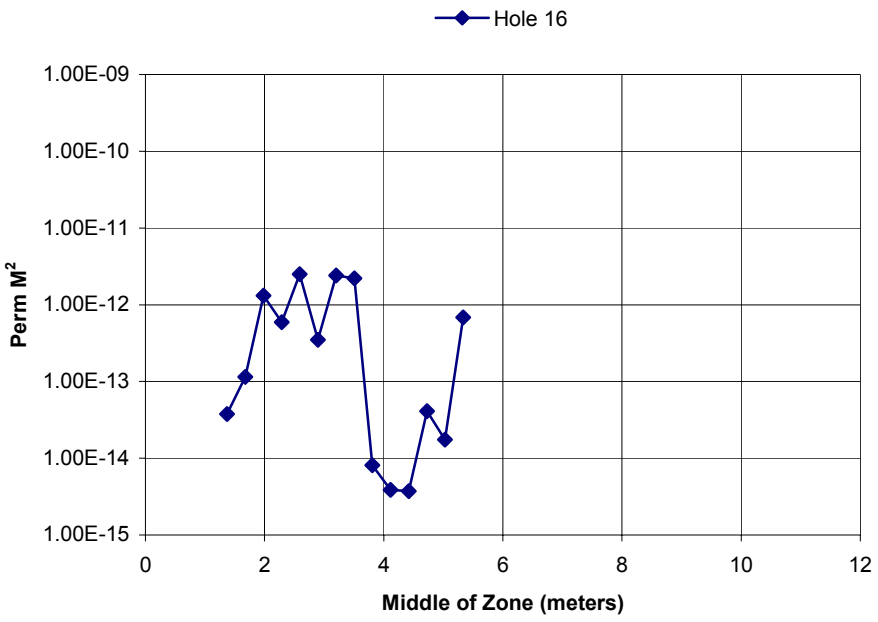

DTN: LB980901233124.009 [105856]

Figure 6.5.2-2. Air-Permeability Profiles along Boreholes in Alcove 4 (continued)

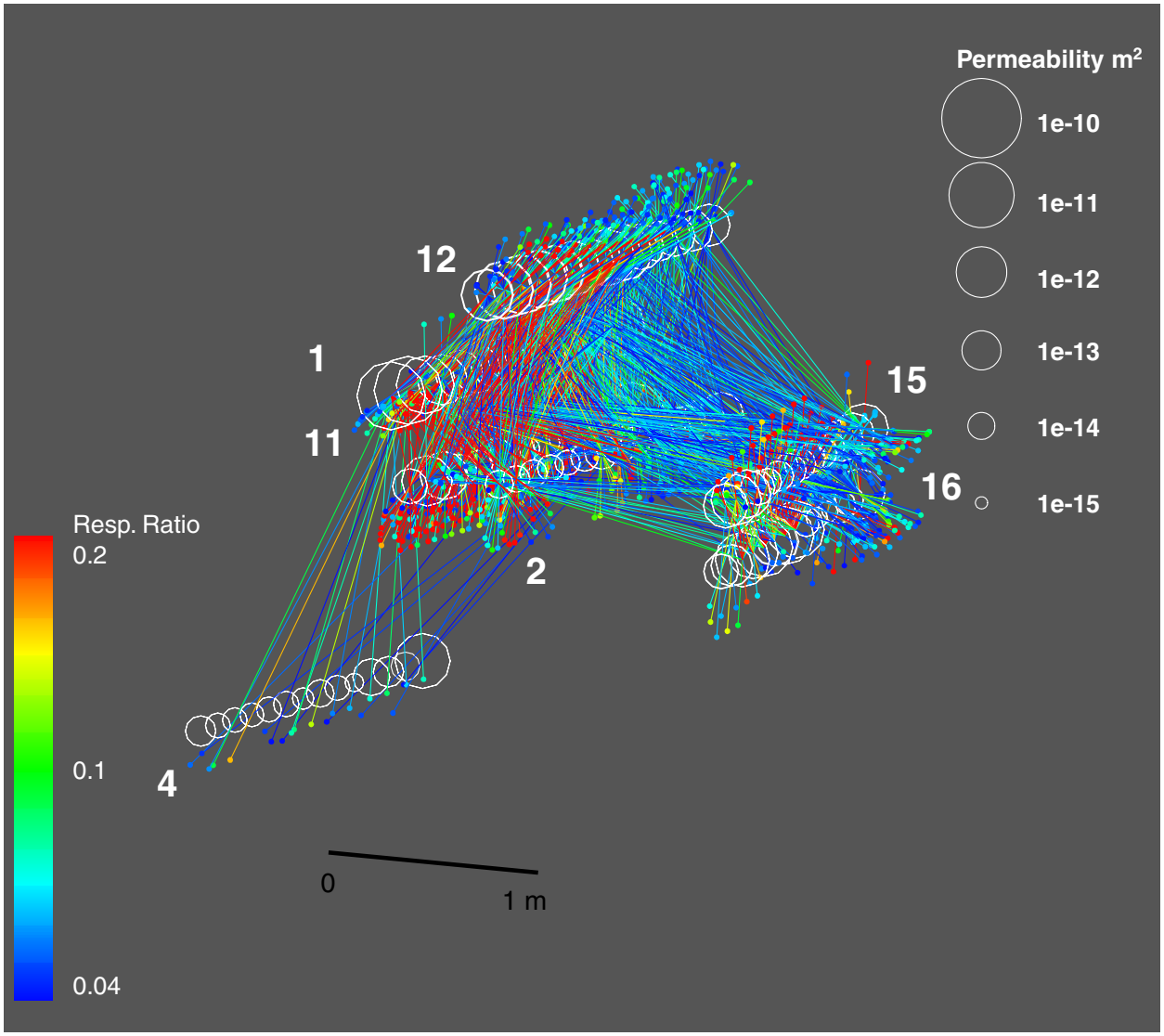

DTN: LB990901233124.004 [123273]

Figure 6.5.2-3. Crosshole Responses for the Borehole Cluster at Alcove 4 PTn Test Bed with All Response Pressure (Resp.) Ratios below 0.2 Included

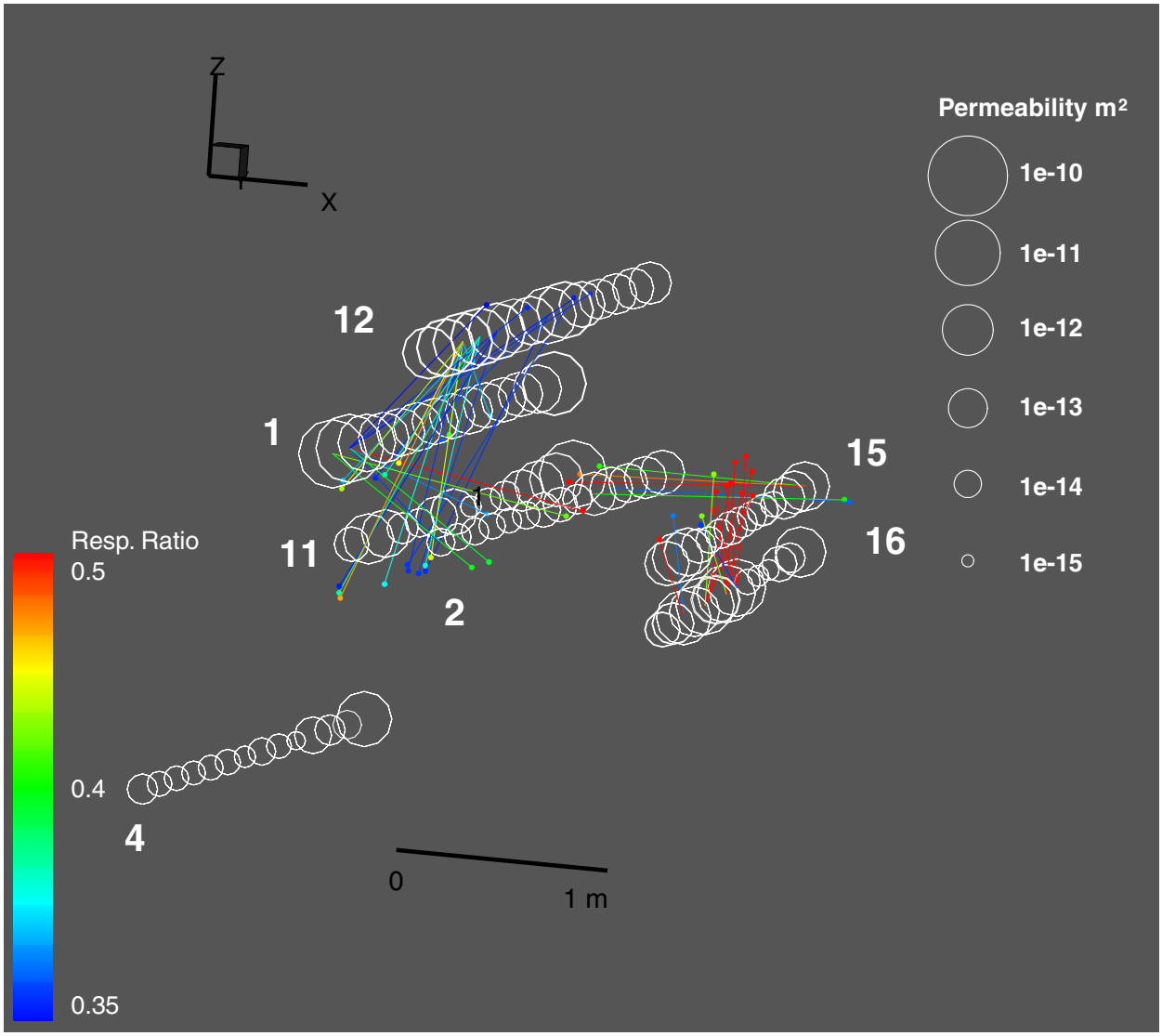

DTN: LB990901233124.004 [123273]

Figure 6.5.2-4. Crosshole Responses for Borehole Cluster at Alcove 4 PTn Test Bed with Small Response Pressure (Resp.) Ratios Filtered

6.6 ANALYSES OF FRACTURE FLOW IN FRACTURE-MATRIX TEST BED AT ALCOVE 6

Wetting-front movement, flow-field evolution, and drainage of fracture flow paths were evaluated in a test bed with a slot excavated below a cluster of boreholes. The slotted test bed is located within the Topopah Spring welded tuff (TSw) at Alcove 6 in the ESF at Yucca Mountain, Nevada. Hydraulic parameters such as formation intake rates, flow velocities, seepage rates, and fracture volumes were measured under controlled boundary conditions, using techniques developed specifically for *in situ* testing of flow in fractured rock. Below, the test-bed configuration and field instrumentation are described, followed by the results.

6.6.1 Liquid-Release Tests in Low- and High-Permeability Zones

Field tests were conducted at Alcove 6 over a period of six weeks, starting in late July 1998. These included multiple releases of tracer-laced water in one high-permeability zone (HPZ) and one low-permeability zone (LPZ) along an injection borehole. The permeabilities of these zones were determined from air-permeability measurements conducted over 0.3 m sections along the borehole, using a straddle packer that also was used for liquid releases. The HPZ had an air-permeability value of 6.7×10^{-12} m^2, and the LPZ had an air-permeability value of 2.7×10^{-13} m^2 (Salve 1999 [155692], pp. 48–49 and Cook 2001 [156902], pp. 51–53). During and following liquid-release events, changes in saturation and water potential in the fractured rock were measured in three monitoring boreholes, with changes continuously recorded by an automated data acquisition system. The water that seeped into the excavated slot below the injection zone was collected, quantified for volumes and rates, and analyzed for tracers.

6.6.1.1 The Test Bed

The test bed was located at Alcove 6 in the ESF (Figure 6.6.1-1a), lying within the middle nonlithophysal zone of the TSw. The rock was visibly fractured, with predominantly vertical fractures and a few subhorizontal fractures. The relatively wide fracture spacing (on the order of tens of centimeters) facilitated the choice of injection zones, allowing discrete fractures and well-characterized fracture networks to be isolated by packers for localized flow testing.

A horizontal slot and a series of horizontal boreholes are the distinct features of the test bed (Figure 6.6.1-1b). The slot, located below the test bed, was excavated by an over-coring method. The excavation sequence required (first) the drilling of parallel pilot holes, 0.10 m in diameter, over 4 m in length with a 0.22 m spacing, normal to the alcove wall. The pilot holes were then over-cored by a 0.3 m drill-bit to excavate the 2.0 m wide, 4.0 m deep and 0.3 m high slot located approximately 0.8 m above the alcove floor. Three I-beam supports were installed along the length of the slot for support. Four horizontal boreholes, 0.1 m in diameter and 6.0 m in length, were drilled perpendicular to the alcove wall above the slot. Boreholes A and B were located 1.6 m above the slot ceiling, while boreholes C and D were 0.9 m and 1.0 m above the slot ceiling, respectively, and 0.7 m apart (Figure 6.6.1-1b).

Borehole A was used for fluid injection, while boreholes B, C, and D were monitored for changes in moisture conditions. The slot was used to collect water seeping from the fractured

rocks above. A flexible plastic curtain 3.0 m wide and 0.9 m high was installed to cover the slot face and to minimize air movement between the alcove and the slot.

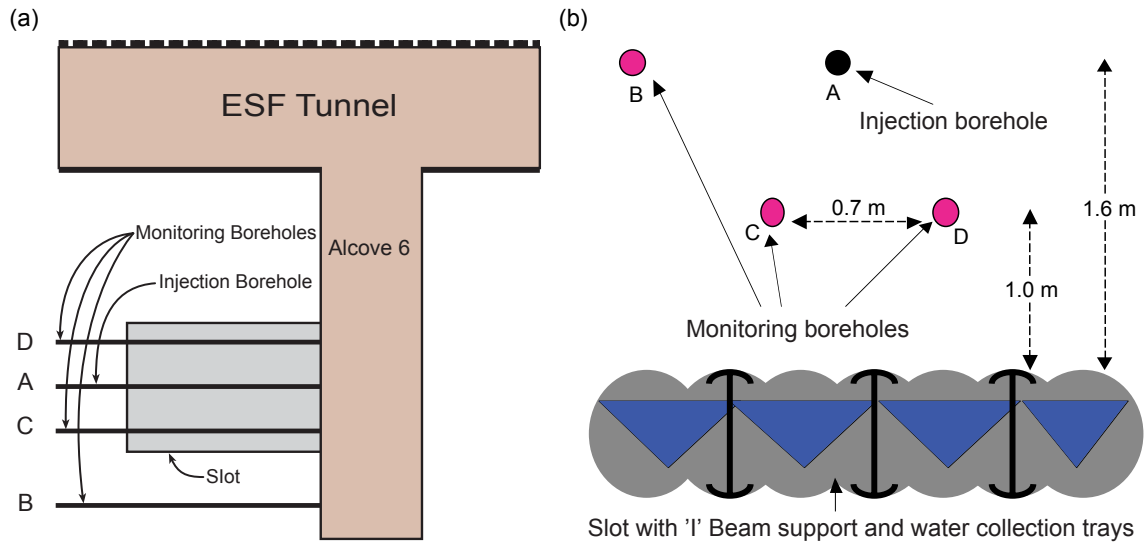

NOTE: Figures are not drawn to scale.

Figure 6.6.1-1. Schematic Illustration of (a) Plan view of Location and (b) Vertical View of Layout of Test Bed at Alcove 6 in the ESF at Yucca Mountain

6.6.1.2 Instrumentation

There were three distinct components to the flow investigation: (1) controlled release of water into isolated zones, (2) borehole monitoring for changes in saturation and water potential, and (3) collection of seepage from the slot ceiling. The key features of new instruments developed for this field investigation are presented in Attachment VI.

6.6.1.3 Liquid-Release Experiments

Air-permeability measurements were done along 0.3 m sections of the injection borehole as described in Section 6.1 and Section 6.5. The HPZ is located 2.3–2.6 m from the borehole collar, whereas the LPZ is 0.75–1.05 m from the collar. In both HPZ and LPZ, a series of constant-head tests were conducted to determine the temporal changes in the rate at which the formation could take in water. In the HPZ, a second series of tests was conducted with different injection rates. Tests conducted in this field investigation are summarized in Table 6.6.1-1. Seepage rates into the slot were monitored.

All the water used in the ESF was spiked with lithium bromide for mining-related activities and for most of the scientific investigations. Additional tracers were added to the water injected into the LPZ and during the first set of experiments in the HPZ (Table 6.6.1-1). During the tests, water that seeped into the slot was periodically sampled and analyzed for tracer concentrations.

Water was released into the LPZ three times over a period of two weeks, starting on July 23, 1998 (Table 6.6.1-1). For the first release, water was injected at a constant pump rate of approximately 56 mL/min. At 66 minutes, water was observed in the overflow line, indicating

that water was being injected at a rate higher than the intake capacity of the zone. At this time, the flow rate on the pump was immediately reduced to approximately 6.0 mL/min. Within 22 minutes, return flow ceased, and water was injected continuously at this rate for the next 4 hours and 23 minutes. Based on the actual flow rate determined from transducers located at the bottom of the water reservoir (see Attachment VI.1), a total of 6.3 liters of water was injected into the zone, of which 0.7 liters was recovered as return flow. The other 5.6 liters was released into the formation. Average net release rate into the formation rate was approximately 17 mL/min.

For the second liquid release in the LPZ, the constant-head injection system was used. The constant-head chamber was located adjacent to the injection borehole, such that the head of water was 0.07 m in the injection zone. This constant head was maintained for 4 hours in the injection zone, while the water level in the reservoir was continuously monitored. At the end of this constant-head period, water supply to the injection zone was discontinued, resulting in a falling-head boundary condition inside the injection zone. A total of 1.4 liters of water was introduced into the LPZ from both the constant-head and falling-head periods.

The final release into the LPZ was initiated on July 29, 1998, when water was introduced into the formation under a constant head (of 0.07 m) maintained for 43 hours, after which the ponded water in the injection zone continued to percolate into the formation under a falling-head condition. During the test, 1.0 liters of water were released under the constant-head boundary, whereas 1.2 liters were released under the falling head.

Summing up all three tests in the LPZ, 9.2 liters of water were released to the formation under a combination of constant and falling-head boundary conditions at the point of injection.

Water was injected into the HPZ during two groups of tests over a period of two weeks (Table 6.6.1-1). The first group of four tests was conducted during August 4–6, 1998, and the second group of four tests were conducted during August 25–28, 1998. The first two tests (Test HPZ-1 and Test HPZ-2) in the first group were constant-head tests (of head 0.07 m) that served to establish the intake rates at which the injection zone could release water to the formation. The HPZ-1 constant-head test rate was ~119 mL/min. The HPZ-2 constant-head test rate was ~98 mL/min. After the HPZ-2 test, tests were conducted at constant flow rates. During the third test (Test HPZ-3) conducted on the next day, water was injected at approximately half the intake rates observed with the constant-head system (i.e., ~53 mL/min). During the fourth test (Test HPZ-4) on August 6, 1998, water was injected at a constant rate of ~ 5 mL/min over 12 hours. During the second group of tests (Tests HPZ-5 through HPZ-8) over a period of four days starting on August 25, 1998, the injection rate was sequentially reduced from ~69, ~38, ~29, and finally to ~14 mL/min.

Table 6.6.1-1. Amount of Water and Types of Tracers Released into the Injection Borehole

Date	Test #	Injection type	Infiltration rate (mL/min)	Volume of water injected (l)	Additional Tracer *
7/23/98	LPZ-1	Constant rate	~16	5.6	Sodium Bromide 2,3,6 Trifluorobenzoic acid
7/24/98	LPZ-2	Constant head	~1.2	0.3	2,4,5 Trifluorobenzoic acid
7/24-25/98	LPZ-2	Falling head		1.1	2,4,5 Trifluorobenzoic acid
7/29-30/98	LPZ-3	Constant head	~0.5	0.4	3,5 Difluorobenzoic acid
7/30-31/98	LPZ-3	Constant head	~0.5	0.6	3,5 Difluorobenzoic acid
7/31-8/4/98	LPZ-3	Falling head		1.2	3,5 Difluorobenzoic acid
8/4/98	HPZ-1	Constant head	~119	16.3	Potassium Fluoride Pentafluorobenzoic acid
8/4/98	HPZ-2	Constant head	~98	17.3	2,3,4 Trifluorobenzoic acid
8/5/98	HPZ-3	Constant rate	~53	17.5	3,4 Difluorobenzoic acid
8/6/98	HPZ-4	Constant rate	~5	3.4	2,3,4,5 Tetrafluorobenzoic acid
8/25/98	HPZ-5	Constant rate	~69	18.4	
8/26/98	HPZ-6	Constant rate	~38	18.4	
8/27/98	HPZ-7	Constant rate	~29	18.2	
8/28/98	HPZ-8	Constant rate	~14	9.4	

DTN: LB990901233124.002 [146883]

NOTES: LPZ located 0.75-1.05 m from borehole collar
HPZ located 2.30-2.60 m from borehole collar
* All injected water was tagged with lithium bromide

6.6.2 Observations of Wetting-Front Migration and Fracture Flow

Water released in the injection borehole flowed through the fractured rock and, in the case of the HPZ, some of the water seeped into the slot located 1.6 m below. Liquid-release rates in the injected zone were measured, saturation and water-potential changes were observed along monitoring boreholes, and seepage water into the slot was collected.

6.6.2.1 Liquid-Release Rates

Measurements of liquid-release rates in the LPZ in this fractured-welded-tuff test bed exhibited a response similar to that observed for (unfractured) porous media. The initially high rates asymptotically approached low steady-state values of ~0.35 mL/min (Figure 6.6.2-1a). Near continuity was observed in the decreasing liquid-release rates, even with a five-day gap between liquid releases into the formation (Figure 6.6.2-1b).

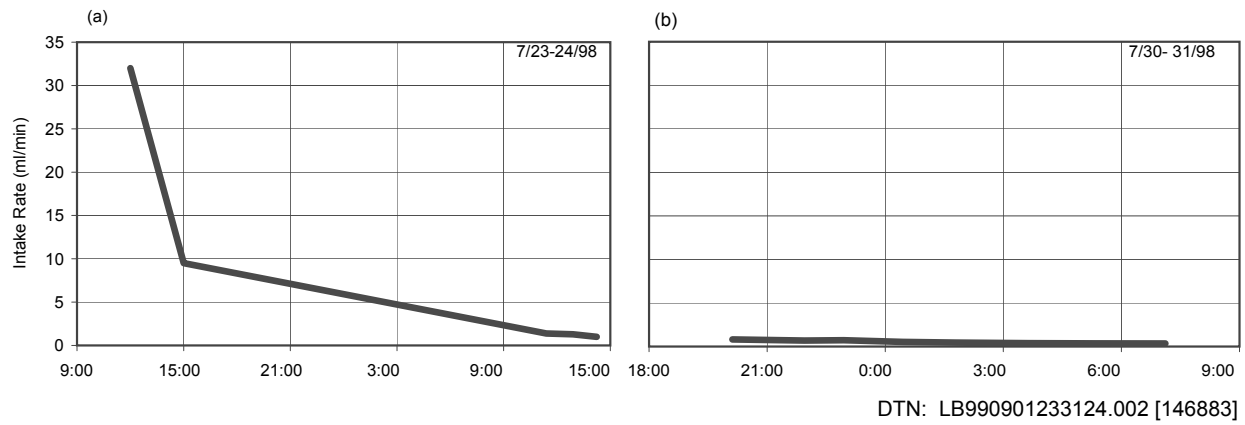

Figure 6.6.2-1. Water Intake Rates Observed in the Low Permeability Zone

For the first two constant-head tests conducted in the HPZ, the rates of liquid release varied significantly during and between tests (Figure 6.6.2-2). In the first test, the liquid-release rate continued to climb for the first sixty minutes and then remained steady for the next 15 minutes before briefly increasing sharply. For the remainder of the test it continued to fluctuate between 70 and 160 mL/min. In the second test, the liquid-release rate rapidly increased for the first 15 minutes. The rate then slowly decreased and steadied off to ~100 mL/min. Ninety minutes into the test, the liquid-release rate briefly fell to 35 mL/min, sharply increased to 130 mL/min, and slowly decreased to a quasi-steady rate of 90 mL/min in the next 80 minutes.

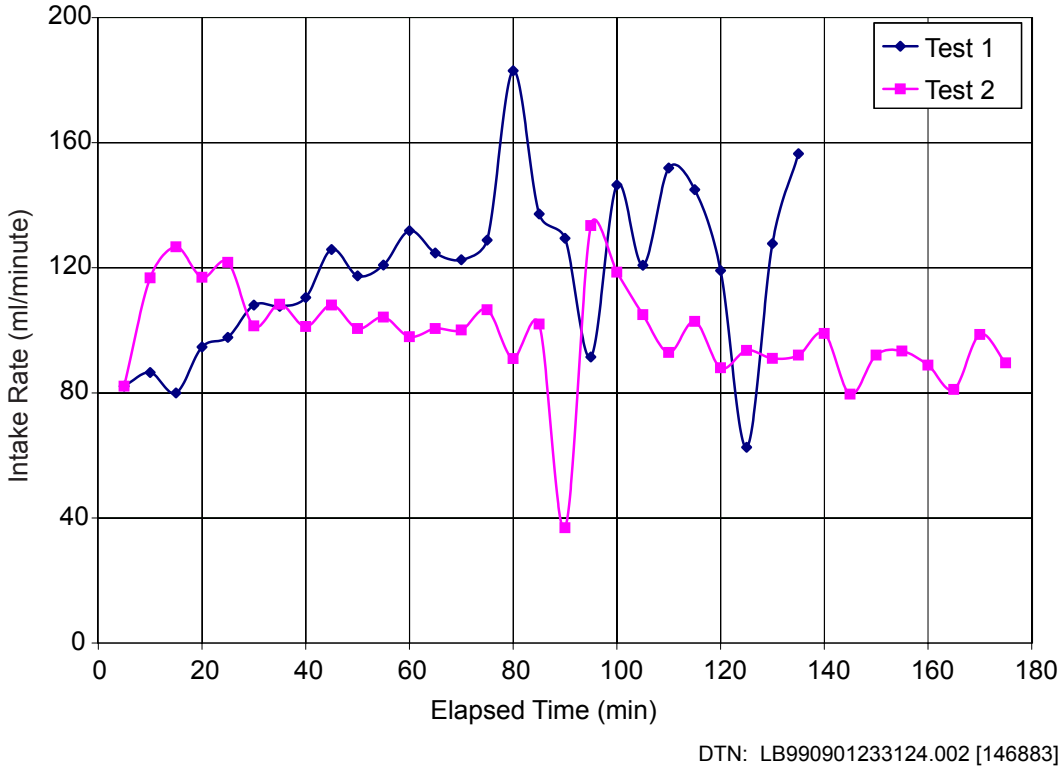

Figure 6.6.2-2. Water Intake Rates Observed in the High Permeability Zone

6.6.2.2 Formation Wetting and Drying

In the two monitoring boreholes (C and D, shown in Figure 6.6.1-1b) located below the injection borehole (A), changes in saturation were detected both by the electrical-resistivity probes (ERPs), as shown in Figure 6.6.2-3a and Figure 6.6.2-3c, and by the psychrometers, as shown in Figure 6.6.2-3b and Figure 6.6.2-3d. The ERPs consisted of two electrical leads sandwiched between pieces of filter paper. The results in Figure 6.6.2-3 are the responses to liquid release in the LPZ located 0.75–1.05 m from the borehole collar. In both boreholes, large changes in saturation were detected by either ERPs or psychrometers or both, located between 0.9 and 1.9 m from the collar. At a distance of 2.15 m from the borehole collar, the changes were much smaller.

The wetting process reduces electrical resistance and increases the water potential (making it less negative). The drying process induces the opposite changes. In borehole C, the first drying response was detected by the ERP 0.90 m from the borehole collar, as illustrated in Figure 6.6.2-3a. A step increase in resistance was observed 30 minutes after water had been released, suggesting some initial drying with dry air preceding a wetting front. Two hours later, an abrupt increase in wetting was indicated by a stepped decrease in resistance. ERPs located at 1.15, 1.40, and 1.65 m also detected the arrival of a wetting front within 2 to 4 hours of liquid release. In borehole D (Figure 6.6.2-3c), the ERPs located at 0.9 and 1.15 m from the collar were first to detect increases in saturation, 30 minutes after the first release of water. At distances of 1.40 and 1.65 m, the wetting front arrived 6 hours later.

In both boreholes, the probes that had the largest and quickest responses (i.e., probes located between 1.15 and 1.65 m) were also the ones that showed some drying between the two injection events. Probes located at a distance of 0.90–1.15 m detected a continuous drying trend after the initial period of injection.

The borehole C psychrometer data in Figure 6.6.2-3b supported the ERP data in Figure 6.6.2-3a with smoother and more systematic changes induced by wetting-front arrivals. The sensors closer to the release point had larger changes in water potential. At distances between 1.40 and 2.15 m from the collar, water potentials were between -140 and -75 m before the first injection. Immediately after water was introduced, water potentials began to rise steadily for the next four days, reaching values between -70 and -30 m. In response to the second injection period (i.e., July 29–August 4, 1998, in Table 6.6.1-1), the most noticeable increases in potentials were observed in the psychrometer located at 1.40 m, where water potentials increased from -40 to -15 m after the second injection period. In borehole D, illustrated in Figure 6.6.2-3d, changes in water potential were observed between 0.90 and 1.90 m following the first injection. However, the extent of drying, as seen in the decrease in water potentials at 1.40 and 1.65 m, was greater than observed in borehole C. During the second wetting event, water potentials in this zone were similar to those observed following the first event. Oscillatory responses could be related to variations of drift conditions for sensors near the borehole collars. This is a speculative interpretation, to be substantiated or refuted.

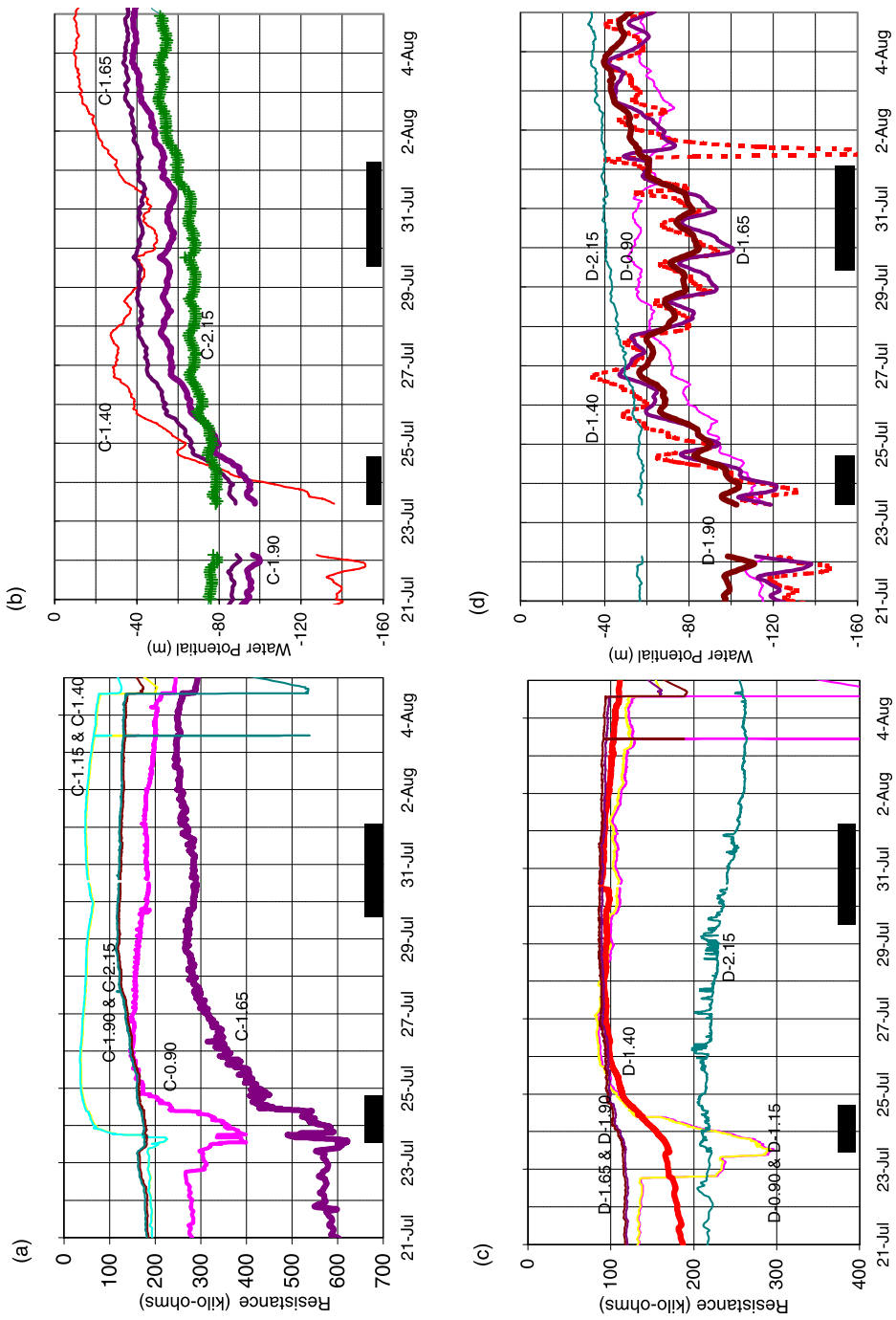

DTN: LB990901233124.002 [146883]

NOTE: The legend identifies the sensor location in borehole (C & D) and distance of sensor from the borehole collar. Shaded zones indicate the duration of liquid-release events. Note resistance axis is inverted.

Figure 6.6.2-3. Changes in Electrical Resistance and Water Potential Detected during Liquid Release into the Low Permeability Zone

Similar to the injection response in the LPZ, changes in saturation were detected both by the ERPs and psychrometers in the monitoring boreholes (Figure 6.6.2-4) from liquid releases into the HPZ located 2.30–2.60 m from the borehole collar. In borehole C, changes in saturation were observed between 1.9 and 3.4 m from the borehole collar, with the largest changes observed between 2.15 and 3.15 m. Both the ERPs and the psychrometers detected the changes. The largest changes in water potentials were detected between 2.15 and 2.40 m from the borehole collar in borehole C, where pre-injection water potentials, which were between -70 to -60 m, climbed to between -20 and -10 m after the first set of releases. These values persisted after the second set of releases. In borehole D, saturation changes were observed over a slightly wider span along the borehole (i.e., 1.65 to 3.65 m from the borehole collar), with the noticeable changes observed between 1.90 and 3.40 m from the borehole collar. After the initial release of water in the HPZ, water potentials between locations 2.15 and 2.90 m increased over a period of a week. These were between -15 to -5 m for the duration of the remaining liquid releases.

In both boreholes, the psychrometer data suggest that after the first batch of water releases (i.e., August 4–6, 1998), water potentials significantly increased (e.g., -60 to -20 m), which then persisted until the start of the second period of injection (August 25–28, 1998). During this second set of injections, more water was retained by the formation, resulting in further increases in water potentials. The ERP and psychrometer data indicate that the zones between 2.15 and 2.40 m in borehole C, and between 2.15 and 2.65 in borehole D, showed the largest changes during active testing.

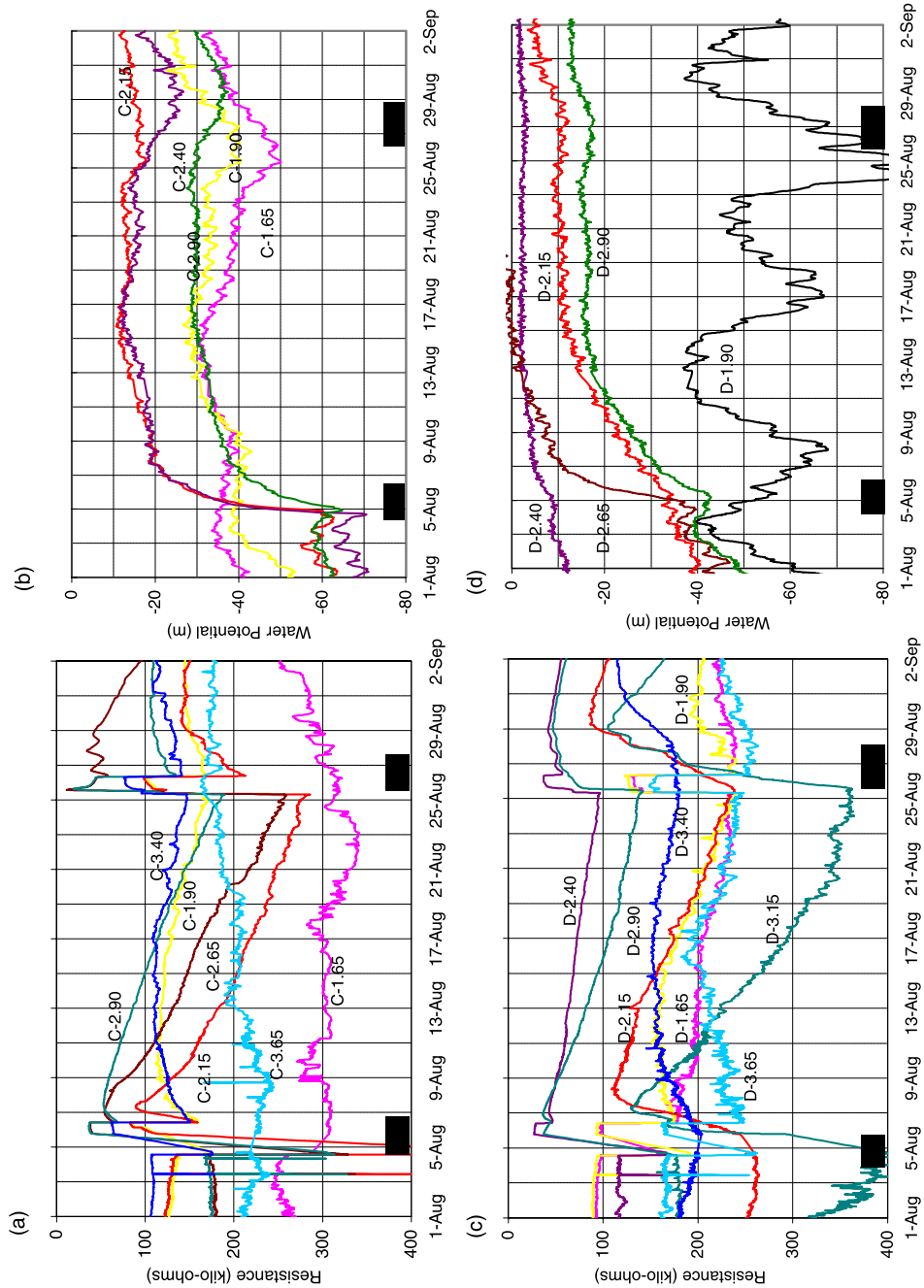

DTN: LB990901233124.002 [146883]

NOTE: The HPZ is located between 2.30 and 2.60 m from the borehole collar. The legend identifies the sensor location in borehole (C & D) and distance of sensor from the borehole collar. Shaded zones indicate the duration of two groups of liquid-release events. Note resistance axis is inverted.

Figure 6.6.2-4. Changes in Electrical Resistance and Water Potential Detected during Liquid Release into the High Permeability Zone

6.6.2.3 Seepage into the Slot

Seepage into the slot was observed during all eight tests in the HPZ (and none in the LPZ tests). The eight tests were conducted in two groups (Table 6.6.1-1). The test results are summarized in Table 6.6.2-1 and illustrated in Figure 6.6.2-3 and Figure 6.6.2-4 as two shaded test duration zones. During the first test in the first group (Test HPZ-1), water was first observed on the slot ceiling five minutes after the start with 0.41 liters of water released under constant-head conditions. In the HPZ-2 and HPZ-3 tests, water appeared in the slot within 3 minutes after 0.17 and 0.14 liters, respectively, had been released. In the HPZ-4 test, water appeared in the slot after five hours with 1.50 liters of water injected at a rate of 5 mL/min.

In the second group of tests, travel time for the first drop of water was 3 minutes after 0.14 liters was injected at a rate of ~69 mL/min (Test HPZ-5). In the HPZ-6 and HPZ-7 tests, the arrival time of the wetting front was 7 minutes after 0.26 and 0.20 liters of water were injected at a rate of 38 and 29 mL/min, respectively. In the final HPZ-8 test, water first appeared in the slot after 1:08 hr, with 0.90 liters injected into the formation at a rate of 14 mL/min.

Table 6.6.2-1. Summary of Liquid-Injection Tests in the High Permeability Zone.

Test Number	Injection Rate (mL/min)	Duration of Injection (hh:mm)	Volume Recovered (liters)	Travel Time of First Drop (hh:mm)	Volume of Water In Formation (liters)		Water Retained in Formation (%)
					At First Drop	At End of Injection	
HPZ-4	5	11:54	0.36	5:00	1.51	3.03	89
HPZ-8	14	11:19	4.56	1:08	0.90	4.82	51
HPZ-7	29	10:36	13.21	0:07	0.20	5.02	28
HPZ-6	38	8:00	14.73	0:07	0.26	3.71	20
HPZ-3	53	5:25	11.14	0:03	0.14	6.31	36
HPZ-5	69	4:26	11.47	0:03	0.14	6.90	38
HPZ-2	98	2:56	12.17	0:03	0.17	5.15	30
HPZ-1	119	2:17	11.61	0:05	0.41	4.67	29

DTN: LB990901233124.002 [146883]

The fraction of injected water recovered in the slot continued to increase as each test progressed. Significant variability was observed in the percentage of water recovered and the seepage rate during and between tests (Figure 6.6.2-5a and b). Seepage variability was related to both the amount of water injected and the rate at which water was released into the formation. Early in each test, the amount of water recovered sharply increased. The percentage of injected water recovered approached relatively constant values after approximately 10 liters of water had been injected. Intermittent seepage behavior (Figure 6.6.2-5b) was observed during all the tests.

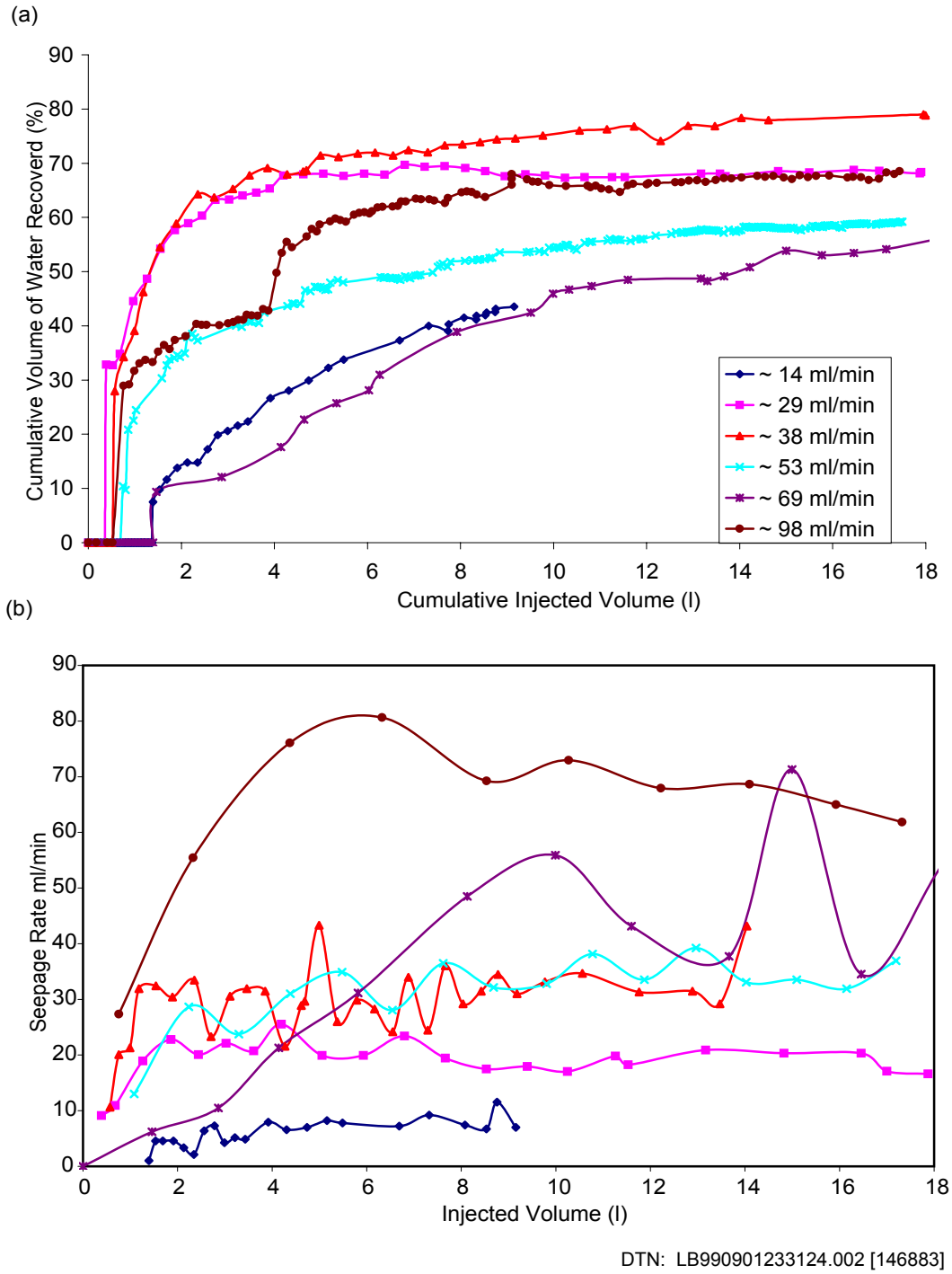

Figure 6.6.2-5. Seepage into Slot: (a) Percentage of Injected Water Recovered and (b) Seepage Rates for Various Release Rates

As illustrated in Figure 6.6.2-6, the percentage of the amount of injected water recovered at the release rate of 38 mL/min was higher than the percentages at other injection rates. The first maximum percentage could be associated with the dominant flow path connecting the injection zone with the outflow slot boundary. With increasing injection rate, additional flow paths, either through other fractures or through other areas in the same fracture, could contribute to the storage and flow of additional water.

Figure 6.6.2-6 also illustrates the distribution of seepage among the collection trays in the slot. As each test progressed, water initially appeared on the slot ceiling at one single point directly below the injection zone, and seepage water was collected from four trays located around the point of entry. During these tests, water seeping into the slot was largely concentrated in a single tray, with the three other trays collecting significantly smaller amounts of water. Slight increases at higher injection rates were noticeable in some of the secondary trays. The remaining 24 trays stayed dry during all the liquid-release tests.

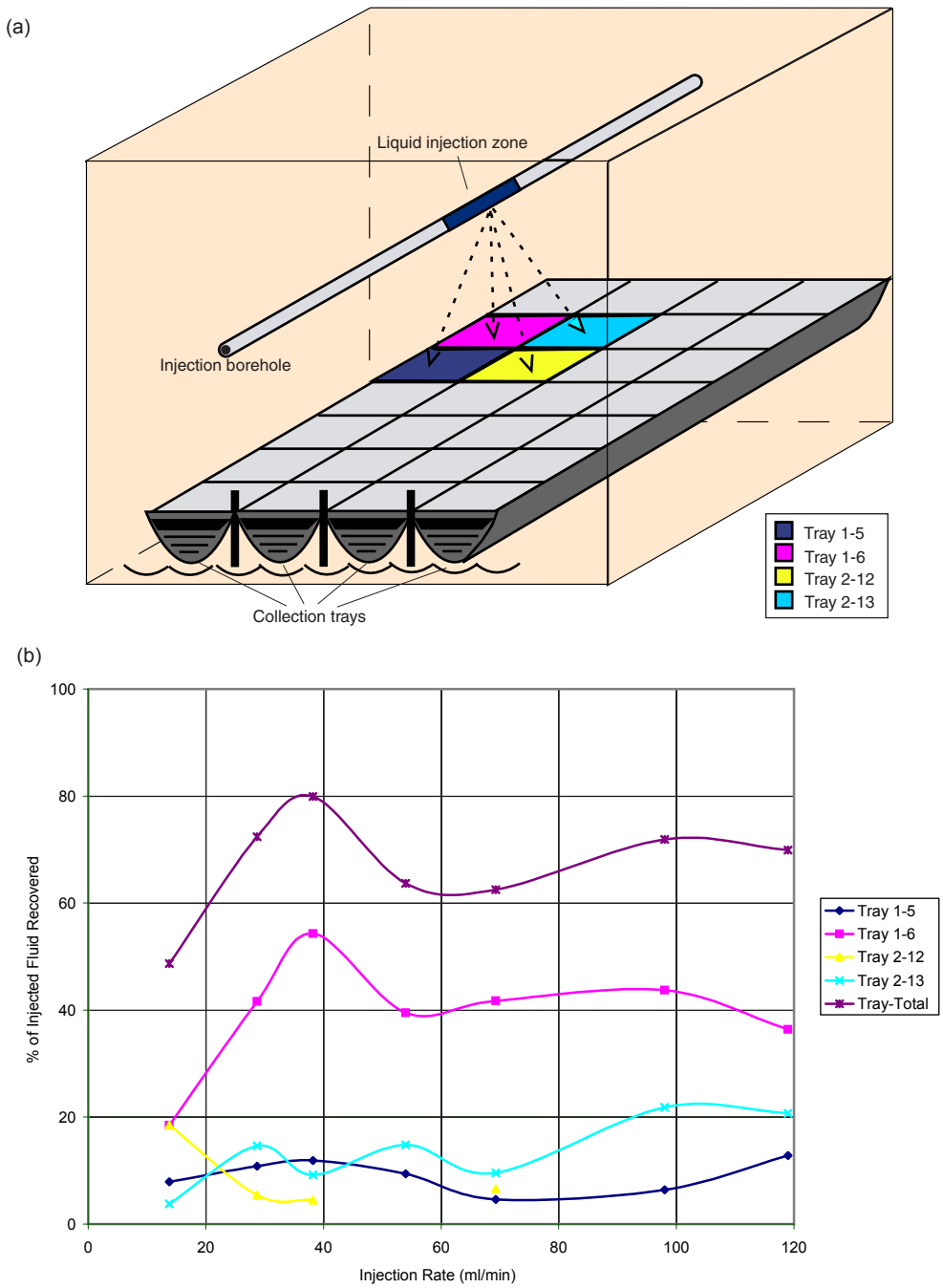

DTN: LB990901233124.002 [146883]

Figure 6.6.2-6. Seepage into Collection Trays in the Slot: (a) Tray Configuration and (b) Percentages of Injected Water Recovered for Different Trays

In all the tests during which there was seepage, 0.5 to 1.3 liters of water entered the slot after the water supply to the formation was switched off (Figure 6.6.2-7). Most of this water was collected within one hour, with recovery rates being largest immediately after the test. The constant-head test with ~98 mL/min release rate had a "stepped" nature to the post-injection recovery. During the first fifteen minutes, the 0.8 liters of collected water appeared in four bursts, each containing 0.1–0.3 liters of water. Changes of similar magnitudes were observed in the tests with injection rates of ~53 mL/min and ~14 mL/min (with one late burst each shown in Figure 6.6.2-7).

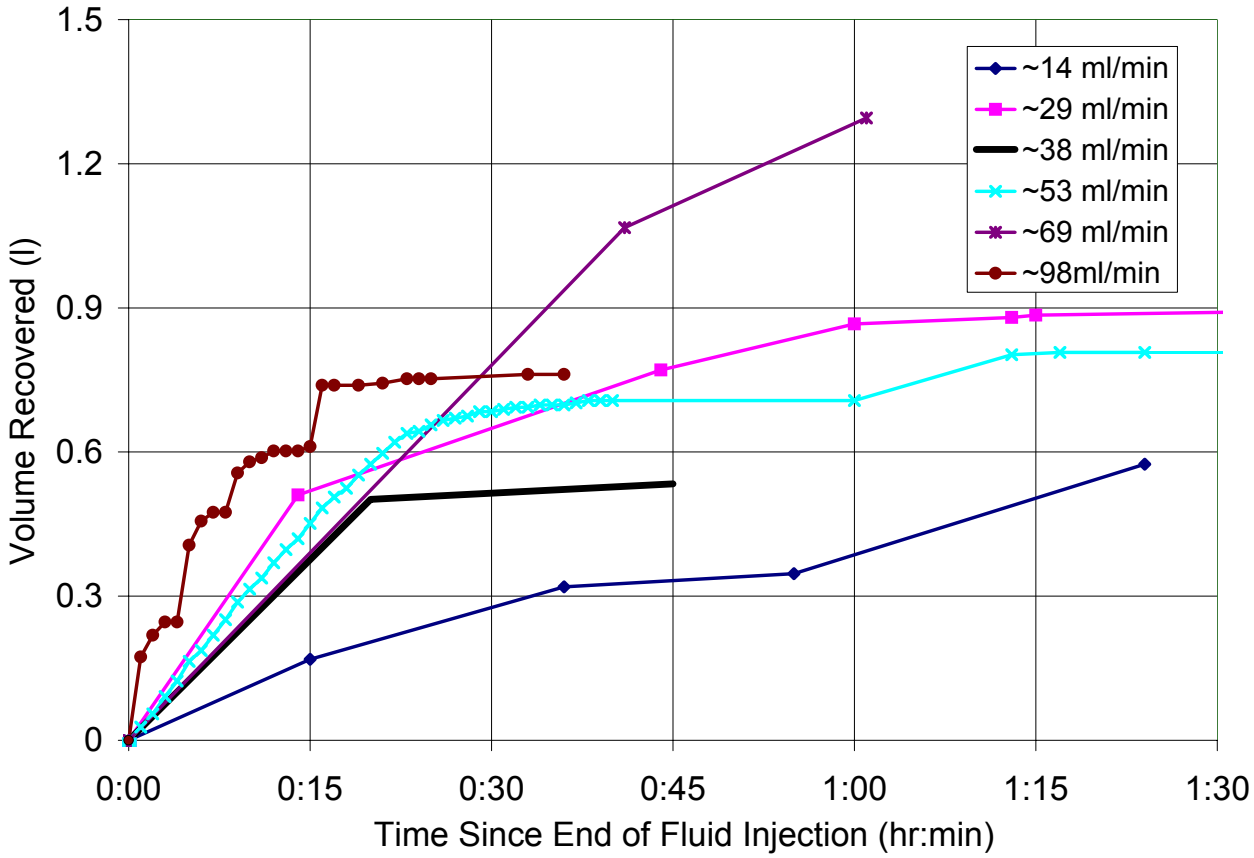

DTN: LB990901233124.002 [146883]

Figure 6.6.2-7. Volume of Water Recovered in the Slot after Liquid Injection at Various Rates into the High Permeability Zone was Stopped

6.6.2.4 Tracer Recovery

Tracers injected in the HPZ were detected in the water samples collected in the slot. (None of the traced water introduced in the LPZ was recovered.) Typically, tracers introduced in one test were rapidly flushed out of the system during the subsequent test (Figure 6.6.2-8). The pattern of recovered concentrations of tracers suggests that plug flow was the dominant process by which "new" water replaced "old" water from the previous test. Some recovery of tracers from the formation was observed during subsequent tests.

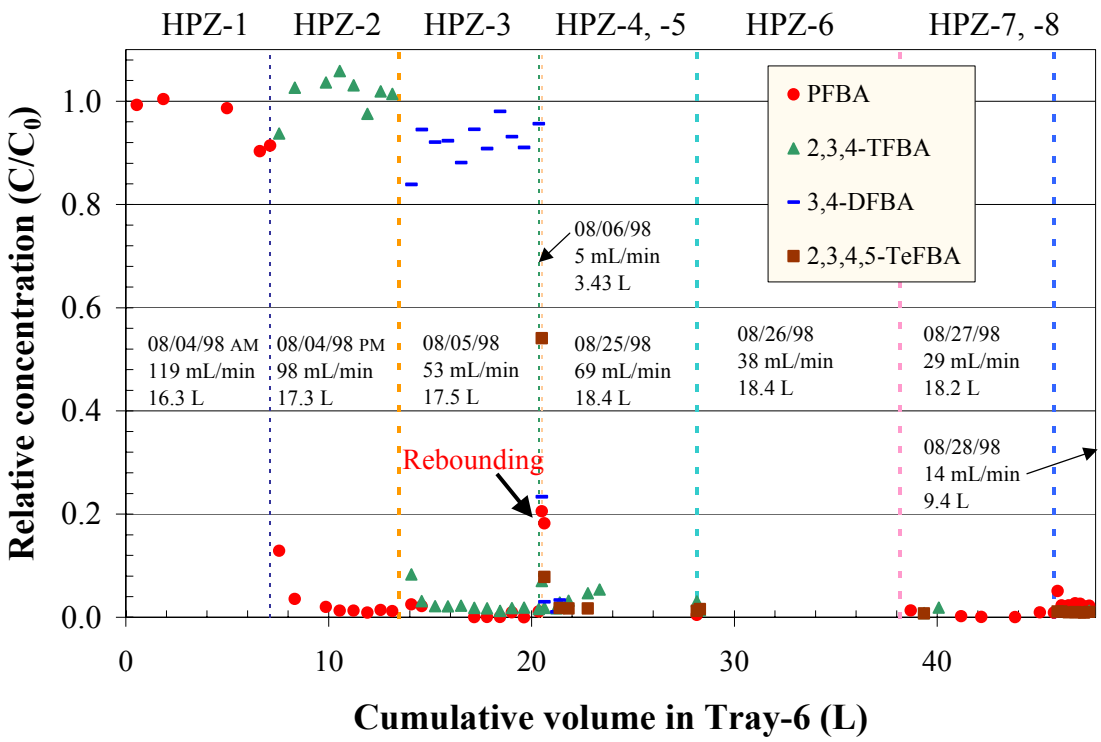

DTN: Flow Rate Data: LB990901233124.002 [146883] and Chemical Data: LB990901233124.001 [155694]

Figure 6.6.2-8. Tracer Concentrations in Seepage Water Following Injection into the High Permeability Zone

INTENTIONALLY LEFT BLANK

6.7 ANALYSES OF FLOW THROUGH THE FAULT AND MATRIX IN THE TEST BED AT ALCOVE 4

To investigate the potential for damping fast flow through the Paintbrush nonwelded tuff (PTn), the evolution of a flow field and the migration of a wetting front following the release of liquid into a fault and matrix were evaluated in a test bed using a cluster of horizontal boreholes at Alcove 4.

6.7.1 Flow Tests in Paintbrush Tuff Unit Layers and Fault

Field experiments were conducted in the PTn within the ESF at Yucca Mountain. These experiments included multiple releases of tracer-laced water in isolated zones along three horizontal boreholes. The zones into which water was released were selected based on air-permeability measurements conducted over 0.3 m sections of borehole (Section 6.5.2). The plumes that developed from these releases were monitored in six separate horizontal boreholes. During and following liquid-release events, changes in saturation and water potential along horizontal monitoring boreholes were continuously recorded by an automated data acquisition system.

6.7.1.1 The Test Bed

The test bed is located at Alcove 4 in the ESF. It is accessed through an alcove excavated (by an Alpine miner) at approximately 67 degrees to the central axis of the ESF North Ramp. Alcove 4 transects portions of the lower Pah Canyon Tuff (Tpp) and the upper pre-Pah Canyon bedded tuffs (Tpbt2) of the PTn (nomenclature of Buesch et al. 1996 [100106], p. 7). The central axis of the alcove has an azimuth of 6 degrees, which coincides with the approximate strike of the PTn units in the vicinity. The north face of the alcove, in which the test bed is located, is approximately 6 m wide and 5.3 m high (Figure 6.7.1-1).

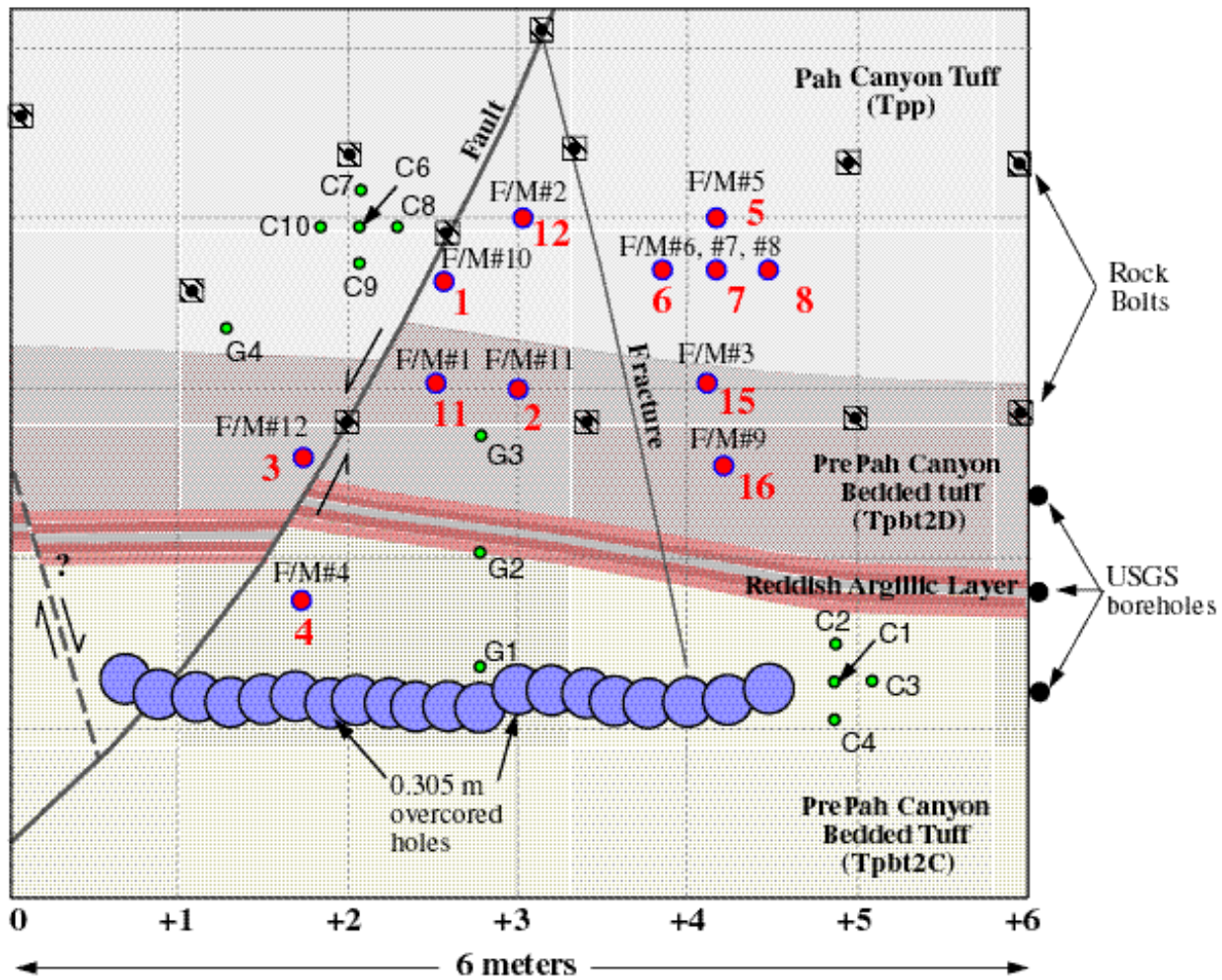

0.0762 m diameter (NQ) boreholes, approximate depth = 6 m

0.0254 m diameter boreholes, depth of "G" holes = 1 m, depth of "C" holes = 2 m

NOTE: Also included are location of boreholes and the slot.

Figure 6.7.1-1. Geological Sketch and Schematic Illustration for the North Face of Alcove 4 in the ESF at Yucca Mountain

The lower Tpp and upper Tpbt2 units D and C (units from Moyer et al. 1996 [100162], pp. 46-50) are exposed along the north face of Alcove 4. Tpp is nonwelded and pumice-rich. It exhibits a chalky-white color and is apparently zeolitically altered (based on destruction of the texture of the matrix ash and destruction of the integrity of the glass shards, Moyer et al. 1996 [100162], p. 46). Zeolitic alteration in the North Ramp of the ESF commonly follows fractures and faults that cut through the Tpp and Tpbt2 units (Barr et al. 1996 [100029], p. 44). The contact between the lower Tpp and upper Tpbt2D is sharp in Alcove 4, marked by distinct color changes. Tpbt2D is also nonwelded, possibly reworked, and has variably abundant (while zeolitically altered) pumice within a fine- to coarse-grained, medium-brown matrix.

Below Tpbt2D, lying in the upper Tpbt2C, is a thin (0.20–0.30 m), light-pink-to-red argillically altered layer that is almost completely offset by a small, westward-dipping normal fault. Alteration within this layer can be traced from the end of Alcove 4 out into the North Ramp. It is uncertain whether the argillic alteration seen in Alcove 4 is laterally continuous, though reddish alteration is commonly observed in several boreholes and in outcrops across Yucca Mountain at the same stratigraphic horizon (Moyer et al. 1996 [100162], pp. 54–55). The remaining Tpbt2C exposed along the north face below the argillic layer is massive and nonwelded, has very pale tan coloring, and contains abundant, coarse pumice and lithic fragments.

Cutting the north face of Alcove 4 is a normal fault with a small offset (0.25 m). As mapped along the crown at the end of the alcove (Barr et al. 1996 [100029], full-periphery geological map OA-46-289, DTN: GS960908314224.020 [106059] for the crown, but not for the end face), the fault has a strike of approximately 195 degrees and a westward dip of 58 degrees. The fault is open in the ceiling and is closed, with knife-edge thickness, near the invert on the north face. Intersecting the fault near the alcove crown along the north face is a high-angle fracture. The cause of the fracture is uncertain and could have been induced by drilling or drying, considering the location of rock bolts and the clay content of the rocks. The orientation of the fracture is unknown, though it has an apparent eastward dip of about 75 degrees. Similar to the fault, the fracture appears to have a large aperture near the ceiling and a much smaller aperture (eventually becoming undetectable) near the invert.

Two distinct features that were imposed on the formation define the layout of the field experiment, i.e., a horizontal slot and a series of horizontal boreholes. The slot, located immediately below the test bed, was designed to capture any seepage resulting from gravity drainage. It was excavated by a drilling sequence that required 0.10 m diameter pilot holes drilled parallel at 0.22 m spacing, perpendicular to the alcove wall. These pilot holes were then over-cored by a 0.3 m drill-bit to excavate a 6.0 m wide, 4.0 m deep and 0.3 m high cavity located approximately 1.5 m above the alcove floor. I-beam supports were installed along the length of the slot to prevent it from collapsing during the duration of the field tests.

Twelve 6.0 m long, 0.1 m diameter boreholes were drilled into the alcove face, as illustrated in Figure 6.7.1-1 and Figure 6.7.1-2. Borehole 1, borehole 4, borehole 11, and borehole 12 were positioned to intersect the fault for the purpose of conducting flow tests within the fault. Borehole 2 was located to detect moisture that could migrate through the matrix below borehole 12. Borehole 12 was the injection borehole for the fault flow tests conducted. The configuration of borehole 5, borehole 6, borehole 7, and borehole 8 was designed to investigate the nature of matrix flow in the Tpp, with borehole 5 serving as the injection borehole and borehole 6, borehole 7, and borehole 8 equipped with probes to detect changes in moisture conditions. Borehole 3 on the left side of the fault, and borehole 15 and borehole 16 away from the injection boreholes, were not instrumented for the tests conducted. (Borehole 9, borehole 10, borehole 13, and borehole 14 were planned but not drilled.)

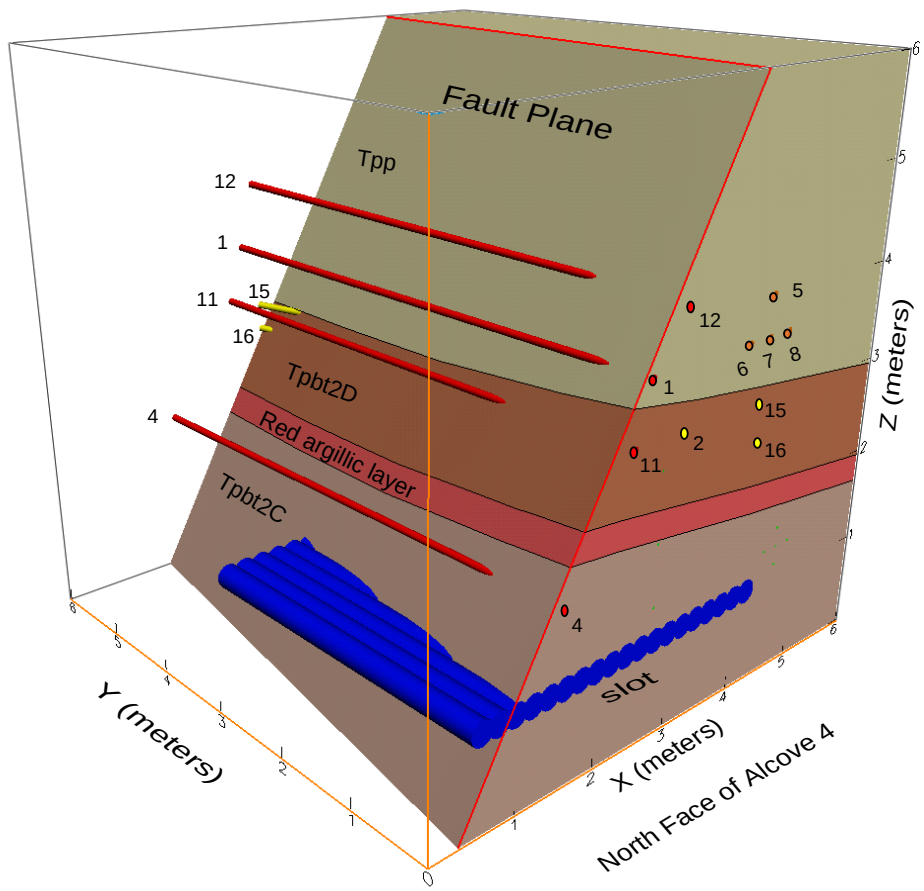

Figure 6.7.1-2. Perspective Illustration of Three-Dimensional View of the Boreholes, Slot, and Lithological Unit Contacts in the Alcove 4 Test Bed

6.7.1.2 Instrumentation

The flow investigation had three distinct components: (1) controlled release of water into isolated zones, (2) borehole monitoring for changes in saturation and water potential, and (3) the monitoring of seepage from the slot ceiling. For each component, new instruments were developed, details for which are described in Attachment VI. Because water did not seep into the slot, the seepage monitoring system was not used. Key features of the liquid-injection and borehole-monitoring system are presented in the following subsections.

6.7.1.2.1 Fluid Injection

The liquid-release experiments required water to be injected into the formation over a 0.3 m section of borehole with a constant-head boundary condition to determine the maximum rates at which the zone could take in water. The main components of the fluid-release apparatus included an inflatable packer system used to isolate the injection zone, a pump to deliver water to a constant-head chamber from which water was introduced into the injection zone, and a reservoir to provide a continuous supply of water. To capture the temporal variability in vertical flux of

water from the injection zone, an automated liquid-release system was developed to measure changing flow rates on a ponded surface. This system allowed for continuous measurement of local liquid-release rates during the entire experiment.

6.7.1.2.2 Borehole Monitoring

In six monitoring boreholes (borehole 1, borehole 2, borehole 11, borehole 6, borehole 7, and borehole 8 in Figure 6.7.1-2) located above the slot, changes in saturation and water potential were continuously recorded during the entire investigation. Changes in saturation along boreholes were measured with ERPs located at 0.25 m intervals along a 6.0 m length of each borehole. Water–potential measurements were made with psychrometers, as described in Attachment VI.2 for Alcove 6 testing. The psychrometers and ERPs were housed in special Borehole Sensor Trays (BSTs) installed along the length of each monitoring borehole.

6.7.1.3 Liquid-Release Experiments

Air-permeability measurements were made along 0.3 m sections of all nine boreholes to determine the exact location of the fault in borehole 4, borehole 11, and borehole 12, as discussed in Section 6.5.2. All water used in the ESF (for mining-related activities and scientific investigations) was spiked with the same concentration of lithium bromide. For the entire duration of the experiments, saturation and water-potential changes along the monitoring boreholes were continuously measured.

A total of 193 liters of water was released into borehole 12 during seven events, under constant-head conditions, between October 21 and November 5, 1998, as summarized in Table 6.7.1-1. In this borehole, as in all others, water was released over a 0.30 m interval. Here, the injection interval was centered at a distance 1.4 m from the borehole collar, determined from air-permeability measurements to be the location of the fault.

Table 6.7.1-1. Summary of Liquid Releases into the Fault Zone in Borehole 12

Test Number	Date (mm/dd/yy)	Volume Injected (l)	Duration (hh:mm)	Average Intake Rate (mL/min)
1	10/21/98	42.90	5:12	138
2	10/22/98	41.44	5:59	115
3	10/26/98	21.34	4:22	81
4	10/27/98	29.53	6:59	70
5	10/28/98	22.16	6:10	60
6	11/04/98	17.08	5:48	49
7	11/05/98	18.85	6:31	48

DTN: LB990901233124.005 [146884]

In borehole 5 away from the fault, water was released into two zones. In the first zone (located 1.50 to 1.80 m from the collar) 1.37 liters of water were released to the zone on October 19, 1998, and a similar volume was released on October 20, 1998. Because a problem was detected with the constant-head system, no more water was injected into this zone. On October 27, 1998, after the injection system was repaired, water was released into borehole 5 at a distance of 2.44–2.74 m from the borehole collar. In this zone, 6.5 liters of water were released under constant head conditions over a period of 23 days.

6.7.2 Observations of Fault Flow and Matrix Flow

During and following the release of water into the test bed, intake rates (rates of water moving into the formation during constant-head tests), travel times, and lateral dispersion of the plume (as seen along the length of horizontal boreholes) were continuously monitored. In the following section, the observed hydrological responses to liquid releases in the three zones as detected by ERPs and psychrometers are presented.

6.7.2.1 Fault Responses

6.7.2.1.1 Intake Rates

Water was injected into the section of borehole 12 that intercepted the fault approximately 1.40 m from the collar. Here, 193 liters of water were released into the formation during seven events that extended over a period of two weeks, as illustrated in Figure 6.7.2-1. Each event lasted between 4 and 7 hours, during which 20–43 liters of water entered the injection zone. Each release event began with water filling the 1.37-liter injection cavity in about 3 minutes, after which the liquid-release apparatus kept the injection zone filled by maintaining a constant-head boundary for the period of injection. After water was injected into the formation, the 1.37 liters of water occupying the injection zone were released to the formation under falling head conditions.

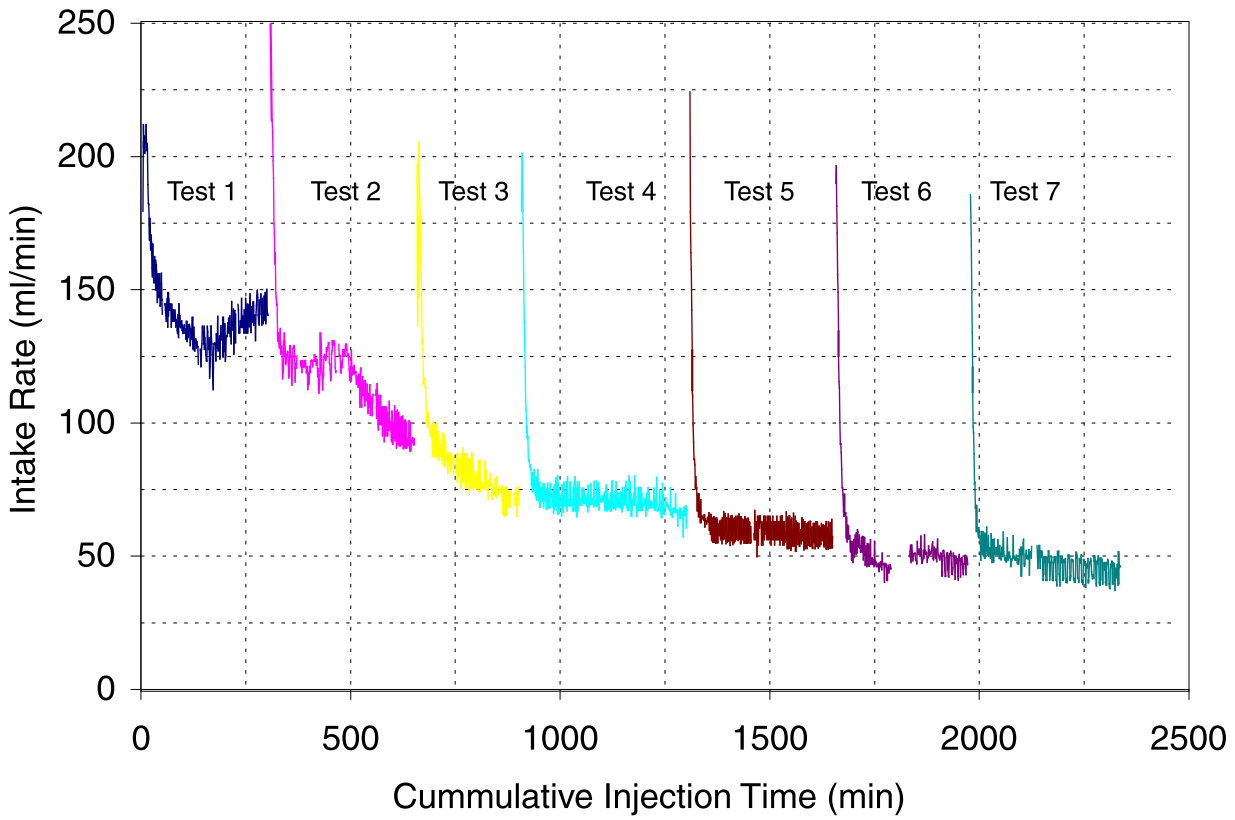

DTN: LB990901233124.005 [146884]

Figure 6.7.2-1. Intake Rates along the 0.3 m Zone Located on the Fault in Borehole 12

During Test 1 into the fault, the intake rate dropped from 200 mL/min to 120 mL/min over a period of 180 minutes, before recovering to 145 mL/min in the next 120 minutes. In Test 2, conducted one day later, the intake rate dropped from 200 mL/min to 120 mL/min over a period of 80 minutes before remaining fairly constant for the next 100 minutes. Approximately 180 minutes after this release event started, the intake rates began to drop steadily, reaching a rate of 95 mL/min by the end of the test. In Test 3, which was initiated four days later, the intake rates rapidly dropped to 95 mL/min during the first 40 min and then continued to decrease at a more gradual rate for the next 200 minutes to a rate of 70 mL/min. During Test 4 and Test 5, conducted during the next two days, the pattern of rate change was similar, with an initially high intake rate quickly dropping to a near constant value (70 to 60 mL/min, respectively). In Test 4, this constant value persisted 300 minutes into the test, after which there was a gradual decrease in intake rates for the remainder of the test. During Test 6, which began after a six-day hiatus, water was injected during two intervals. During this test, water was introduced under constant-head conditions for 140 and 158 minutes periods with a gap of 22 minutes, during which water imbibed into the formation under a falling head. The intake rates rapidly dropped to 50 mL/min. In Test 7 into this zone, the intake rates again dropped to 50 mL/min after 100 minutes of release. The rates gradually decreased during the 200 minutes of injection, which approached 40 mL/min after 18 liters of water had been injected.

6.7.2.1.2 Travel Times in Fault

When water was introduced into borehole 12, the time taken for the wetting front to travel 1.07 m along the fault to borehole 11 varied among the seven tests (Figure 6.7.2-2). In the first test, water was detected in the lower borehole ~300 minutes after the first release, while in the second test, the travel time was reduced to ~200 minutes. For the third test, this travel time was ~250 min; in the fourth test, water appeared in the fault in borehole 11 within ~150 minutes. The fastest travel time was observed for the fifth test, when the front arrived within ~120 minutes in borehole 11. In the last two tests, the travel times were significantly slower, with increasing saturations observed 400 and 700 minutes after the initial release of water.

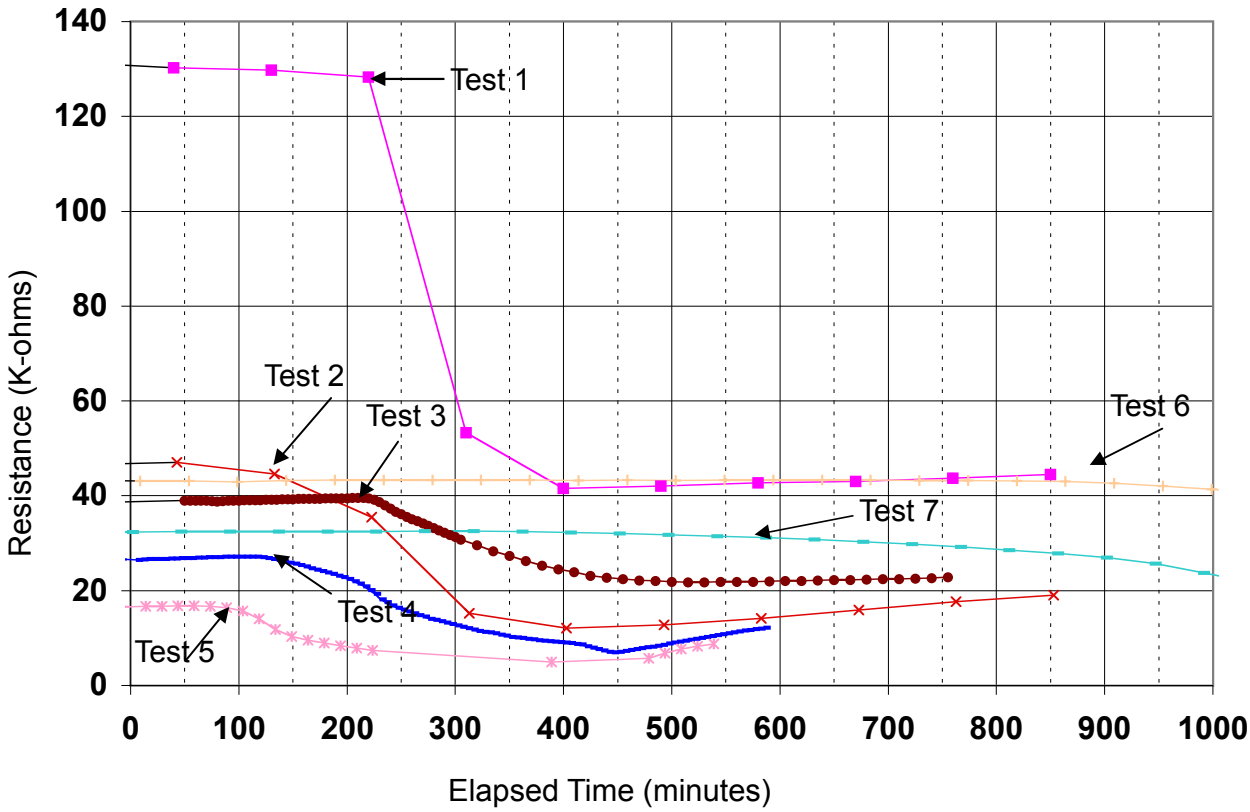

DTN: LB990901233124.005 [146884]

Figure 6.7.2-2. Wetting Front Arrival in Borehole 11 Following Liquid Released into the Fault in Borehole 12

6.7.2.1.3 Dispersion

Water injected into the fault in borehole 12 was detected along the length of borehole 11 by ERPs located between 0.65 and 2.40 m (Figure 6.7.2-3). Unlike the ERP located on the fault (1.40 m from the collar), which showed a stepped response to individual release events, these other ERPs showed a slow, gradual decrease in resistance measurements. The first response was seen in the ERPs located on either side of the fault, with the one at 1.65 m responding first. ERPs located between the alcove face and the fault appeared to be significantly drier at the start of the experiment than those located deeper in the test bed. These ERPs responded with larger decreases in resistance measurements following the start of the release water. The largest response to the injection events in borehole 12 was detected between 0.9 and 1.65 m from the collar in borehole 11.

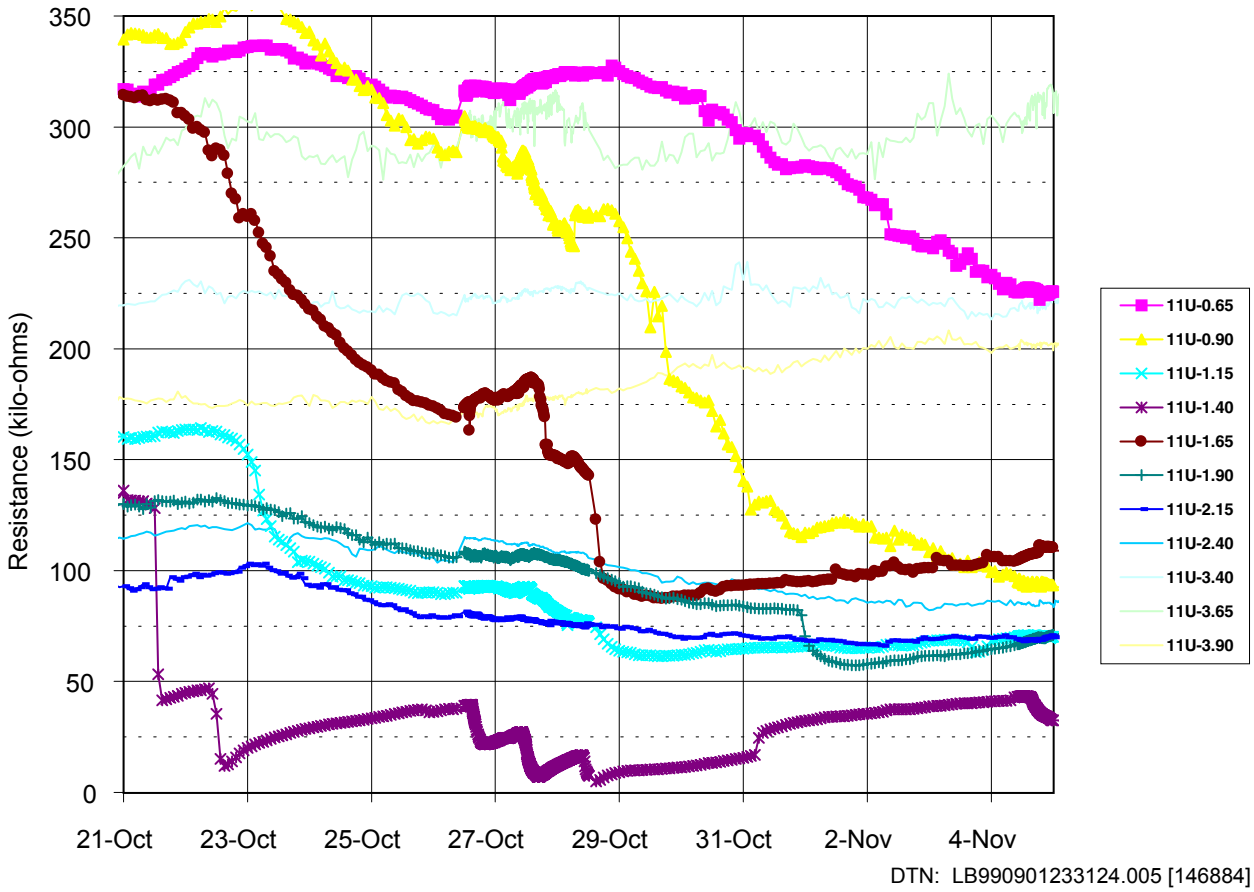

NOTE: The legend indicates the location of the measurement (in meters) from the collar. The 'U' indicates that these are measurements from the upper BSTs in the borehole.

Figure 6.7.2-3. Changes in Electrical Resistance in Borehole 11 in Response to Liquid Released into the Fault in Borehole 12

In borehole 2 located 0.97 m vertically below borehole 12, the first ERPs to detect the wetting front were centered immediately below the fault (Figure 6.7.2-4). Here, at a distance of 1.15 to 1.65 m from the borehole collar, changes in saturation were detected almost one week after the first injection event on October 21, 1998. Over the next three weeks, ERPs at 1.15 and 1.40 m continued to detect increasing saturations, while the ERP at 1.65 m wetted for four days before maintaining a relatively constant saturation level for the next 18 days. At depths between 1.90 and 2.40 m, the response was delayed very slightly.

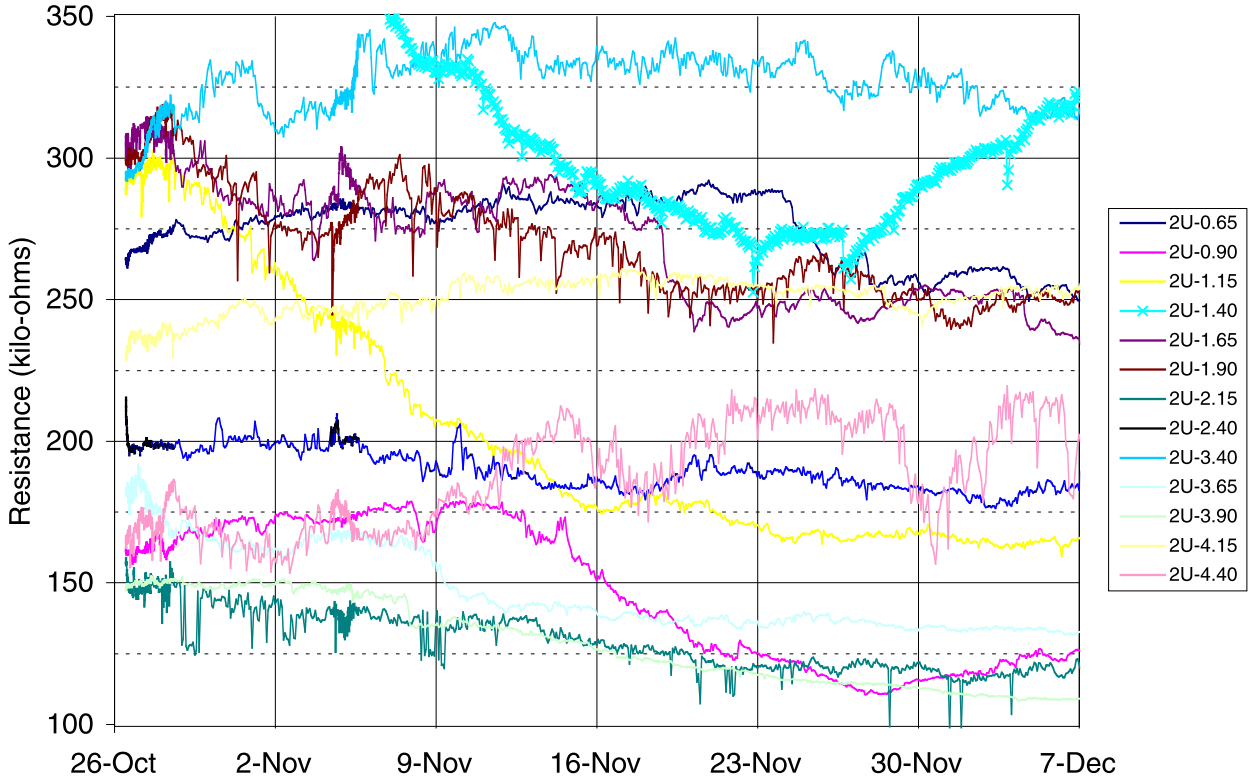

DTN: LB990901233124.005 [146884]

NOTE: The legend indicates the location of the measurement (in meters) from the collar. The 'U' indicates that these are measurements from the upper BSTs in the borehole.

Figure 6.7.2-4. Changes in Electrical Resistance in Borehole 2 in Response to Liquid Released into the Fault in Borehole 12

6.7.2.2 Matrix Responses

6.7.2.2.1 Intake Rates

When water was released into borehole 5, in the zone 2.44–2.74 m from the collar, the intake dropped steeply to 1 mL/min within 150 minutes (Figure 6.7.2-5). The intake rate then continued to gradually decrease over the next 2,000 minutes before reaching a constant rate of ~0.1 mL/min. This rate remained approximately constant for the entire duration of the test.

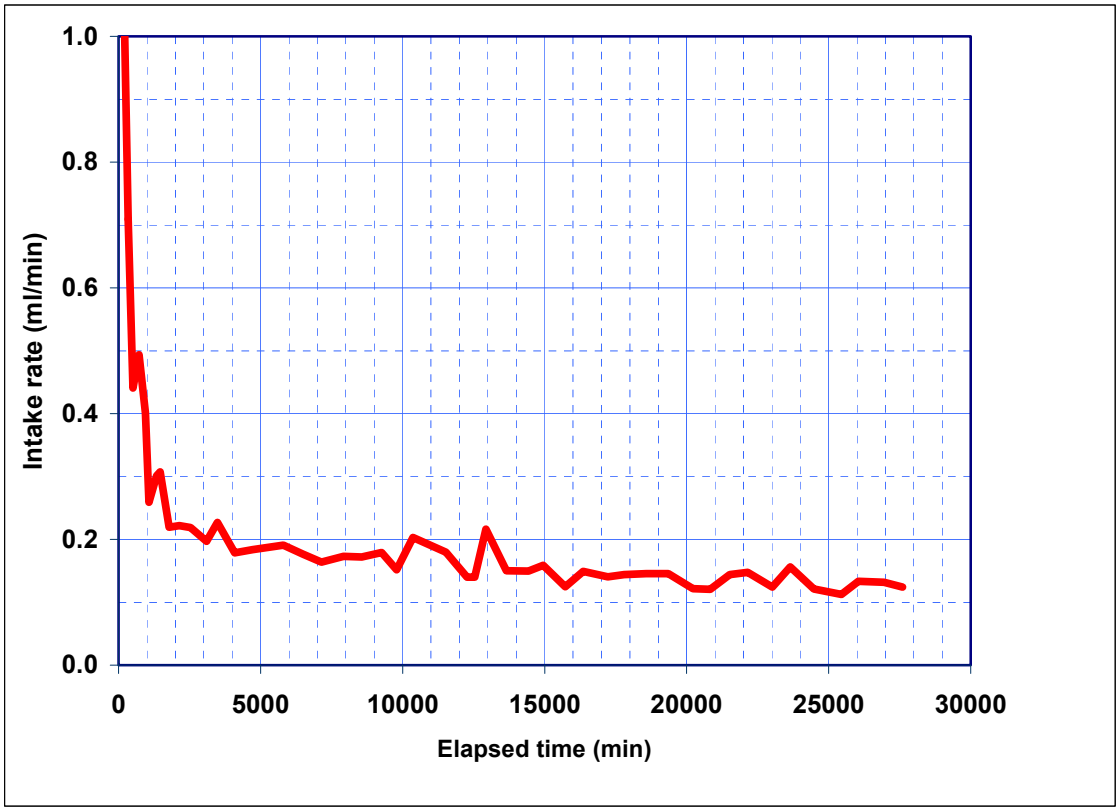

DTN: LB990901233124.005 [146884]

Figure 6.7.2-5. Intake Rates along a 0.3 m Zone in the Matrix Located 2.44–2.74 m from the Collar in Borehole 5

6.7.2.2.2 Wetting Front Migration

Following the first release of water in borehole 5 on October 27, 1998 (at 2.44–2.74 m from the collar), the wetting front was detected in the upper section of borehole 6 (located 0.45 from borehole 5) after a period of 14 days on November 10, 1998, at a distance of 2.90 m from the collar (Figure 6.7.2-6). Some of the sensors near the collar had high resistance values and fluctuating changes that might represent responses to additional drying and wetting processes near the borehole collar.

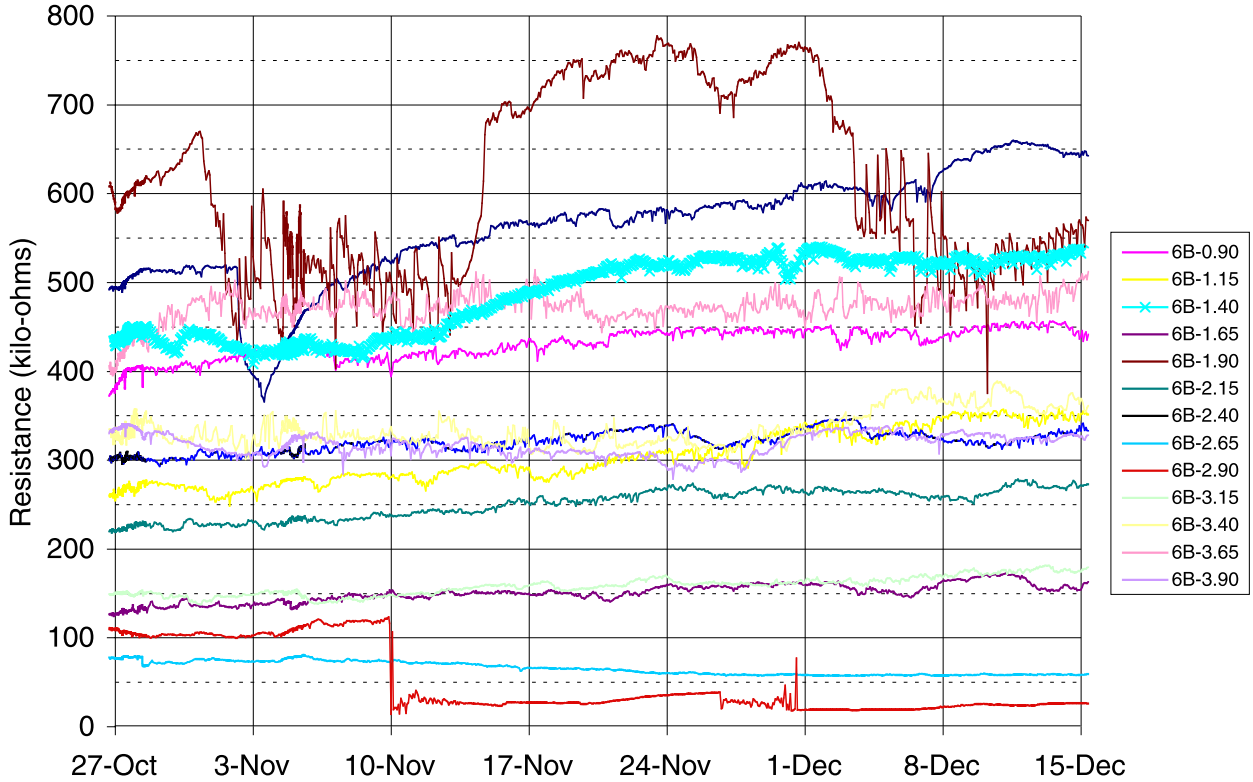

DTN: LB990901233124.005 [146884]

NOTE: The legend indicates the location of the measurement (in meters) from the collar. The 'B' indicates that these are measurements from the lower BSTs in the borehole.

Figure 6.7.2-6. Changes in Electrical Resistance in Borehole 6 in Response to Liquid Released in Borehole 5

6.8 COMPILATION OF WATER-POTENTIAL MEASUREMENTS IN NICHES

Measurements of water potentials from three niche sites in the ESF are presented. These sites are located on the west side of the ESF Main Drift at Niche 3566 (Niche 1), Niche 3650 (Niche 2), and Niche 3107 (Niche 3). Niche 3566 (Niche 1) lies between the Sundance fault and a cooling joint branching out from the fault. The primary objective of this effort was to determine the water potential at various points within the three niche sites to determine if wet conditions exist at Niche 3566 (Niche 1) near the fault while other niches are drier.

To meet this objective, we used psychrometers (a method to measure water potential, in boreholes). The psychrometers were also used in wetting-front detection, as described in Section 6.6 for Alcove 6 and Section 6.7 for Alcove 4. The sensitivity of psychrometer performance is described in Attachment VII. The results of this section need to take into account the uncertainties associated with the sensitivities of psychrometer readings (to operating conditions and to handling of the sensors, as discussed in Attachment VII.)

6.8.1 Location and Timing of Water-Potential Measurements at Niches

Water potentials were measured either along the length or at the ends of 0.0762 m diameter boreholes. Three different types of housing units were used to locate psychrometers in the boreholes. The main feature of the housings was the creation of a small air chamber that allowed for quick equilibration and measurements of humidity close to the borehole wall.

At Niche 3566 (Niche 1), two separate sets of measurements were made: before and after niche excavation. Pre-excavation measurements were made during May 1997 in three holes (U, M, and B) at a distance of 10 m from the borehole collar (Figure 6.8.1-1a). Between July and September 1997, two sets of measurements were made along borehole U at distances between 3.5 and 8.0 m from the collar. Post-excavation measurements of water potential were made in October 1997 in five boreholes extending radially along a horizontal plane from the niche cavity (Figure 6.8.1-1b).

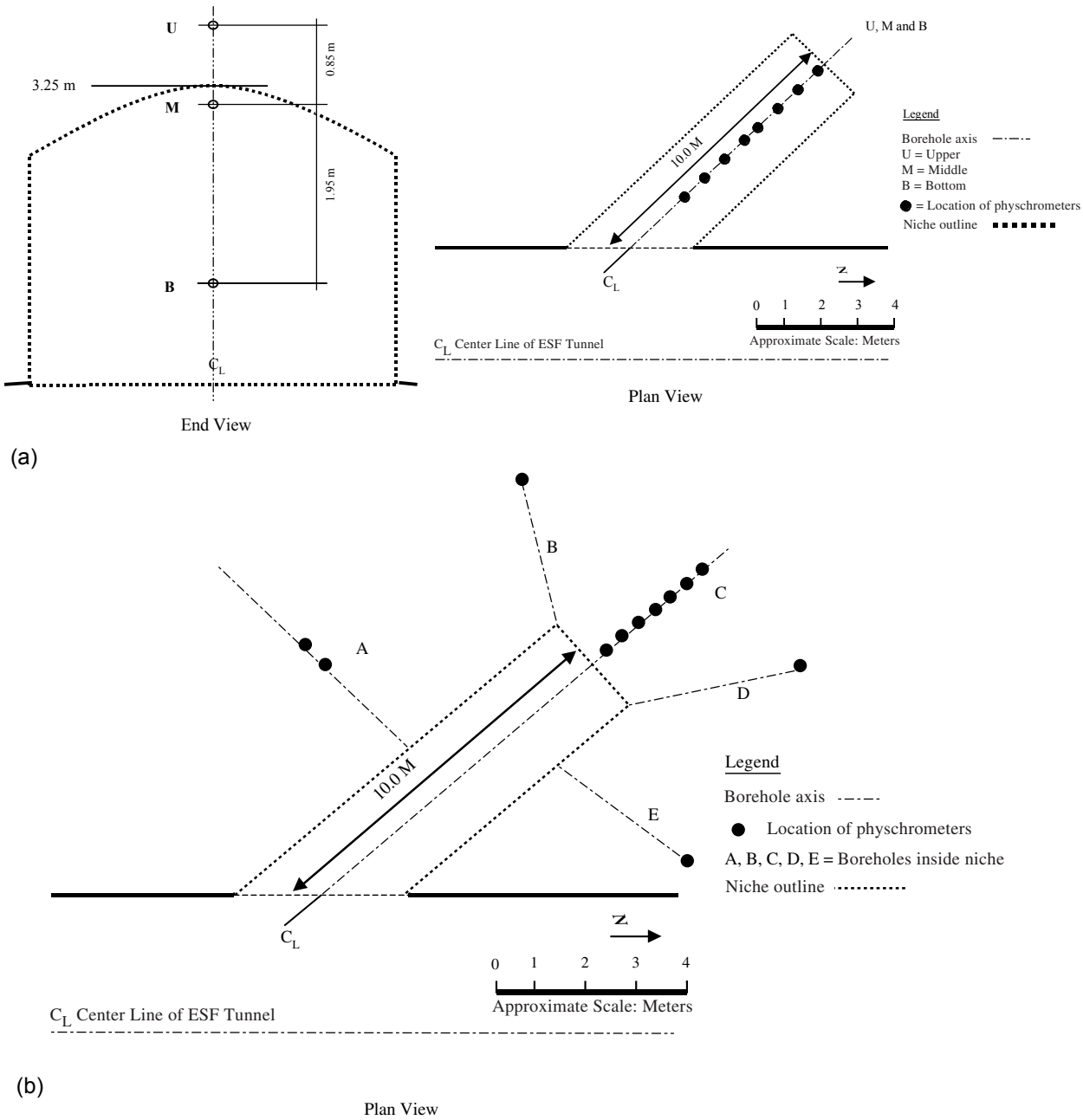

Figure 6.8.1-1. Schematic Illustration of the Location of Psychrometers in Niche 3566 (Niche 1) (a) in Pre-Excavation and (b) in Post-Excavation Conditions

At Niche 3650 (Niche 2), two separate sets of water-potential measurements were made in July 1997, before and after air-permeability tests were conducted in the boreholes. In three boreholes at this location (ML, BR, and BL), water potentials were measured at the end of the boreholes (10 m). In borehole UM, measurements were made close to the borehole collar, i.e., between 0.6 and 1.2 m (Figure 6.8.1-2).

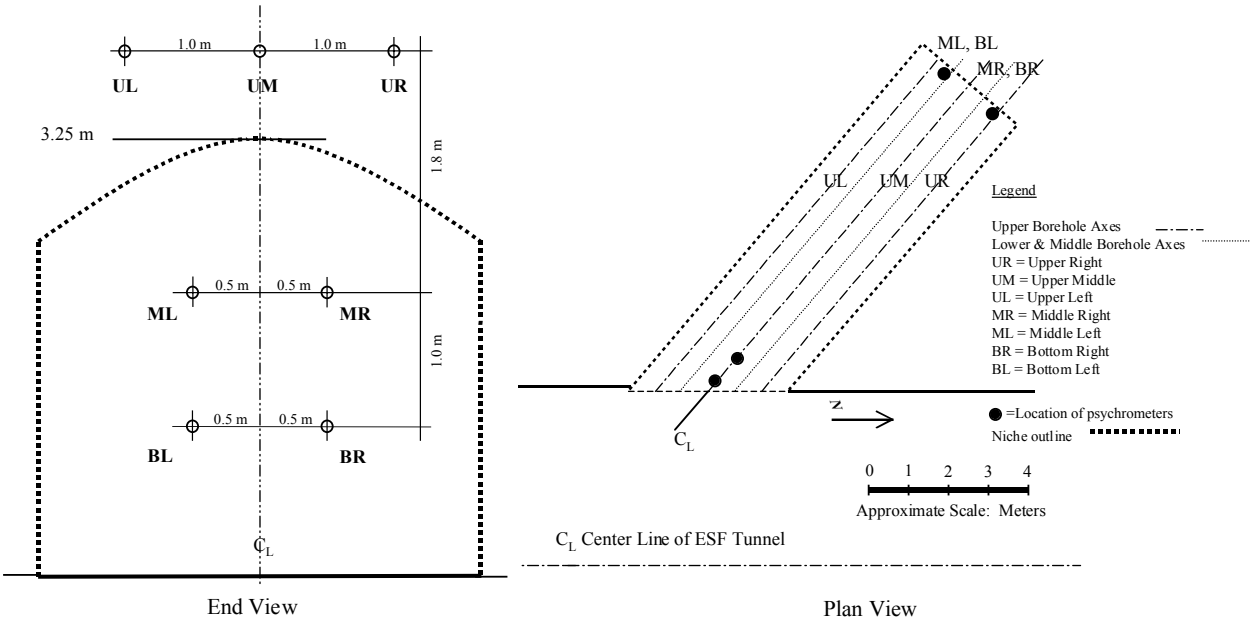

Figure 6.8.1-2. Schematic Illustration of Location of Psychrometers in Niche 3650 (Niche 2)

At Niche 3107 (Niche 3), four boreholes were instrumented with psychrometers (Figure 6.8.1-3). One set of potential measurements were made in December 1997 and January 1998. In the upper middle (UM) borehole, multiple measurements were made along the first 3.0 m, while in the remaining three boreholes (ML, UL, UR), single measurements were made using different lengths of borehole cavity. In the upper-right borehole (UR), sensors were located at the back of the borehole and sealed off with inflation packers such that the borehole cavity was less than 0.04 m long. In the upper-left borehole (UL), sensors were located 5 m from the borehole collar, with the cavity sealed off by inflation packers. In this case, the sensing cavity extended over 5 m of the borehole. In the middle-lower borehole (ML), sensors were located 0.3 m from the borehole collar, with an inflation packer installed to isolate the entire 10 m length of borehole from the ESF Main Drift.

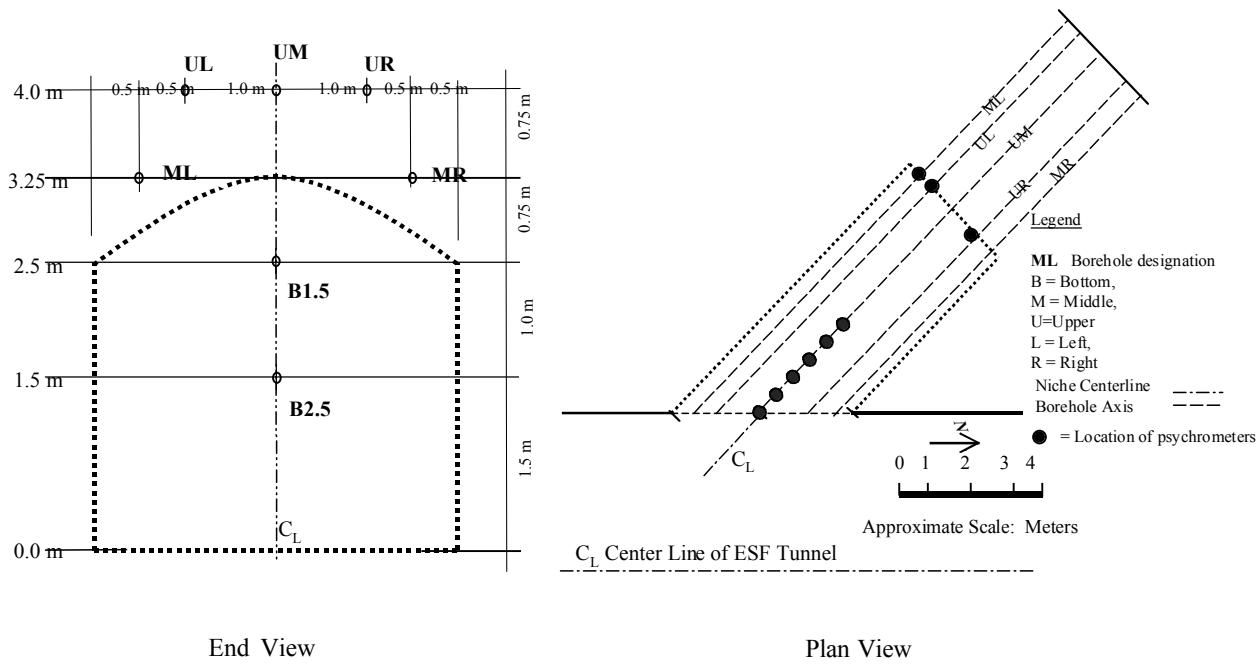

Figure 6.8.1-3. Schematic Illustration of Location of Psychrometers in Niche 3107 (Niche 3) (Pre-Excavation)

6.8.2 Observations of Dryout in Niche Boreholes

Water-potential measurements obtained from the three niches are summarized in Table 6.8.2-1 and Table 6.8.2-2. The time and duration of measurements are presented for each location.

Table 6.8.2-1. Water-Potential Measurements in Niche 3566 (Niche 1)

Borehole ID	Dist. from Collar (m)	Duration of Measurement	Psych #	Water Potential (m)
Pre-Excavation				
U	10.0	5/9-16/97	Psy -51	-13
U	10.0	5/9-16/97	Psy -52	-13
M	10.0	5/9-16/97	Psy -53	-7
M	10.0	5/9-16/97	Psy -54	0.4
B	10.0	5/9-16/97	Psy -55	-12
U	6.1	7/8-14/97	Psy -42	-49
U	5.5	7/8-14/97	Psy -43	-46
U	5.5	7/8-14/97	Psy -44	-34
U	4.9	7/8-14/97	Psy -45	-46
U	4.3	7/8-14/97	Psy -48	-68
U	3.7	7/8-14/97	Psy -50	-62
U	7.9	9/16-24/97	Psy -42	-49
U	7.3	9/16-24/97	Psy -60	-46
U	6.7	9/16-24/97	Psy -45	-71
U	6.1	9/16-24/97	Psy -48	-67
U	5.5	9/16-24/97	Psy -50	-36
Post-Excavation				
A	6.25	10/18-21/97	Psy-43a	-2
A	6.75	10/18-21/97	Psy-60	-30
B	6.00	10/18-21/97	Psy-51	-43
C	0.15	10/18-21/97	Psy-49	-132
C	0.76	10/18-21/97	Psy-42	-33
C	1.98	10/18-21/97	Psy-45	-22
C	1.98	10/18-21/97	Psy-47	-47
C	1.37	10/18-21/97	Psy-48	-40
C	2.60	10/18-21/97	Psy-43	-57
D	6.00	10/18-21/97	Psy-54	-22
D	6.00	10/18-21/97	Psy-56	-32
E	6.00	10/18-21/97	Psy-57	-75
E	6.00	10/18-21/97	Psy-59	-81

DTN: LB980001233124.001 [105800]

Table 6.8.2-2. Water-Potential Measurements in Niche 3650 (Niche 2)

Borehole ID	Dist. from Collar (m)	Duration of Measurement	Psych #	Water Potential (m)
Pre-Air-Injection Testing				
UM	1.2	7/1-8/97	Psy -48	-127
UM	0.6	7/1-8/97	Psy -49	-139
UM	0.6	7/1-8/97	Psy -50	-165
BR	10.0	7/1-8/97	Psy -51	-37
BR	10.0	7/1-8/97	Psy -52	-39
BR	10.0	7/1-8/97	Psy -53	-32
BL	10.0	7/1-8/97	Psy -54	-24
BL	10.0	7/1-8/97	Psy -55	-36
ML	10.0	7/1-8/97	Psy -57	-1
Post-Air-Injection Testing				
ML	10.0	7/24-28/97	Psy -51	-29
ML	10.0	7/24-28/97	Psy -52	-38
ML	10.0	7/24-28/97	Psy -53	-39
BR	10.0	7/24-28/97	Psy -54	-58
BR	10.0	7/24-28/97	Psy -55	-49
BR	10.0	7/24-28/97	Psy -56	-48
BL	10.0	7/24-28/97	Psy -57	-21
BL	10.0	7/24-28/97	Psy -58	-15
BL	10.0	7/24-28/97	Psy -59	-28

DTN: LB980001233124.001 [105800]

Table 6.8.2-3. Water-Potential Measurements in Niche 3107 (Niche 3)

Borehole ID	Dist. from Collar (m)	Duration of Measurement	Psych #	Water Potential (m)
UM	0.45	12/22/97-1/8/98	Psy-86	-273
UM	1.06	12/22/97-1/8/98	Psy-83	-154
UM	1.67	12/22/97-1/8/98	Psy-75	-83
UM	2.90	12/22/97-1/8/98	Psy-68	-28
UL	10.00	12/22/97-1/8/98	Psy-64	-15
ML	10.00	12/22/97-1/8/98	Psy-66	-84

DTN: LB980001233124.001 [105800]

6.8.2.1 Niche 3566 (Niche 1) Pre-Excavation

Water potentials measured at the ends of the three pre-excavation boreholes (U, M, and B) in Niche 3566 (Niche 1) were close to saturation values, indicating that approximately 10 m from

the ESF, the formation is relatively wet. Of the three, the end of the middle borehole appeared to be wettest, with water potentials between 0.4 and -7 m. Measurements made along the profile of borehole U (between 3.7 and 7.9 m from the collar) ranged between -34 and -71 m (Figure 6.8.2-1 and Table 6.8.2-1).

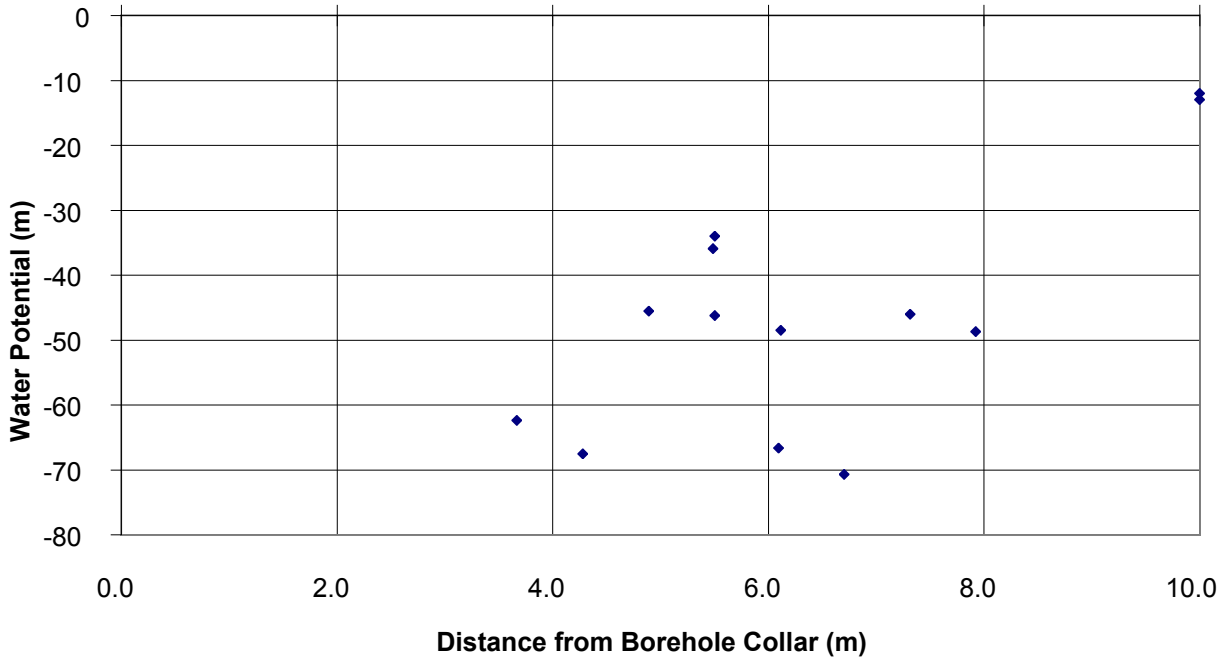

DTN: LB980001233124.001 [105800]

Figure 6.8.2-1. Pre-Excavation Water Potential Measured along Borehole U in Niche 3566 (Niche 1)

6.8.2.2 Niche 3566 (Niche 1) Post-Excavation

In the excavated niche cavity, water potentials were monitored in five boreholes. The monitored locations in borehole A (Figure 6.8.1-1b) were at 6.25 and 6.75 m from the collar. High water potentials were measured at these points (-2 and -30 m respectively). In three of the remaining boreholes (B, D, and E) water potentials measured at depths of 6.0 m varied significantly between boreholes. Borehole D (-27 m) was wettest, followed by B (-43 m) and then E (-78 m). These observations appear to be consistent with those made in the pre-excavation boreholes, which indicated that the formation tended to get wetter with increasing distance from the Main Drift.

Measurements made close to the collar in borehole C suggest that there was significant dryout in the rock surrounding the niches to a depth of at least 0.15 m, extending possibly to 2.6 m.

6.8.2.3 Niche 3650 (Niche 2) Pre-Excavation

Measurements were made at the end of three boreholes BR, BL, and ML (Figure 6.8.1-2, Table 6.8.2-2), each 10 m long, before and after a series of air-permeability tests. Pre-test water-potential values ranged between -1 and -39 m. However, following the test, water potentials in one hole (BR) dropped to between -48 and -58 m, while in another hole (BL) the measurements did not show significant changes. Closer to the borehole collar of borehole UM, readings made between 0.6 and 1.2 m indicate a relatively dry zone, with water potentials between -125 and -137 m.

6.8.2.4 Niche 3107 (Niche 3)

The observations made in Niche 3107 (Niche 3) in Table 6.8.2-3 indicate significant variability among the boreholes in the niche. Measurements made at the ends of boreholes UL (-15 m) and ML (-84 m) indicate that at a depth of 10 m, with a separation distance of 0.9 m (0.75 m vertically and 0.5 m horizontally, as illustrated in Figure 6.8.1-3), there is a steep potential gradient. Furthermore, from observations within borehole UM, it is clear that a prominent dryout zone (Figure 6.8.2-2) is associated with the Main Drift of the ESF.

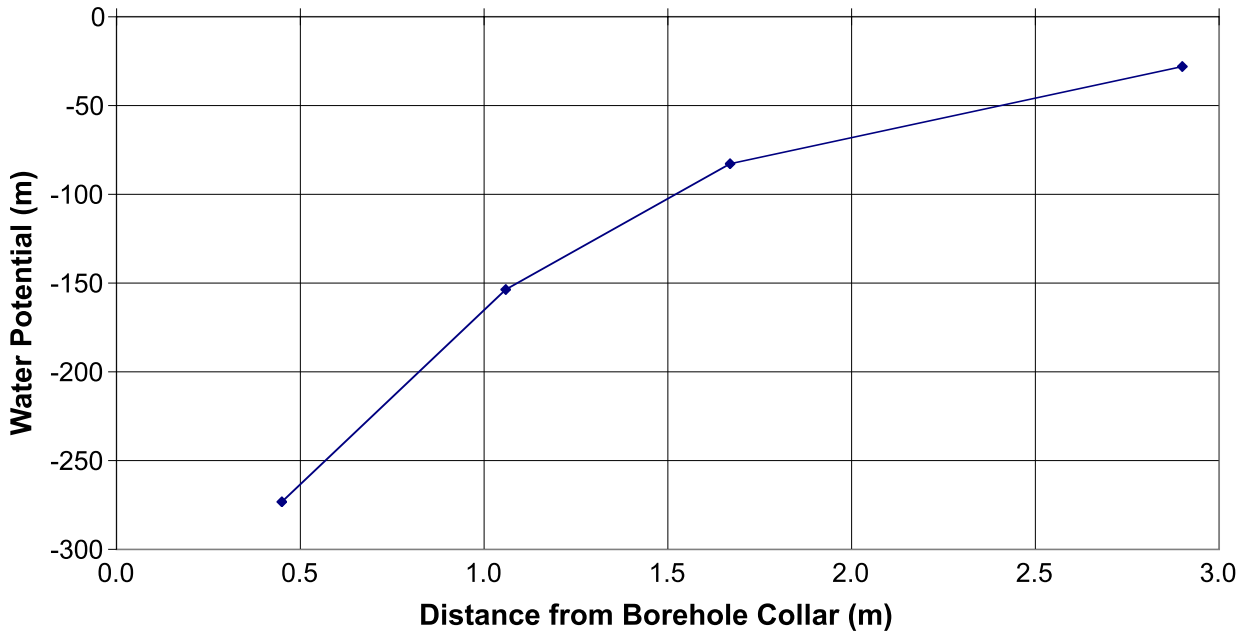

DTN: LB980001233124.001 [105800]

Figure 6.8.2-2. Water Potential Measured along Borehole UM in Niche 3107 (Niche 3)

6.9 OBSERVATIONS OF CONSTRUCTION-WATER MIGRATION

During the ECRB Cross Drift excavation, sensors and water-collection trays were placed in a borehole below the Starter Tunnel and along the ESF Main Drift at the cross-over point. This section summarizes the results of monitoring the migration of water plumes from tunneling activities. A secondary objective was to evaluate the performance of ERP as a tool to detect the migration of wetting fronts in the unsaturated zone of fractured tuffs. Time-domain reflectometry (TDR) was also used to monitor construction-water arrivals in drift walls. TDR is based on electric measurement of waveguide reflection signals from changes in dielectric constant associated with water-content changes.

6.9.1 Equipment Setup for Construction-Water Monitoring

6.9.1.1 Starter Tunnel Borehole

To monitor the migration of a water plume resulting from construction of the ECRB Cross Drift, a 30 m long borehole (0.10 m ID), at an angle of 30 degrees (from the horizontal), was constructed along the proposed path of the ECRB Cross Drift tunnel (Figure 6.9.1-1). This borehole was located in the Tptpul unit. The borehole originated at the end of a starter tunnel that was the launching pad for the Tunnel Boring Machine (TBM) used to excavate the ECRB Cross Drift. Changes in water saturation and potential were monitored along the entire length of theborehole, using psychrometers and ERPs, as the TBM advanced through the formation above.

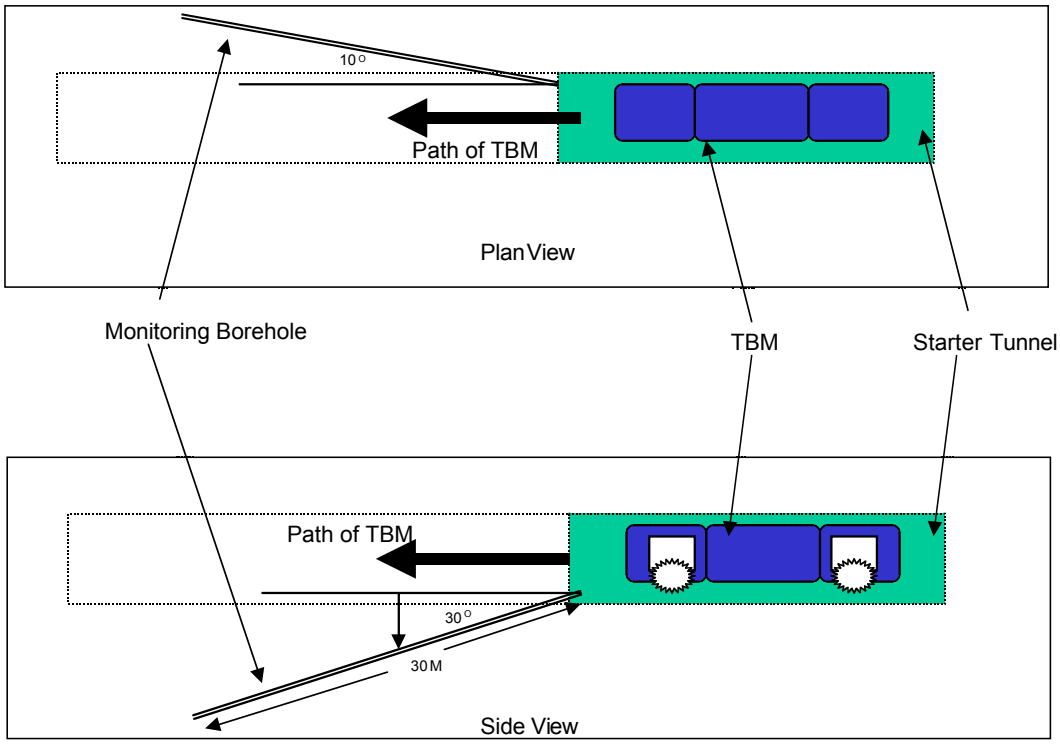

Figure 6.9.1-1. Schematic Illustration of the Location of Wetting-Monitoring Borehole at the Starter Tunnel of the ECRB Cross Drift

6.9.1.2. Electrical Resistivity Probes and Psychrometers

The psychrometers and ERPs were housed in PVC trays. These trays were fabricated from PVC pipes (0.10 m OD) bisected along the lengths. On each tray, psychrometers were installed at a spacing of 1.0 m along the borehole, while ERPs were located at 0.5 m intervals. To locate the psychrometers, squares of PVC (0.02 m) were glued at the 1.0 m mark and small diameter holes (~0.003 m ID) were drilled through the tray. Psychrometers were then installed in these holes (Figure 6.9.1-2). ERPs were attached to the outer surface of the PVC trays with strips of Velcro. This housing permitted close contact between the ERPs and borehole wall, while allowing the psychrometers to contact the borehole wall through a small cavity.

A steel spoon, 3.0 m long and having the same configuration as the trays, was used to locate each PVC tray along the borehole. Typically, each tray was placed on the steel spoon and carried to the desired location, at which point the spoon was slipped out, allowing the tray to settle snugly against the borehole wall.

Twenty-seven psychrometers and 54 electrical resistivity probes located on nine PVC trays were installed in the borehole (Figure 6.9.1-2) on February 26, 1998. Psychrometer data were collected at 1.5-hour intervals starting on February 28, 1998, for a period of four months. ER data collection started on March 25, 1998, and was collected at the same frequency and for the same duration as the psychrometers.

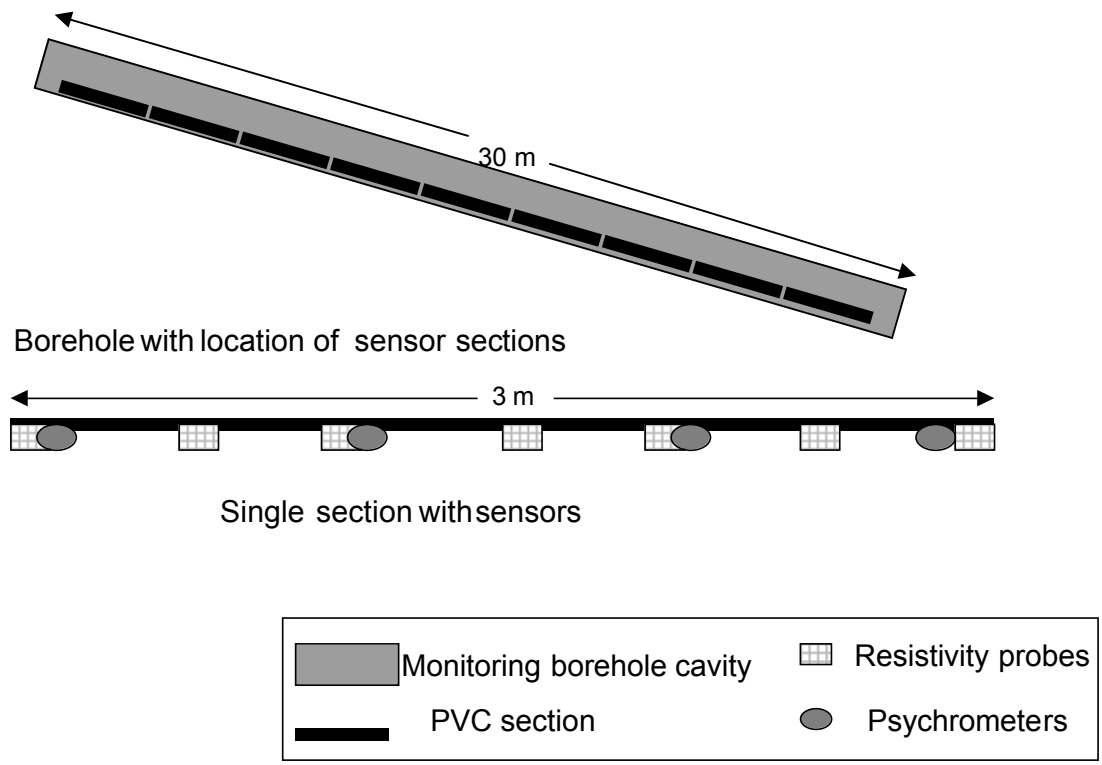

Figure 6.9.1-2. Schematic Illustration of the Borehole Wetting Front Monitoring System with Psychrometers and Electrical Resistivity Probes

6.9.1.3 Drift Monitoring at the Crossover Point

The schematics of the seepage detection system, with fluid collection trays hanging below the ceiling of the ESF Main Drift, are illustrated in Figure 6-2. The schematics of the associated sensor arrays are illustrated in Figure 6.9.1-3. The seepage monitoring system was used to detect the wetting front in the ESF Main Drift as the result of releases of traced water in the ECRB Cross Drift above.

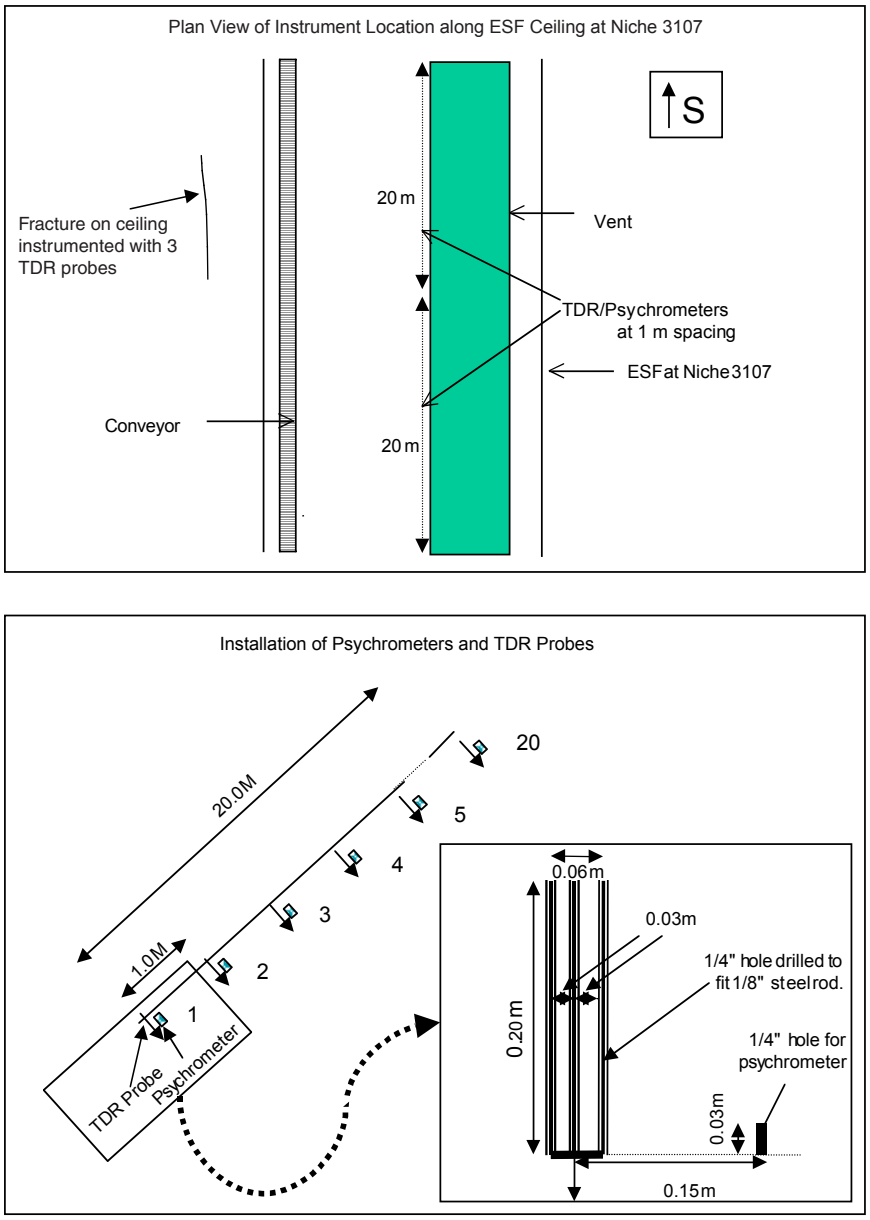

Figure 6.9.1-3. Schematic Illustration of Sensor Arrays for Wetting Front Monitoring

At the cross-over monitoring station, 132 collection trays were installed, each 0.3 m wide and 1.23 m long, from station 30+40 to 30+80 m. The trays were hung below the tunnel ceiling next to the ventilation duct along the ESF Main Drift. On the drift walls above the spring line (3.18 m

above the floor), psychrometers and TDR probes were installed. A horizontal sensor array with 40 psychrometer-TDR pairs at 1 m spacing was installed along the west wall (right rib). At the crossover location, vertically along the west wall, between the spring line and the ventilation duct, three psychrometers were installed. On the east wall (left rib), three TDR probes were installed along the trace of a major fracture. In addition to the sensor on the walls, an infrared camera and a video camera periodically monitored the area around one TDR probe on the fracture trace. Infrared images are sensitive to temperature changes associated with evaporation processes.

6.9.2 Wetting-Front Detection and Monitoring Below the ECRB Cross Drift

The following results are presented to show that the wetting front was detected up to 12.15 m below the ECRB Cross Drift Starter Tunnel, and no seepage was observed at the crossover point in the Main Drift 17.5 m below the ECRB Cross Drift. The Starter Tunnel is located in the upper lithophysal TSw tuff unit, and the crossover point is located in the middle nonlithophysal TSw tuff unit.

6.9.2.1 Wetting-Front Detection at the Starter Tunnel

The responses of all psychrometers and ERPs used in this investigation are summarized in Table 6.9.2-1 and Table 6.9.2-2. In the last columns of both tables, all working sensors with signals in response to construction-water usage are labeled “yes,” and those not in response are labeled “no.” With the arrival of a wetting front, the water potential measured by psychrometers and the electrical resistance measured by ERPs change to near-zero values.

Table 6.9.2-1. Psychrometers Response to Excavation at the Starter Tunnel of the ECRB Cross Drift

PSY_ID	Dist. Collar (m)	Vertical Depth (m)	Response to Tunneling
Psy_30.3	30.3	15.15	-
Psy_29.3	29.3	14.65	-
Psy_28.3	28.3	14.15	No
Psy_27.3	27.3	13.65	-
Psy_26.3	26.3	13.15	No
Psy_25.3	25.3	12.65	No
Psy_24.3	24.3	12.15	Yes
Psy_23.3	23.3	11.65	No
Psy_22.3	22.3	11.15	Yes
Psy_21.3	21.3	10.65	No
Psy_20.3	20.3	10.15	No
Psy_19.3	19.3	9.65	-
Psy_18.3	18.3	9.15	Yes
Psy_17.3	17.3	8.65	Yes
Psy_16.3	16.3	8.15	Yes
Psy_15.3	15.3	7.65	Yes
Psy_14.3	14.3	7.15	Yes
Psy_13.3	13.3	6.65	Yes
Psy_11.4	11.4	5.7	Yes
Psy_10.4	10.4	5.2	Yes
Psy_9.4	9.4	4.7	Yes
Psy_7.2	7.2	3.6	-
Psy_6.2	6.2	3.1	Yes
Psy_5.2	5.2	2.6	Yes
Psy_3.9	3.9	1.95	-
Psy_2.6	2.6	1.3	-
Psy_1.6	1.6	0.8	Yes

NOTE: This table summarizes the interpretation of water-potential data in DTN: LB98091233124.014 [105858] with detailed example curves shown in Figure 6.9.2-1.

Table 6.9.2-2. Electrical Resistivity Probe Responses to Excavation at the Starter Tunnel of the ECRB Cross Drift

ER_ID	Dist. Collar (m)	Vertical Depth (m)	Response to Tunneling
ER_30.3 m	30.3	15.2	No
ER_29.8 m	29.8	14.9	No
ER_29.3 m	29.3	14.7	No
ER_28.8 m	28.8	14.4	No
ER_28.3 m	28.3	14.2	No
ER_27.8 m	27.8	13.9	No
ER_27.3 m	27.3	13.7	Yes
ER_26.8 m	26.8	13.4	Yes
ER_26.3 m	26.3	13.2	No
ER_25.8 m	25.8	12.9	No
ER_25.3 m	25.3	12.7	No
ER_24.8 m	24.8	12.4	No
ER_24.3 m	24.3	12.2	Yes
ER_23.8 m	23.8	11.9	No
ER_23.3 m	23.3	11.7	No
ER_22.8 m	22.8	11.4	No
ER_22.3 m	22.3	11.2	Yes
ER_21.8 m	21.8	10.9	Yes
ER_21.3 m	21.3	10.7	Yes
ER_20.8 m	20.8	10.4	No
ER_20.3 m	20.3	10.2	Yes
ER_19.8 m	19.8	9.9	Yes
ER_19.3 m	19.3	9.7	Yes
ER_18.8 m	18.8	9.4	Yes
ER_18.3 m	18.3	9.2	Yes
ER_17.8 m	17.8	8.9	Yes
ER_17.3 m	17.3	8.7	Yes
ER_16.8 m	16.8	8.4	Yes
ER_16.3 m	16.3	8.2	Yes
ER_15.8 m	15.8	7.9	Yes
ER_15.3 m	15.3	7.7	Yes
ER_14.8 m	14.8	7.4	Yes
ER_14.3 m	14.3	7.2	Yes
ER_13.8 m	13.8	6.9	Yes
ER_13.3 m	13.3	6.7	Yes

Table 6.9.2-2. Electrical Resistivity Probe Responses to Excavation at the Starter Tunnel of the ECRB Cross Drift (continued)

ER_ID	Dist. Collar (m)	Vertical Depth (m)	Response to Tunneling
ER_12.8 m	12.8	6.4	Yes
ER_11.4 m	11.4	5.7	Yes
ER_10.9 m	10.9	5.5	Yes
ER_10.4 m	10.4	5.2	Yes
ER_9.9 m	9.9	5.0	Yes
ER_9.4 m	9.4	4.7	Yes
ER_8.9 m	8.9	4.5	Yes
ER_7.2 m	7.2	3.6	Yes
ER_6.7 m	6.7	3.4	Yes
ER_6.2 m	6.2	3.1	Yes
ER_5.7 m	5.7	2.9	Yes
ER_5.2 m	5.2	2.6	Yes
ER_4.7 m	4.7	2.4	Yes
ER_3.9 m	3.9	2.0	Yes
ER_3.1 m	3.1	1.6	Yes
ER_2.6 m	2.6	1.3	Yes
ER_2.1 m	2.1	1.1	Yes
ER_1.6 m	1.6	0.8	Yes
ER_1.1 m	1.1	0.6	Yes

NOTE: This table summarizes the interpretation of electrical resistivity data in DTN: LB98091233124.014 [105858] with detailed example curves shown in Figure 6.9.2-2.

6.9.2.1.1 Psychrometers

The data from the psychrometers illustrated in Figure 6.9.2-1 show that along the entire length of the borehole, the walls were at water potentials approximately -500 m when the sensors were installed in late February 1998. A uniform, steep increase in water-potential values over the first two weeks in March 1998 suggests the recovery of the borehole wall from drying that occurred during the dry drilling of this borehole. The following four months of data show all psychrometers approaching equilibrium values, with water potentials ranging from -70 to 0 m (Figure 6.9.2-1).

Superimposed on this asymptotic trend in water-potential values are periodic deviations, with psychrometers nearer the borehole collar showing a larger number of such events. These events were restricted to the first two months of monitoring, and by the third week of April, the last of these events had occurred. Three of the psychrometers (located at distances of 1.6, 6.2, and 9.4 m

from the borehole collar) showed evidence of wetting events, which increased water potential to (near) zero. The psychrometer at 1.6 m had near-zero water potential for three distinct periods. The first extended from the start of monitoring until March 3, and the second extended for four days beginning on March 8. A final period, significantly shorter, lasted for almost 24 hours on March 22. The psychrometer located at 6.2 m measured water potential close to zero for a three-day period starting on March 8th. The psychrometer located at 9.4 m detected water-potential values close to zero for a single event on March 13, for nearly eleven hours.

One concern that could arise from the use of a slanting borehole to measure wetting-front migration is the possibility of the bore cavity short-circuiting flow paths. For this particular investigation, this short-circuiting does not appear to be happening, as indicated by the analysis of recovery responses observed at the depth of 5.2 m. Here, the response to a wetting event was negligible when compared with other psychrometers close to this location (above and below), suggesting that this zone was well isolated (hydraulically) from the adjacent zones and did not detect the wetting front. In the remaining eight psychrometers located between 9.4 m and 17.3 m from the borehole collar, investigators found evidence of small increases in water potential that extend beyond the projected recovery rate. Some of these increases coincided with periods when the psychrometers at distances of 1.6, 6.2, and 9.4 m along the borehole showed near-zero potentials; the rest of the psychrometer data remained uncorrelated until the end of April 1998. The psychrometers up to a distance of 10.4 maintained a sinusoidal response, which fluctuated around a trend of slow water-potential increase.

By early May 1998, the rates at which water potential was increasing had decreased significantly, and by mid-June all psychrometer readings appeared to have stabilized. In the case of two deep psychrometers (i.e., at 18.3 m and 22.3 m), there appears to have been individual events that for brief periods increased the rate at which water potentials were increasing. The deep psychrometers maintained nearly constant readings once they approached equilibrium, without the oscillations observed for shallow psychrometers.

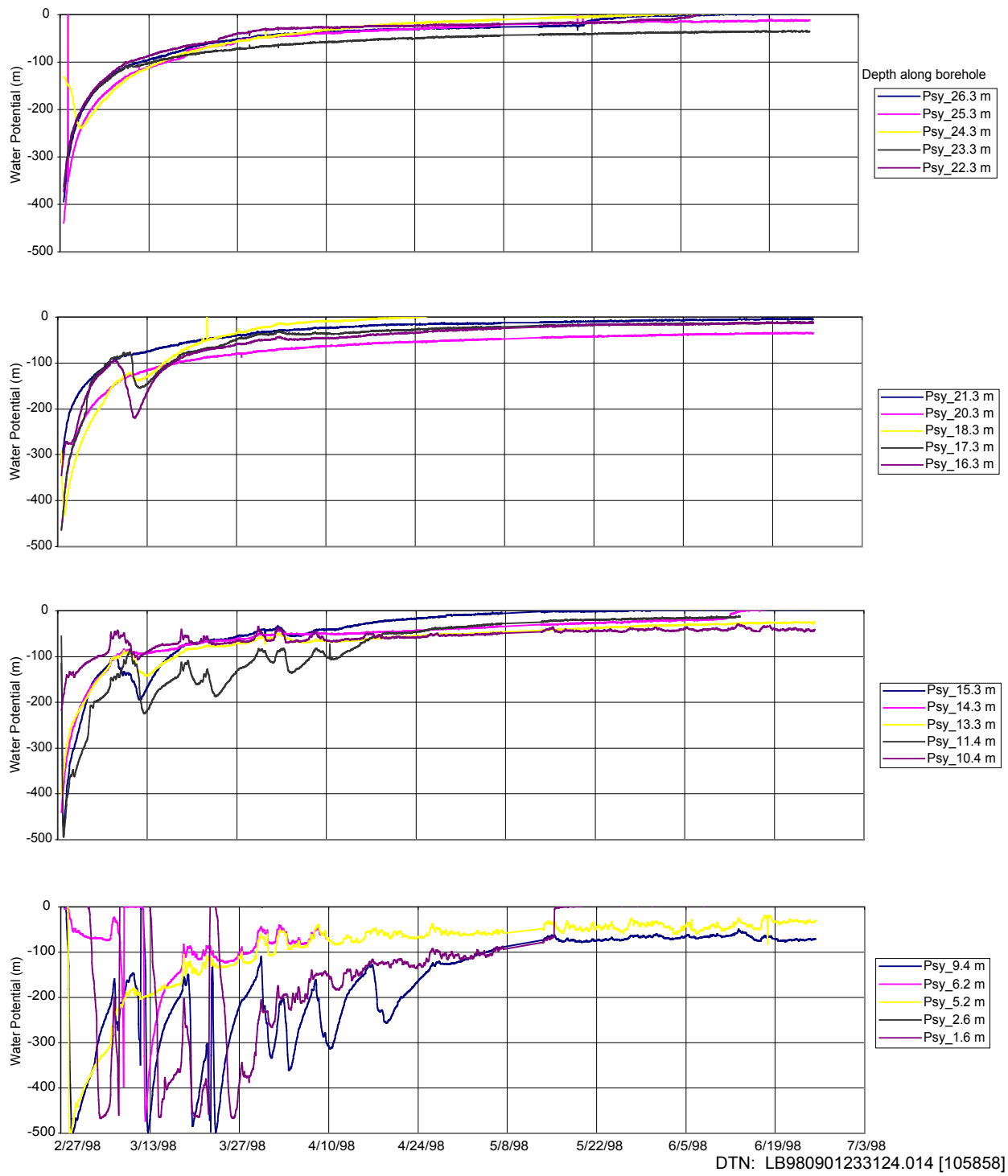

DTN: LB980901233124.014 [105858]

Figure 6.9.2-1. Changes in Water Potential Observed along the Wetting Front Monitoring Borehole at the Starter Tunnel of ECRB Cross Drift

6.9.2.1.2 Electrical Resistivity Probe

Measurements of electrical resistance were initiated in late March and continued until late June. Figure 6.9.2-2 summarizes the responses observed from probes located at 0.5 m intervals along the walls of the borehole between 17.3 and 29.8 m from the borehole collar.

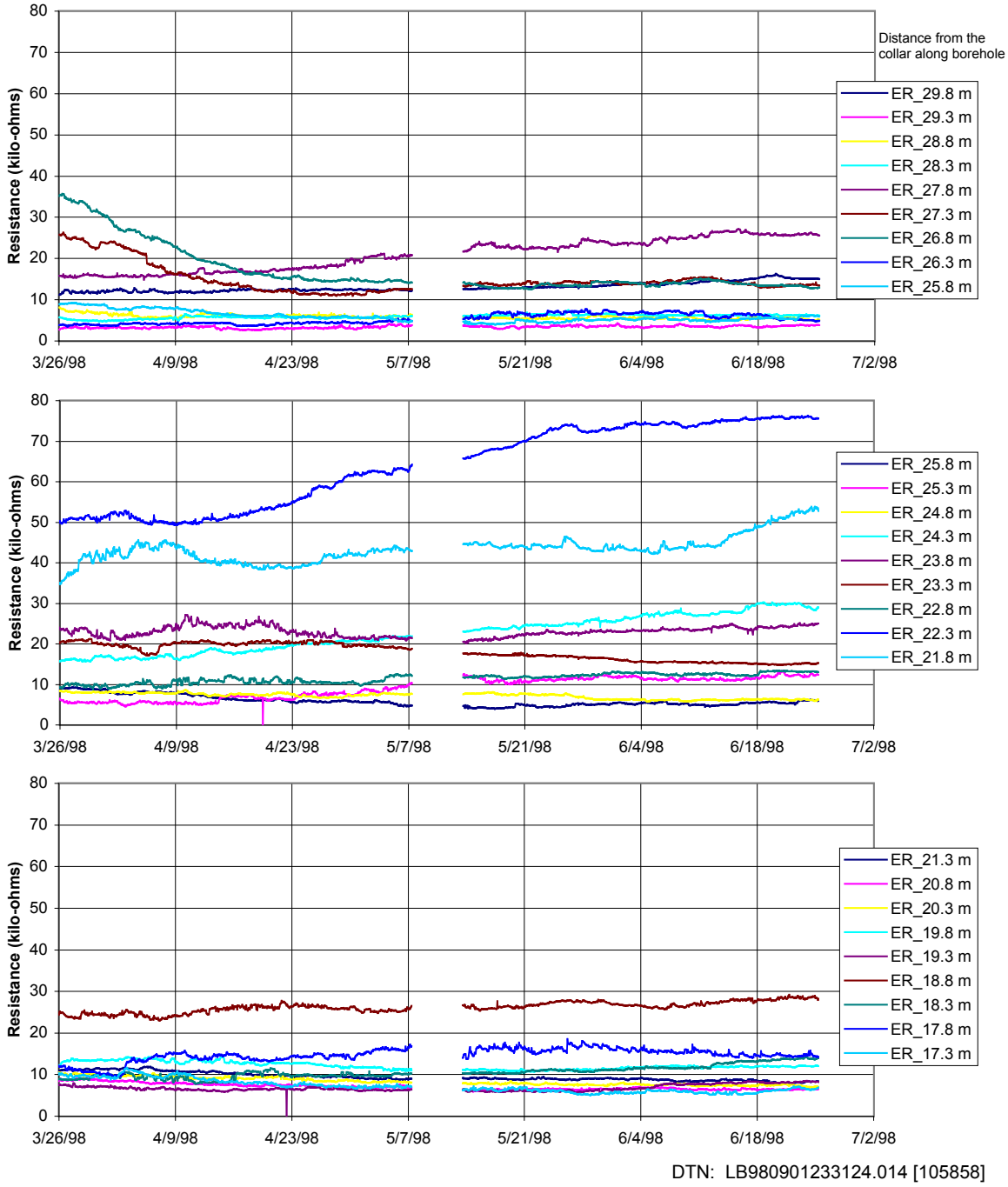

DTN: LB980901233124.014 [105858]

Figure 6.9.2-2. Changes in Electrical Resistance Observed along the Wetting-Front Monitoring Borehole at the Starter Tunnel of the ECRB Cross Drift

6.9.2.1.3 Potential Sensor Comparison

As part of an effort to evaluate the performance of ERPs as a sensor to monitor the arrival and movement of a wetting front, a series of probes was installed adjacent to psychrometers along the borehole length. The performance of the ERPs was compared with those of psychrometers.

From the psychrometer data collected between late March and June 1998, as illustrated in Figure 6.9.2-3, the events of interest were:

- Sinusoidal responses in the shallower psychrometers (e.g., psychrometers at a distance of 5.2 m)
- The wetting and drying cycles observed in the shallower zones as the borehole walls approached equilibrium (e.g., psychrometers at a distance of 9.4 m)
- Steady approaches to equilibrium as seen in the deeper psychrometers (i.e., at depths greater than 10.4 m).

Figure 6.9.2-3a to Figure 6.9.2-3c summarize responses of both psychrometers and ERPs for the three response patterns observed in the psychrometer data. (The y-axes for resistance were presented in decreasing scales, so that wetter sensors have higher y-values.) In two of the three cases, the ERPs responded in a pattern similar to that of psychrometers located adjacent to the probes. With the exception of the sensor at 5.2 m, the sinusoidal response observed by the psychrometer was well tracked by the ERPs, with points of changing trends fairly well synchronized. However, the direction of the trends between small time intervals is not consistent, suggesting that the response times of the probes are significantly different. The ERPs at shallow depths might be sensitive to air flows through the fractures in addition to moisture conditions in the vicinity of the probes. The psychrometers measure the moisture conditions in the vicinity of the probes.

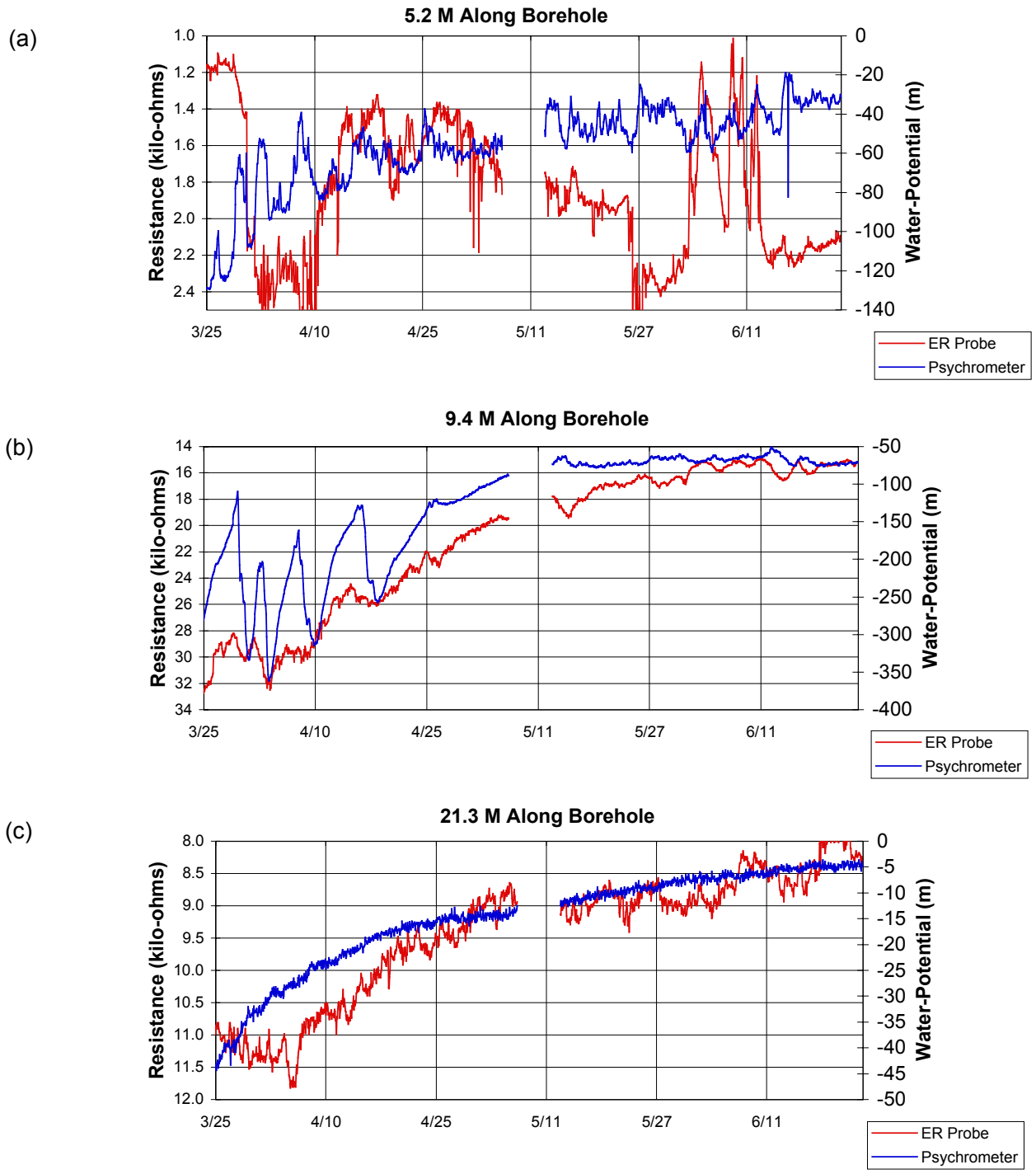

DTN: LB980901233124.014 [105858]

Figure 6.9.2-3. Comparison of Performance of Electrical Resistivity Probe and Psychrometer

At a distance of 9.4 m, the potential increased steadily from -400 m to -70 m between late March 1998 and June 1998, and the corresponding ERP measurements followed a similar pattern. Here, large fluctuations in water potentials in relatively short periods of time (-200 m in 4 days) were comparably detected by both types of probes. The slower, more gradual recovery observed by psychrometers deeper in the formation was generally well tracked by the ERPs (e.g., at 21.3 m).

6.9.2.2 Wetting-Front Monitoring at the Crossover Point

Figure 6-2 illustrates the potential movement from ECRB Cross Drift to the ESF Main Drift seepage collection system to study the migration of water and tracer flow from one drift to another. The seepage monitoring system was used to monitor the migration of construction water from the ECRB Cross Drift. Niche 3107 (Niche 3) is currently part of the drift-to-drift study as a monitoring station. The existing horizontal boreholes at Niche 3107 (Niche 3) are used in wetting-front monitoring for liquid released from a new alcove excavated horizontally from the ECRB Cross Drift and directly above the niche.

The ECRB Cross Drift passed over the ESF Main Drift on the second shift of July 1, 1998. No seepage was observed. The observers in the ESF Main Drift could hear rumbling noises from the TBM and feel vibrations on the railroad tracks and tunnel wall. However, no falling of loose rock was observed.

Figure 6.9.2-4 illustrates an example of the data collected by the TDR probes. No evident signals were associated with wetting-front arrivals. These null results from the sensors substantiated the field observations of no seepage associated with TBM passing over the ESF Main Drift. The confirmation of no seepage at the crossover point establishes the lower limit for the drift-to-drift flow and drift seepage processes associated with localized construction-water usage. It also provides a guide to the design of controlled drift-to-drift experiments at this unique location, with one drift above another drift.

The underground water usage in the ECRB Cross Drift is being monitored by YMP Science and Engineering Testing on a shift-by-shift basis; the tunnel-water use logs are being evaluated by the YMP Testing Safety Assurance group.

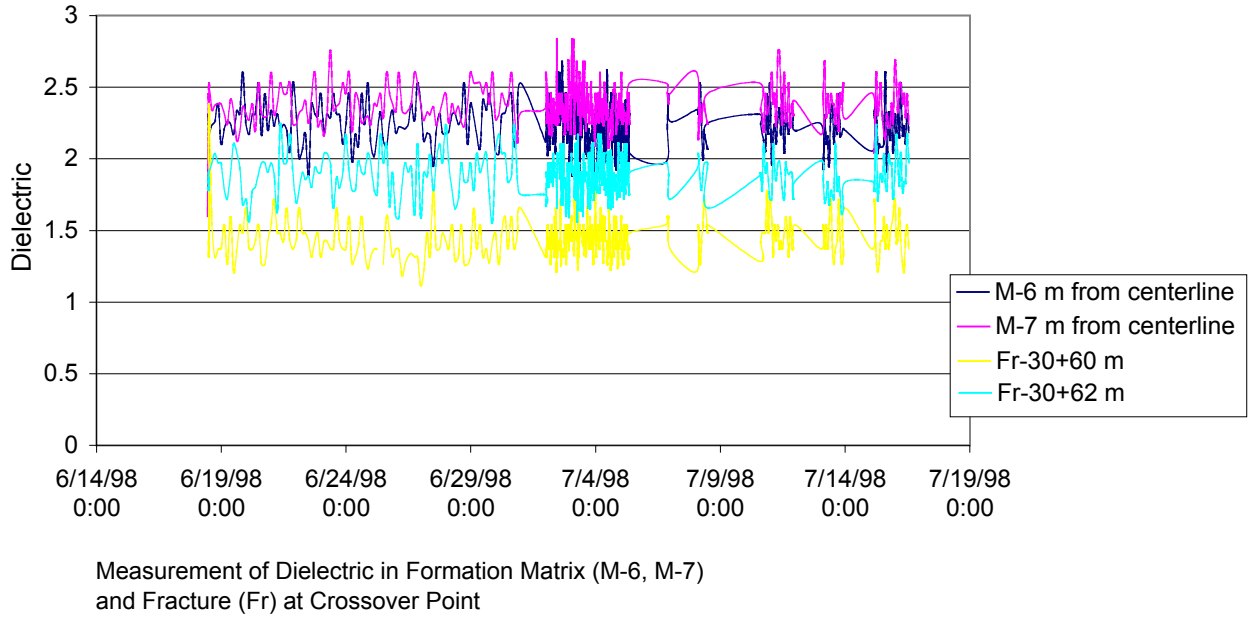

DTN: LB980901233124.014 [105858]

Figure 6.9.2-4. Example of Time Domain Reflectometry Probe Data at the Crossover Point in the ESF Main Drift

6.10 MOISTURE MONITORING AND WATER ANALYSIS IN UNDERGROUND DRIFTS

In ventilated drift sections, no continuous dripping (or seepage) was observed in either the ESF Loop or in the ECRB Cross Drift. This lack of seepage may be explained by the capillary barrier mechanism, as described in Section 6.2, with capillary forces holding water within the rock mass. The other explanation is related to ventilation. Ventilation can remove large amounts of moisture, dry the rock behind the drift walls, and suppress seepage. To determine if seepage returns when ventilation effects are mitigated, the last one-third of the ECRB Cross Drift was sealed with multiple bulkheads. Section 6.10.1 summarizes the moisture conditions and construction-water migration associated with drift excavation. Section 6.10.2 describes the preliminary results from the ongoing moisture monitoring in the ECRB Cross Drift. This section summarizes the current information on both the moisture conditions during drift operation and the post-emplacement environment in sealed drifts.

6.10.1 Construction (Drift Excavation) Effects on Moisture Conditions

6.10.1.1 Status of the ESF Moisture Monitoring Study

The moisture conditions in the ESF tunnels were monitored at 17 stations in the ESF main tunnel (from station 7+20 to station 73+50) and 10 stations in the ECRB Cross Drift (from station 0+25 to station 25+55), as summarized in Table 6.10.1-1. Relative humidity, temperature, barometric pressure, and air velocity were measured at various stations. The moisture-monitoring stations were supplemented by measurements from sensors with humidity/temperature probes and barometers mounted on the TBM during excavations. Additionally, periodic surveys were conducted along the tunnels with these sensors, mounted on a mobile cart. An infrared camera was used in mobile surveys to measure the temperature changes on the tunnel walls.

Table 6.10.1-1. Moisture-Monitoring Stations in the Exploratory Studies Facility

Moisture-Monitoring Station Location/ ID*	Description**	DTN
21+00/LB20, 28+30/LB50, 35+00/LB40, 42+50/LB60, 47+00/LB70, 51+73/LB80, 57+50/LB90, 64+59, 67+00, 73+50, AOD5, BKH5	Relative Humidity, Temperature, and Pressure in ESF Monitoring Stations in Report "Evaluation of Moisture Evolution in the Exploratory Studies Facility." VA Supporting Data	LB960800831224.001 [105793]
	Moisture Data Report from October, 1996 to January, 1997	LB970300831224.001 [105794]
	Moisture-Monitoring Data Collected at ESF Sensor Stations, Moisture Monitoring Before and After the Completion of the ESF	LB970801233124.001 [105796]
	Moisture-Monitoring Data Collected at Stationary Moisture Stations	LB970901233124.002 [105798]
7+20/GS#3, 10+93/GS#4, 28+93, 51+64, 67+20, Operator-Shack/GS#1 (on TBM), Vent-Line-Intake/GS#2 (on TBM)	Moisture Monitoring in the ESF, Oct. 1, 1996 through Jan. 31, 1997	GS970208312242.001 [135119]
	Moisture Monitoring in the ESF, Feb. 1, 1997 through July. 31, 1997	GS970708312242.002 [135123]
	Moisture Monitoring in the ESF, August 1, 1997 through July. 31, 1998	GS980908312242.024 [135132]
ECRB Cross Drift GS: 0+25, 2+37, 2+88, 3+38, 10+03, 21+07, 24+75; LB: 14+35, 21+40, 25+55	Moisture Monitoring in the ECRB CROSS DRIFT, 04/08/98 to 7/31/98	GS980908312242.035 [135133] LB990901233124.006 [135137] (This Scientific Analysis Report/Section 6.10.2.2)

NOTES: * LB for stations maintained by LBNL, and GS for stations maintained by USGS in this cooperative moisture-monitoring study.

* From ATDT or equivalent description.

The moisture data in the drifts, together with ventilation data and construction-water usage data, can be used to evaluate the amounts of moisture removed from the ESF drifts and the net quantities of construction water drained into the surrounding tuff formations. In this scientific analysis report, examples of moisture-monitoring data collected right after excavation of the ECRB Cross Drift are presented. Simple observations are qualitatively discussed to highlight the importance of excavation and operation data for determining site perturbations. Potential sources for corroborative evidence of the induced effects are presented in Table 6.10.1-1 through Table 6.10.1-3.

Table 6.10.1-1 summarizes the data collected in moisture monitoring stations during and after drift excavations. Moisture removals in the drift dry up the surrounding tuffs. Water-potential measurements are listed in Table 6.10.1-2. Use of construction water changes the saturation of

the tuffs along flow paths. Table 6.10.1-3 summarizes the saturation measurements for both perturbed conditions and for ambient conditions.

Table 6.10.1-2. Water-Potential Measurements in the Exploratory Studies Facility

Potential Measurement	Description*	DTN
Niche 3566 (Niche 1)—psychrometer Niche 3650 (Niche 2)—psychrometer	3 main boreholes, 5 lateral boreholes in Niche 3566 (Niche 2), 5/9/97—10/21/97; 6 main boreholes in Niche 3650 (Niche 2), 7/1/97—7/28/97	LB980001233124.001 [105800]/ This Scientific Analysis Report/Section 6.8.2
Niche 3566 (Niche 1)—heat dissipation probe	21 heat dissipation probe drill holes, 11/4/97—7/31/98	GS980908312242.022 [135157]
Niche 3107 (Niche 3)—psychrometer	3 main boreholes, 12/22/97—1/8/98	LB980001233124.001 [105800]/ This Scientific Analysis Report/Section 6.8.2.4
Alcove 7—heat dissipation probe	Heat dissipation probe drill holes, 12/9/97—1/31/98	GS980908312242.022 [135157]
Alcove 3—filter paper Alcove 4—filter paper	1 core hole in Alcove 3, 2 core holes in Alcove 4	GS980908312242.033 [107168], GS980908312242.032 [107177]
North Ramp 7+27 to 10+70 South Ramp 69+65 to 76+33—filter paper	18 North Ramp boreholes, 3 Alcove 4 boreholes, and 46 South Ramp boreholes, HQ, 2-m length	GS980308312242.004 [107172]
South Ramp—heat dissipation probe	Heat dissipation probe drill holes, 8/1/97—1/4/98	GS980308312242.002 [135163]
Cross-Over Point 30+62 in the ESF Main Drift Below the ECRB Cross Drift—psychrometer	43 psychrometers on ESF drift walls, 6/19/98—7/16/98	LB980901233124.014 [105858]/ This Scientific Analysis Report/Section 6.9.2.2
ECRB Cross Drift Starter Tunnel—psychrometer & electrical resistivity probe	1 slant borehole below the invert	LB980901233124.014 [105858]/ This Scientific Analysis Report/Section 6.9.2.1
ECRB Cross Drift 0+50 to 7+75—heat dissipation probe	6 heat dissipation probe drill holes, 4/23/98—7/31/98	GS980908312242.036 [119820]
Surface Based Boreholes—psychrometer	USW NRG-7a, UE-25 UZ#4, UE-25 UZ#5, USW UZ-7a and USW SD-12; 1/1/97—6/30/97; 7/1/97—9/30/97; 10/1/98—3/31/98; 4/1/98—9/30/98	GS970808312232.005 [105978] GS971108312232.007 [105980] GS980408312232.001 [105982] GS981208312232.002 [156505]

NOTE: * ATDT or equivalent description.

Table 6.10.1-3. Saturation Measurements in the Exploratory Studies Facility

Saturation Measurement	Description*	DTN
Niche 3566 (Niche 1) - core Niche 3650 (Niche 2) - core	3 main boreholes, 6 lateral boreholes in Niche 3566 (Niche 1) and 7 main boreholes in Niche 3650 (Niche 2)	GS980908312242.018 [135170], GS980908312242.020 [135172]
Alcove 6 - core Alcove 7 - core	3 boreholes in Alcove 6, 1 borehole in Alcove 7	GS980908312242.029 [135175], GS980908312242.028 [135176]
Alcove 3 - core Alcove 4 - core	1 core hole in Alcove 3, 2 core holes in Alcove 4	GS980908312242.033 [107168], GS980908312242.032 [107177]
North Ramp 7+27 to 10+70 South Ramp 59+65 to 76+33 – core	Borehole samples	GS980308312242.005 [107165], GS980308312242.003 [135180]
South Ramp - time domain reflectometry	TDR measurements, 8/1/97 - 1/4/98	GS980308312242.001 [135181]
ECRB Cross Drift Starter Tunnel - Core	1 slant borehole core	GS980908312242.030 [135224]
Cross-Over Point 30+62 in the ESF Main Drift Below the ECRB Cross Drift - time domain reflectometry	43 TDR probes on ESF drift walls, 6/19/98 - 7/16/98	LB980901233124.014 [105858]/ This Scientific Analysis Report/Section 6.9.2.2

NOTE: * From ATDT or equivalent description.

6.10.1.2 Moisture Conditions and Perturbations Observed in Drifts

6.10.1.2.1 Observation of Moisture Conditions in Ventilated ESF Main Drift

Preliminary evaluation of the moisture data during ESF excavation showed that the moisture conditions were sensitive to construction activities. The daily usage of water for excavation, muck transport, dust-control, and other operations introduced rapid changes in moisture conditions throughout the tunnel atmosphere and in the wall rock. During weekends in 1996, when construction activities were absent, the tunnel atmosphere generally stabilized to either high-humidity conditions if the ventilation was turned off, or low-humidity conditions if the ventilation was left on (DTN: LB960800831224.001 [105793]). After completion of the ESF main tunnel with two portals for entrance and exit, high-humidity conditions were suppressed by natural ventilation through the portals (DTN: LB970801233124.001 [105796]).

The following order-of-magnitude estimate of moisture removal capacity represents the ESF system in August 1996 conditions when the ESF Main Drift was excavated but the ESF South Ramp was not, with the total length of 6,250 m. (The ESF was excavated from 1994 to 1997.) For a 6,250 m long tunnel with cross-sectional area of 40 m^2 (circular cross-sectional area with invert, vent line, and conveyor blockage areas subtracted), the humid tunnel air can contain 2,500 kilograms of excess water mass if we estimate that the tunnel is on average 50% higher in relative humidity than the outside air, with the corresponding vapor density difference on the

order of 0.01 kg/m^3. If the tunnel air is ventilated with a flow rate of 47 m^3/s or 100,000 ft^3/min (cubic feet per minute, or cfm), it will take 5,300 seconds or 1.5 hours to remove and replace the tunnel air. The water-removal rate of 2,500 kg over 1.5 hours corresponds to 285 m^3/week (285 kiloliter/week or 75,000 gallon/week). If all the moisture in the tunnel air is from evaporation, the equivalent evaporation rate from the tunnel walls and inverts (with area 6250 m × 23.7 m) is on the order of 100 mm/yr (Wang et al. 1996 [101309]).

More specific estimates were made for sections in different tuff units, using measured relative humidity changes. Vapor-density differences between different locations, together with a simple approximation of air flow in the tunnel, were used to estimate the moisture removal rate and the equivalent evaporation rate. Weekly rates of the amount of water removed by ventilation were a substantial fraction of water used in the tunnel. Estimated equivalent evaporation rates were on the order of 200 mm/yr, with standard deviation over 90 mm/yr, for both the Topopah Spring welded tuff units in a 1400 m section centered at Alcove 5 (the thermal test alcove) and the Paintbrush nonwelded units in a 380 m section between Alcove 3 and Alcove 4. The uncertainties were related to fluctuations in the moisture conditions introduced by construction activities, including air ventilation and water usage.

The equivalent evaporation rate over 100 mm/yr is an order of magnitude larger than the ambient percolation flux. The large evaporation rate could suppress the observations of active seeps and contribute to the apparent dry tunnel conditions. Rock temperatures near the TBM were observed to change spatially and temporally and could be related to evaporation from rock surfaces. Water potentials near the rock surfaces were measured with heat dissipation probes, and water potential profiles along boreholes were measured by psychrometers in niches and alcoves along the ESF Main Drift and along the ECRB Cross Drift, as summarized in Table 6.10.1-2. Field measurements in boreholes and laboratory measurements of physical and hydrological properties of cores were conducted to measure saturation distributions, as summarized in Table 6.10.1-3 and Section 6.8. The dryout zones could extend nominally 1 to 3 m into the walls, with fractures and faults likely extending the depths of drying influence.

The advances of the ESF tunnel excavations were detected pneumatically by sensors in 10 surface-based boreholes within 200 m of the ESF. In comparison to the damping of barometric signals from the ground surface, less attenuation and phase lag were observed for signals from the ESF. For the borehole NRG-7a, within 30 m in horizontal distance from the ESF tunnel, the changes in water potential could also be related to the ESF dryout (see last entry of Table 6.10.1-2 for DTNs of surface-based boreholes).

The main effects of ESF ventilation are the drying of rocks around the tunnel, the suppression of potential seepage into tunnels, and the perturbation of the gas flow field around the tunnel. Niche 3566 (Niche 1), Alcove 7, and the last section of the ECRB Cross Drift have been closed for long time periods to gain additional information on the rewetting processes and potential seepage events. Both the data collected during active ventilation phases and passive nonventilation phases will contribute to the assessment of UZ responses to large-scale perturbations at Yucca Mountain.

6.10.1.2.2 Observation of Moisture Effects in Alcove 3 and Alcove 4

Corroborating studies have been performed between Alcove 3 and Alcove 4 that quantified *in situ* water-potential, moisture, and temperature fluctuations in the nonwelded units of the Paintbrush Group (PTn), to identify gradients between the PTn and adjacent Tiva Canyon tuff and Topopah Spring tuff (DTN: GS021008312242.003 [162178]). The studies identified an effect of ventilation-induced drying to a depth of 4.9 m into the tuff from the ESF. As a result, water-potential values were more negative (lower moisture content) near the tunnel surface and greater (higher moisture content) beyond the zone influenced by ventilation. From surface to depth, water-potential values (in bars) were: Tiva Canyon -27.0 to –3.5 (ventilation effects), Paintbrush nonwelded –1.7 to –0.1, and Topopah Spring –1.4 to -0.6. The combined evidence of high moisture values at the Bt2/Tptrv3 contact (–0.1 and –0.3 bars), along with the 10-degree east dip of the beds, indicates a high potential for lateral water flow in the PTn (DTN: GS021008312242.003 [162178]; LeCain et al. 2002 [158511]).

6.10.1.2.3 Observation of Moisture Conditions in Ventilated ECRB Cross Drift

The drift conditions at the ECRB Cross Drift in 1998 were similar to the conditions of the ESF Main Drift in 1996. High-humidity conditions existed in the new sections just excavated. Relative humidity data from three moisture stations in the ECRB Cross Drift are illustrated in Figure 6.10.1-1 and Figure 6.10.1-2 for the month of November 1998, right after the completion of TBM excavation. The moisture sensor assembly at ECRB Cross Drift Construction Station CD 25+55 (2,555 m from the ECRB Cross Drift entrance) is located near the Solitario Canyon fault on the western boundary of the repository block. The other two stations, at CD 14+43 and CD 21+40, measured the moisture conditions in the middle part of the ECRB Cross Drift within the repository block.

The figures illustrate the temporal fluctuations and the spatial distributions of moisture conditions along the ECRB Cross Drift. The data were collected every 15 minutes. CD 25+55 was much more humid than the other two stations under the control of the same ventilation system. The day shifts had more activities than the other two shifts. During the week of the Thanksgiving holiday (November 26, 1998), there were increases in moisture conditions that might be correlated with ventilation shutdown. The monthly averaged relative-humidity values are 15 ± 3% for CD 14+43, 18±4% for CD 21+40, and 28±5% for CD 25+55.

The spatial variations illustrated in Figure 6.10.1-2 are based on weekly averaging over the day shifts. The differences in relative humidity are more clearly shown with the spatial distribution plot. While the magnitude varies from week to week, the spatial gradients were relatively constant. Average gradients for the two sections were 3.4% per kilometer between CD 14+35 and CD 21+40, and 25.2% per kilometer between CD 21+40 and CD 25+55. The section near the end of the tunnel apparently had more moisture removed than the section near the entrance.

The temporal and spatial distributions in Figure 6.10.1-1 and Figure 6.10.1-2 are presented to illustrate the characteristics of the moisture evolution in a newly excavated tunnel. Moisture gradients, together with the ventilation rates, are needed to calculate the moisture removal rates. The ECRB Cross Drift is a simple tunnel system compared to the ESF Main Drift. There is only one ventilation line operating along the ECRB Cross Drift, without any secondary branches separating the air flows into side alcoves and niches.

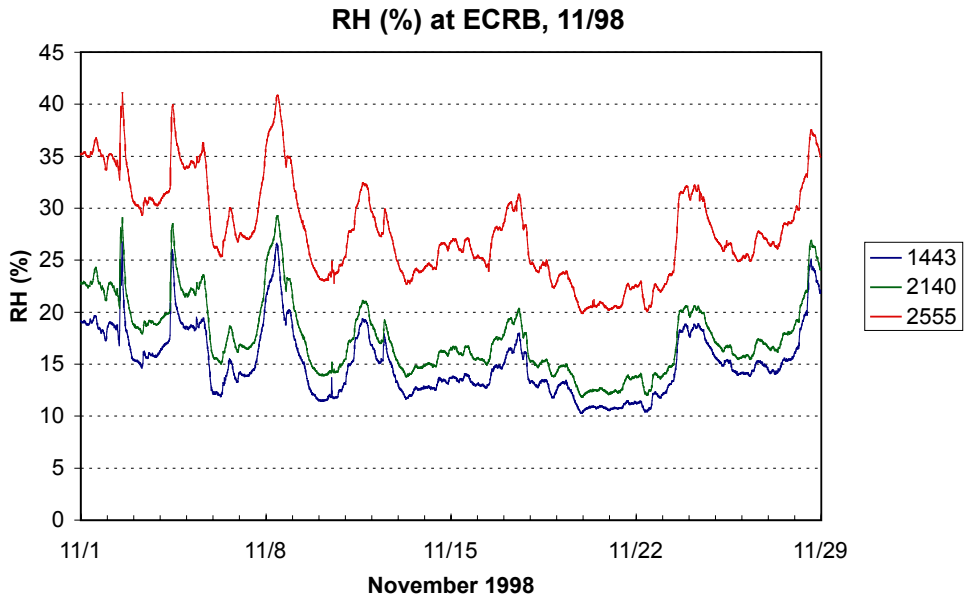

DTN: LB990901233124.006 [135137]

NOTE: The data were collected in November 1998 after completion of excavation. The legends are the distances in meters from the moisture station to the ECRB Cross Drift entrance.

Figure 6.10.1-1. Relative Humidity Temporal Variations in the ECRB Cross Drift

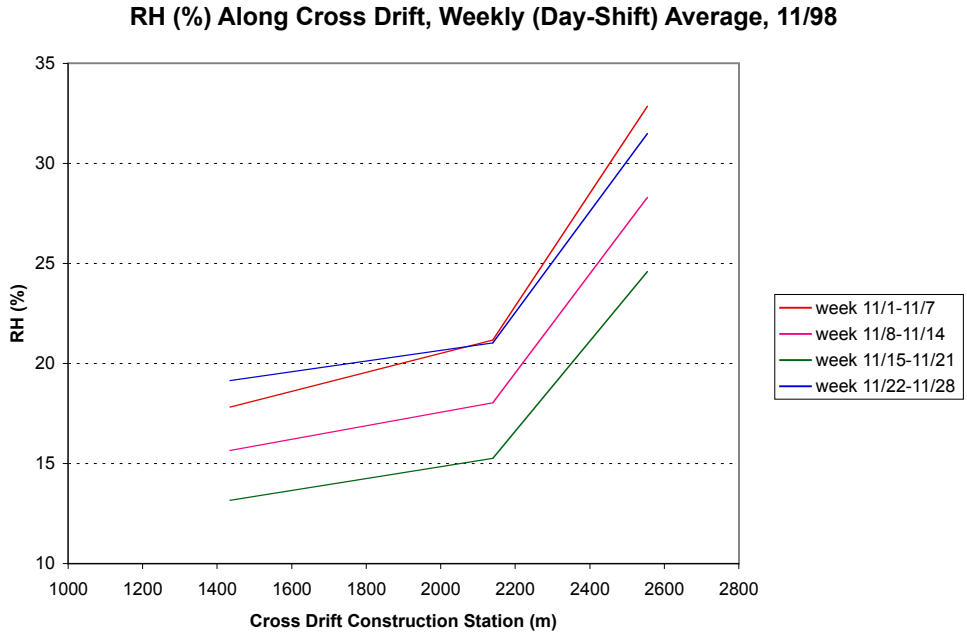

DTN: LB990901233124.006 [135137]

NOTE: The weekly averages of day shift data are presented for November 1998 after completion of excavation.

Figure 6.10.1-2. Relative Humidity Spatial Variations along the ECRB Cross Drift

6.10.1.3 Construction Water Migration Below Invert from Excavation

Construction water used in the excavation of the ESF contained lithium bromide as a tracer. The presence of the tracer (measured as bromide to chloride ratio, Br/Cl, leached out of crushed borehole samples) is illustrated in Figure 6.10.1-3 along three construction-water (CWAT) boreholes drilled in the ESF. The deepest tracer penetration was at borehole CWAT#2, in which construction water had reached the bottom of the borehole (30 m). CWAT#2 is located in an intensely fractured zone of the middle nonlithophysal zone of the TSw. In CWAT#1, the construction water was detected in all samples to a depth of 2.4 m, with two isolated peaks at greater depths. In CWAT#3, located in the upper lithophysal zone, the construction water was detected only in the top 2 m. Figure 6.10.1-3 also illustrates the areal distributions of three tuff units in the repository horizon: the middle nonlithophysal zone, the lower lithophysal zone, and the lower nonlithophysal zone, all of the Topopah Spring welded hydrogeologic unit. Both the variations in hydrological properties of different tuff units and in the construction usage rates could have affected the construction-water penetrations.

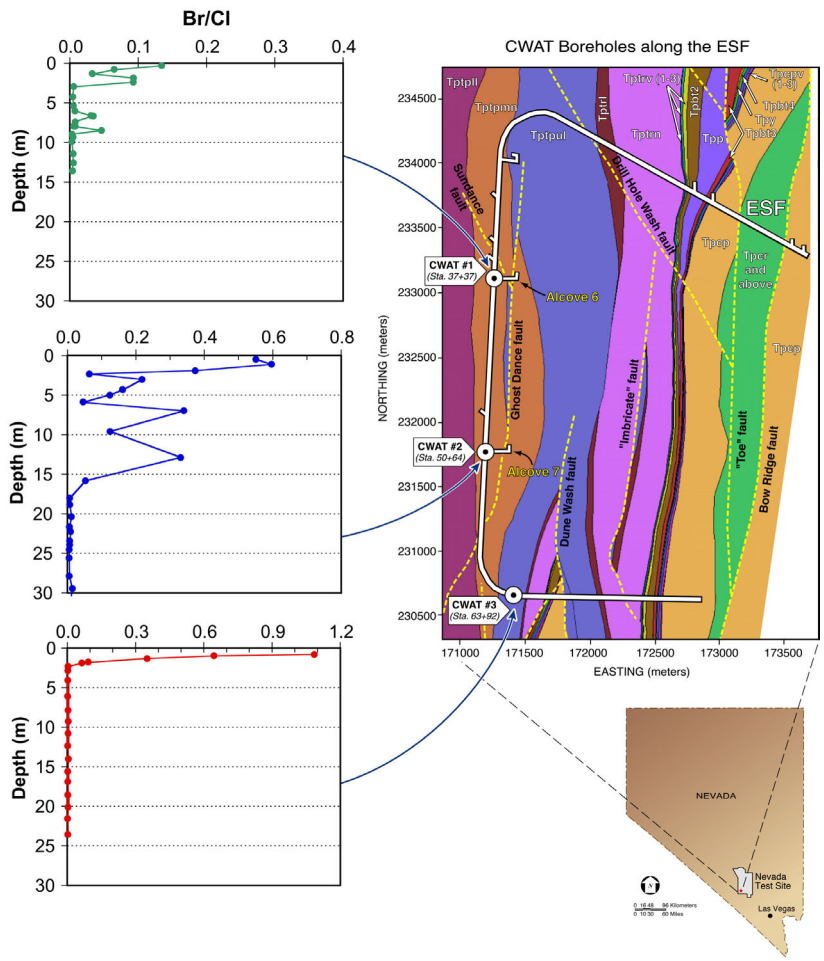

DTN: LAJF831222AQ98.007 [122730]

Source: Geological framework model GFM3.1 (BSC 2001 [154622]).

Figure 6.10.1-3. Construction Water Distribution below Exploratory Studies Facility Drift

6.10.2 Observation along the Nonventilated Sections of the ECRB Cross Drift

The moisture monitoring study conducted in the ECRB Cross Drift is designed to detect drips in sealed drift sections. To observe potential seepage, ventilation effects to the terminal section of the ECRB Cross Drift have been minimized with the construction of a series of four bulkheads (Figure 6.10.2-1). The nonventilated sections include the area below the Solitario Canyon wall and intercept the Solitario Canyon fault.

The first two bulkhead doors were located at Stations CD 17+63 and CD 25+03 on June 1999. A third bulkhead door was located at Station CD 25+99 on July 2000, and then a fourth bulkhead was located at Station CD 22+01 on November 2001.

Along seven boreholes in the ECRB Cross Drift shown in Figure 6.10.2-2, psychrometer measurements of water potential have been made. Within the drift opening, humidity, temperature, wind speed, and barometric pressure are being measured at various stations to provide information on moisture dynamics along the ECRB Cross Drift. During November 2002, Electrical Resistance Probes (ERPs) were laid out at 0.5 m intervals between Stations CD 24+00 and CD 26+36 to measure saturation changes along the drift wall. Additionally, relative humidity and temperature probes were located in Stations CD 15+02, CD 20+40, CD 21+40, CD 21+90, CD 22+50, CD 23+45, CD 24+40, CD 25+10, CD 25+36, CD 25+52, CD 25+90, CD 26+00, CD 26+30, and CD 26+60. Six water collection units were also installed between Stations CD 24+85 and CD 24+95. Figure 6.10.2-2 shows the location of moisture monitoring stations along sections of the ECRB.

Additional information on moisture conditions within the nonventilated zone has been gleaned during periods when the bulkhead doors were opened, including before 2003: (1) January 12–13, 2000; (2) May, June, and July 2000 to install the third bulkhead, (3) January 22–25, 2001, (4) May 22, 2001, to repair electrical power, (5) October 1–December 20, 2001, and (6) June 24-27, 2002. During most of the entries, the entire ECRB was accessible for visual inspection. The June 2002 entry was restricted to the area between bulkhead at CD 17+63 and bulkhead at CD 22+01. During each of these entries, observations of wet spots were documented, and water samples were manually collected from small pools of water if feasible.

Figure 6.10.2-3 provides a geological cross section at the terminal end of the ECRB Cross Drift, showing the locations of the last two bulkheads and the TBM. These sections have higher potential for seepage because of higher surface net-infiltration rates and higher percolation flux distributions in the repository level. The high flux region could be located especially in areas with no overlying nonwelded tuff. The section between Station CD 25+03 and Station CD 26+01 also intersects the Solitario Canyon fault at CD 25+84. The section behind the bulkhead at CD 25+99 contains the TBM used for ECRB Cross Drift excavation. The TBM is a heat source because of power being supplied to the TBM. Table 6.10.2-1 provides rock unit contacts intersected by the tunnel sections behind the bulkheads.

Section 6.10.2.1 summarizes the water potential and moisture monitoring data. Section 6.10.2.2 presents the observations in periodic entries behind the bulkheads to observe wet zones. Section 6.10.2.3 presents data from water samples collected during early entries.

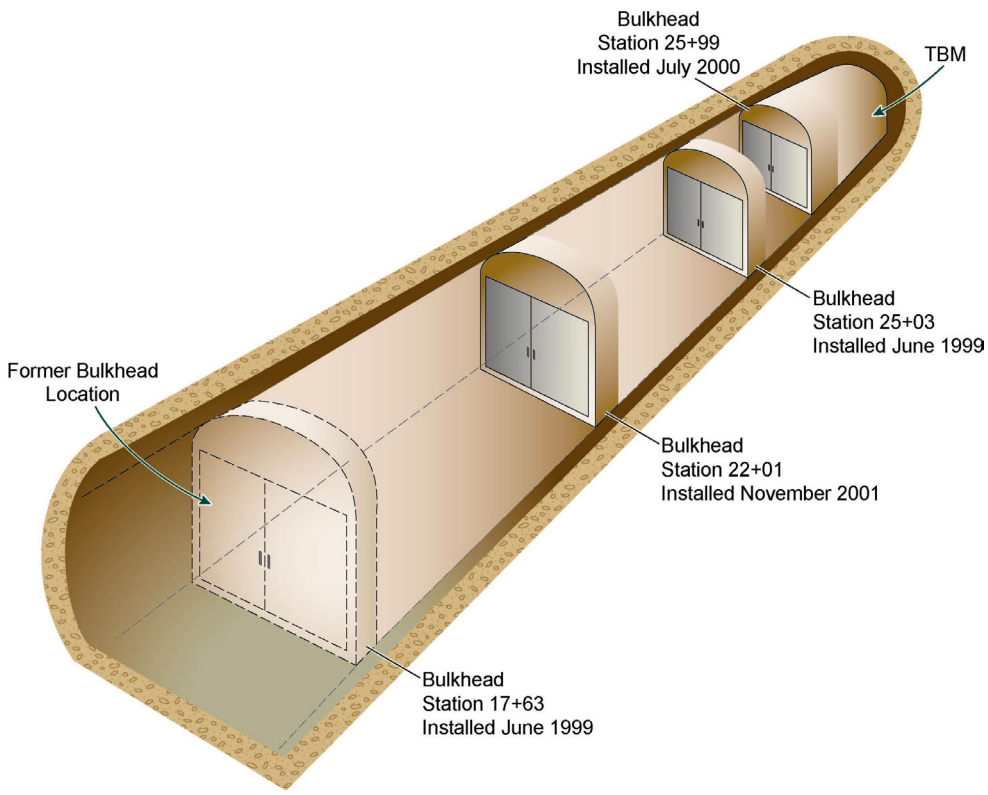

Figure 6.10.2-1. Schematic Illustration of Bulkhead Locations in the ECRB Cross Drift

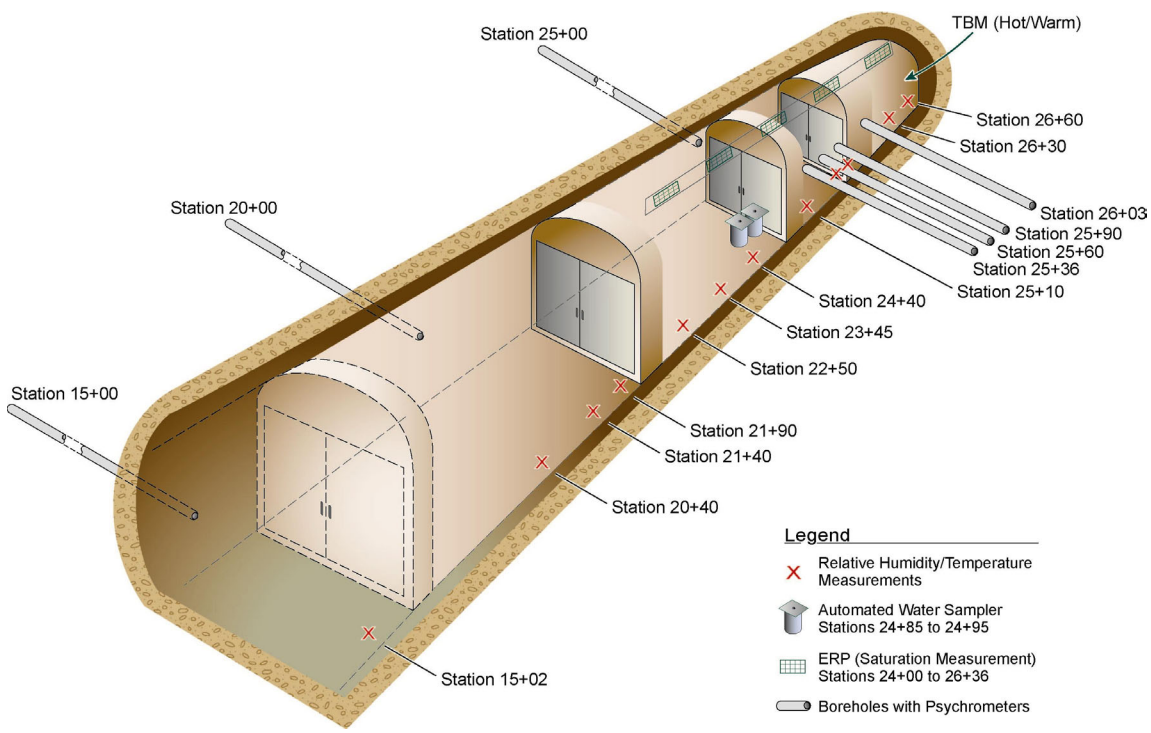

Figure 6.10.2-2. Schematic Illustration showing Berkeley Lab Monitoring Station in Locations in the ECRB Cross Drift

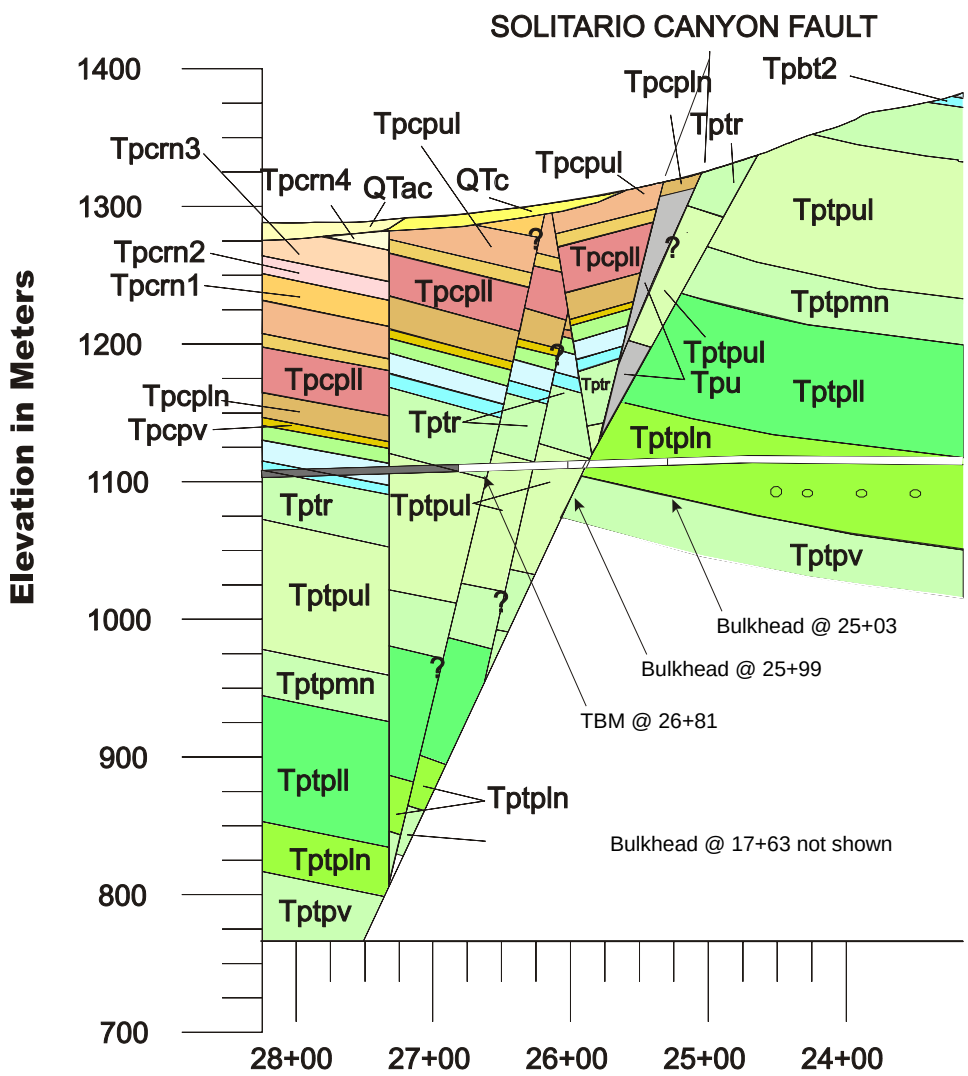

DTN: GS990908314224.010 [152631]

NOTE: For stratigraphic abbreviations, refer to Drawing OA-46-345 "Comparative Geologic Cross Section along the Cross Drift".

Figure 6.10.2-3 As-Built Cross Section of the Terminal End of the ECRB Cross Drift (23+00 m to 26+81 m) Showing the Bulkhead Locations

Table 6.10.2-1 Rock Unit Contacts Intersected by the Bulkhead Sections (All within the Topopah Spring Tuff)

Station	Mapped Contact
23+26	Tptpll / Tptpln (Topopah Spring Tuff lower lithophysal / lower nonlithophysal Contact)
25+84	Tptpln / Tptpul (Topopah Spring Tuff lower nonlithophysal / upper lithophysal Solitario Canyon Fault Zone)
26+64	Tptpul / Tptr (Topopah Spring Tuff upper lithophysal / crystal rich lithophysal Solitario Canyon Fault Zone)

DTN: GS990408314224.006 [108409]

6.10.2.1 Water-Potential Measurements and Drift Relative Humidity and Temperature Variations

Past observations have shown that, in an open tunnel, the evaporation potential of ventilation is much greater than any expected seepage. Observations from boreholes installed perpendicular to the tunnel wall suggest a clear dryout zone associated with ventilation of the tunnel. General conclusions from our understanding of the unsaturated zone suggest that if seepage into drifts were to occur, it would most likely be in the western portion of the repository block, where geological conditions are most conducive to infiltration, percolation, and seepage. The characteristics in this portion of the tunnel that make it most suitable for locating seeps are the absence of an overlying PTn past about CD 23+50 and the relatively high percolation rates, caused by high infiltration from shallow soils and higher elevation at the surface.

The 918 m long drift section (from bulkhead at CD 17+63 to the TBM end at CD 26+81) is located in the Topopah Spring lower lithophysal (Tptpll) and the lower nonlithophysal (Tptpln) tuff units, and includes the Solitario Canyon fault (the western boundary of the primary repository block) (Figure 6.10.2-1).

6.10.2.1.1 Water-Potential Measurements

Water-potential measurements along three horizontal boreholes in the ECRB Cross Drift are summarized in Figure 6.10.2-4. These three boreholes are located at CD 15+00, CD 20+00 and CD 25+00, and are 6 m long. The borehole at CD 15+00 is located before the first bulkhead, while the boreholes at CD 20+00 and CD 25+00 are located in bulkheaded sections.

There are three aspects to the water-potential measurements in the ECRB Cross Drift: (a) spatial variability within boreholes, (b) spatial variability between boreholes, and (c) the temporal variability within boreholes located between the first and second borehole. Spatial variability within boreholes begins with low water potentials close to the drift, increases rapidly over a distance of 1-2 m, and then remains close to saturated values along the deeper profile. Among the three monitored boreholes, the one located at CD 15+00 had its lowest water potential (i.e., driest) close to the drift wall. The borehole at CD 20+00 also had lower water potentials up to a distance of ~1.5 m from the borehole collar in (prior to the location of the bulkhead doors), which have since increased. The borehole located farthest into the ECRB Cross Drift at CD 25+00 did not show large drops in water potential closer to the collar, nor did the borehole show any increases in water potentials following the installation of the bulkhead doors.

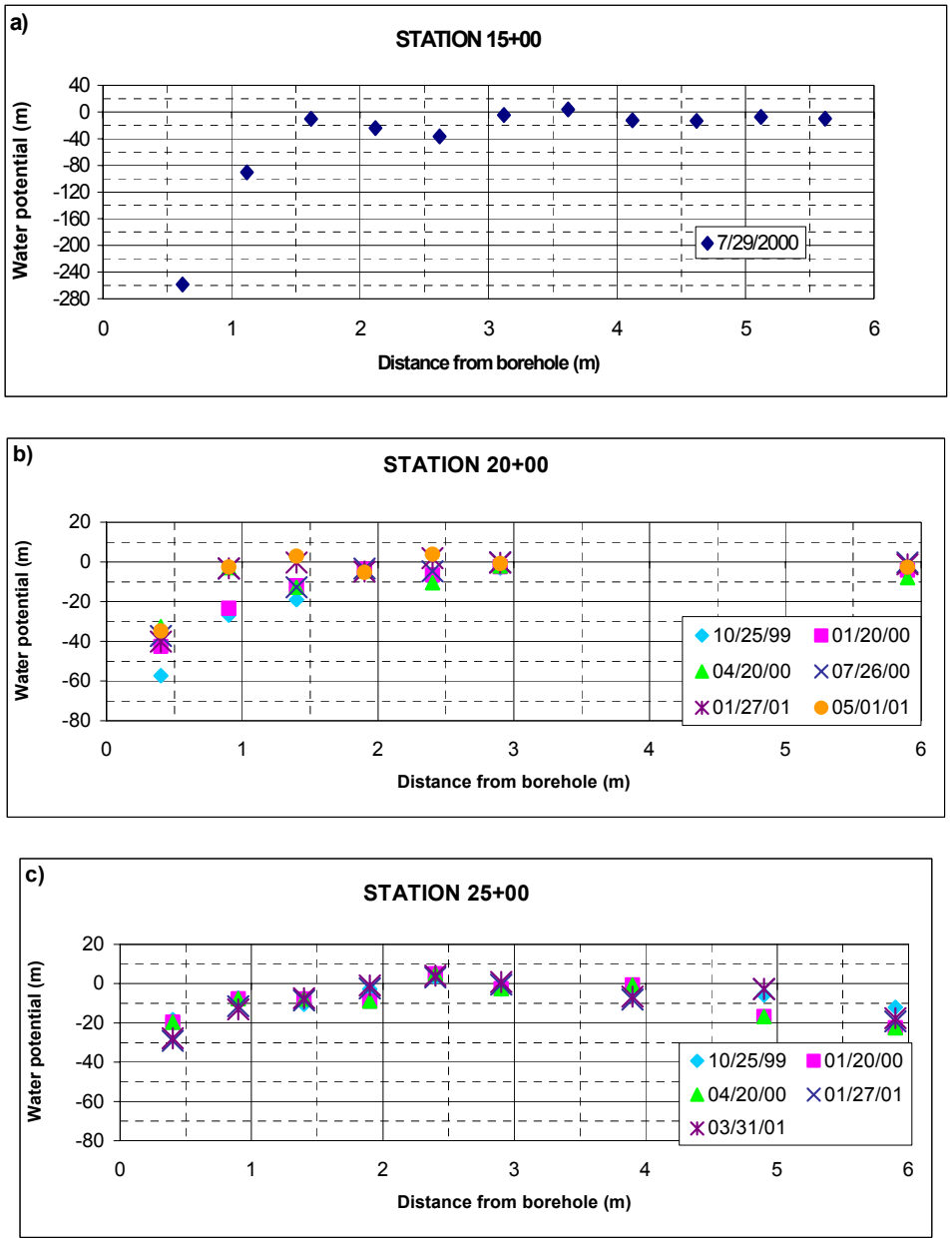

DTN: LB0110ECRBH2OP.001 [156883]

Figure 6.10.2-4. Water-Potential Measurements along the ECRB Cross Drift: (a) Station 15+00; (b) Station 20+00; (c) Station 25+00

6.10.2.1.2 Barometric Pressure Variations

Barometric pressure measured in the ECRB Cross Drift did not show any spatial variability, but had a pronounced change over time (Figure 6.10.2-5). The range of the temporal variability was between ~870 and ~905 millibars (mbars). From May to September 2000, the barometric pressure along the ECRB Cross Drift was restricted between ~880 and ~895 mbars. Larger fluctuations in the barometric pressure were observed between October 2000 and May 2001.

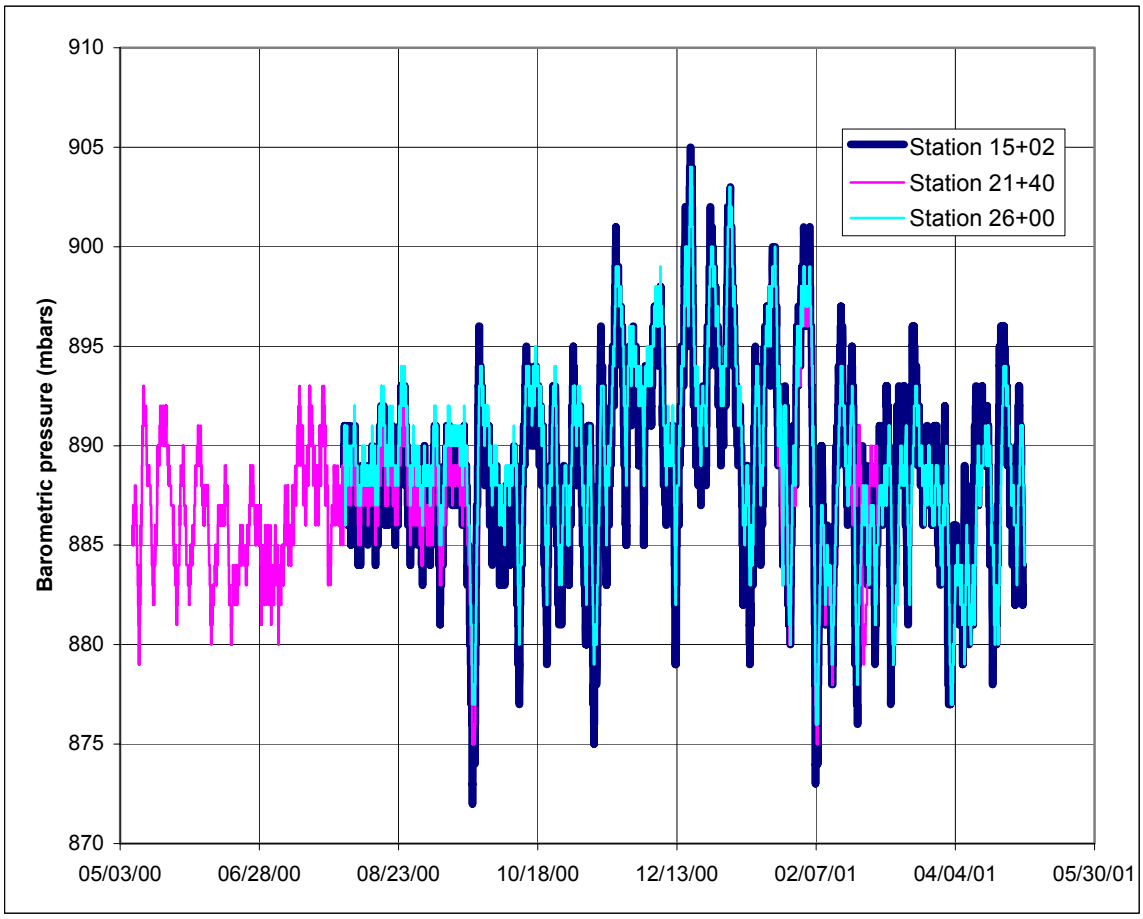

DTN: LB0307ECRBRHTB.001 [164843]

Figure 6.10.2-5. Barometric Pressure Measured along the ECRB Cross Drift

6.10.2.1.3 Temperature Variations between May 2000 and May 2001

Temperature measurements along the ECRB Cross Drift made over a period of nine months, starting in early August 2000, show a clear temperature gradient extending through the section of the ECRB Cross Drift behind the bulkhead doors (Figure 6.10.2-6).

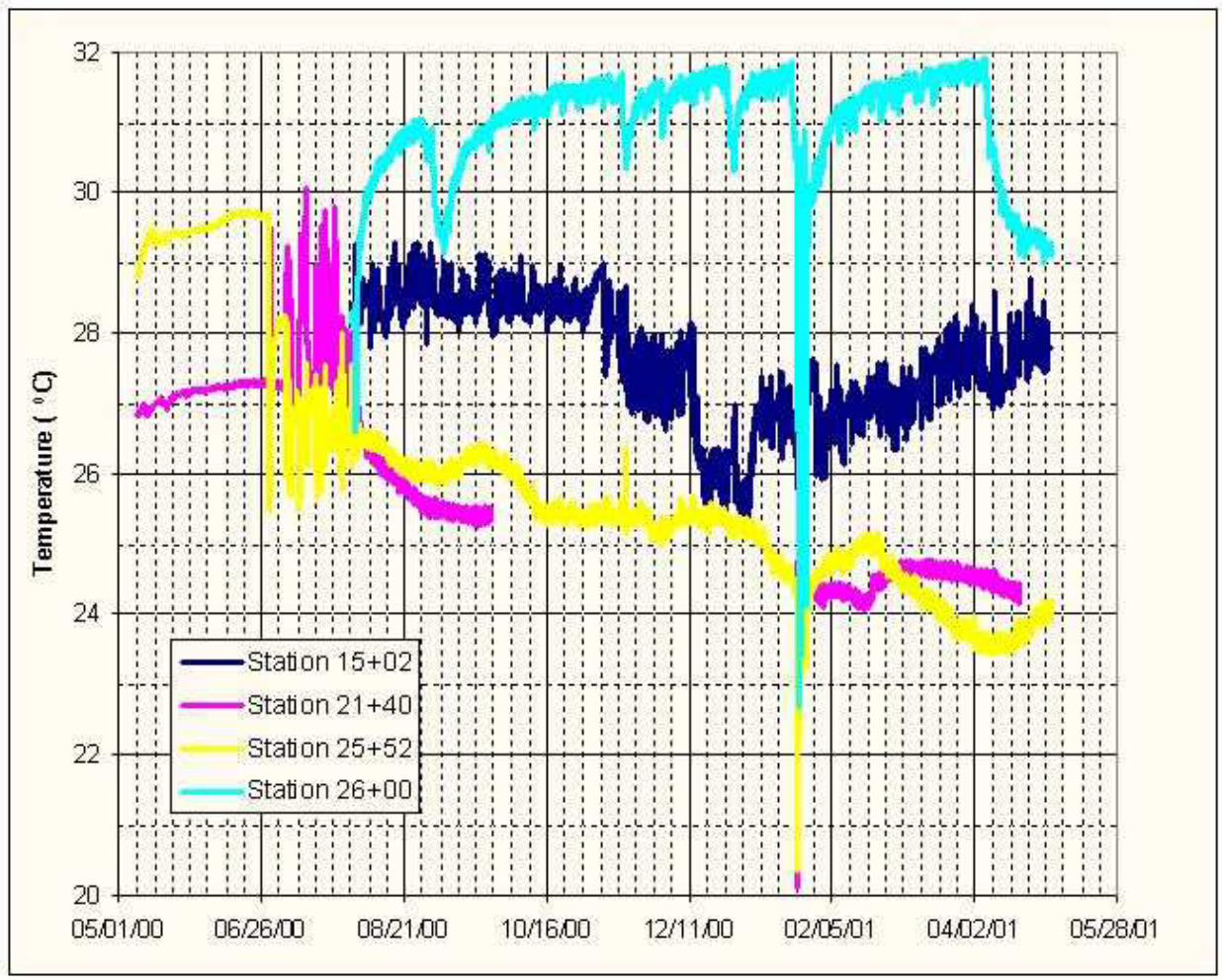

DTN: LB0307ECRBRHTB.001 [164843]

Figure 6.10.2-6. Temperature Measured in the Four ECRB Cross Drift Stations

The highest temperatures were recorded in the zone behind the last bulkhead, which houses the TBM. In this zone, the temperature fluctuated between 30˚ and 32˚C during most of the monitoring periods. However, there were three distinct periods when the temperature in this zone dropped below 30˚C. The first occurred in early September 2000 and was likely caused by power interruptions, which in turn caused the TBM to cool. The second temperature drop was in late January 2001, when all the bulkhead doors were opened. During this brief period, the temperature in the vicinity of the TBM dropped to ~22.5˚C. The temperature in this zone again dropped to below 30˚C in early April 2001, likely because of the powering-off of the TBM.

In the zone between the third and fourth bulkheads, the temperature tended to continuously drop from ~26.5˚C to ~ 24˚C between August 2000 and May 2001. Significant deviations from trend were observed in early September 2000, when the temperature increased briefly. These deviations coincide with the temperature decreases in the zone housing the TBM. Because similar observations were not recorded before the first bulkhead, it is likely that this perturbation was caused when the fourth bulkhead door was left open for a few days.

The temperature data collected between the first and second bulkhead shows the region steadily cooling immediately following the closure of the bulkhead doors in July 2000. (Because of the lack of temperature data from this location between late September 2000 and February 2001, temperature dynamics in this zone cannot be compared with the other two zones during this time.) Following the closure of the bulkhead doors in late January 2001, the temperature in this zone immediately reached ~24˚C and remained close to that value over the next two months.

Temperature in the ECRB Cross Drift measured immediately before the first bulkhead shows diurnal and seasonal fluctuations. While the diurnal fluctuations appear to be restricted to within 3˚C, the seasonal temperature changes from ~29˚C in late August 2000, to ~25˚C in late December 2000.

In summary, the zones defined by the bulkhead in the ECRB Cross Drift appear to be partially thermally isolated from each other and also from the area before the bulkhead *when the doors are closed*. The zone housing the TBM was warmer than the area before the first bulkhead, while the other two zones were consistently cooler when the doors were closed. During the period when the bulkhead doors were opened, the temperature in each of the zones rapidly approached that of the zone outside the bulkheads.

6.10.2.1.4 Relative Humidity Variations between May 2000 and May 2001

The relative humidity in the three zones defined by the bulkheads shows spatial variability similar to the temperature data (Figure 6.10.2-7). The lowest humidity was observed in the area before the first bulkhead, where it fluctuated between ~10 and 40%, with a few instances where the humidity was greater than 60%. In the two zones monitored behind the bulkheads, the relative humidity remained close to ~95%, with some changes observed in March 2001, when the humidity in the third zone gradually fell closer to ~90%.

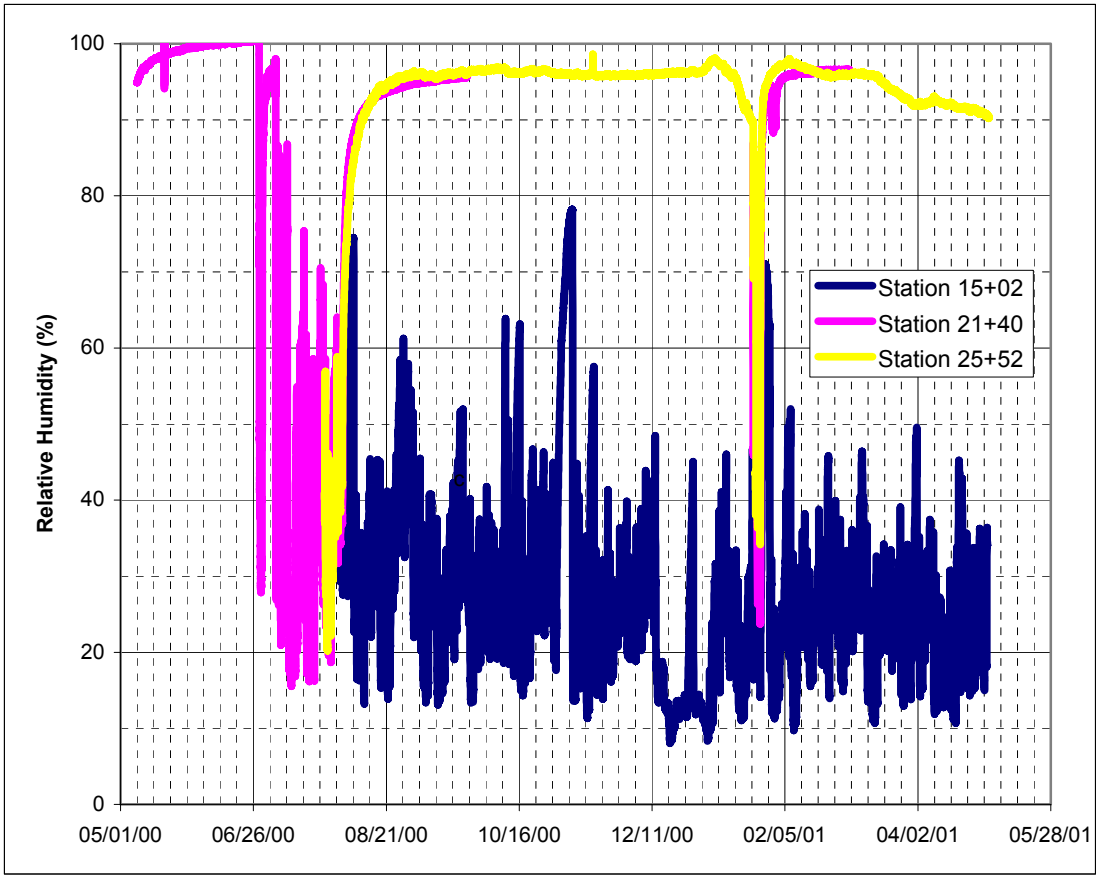

DTN: LB0307ECRBRHTB.001 [164843]

Figure 6.10.2-7. Relative Humidity Measured in the ECRB Cross Drift Stations

6.10.2.2 Observations of Wet Zones During Bulkhead Entries

Additional information on the moisture conditions within the nonventilated zone has been collected during periods when the bulkhead doors were opened. During periodic entries for visual inspection, wet spots were observed and water samples were manually collected. Observations have been made in the nonventilated sections that show the existence of liquid water, as well as rust spots and organic growths (i.e., indicators of the prolonged presence of water). While the presence of liquid water is evident, no continuous seepage from the rock into the closed sections of the ECRB Cross Drift has been observed to date. Figure 6.10.2-8 summarizes the timing and locations of liquid water observed during bulkhead entries, with details described in the following subsections. Photographic evidence is presented for the October 1-2, 2001 entry (DTN: LB0301ECRBRHTB.001 [164605]) to represent similar observations during other entries (DTN: GS030608312231.002 [165547] for additional images of ECRB moisture monitoring entries, January 22, 2002, to February 3, 2003).

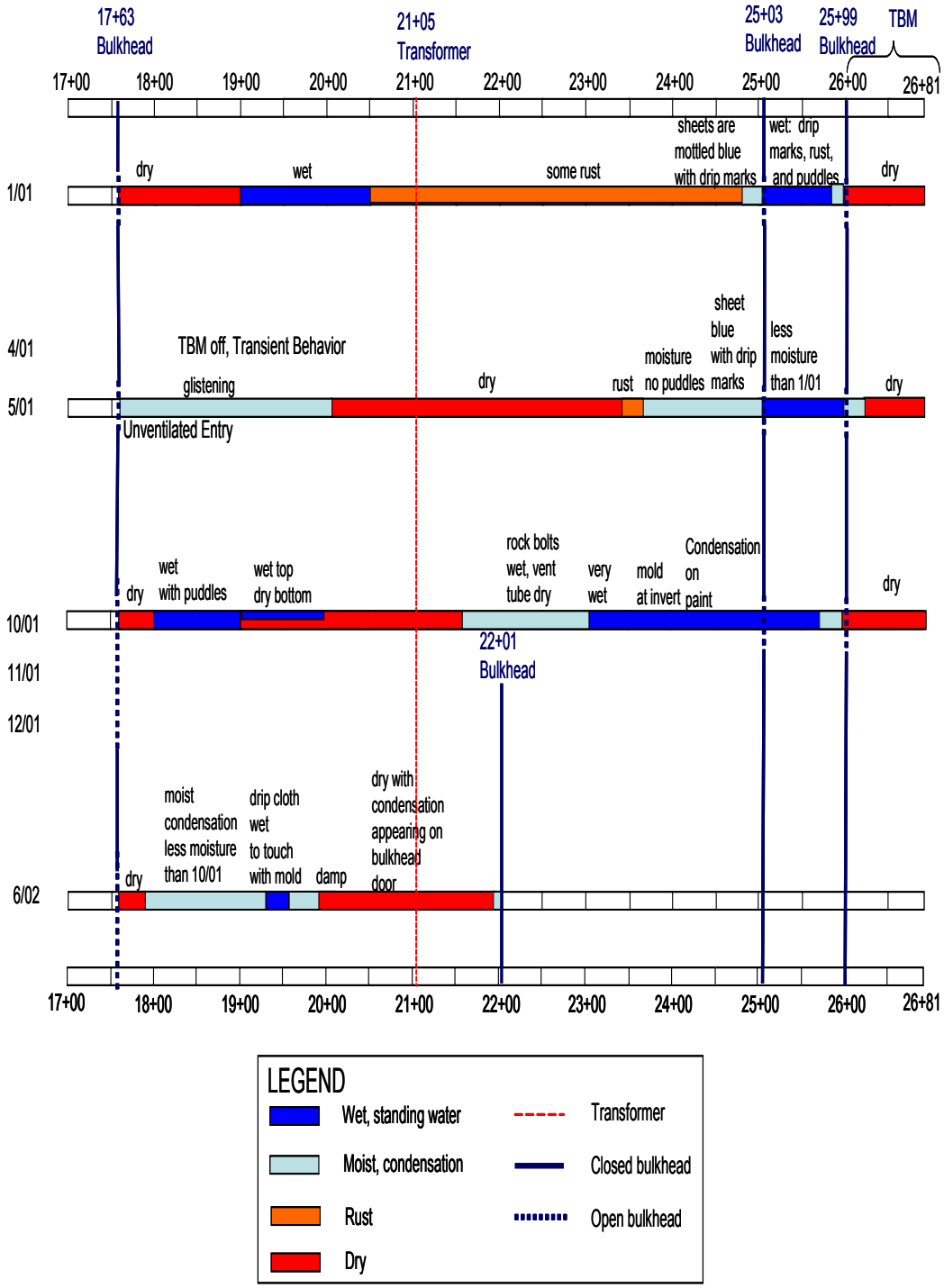

Sources: Entry 1/23/01 to 1/25/01: Hudson 2002 [165391] pp. 23-24, 91-98;
Entry 5/22/01: Hudson 2002 [165391] pp. 38-39, 140-150;
Entry 10/1/01 to 12/20/01: Hudson 2002 [165391] pp. 218-301;
Hudson 2002 [163398] pp. 1-47;
Entry 6/24/02 to 6/27/02: Hudson 2002 [163398] pp. 143-147.

Figure 6.10.2-8. Distribution of Wet Zones During ECRB Bulkhead Entries

6.10.2.2.1 Comparison of Observations During Nonventilated Entries in January 22–25, 2001 and May 22, 2001

In the entry on January 22-25, 2001, distinctly wet zones were observed, as shown in Figure 6.10.2-8. The power was off in April 2001. To avoid loss of data, an unventilated entry behind the bulkheads was done on May 22, 2001, to restore power to the dataloggers and to the TBM. The first bulkhead at CD 17+63 was opened at 11:10 am on May 22, 2001. No ventilation was established, and entry was permitted at 11:20 am. This entry was restricted to the same day, with bulkheads closed after the entry.

Less moisture was observed during the May 22, 2001, entry than had been observed during the January 22–25, 2001, entry. The moisture had not accumulated into puddles. The canvas drip detection sheet at CD 24+10 and the observed rust spots at CD 23+50 indicate that liquid moisture had been present at least this far up the tunnel. The continued power loss to the TBM resulted in a decreased temperature gradient within the tunnel. Moisture behind the third bulkhead and the smaller amount of moisture between the second and third bulkhead indicate that as the temperature gradient decreases, observable moisture tends to move toward the TBM.

The existence of water (glistening) was initially observed on the utility and vent lines in the first 250 m. The water appeared to be present only on the surface. Within two hours the moisture had evaporated. At CD 21+00, everything was dry. Moisture began reappearing on the utility and vent lines at about CD 23+50. There were rust spots on the steel channels and on the tracks. There was moisture at about a meter interval on the conveyor belt, but the water had not accumulated into puddles. A canvas sheet further up the tunnel than the others and hung on January 25, 2001, at CD 24+10, was mottled blue, with drip marks covering the entire sheets. The sheets between CD 24+75 and CD 24+95 were moist, and moisture also appeared on the utility and vent lines and on the bulkhead at CD 25+03, opened at 12:06 pm. Between the CD 25+03 and the CD 25+99 bulkhead, the canvas sheets were moist, but there was much less puddled water than for the January 22–25, 2001 entry. Moisture was evident on the canvas sheets, conveyor belt, and metal surfaces, and there were some small rocks on the conveyor belt. The bulkhead at CD25+99 was opened at 12:17 pm. There was moisture on utility lines and instruments cables to about 10 m behind the bulkhead. Beyond 10 m behind the bulkhead at CD 25+99, everything was dry.

6.10.2.2.2 Observations of Entry Made on October 1–2, 2001

An entry occurred on October 1 and a follow-up entry occurred on October 2, 2001. Four sections of alternating dry and wet conditions were observed between the first and second bulkhead on the first day, October 1, 2001 (12:03 pm to 13:37 pm). On the next day October 2, 2001, most water droplets had evaporated. Some of the rock and especially the in-filled fractures remained damp. Note that DTN: LB0301ECRBRHTB.001 [164605] includes photos for this entry.

On October 1 in the wet sections, the dampness was more pronounced on the upper part of the drift walls. The fault between the CD 25+03 and CD 25+99 bulkhead was dry. The last section behind the CD 25+99 bulkhead was also dry, with no rust was observed (implying that the section was not wet during the closure period). On the next day, October 2, 2001, most of water

droplets were evaporated, with some of the rock remaining damp. A patch of paint was observed to have beads of water drops on its surface, with no similar beads observed on the surrounding rock surfaces (Figure 6.10.2-9). Since the paint is impermeable, the observed beads are likely the results of condensation, not from seepage through the rocks below the painted patch. This observation substantiates the hypothesis that the observed water originates from condensation as the result of local temperature variations. This hypothesis is based on observations of early bulkhead entries and on chemical analyses (Section 6.10-3) from the limited water samples collected.

Detailed Descriptions of Visual and Photographic Observations

The bulkhead at CD 17+63 was entered on October 1, 2001, 12:03. Dry stalactites were observed on the vent tube just inside of the first bulkhead (Figure 6.10.2-10). The deposits were probably from redistribution of vent tube materials from dissolutions associated with early condensations, driven by temperature variations near the bulkhead. The lights in the same area have precipitate on them, but were dry during the observation. The drift was dry from the first bulkhead to about CD 18+00.

The drift was wet from CD 18+00 to about CD 19+00. First sign of moisture was observed on the left rib at CD 17+90, with condensate drips on utilities from overhead cables. The drops on the utilities were dry and a little bit rusty. Ventline and walls were very wet, and there were puddles on the belt and condensate all over the belt. There was a large puddle on the conveyer belt at CD 18+25 (Figure 6.10.2-11).

The wet sections conveyer belt had very clear water droplets (presumed to be condensate), all approximately evenly spaced on all rubber surfaces (top, bottom, in-between top bottom belts, etc.). The droplets sometimes ran together if there were depressions in the belt, creating puddles.

The surfaces of the rock in the wet areas were clearly damp but only on the top half of the drift. On the second day, the outer wet area was much drier. There was visual evidence of moisture retention in the little calcite infilled fractures but not in the matrix (Figure 6.10.2-12). This infill occurred more on the upper half of the drift than on the lower half. The infilled fractures looked like collapsed lithophysal cavities, even though the observation was in the lower nonlithophysal zone. In comparison with the observation first day, the inner wet area was not drier on the 2nd day. The main difference was that the droplets on the conveyer had mostly disappeared on the 2nd day.

Condensate was prevalent on the shotcrete after the CD 25+03 bulkhead (Figure 6.10.2-13) and behind the CD 25+99 bulkhead. The drift was dry again from CD 19+00 to about CD 21+50. The walls began to dry out moving towards the TBM. The Solitario Canyon fault appeared quite dry (Figure 6.10.2-14). The cloth tarp hanging on the portal side of the CD 25+99 bulkhead showed discoloration (blue for about 6 m or 20 feet from the bulkhead), indicating that it was wet at some point. Further towards the portal there was no discoloration (Figure 6.10.2-15). The water was likely located only near the bulkhead. Inside the CD 25+99 bulkhead, the drift was quite dry (Figure 6.10.2-16).

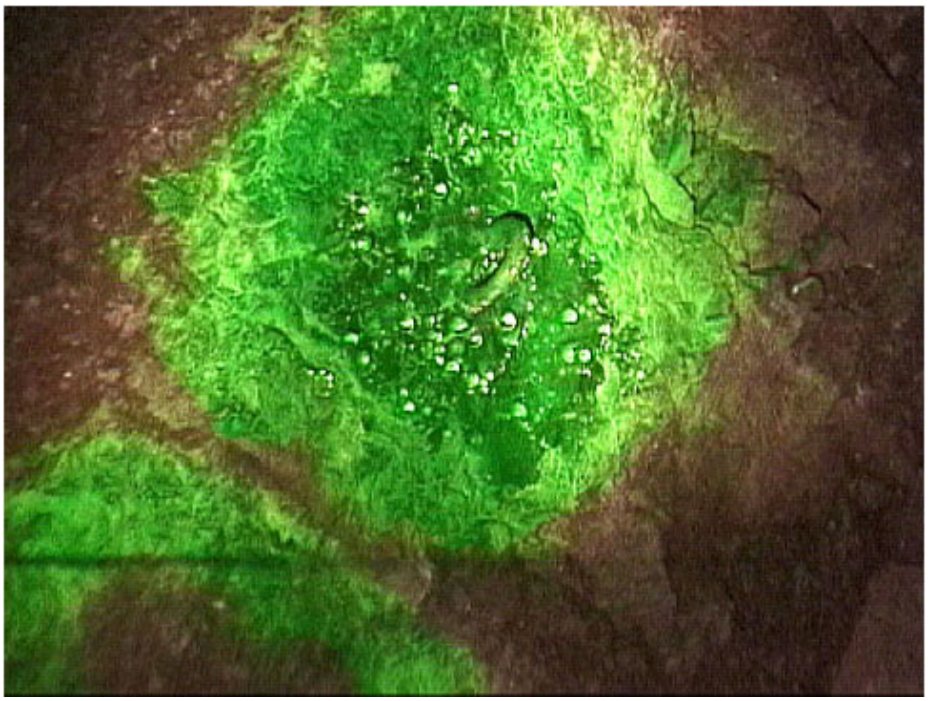

DTN: LB0301ECRBRHTB.001 [164605]

NOTE: Photo taken on 10/2/2001.

Figure 6.10.2-9. The Green Paint on the Crown of the ECRB Had Condensate Hanging from It, but Surrounding Rock Surface Did Not at CD 24+70.

DTN: LB0301ECRBRHTB.001 [164605]

NOTE: Photo taken on 10/1/2001 at 11:43.

Figure 6.10.2-10. Stalactites near 1st Bulkhead at CD 17+63

DTN: LB0301ECRBRHTB.001 [164605]

NOTE: Photo taken on 10/1/2001 at 12:26.

Figure 6.10.2-11. Water Puddle and Condensate on Conveyer at CD 18+25

DTN: LB0301ECRBRHTB.001 [164605]

NOTE: Photo taken on 10/2/2001 at 14:30.

Figure 6.10.2-12. Water Surrounding Inclusions

DTN: LB0301ECRBRHTB.001 [164605]

NOTE: Photo taken on 10/1/2001 at 13:19.

Figure 6.10.2-13. Condensate on Shotcrete after 2nd Bulkhead

DTN: LB0301ECRBRHTB.001 [164605]

NOTE: Photo taken on 10/1/2001 at 13:14.

Figure 6.10.2-14. Solitario Canyon Fault Left Rib

DTN: LB0301ECRBRHTB.001 [164605]

NOTE: Photo taken on 10/1/2001 at 13:15.

Figure 6.10.2-15. Tarp Discoloration before CD 25+99 Bulkhead

DTN: LB0301ECRBRHTB.001 [164605]

NOTE: Photo taken on 10/1/2001 at 13:13.

Figure 6.10.2-16. Inside Bulkhead at CD 25+99 (with TBM)—Quite Dry

6.10.2.2.3 Observations of Entry Made on June 24, 2002

During the nonventilated entry made on June 24, 2002, access to the ECRB was restricted to the areas between Station CD 17+63 and Station CD 22+01. During this entry, no standing pools of water were observed. However, there was some evidence of water at various locations. For example, at Station CD 19+15, a few brown spots of water were visible on plastic sheets that lay over the railroad tracks. Similar brown spots were visible on plastic sheets suspended from the ceiling at the same location. Mold was visible along certain sections of the rail tracks (e.g. Station CD 19+50) and on some of the canvas tarps suspended from the ceiling. Note that DTN: LB0301ECRBRHTB.001 [164605] also contains photos for this entry.

At Station CD 20+00, where a canvas sheet was located next to the transformer, a color contrast observed on the canvas sheet suggests the existence of a microclimate resulting from temperature gradients. Large quantities of water were observed as rivulets along the bulkhead doors at Station CD 22+01. However, immediately above the doors, the bulkhead remained dry.

6.10.2.3 Estimates of Mass of Vapor in Nonventilated Sections of the ECRB

From measurements of relative humidity (i.e., the ratio of the existing vapor pressure to the saturation vapor pressure at the same temperature), the density of water vapor (i.e., the mass of water vapor per unit volume of air) along the ECRB can be estimated from the relationship between temperature and the vapor density in saturated air (Figure 6.10.2-17). This relationship is accurately captured ($R^2 = 0.999$) by the second-order polynomial equation:

$$V_{\sigma s} = 0.00002t^2 + 0.0001t - 0.0053 \qquad [6.10\text{-}1]$$

where $V_{\sigma s}$ is the vapor density of saturated air (kg m^{-3}) and t is the temperature (^{0}C) of the saturated air.

The actual vapor density ($V_{\sigma a}$) is then calculated from the relative humidity as:

$$V_{\sigma a} = V_{\sigma s} \times Rh \qquad [6.10\text{-}2]$$

Subsequently, for a given length of drift, along which the temperature and relative humidity are approximated to be fairly constant, the flux of moisture in to or out of the drift, and the amount of moisture contained per unit length of drift at any given time can also be determined (see Attachment IX.4 for calculation).

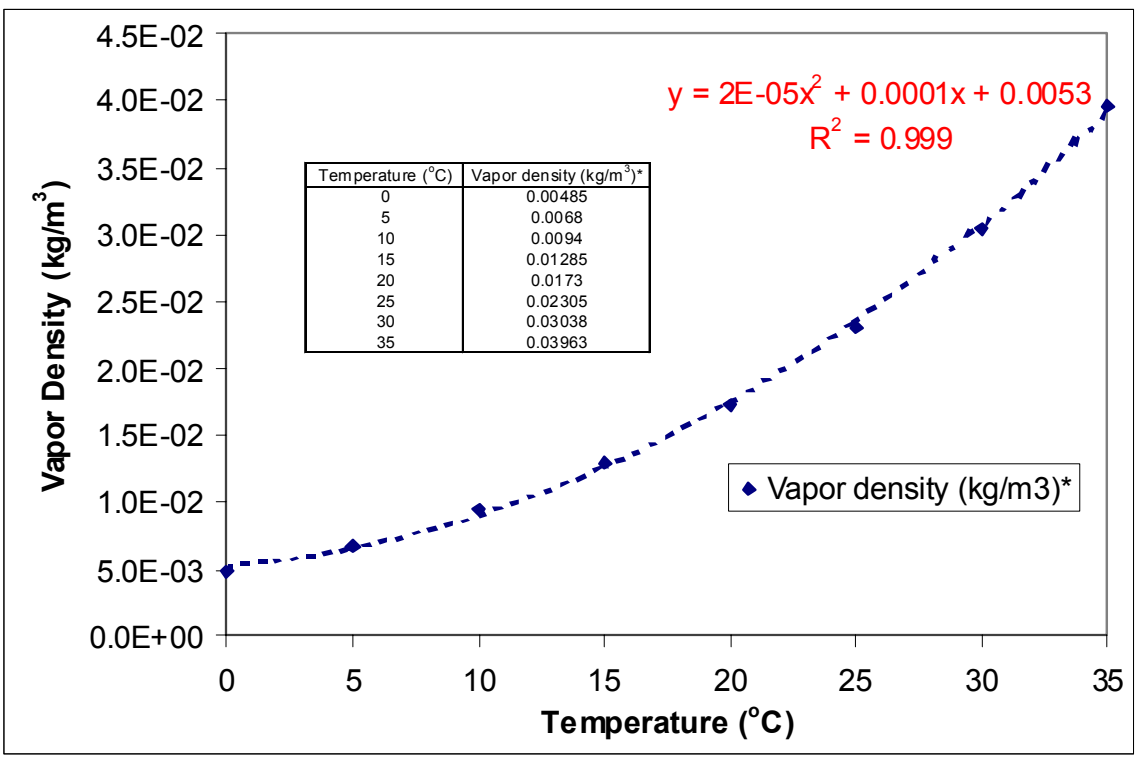

Temperature (°C)	Vapor density (kg/m^3)*
0	0.00485
5	0.0068
10	0.0094
15	0.01285
20	0.0173
25	0.02305
30	0.03038
35	0.03963

DTN: LB0307ECRBRHTB.001 [164843]

NOTE: Table shows the data from which the plot was developed. The polynomial equation describing this relationship is included in the plot. Data for table is from Hillel (1998 [165404], page 37).

Figure 6.10.2-17. Vapor Density at Various Temperatures

For example, after the bulkhead doors in the ECRB were closed during the last week of January 2001, the relative humidity measured at the monitoring stations CD 21+40, CD 25+52 (See DTN LB0307ECRBRHTB.001 [164843]) show a rapid rise in the in-drift humidity measurements (Figure 6.10.2-7).

A first-order estimate of the amount (mass) of vapor for the period immediately following the closure of the bulkhead doors can be made by determining the mass of vapor associated at a given temperature using Equation 6.10-1 and Figure 6.10-2. The temporal response of the mass of vapor is presented in Figure 6.10.2-18. This figure shows that once nonventilated conditions prevail behind closed bulkheads, the mass of vapor rapidly increases to ~37 kg per 100 m section of tunnel.

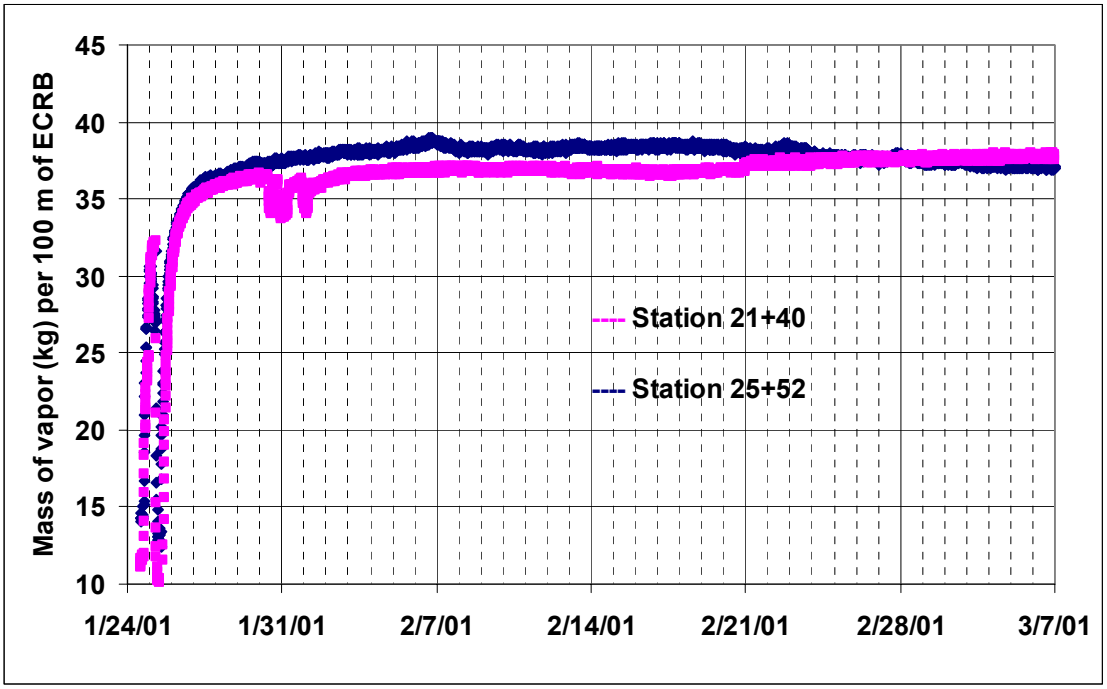

DTN: LB0307ECRBRHTB.001 [164843]

Figure 6.10.2-18. Mass of Vapor in Sections of ECRB Determined from Temperature and Relative Humidity Measurements at Station CD 21+40 and Station CD 25+52

6.10.3 Chemical and Isotopic Analysis of Water Samples Collected During Bulkhead Entries

The nonventilated sections of the ECRB Cross Drift were opened four times from January 2000 to January 2001, and water samples were collected. Both chemical analysis and isotopic measurements were conducted on the samples. The chemical analyses were on major anionic and cationic constituents (including bromide, chloride, and lithium) in the liquid samples. The hydrogen (δD) and oxygen ($\delta^{18}O$) isotope compositions were also analyzed.

6.10.3.1 Chemical Analysis

Most of the initial samples were collected directly from pools that had formed on the conveyor belt, and these samples were of brownish to dark-brown color, with some examples shown in Figure 6.10.3-1. Their chemical compositions show high and spurious concentrations of many constituents, as shown in Table 6.10.3-1. These samples are likely contaminated from the conveyor belt, resulting from the belt usage/operation before ECRB Cross Drift closure, with the degree of contamination unknown and unable to be quantified. Contamination of the conveyor belt may include salt accumulated from water evaporation following transportation of the tuff debris, as well as other miscellaneous contamination. Therefore, these samples may not yield useful information about the origin of the water (condensate or seepage) observed in the ECRB Cross Drift behind bulkheads.

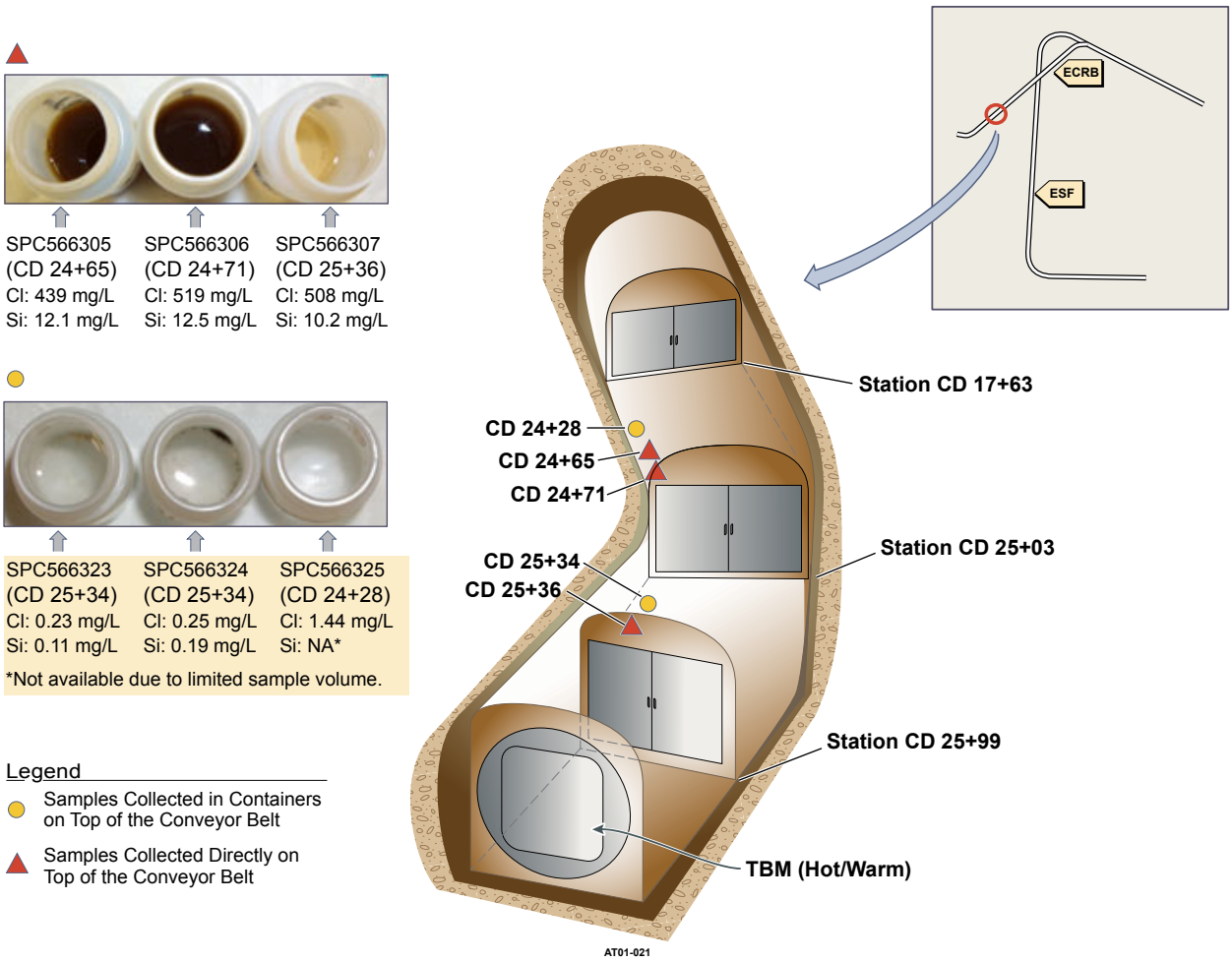

DTN: LB0110ECRBH2OA.001 [156886]

Figure 6.10.3-1. Chemical Analyses of Liquid Samples Collected during Bulkhead Entries

Subsequently, three samples were collected from collection containers placed on the top of the conveyor belt. These samples are clear (Figure 6.10.3-1). Their chemistry, particularly low chloride and silica contents, indicates that this water is condensate (Figure 6.10.3-2). The water does not have the chemical signature of the construction water, which contains about 20 mg/L of lithium bromide added to J-13 well water. Condensate, and subsequent dripping down, could

occur as a result of vapor-to-liquid transition associated with local temperature variations in a humid environment. The moisture conditions measured by humidity and temperature probes support the presence of drift moisture variations (Section 6.10.2.2). These clear samples also show a relatively high amount of calcium and a high sulfate/chloride ratio, suggesting some minor contamination from either rock grout or rock dust (Figure 6.10.3-2). (Some grout or dust present along the drift crown above the sampling containers may have dissolved in the condensate prior to collection.) Samples collected on the drift wall (using a needle syringe for SPC566308 in Table 6.10.3-1, and absorbent pad attached to the wall) show an even higher concentration of calcium and a larger sulfate/chloride ratio, resulting from the direct contact of the sample with the rock.

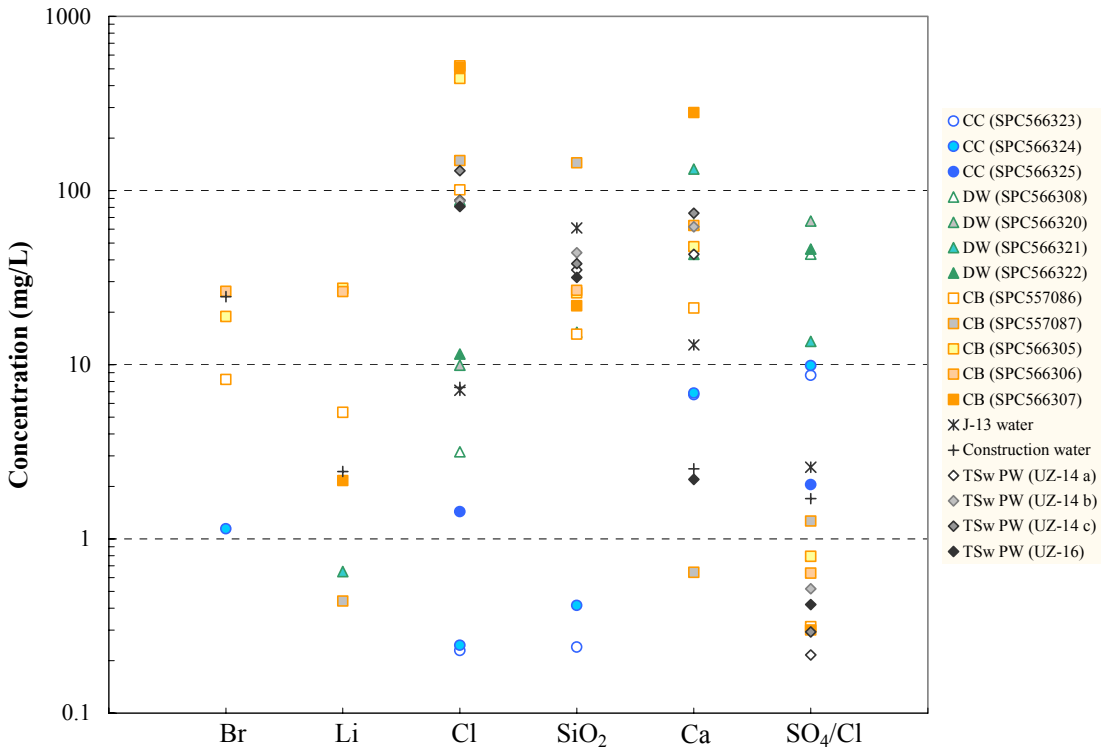

Source: J-13 well water composition from DTN: MO0006J13WTRCM.000 [151029].
TSw pore-water data from BSC 2001 [154874], Table 6.
ECRB water data from DTN: LB0110ECRBH2OA.001 [156886]

NOTE: Unit of the Y-axis is in mg/L, except for the ratio of sulfate to chloride (dimensionless).
ECRB Samples are grouped as follows: CC in collection container, DW on drift wall, and CB on conveyor belt.
Construction water data presented here are an average value from seven samples.
TSw PW: pore water in Topopah Spring welded tuff unit.

Figure 6.10.3-2. Comparison of Chemical Signatures

Table 6.10.3-1. Chemical and Isotopic Data for Liquid Samples Collected in the ECRB Cross Drift

Specimen ID#	Sample Location	Collection Date	Br^-	Cl^-	F^-	NO_3^-	SO_4^{2-}	Ca^{2+}	Li^+	Mg^{2+}	K^+	Na^+	SiO_2	δD	$\delta^{18}O$
			(mg/L)											(%)	
SPC557086	Conveyor belt - Station CD 24+83	1/31/00	8.23	101	ND	ND	31.7	21.2	5.33	3.10	19.0	88.6	15.0	-59	-7.1
SPC557087	Conveyor belt - Station CD 25+17	1/31/00	ND	149	29	ND	188	0.64	0.44	0.10	160	139733	144	-80	-9.3
SPC566305	Conveyor belt - Station CD 24+65	5/03/00	18.9	439	ND	ND	349	47.6	27.5	9.00	27.9	195	25.9	-79	-9.3
SPC566306	Conveyor belt - Station CD 24+71	5/03/00	26.3	519	9.19	ND	330	62.9	26.3	12.0	35.3	230	26.7	-80	-8.9
SPC566307	Conveyor belt - Station CD 25+36	5/03/00	ND	508	6.41	24.1	152	280	2.16	34.0	36.3	191	21.8	-79	-8.7
SPC566308	Shotcrete- Station CD 25+50	5/03/00	ND	3.16	ND	4.29	136	---	---	---	---	---	---	---	---
SPC566300	Construction Water	5/31/00	25.1	6.82	---	ND	13.4	6.64	2.02	---	5.94	59.1	---	---	---
SPC566320	Absorbent pad - Station CD 25+62	6/28/00	ND	9.95	7.05	3.99	665	63.5	ND	11.5	172	105	<1.0	---	---
SPC566321	Absorbent pad - Station CD 25+62	6/28/00	ND	88.0	15.8	5.79	1197	133	0.65	18.1	163	233	15.4	-69	-6.9
SPC566322	Absorbent pad - Station CD 25+62	6/28/00	ND	11.5	8.02	2.20	531	43.0	ND	6.50	141	78.6	<1.0	-71	-7.8
SPC566323	Collection container - Station CD 25+34	6/28/00	ND	0.23	ND	1.63	1.99	6.73	ND	0.40	0.84	1.56	0.24	-83	-9.4
SPC566324	Collection container - Station CD 25+34	6/28/00	1.14	0.25	ND	ND	2.42	6.87	ND	0.40	0.90	1.65	0.42	-84	-9.4
SPC566325	Collection container - Station CD 24+28	6/28/00	ND	1.44	ND	2.34	2.95	---	---	---	---	---	---	-67	-8.1

Table 6.10.3-1. Chemical and Isotopic Data for Liquid Samples Collected in the ECRB Cross Drift (Continued)

Specimen ID#	Sample Location	Collection Date	Br^-	Cl^-	F^-	NO_3^-	SO_4^{2-}	Ca^{2+}	Li^+	Mg^{2+}	K^+	Na^+	SiO_2	δD	$\delta^{18}O$
			(mg/L)											(%)	
SPC573600	Conveyor belt - ~5 m from 2nd bulkhead	1/22/01	45.4	---	---	---	---	---	0.11	---	---	---	---	-90	-10.6
SPC573602	Conveyor belt - Station CD 25+37	1/22/01	79.7	---	---	---	---	---	0.17	---	---	---	---	-74	---
SPC573604	Conveyor belt - ~7 m from 2nd bulkhead	1/22/01	56.3	---	---	---	---	---	12.31	---	---	---	---	-89	-10.7
SPC573605	Conveyor belt - Station CD 25+42	1/22/01	ND	---	---	---	---	---	0.22	---	---	---	---	-55	-3.7
SPC573601	Conveyor belt - Station CD 25+10	1/23/01	72.5	---	---	---	---	---	14.8	---	---	---	---	-48	-5.0
SPC573603	Conveyor belt - Station CD 25+21	1/23/01	52.5	---	---	---	---	---	0.13	---	---	---	---	-55	-4.9

DTN: LB0110ECRBH2OA.001 [156886]; LB0110ECRBH2OI.001 [156887]

NOTE: Liquid samples were filtered through 0.45 μm filters prior to chemical analyses. Phosphate was not detected in any of the liquid samples.
ND: not detected, e.g., below the analytical detection limit (about 0.1 mg/L).
---: Data not available.

6.10.3.2 Isotopic Analysis

Water samples collected were also used for isotopic analyses, with the results presented in Table 6.10.3-1 and illustrated in Figure 6.10.3-3. The δD values of the ECRB Cross Drift water range from -48‰ to -9‰, and the $\delta^{18}O$ values range from -3‰ to -10.7‰. These values are higher than those found in the construction water. The lag time between opening of bulkheads and allowing sample collection (3–4 hours) is sufficient to result in a significant degree of evaporation of the samples. In Figure 6.10.3-3, all samples from the ECRB Cross Drift are shifted from the global meteoric water line, similar to samples from Alcove 5. The offset is characteristic of waters that have undergone some degree of vapor loss. The same degree of shift for both the contaminated samples and the relatively clean samples may indicate that approximately the same degree of evaporation occurred for water collected in the ECRB Cross Drift.

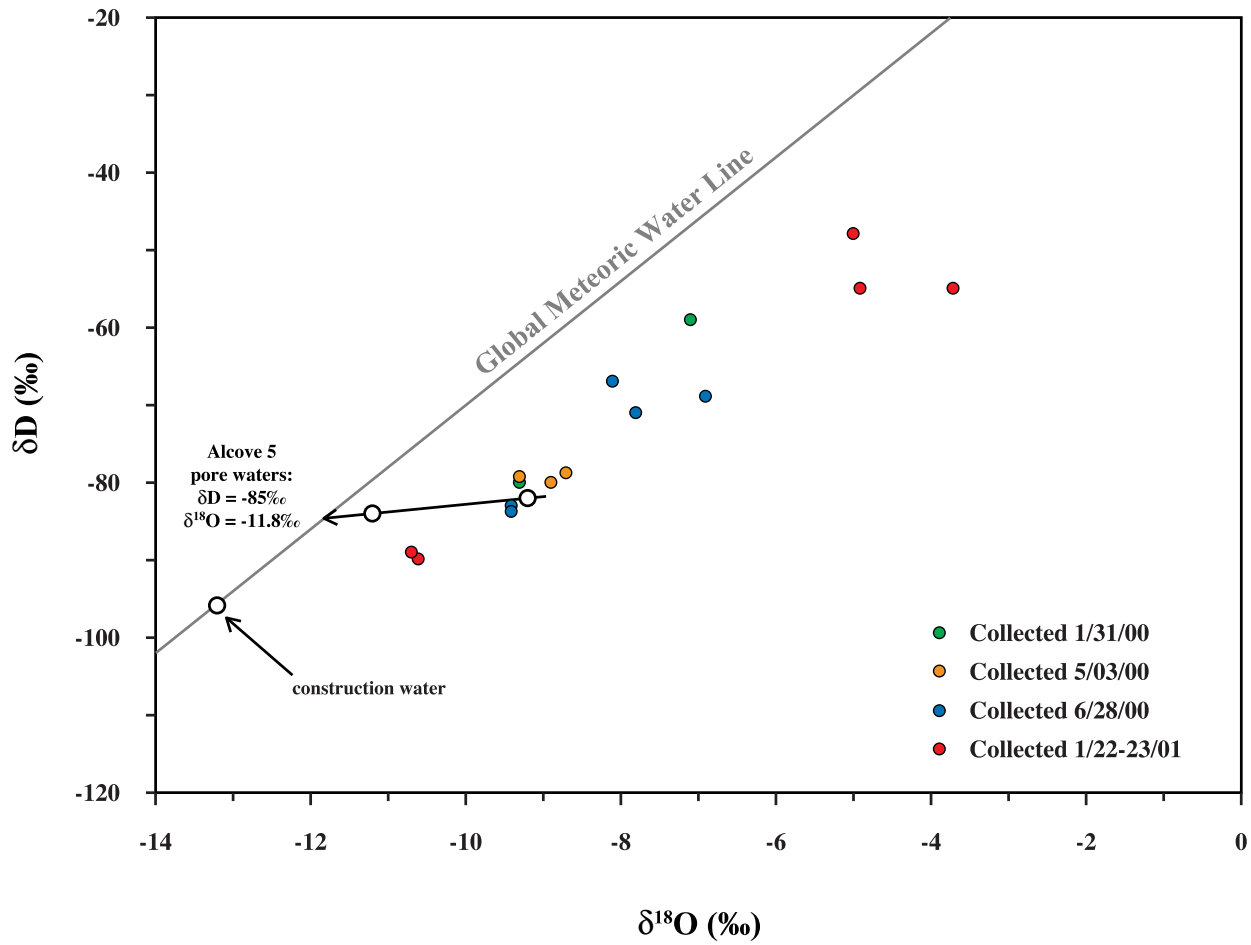

DTNs: LB0110ECRBH2OI.001 [156887], LB0108CO2DST05.001 [156888], LB0011CO2DST08.001 [153460]

NOTE: Also plotted is the isotopic composition of construction water, two pore water samples extracted from core samples from Alcove 5 and the location of the Global Meteoric Water Line.

Figure 6.10.3-3. Plot of the Hydrogen and Oxygen Isotope Compositions of Water Samples Collected from the ECRB Cross Drift

6.10.3.3 Summary of ECRB Entries

During most of the entries, the entire ECRB Cross Drift was accessible for visual inspection. Wet areas were observed and water samples were manually collected from small pools of water. The visual observations suggest that the water observed in the ECRB originated from condensation. (For example, water droplets were observed on the surface of a small patch of paint, an impermeable barrier to the rock.) Water collected from collection containers in the second entry (June 28, 2000) indicated that the water is low in chloride and silicate contents, characteristic of condensate. The water does not have the chemical signature of construction water (i.e., spiked with about 20 mg/L of lithium bromide). Condensates, and consequent dripping down, could occur by water phase transition from vapor to liquid associated with local temperature variations. The moisture conditions measured by humidity and temperature probes support the presence of drift moisture variations. The potential measurements in the boreholes indicate that the tuff matrix is still dry near the borehole collars.

6.10.4 Ambient Monitoring in Alcove 7

Ambient monitoring of temperature, barometric pressure, and relative humidity was also performed inside Alcove 7, located in the ESF at station 50+64. This alcove was constructed to a depth of 203 m and penetrated the Ghost Dance fault at 167 m. Bulkhead doors were installed 64 m and 132 m from the entrance of the alcove during the Fall of 1997 (Kurzmack et al. 2002 [162333]).

The Alcove 7 bulkhead door was first closed on December 11, 1997. Although there were many entries during the period from December 1997 to October 30, 2000, there were relative humidity measurements close to 100%. Fluctuating temperature and relative humidity measurements indicated that the bulkheads were not perfectly sealed (DTN: GS990108312242.005 [166000]).

On September 18, 2001 the bulkheads were opened after being closed since October 30, 2000. Evidence of moisture was observed during this entry. Signs of moisture included drip spots on the drip collection sheets, moisture drops on the utility lines, moisture drops on the shotcrete around the bulkheads, and moisture spots in the dust on an instrument enclosure. Also, the rock in the crown had a dark, moist appearance. The bulkhead doors were next opened on May 20, 2003. There were drip spots on the drip collection sheets, moisture drops on the utility lines, and moisture spots in the dust on an instrument enclosure. The rock in the crown had a dark, moist appearance and the fractures in the rib appeared wet (Hudson 2003 [165273]).

Between September 25, 2001 and June 10, 2002, the relative humidity behind the bulkhead doors was less than 95% (dry end of the thermocouple psychrometers) and was therefore not measured. Pressure monitoring indicated that the transmission of atmospheric pressure fluctuations across the bulkhead doors showed minimal dampening (< 5%) and short time lags (on the order of hours). Large temperature fluctuations (19.5 to 27.5 degrees Celsius) at the monitoring station located 4 m from the entrance of the alcove were caused by seasonal temperature fluctuations down the ESF by the ventilation system. This monitoring station is located outside the bulkhead doors. Diurnal temperature fluctuations caused by ventilation were as large as 1.2 degrees. Temperatures behind the bulkheads indicated no discernable annual fluctuation, and the diurnal temperature fluctuations were less than 0.05 degrees. Abrupt temperature decreases (up to 1.0

degree) were occasionally measured behind the bulkheads. These temperature decreases were correlated with the pressure recovery period following a low-pressure event. The temperature decrease may be caused by a pressure gradient driving warm-dry ESF air through the fractures around the bulkheads, evaporating water and cooling the air.